University of Strathclyde

Department of Mechanical & Aerospace Engineering

Characterisation of metallurgical and mechanical properties of friction stir welded low alloy steels for marine applications

Athanasios I. Toumpis

A thesis submitted in fulfilment of the requirements for the degree of

Doctor of Philosophy

2015

Declaration of Authenticity and Author's Rights

This thesis is the result of the author's original research. It has been composed by the author and has not been previously submitted for examination which has led to the award of a degree.

The copyright of this thesis belongs to the author under the terms of the United Kingdom Copyright Acts as qualified by University of Strathclyde Regulation 3.50. Due acknowledgement must always be made of the use of any material contained in, or derived from, this thesis.

Signed:

Date:

Abstract

Friction stir welding of steel presents numerous advantages across many industrial sectors compared to conventional fusion welding techniques. However, the fundamental knowledge of the process on steel remains relatively limited, hence industrial uptake of friction stir welding is practically non-existent. This thesis reports on a large-scale microstructure and property evaluation of friction stir welded low alloy steel grade DH36 plate, commonly used in marine applications. The extensive study examined butt welds produced by a wide range of process parameters through microstructural characterisation, transverse tensile testing, Charpy impact testing and hardness measurements. A preliminary process parameter envelope has been developed and parameter sets established that deliver high integrity welds and enhance the process's techno-economic competitiveness through a step change increase in the conventionally recognised welding traverse speed.

In parallel, a comprehensive fatigue performance assessment of friction stir welded DH36 steel has been implemented. Original experimental procedures specific to friction stir welding have been put forward and the consequent exhaustive study examined the weld microstructure and hardness distribution in support of tensile and fatigue testing, also accounting for the effect of varying welding parameters. Steel friction stir welds exhibit fatigue lives well above the relevant international recommendations for fusion welding, irrespective of minor surface breaking flaws which have been identified. A detailed fracture surface analysis has concluded that surface breaking irregularities such as these induced by the tool shoulder's features on the weld top surface can be the dominant factor for crack initiation under fatigue loading.

Friction stir welding is a solid state thermo-mechanical deformation process from which the plasticisation behaviour of the stirred material can be evaluated through the study of flow stress evolution. Novel flow stress data on DH36 steel were generated over a range of strain rates and temperatures by hot compression testing; these data and the subsequent innovative metallurgical examination of the tested samples will contribute to the scientific understanding of the process. The evolution of flow stress is found to be considerably affected by the test temperature and deformation rate; this relation has led to a number of significant observations which will inform future refinement of process parameters.

Acknowledgements

Table of Contents

Preface

Friction stir welding (FSW) of low melting point metals and particularly aluminium has been extensively researched in the past decade. The process has achieved a considerable level of maturity, demonstrating that it is a joining method which consistently delivers cost-effective and high quality welds; this has led to its positive reception by many industrial sectors.

In contrast, FSW of steel remains a relatively immature process with insignificant industrial penetration for a number of reasons. The FSW tool for steel with the associated matters of unreliable performance, debatable consistency in weld quality, high costs and short operational life has emerged as the main limiting factor in the economic competitiveness of the process versus well established, traditional fusion welding techniques; this issue is briefly discussed in Chapter 1 of the thesis. The lack of relevant guidelines and specifications is one more obstacle with respect to shipbuilding. However, research has exhibited that FSW of steel produces welds of enhanced properties and furnishes many benefits such as the capability to join dissimilar materials or alloys of poor weldability by fusion methods. It is therefore conceivable that these advantages may counteract the issues outlined above for a few niche applications and this is expected to drive new developments in steel FSW further.

One crucial factor in the wider uptake of FSW that the research work traced in this thesis attempts to address is the scientific understanding of the underlying phenomena during FSW and especially the relation between evolved microstructure and resultant mechanical properties of steel welds. Advancing the scientific knowledge on the manner in which FSW gives rise to these property improvements is essential if the process is to achieve acceptance and large-scale commercialisation. Moreover, this increased knowledge and the corresponding datasets which are recorded will be invaluable to any modelling work on the subject and will favour the progress in process control regimes and tooling design and material, an area in which improvements are greatly desired.

The present thesis is investigating the FSW of low alloy steel in the context of marine applications through a comprehensive microstructural characterisation and mechanical property assessment. The experimental work presented in the following

chapters has been undertaken as part of project HILDA. The European funded (€2.2M FP7 advanced manufacturing) international research project HILDA (High Integrity Low Distortion Assembly) has been formulated with the aim of assisting in the introduction of steel FSW in the European shipbuilding industry. This project has been delivered by a consortium of eight academic and industrial partners across Europe.

The author has been engaged in wide-ranging research activities and implemented the relevant experimental work with respect to the contribution of the University of Strathclyde in HILDA and indeed, the bulk of the experimental testing programmes throughout the project. These highly novel research activities have been concerned with the FSW of steel for the European maritime sector. The corresponding testing programmes have been concentrating on the detailed microstructural examination and mechanical property evaluation of the produced friction stir butt welds on 6 mm thick steel grade DH36, a low alloy steel utilised in the European shipbuilding industry, also focusing on the interactions between weld metallurgy and associated mechanical properties.

The key technical objectives of this extensive research are the development of the fundamental knowledge on FSW of steel in support of the process's future introduction in industry and the generation of data not previously available on steel FSW. The latter have been supplied to international partners for the decisive validation of their predictive local and global models. In summary, 25 friction stir butt welds (out of a total of more than 200 welds created within HILDA using the current state of the art in FSW tool for steel) are explored in terms of metallurgy and mechanical testing and 3 more in fatigue testing, all welds being 2000 mm long. This work is also implemented in order to assess the quality of the produced welds, establish an initial process envelope of acceptable parameter sets and determine original parameter sets of high speed welding which can fabricate high integrity welds, thus improving the process's techno-economic competitiveness.

It is the author's strong belief that the novel findings on the steel friction stir welds' performance and the associated broad datasets which have been generated will substantially advance the scientific understanding of the process. The same research has formed the basis of a number of dissemination activities; these are summarised in Appendix B.

Structure of the thesis

This thesis has endeavoured to offer a balanced account on the two main subjects of microstructural characterisation and mechanical property evaluation. Still, the strong link between microstructure and resultant mechanical properties is consistently highlighted throughout the chapters with relevant metallographic discussion.

Project HILDA (illustrated earlier) is very sparsely referenced in the thesis and only where the scientific collaboration with other partners in the project and their contribution to the author's research work is mentioned. In particular, these contributions are restricted to the development of process parameters through the actual welding (performed by The Welding Institute), the fatigue testing standard operating procedure document and the simple statistical analysis of the fatigue data (drafted in partnership with Lloyd's Register and the Center of Maritime Technologies) and finally, the thermo-mechanical deformation conditions and the temperature distribution map (supplied by The Welding Institute and Cenaero).

Since a number of diverse experimental testing programmes have been conducted and these are divided into individual chapters, there is not one literature review section for the entire thesis, for instance in Chapter 1. Instead, a review of the relevant technical literature on each subject matter is provided in the introductory section of the appropriate chapter. In particular, a general discussion on the FSW process (through the pertinent literature) is provided in Chapter 1, publications on microstructural characterisation of steel FSW are discussed in Chapter 2, suitable commentary on mechanical properties is included in Chapter 3, the literature associated with fatigue is introduced in Chapter 4 and the one on flow stress analysis in Chapter 5. For the same purpose, the thesis has been structured in a way that each chapter can be read and evaluated independently. This is also assisted by the separate literature review made available in the specific chapter for which it is intended. Additionally, a list of references is provided at the end of every chapter to make this a separate entity for the reader who may be interested solely on a particular subject matter. Consequently, every effort has been made to minimise possible overlapping of information but without reducing the clarity of the text or the interconnection of arguments and findings across chapters, where this has been considered useful.

More specifically, Chapter 1 delivers a generic introduction to FSW with an emphasis on steels in shipbuilding applications, explains the welding process, outlines a number of advantages over traditional fusion welding methods mainly relating to the weldable steel grades, the capability of welding alloys of reduced weldability or practically non-weldable by fusion welding methods, also joining dissimilar materials and the possibility to overcome problems related to fusion welding. A discussion on the main challenges of the process is then provided and this is associated primarily with the FSW tool material for steel. The chapter progresses by demonstrating the need for process parameter optimisation and the novelty of the current work. Finally, the development of a steel FSW process envelope is framed and a significant improvement in welding traverse speed which improves the economic potential of FSW on steel is identified.

Chapter 2 describes the material, steel grade DH36 and the welding details which are followed consistently in all testing programmes, also including extensive information on the employed welding machine and FSW tool for steel. A consistent nomenclature of the weld regions is outlined; the chapter then proceeds in discussing the metallographic examination, i.e. the first stage in the assessment of the friction stir welds in terms of quality. This is performed by microstructural characterisation of all welds produced in the process parameter development programme of Chapter 1 and by identification of any flaws which may impact on the quality of the welds.

Since the complex metallurgical system of steel FSW, as displayed in Chapter 2, is expected to influence the welds' mechanical properties, the next significant step in the quality assessment of the newly developed welding parameters is the mechanical property evaluation. Chapter 3 reports on the transverse tensile testing of the 25 friction stir welds along with post testing fracture surface analysis of a characteristic fast traverse speed weld, hardness measurements and Charpy impact pendulum testing with a focus on 6 representative welds.

The fatigue performance of welded components is of critical importance for the marine and shipbuilding industries. As a consequence, the behaviour of the welds in fatigue loading has been evaluated separately in Chapter 4. An original standard operating procedure document was drafted to deliver an innovative and comprehensive examination of the fatigue behaviour of steel FSW with a large number of tests for three stress ranges, also exploring the effect of varying welding

traverse speed on the fatigue performance. New welded plates were produced by adhering to the material and welding details stated in Chapter 2, and based on the process parameter development and quality assessment work described in Chapter 1 through 3. Chapter 4 elucidates the intricate sample manufacturing and preliminary testing methods performed in support of the fatigue testing programme, i.e. surface finish verification, possible weld misalignment, hardness distribution and transverse tensile testing. It then reports on the main experimental steps which involved microstructural characterisation of each weld (concentrating on metallurgical features which may impact on the fatigue life), extensive transverse fatigue testing, an inventive comparison to recommendations by the International Institute of Welding for corresponding fusion welds and on the additional fatigue testing of samples with the critical defect for fracture initiation removed. Finally, a thorough post testing fracture surface analysis is discussed and a relation of fatigue life to various process-related FSW flaws is defined.

For a comprehensive examination of the FSW process on low alloy steel, it is equally important to investigate the thermo-mechanical deformation behaviour of the material under consideration. Chapter 5 presents this novel research programme which has established the flow stress evolution of DH36 steel in conditions simulating actual FSW through hot axisymmetric compression testing. The study is broadened with the use of thermally treated only samples; subsequent microstructural examination of both series of samples and comparison to real friction stir welds is also performed, thus assessing the potential of this testing method to physically simulate the FSW-generated steel metallurgy.

Lastly, the section titled "Concluding remarks" encapsulates the important findings of the present research work and the key research challenges that have emerged. A brief commentary on possible routes for further research is put forward.

1. Friction stir welding of steel – An introduction

1.1. The friction stir welding process

Friction stir welding (FSW) is a solid state joining process patented by Thomas *et al.* [1.1], during which a rotating, cylindrical-shouldered, non-consumable tool with a profiled probe is plunged in the interface between two clamped pieces of butted material and traversed at a constant speed along the joint. The material is thermo-mechanically worked by the specially designed tool [1.2] and heated to a high enough temperature for plastic deformation to occur [1.3] but below the solidus [1.4]. The basic concept and the three stages of the process are shown in Figure 1.1. The tool shoulder produces the bulk of the thermal energy transferred into the weld zone [1.5] as it is advanced along the top of the work piece surface (Figure 1.2). Threads on the probe are intended to decrease the initial plunging force and enhance material stirring during welding [1.6]. Figure 1.3 presents the main parts of a typical state of the art FSW tool for steel. The plasticised material is pushed forwards in the advancing side of the weld by the rotating tool, and then backwards into the retreating side (Figure 1.1). This contrast produces a fundamental asymmetry in the process [1.7]; the two sides experience different thermal cycles and material flow conditions, therefore leading to different properties or even flaws [1.2,1.3].

Frictional heat is generated between the tool and the work pieces. This heat, along with that produced by the mechanical mixing process and the adiabatic shearing within the material causes the stirred materials to soften without melting. As the tool is moved forward, the profiled probe forces plasticised material to the rear (Figure 1.2) where forging forces by the shoulder assist in the consolidation of the weld [1.8,1.9]. FSW is a complex process incorporating mechanical and thermal processing of the material, considerable solid state deformation and high levels of flow stress [1.10]; as no melting of the material takes place, it is a thermo-mechanical deformation process analogous to extrusion and forging [1.3,1.11,1.12] rather than casting which more closely resembles the conditions observed during conventional fusion welding.
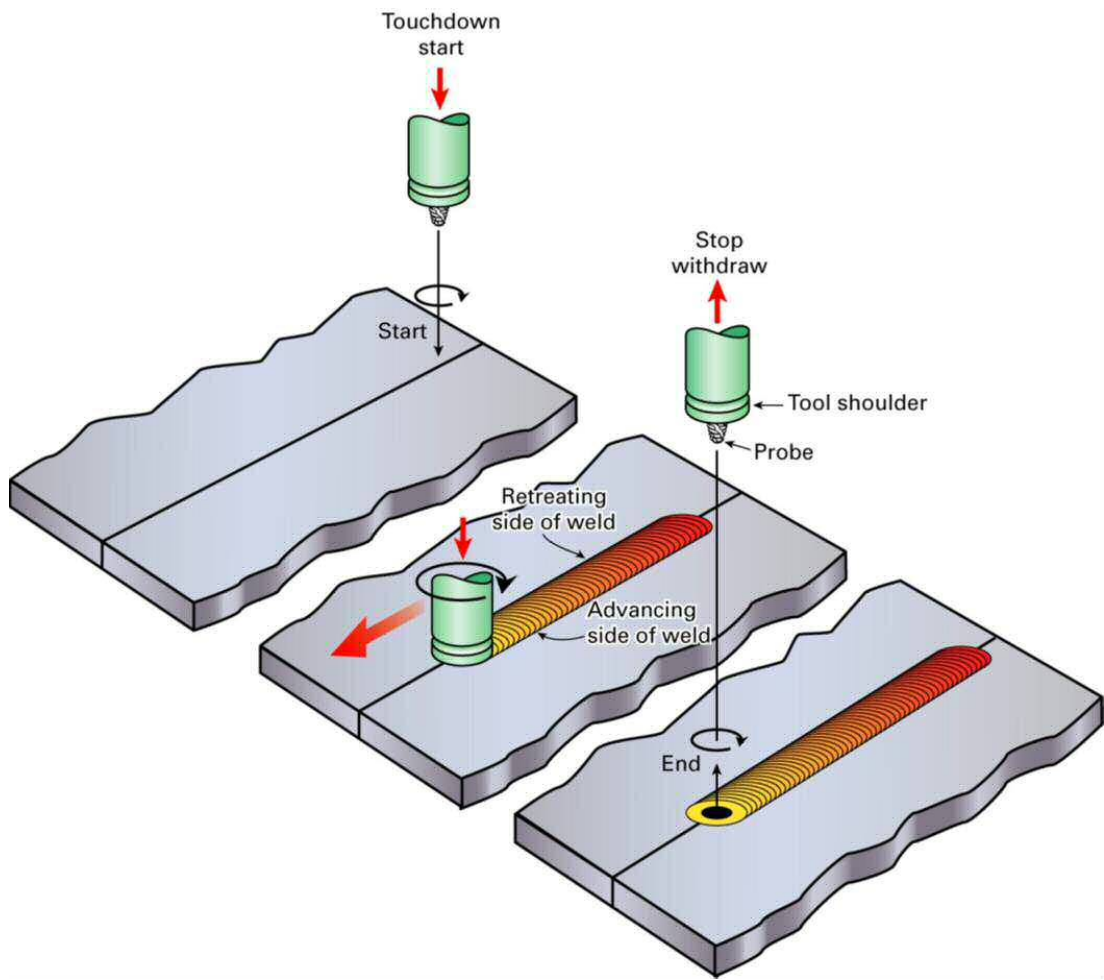
Figure 1.1. The basic concept of FSW [1.7]
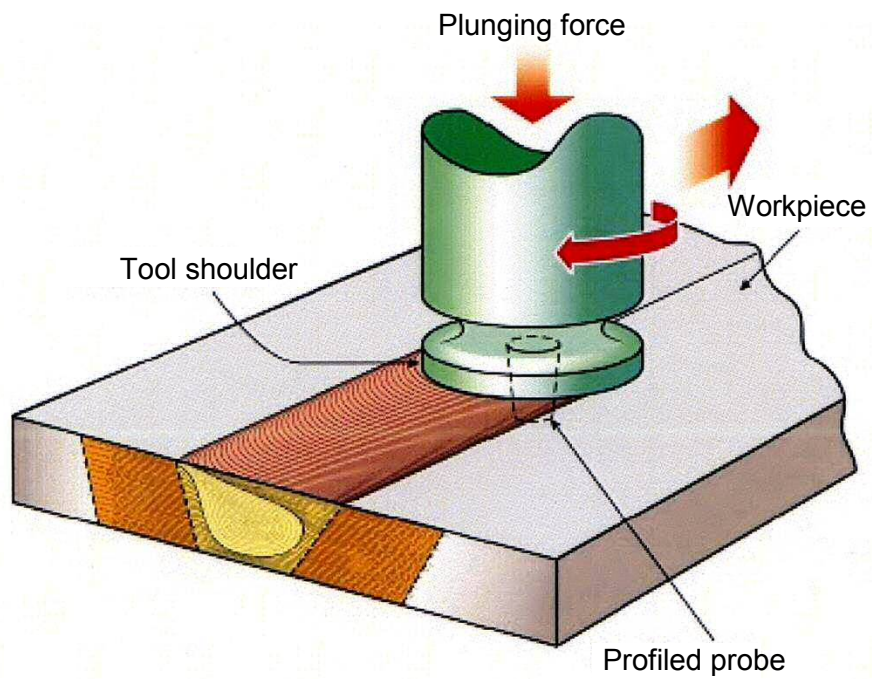
Figure 1.2. Schematic of FSW (adapted from [1.13])
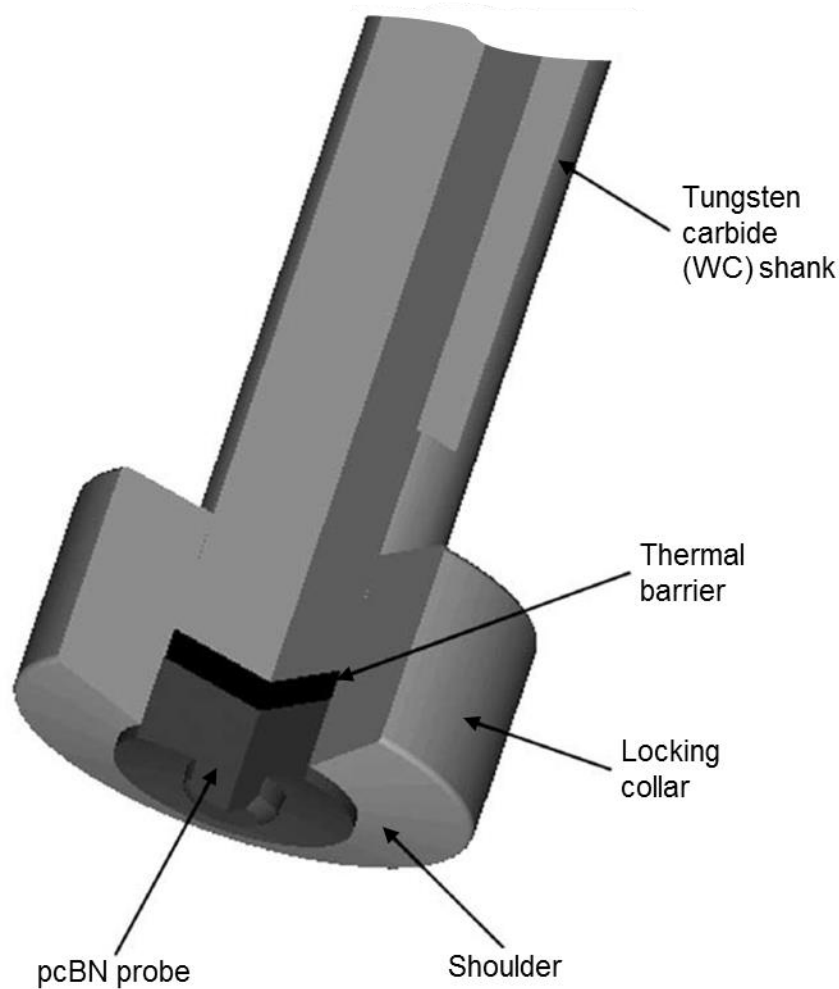
Figure 1.3. Cross section of a typical FSW tool for steel (adapted from [1.14])

FSW is currently being extensively employed in aluminium joining applications [1.7] but there is significant interest by many industrial sectors in transferring the process and its advantages to steel [1.2,1.15]. It has been proposed that the transportation sector, e.g. in automotive [1.16] and rail applications, marine [1.17], shipbuilding [1.6,1.18], and oil and gas industry [1.19,1.20] could make use of technical and potentially financial benefits by implementing steel FSW in their operations. Moreover, research has compared the process to submerged arc welding (SAW) of steel grade DH36 in the context of shipbuilding operations and has reached highly positive conclusions on its technical viability [1.21,1.22]. Previous publications have demonstrated the feasibility of FSW on steel [1.2,1.23], while others report that there are several positive effects on the weld properties such as considerable grain refinement [1.15], overmatching of the parent metal [1.23], minimised distortion [1.18,1.21], and potential for welding speeds which can be technically competitive to fusion welding methods [1.24].

The grain refinement that is consistently observed in the weld zone and particularly in the thermo-mechanically affected zone is caused by severe plastic deformation in high temperatures during welding [1.25], commonly resulting in dynamic recrystallisation of the parent material [1.14,1.26-1.28]. Through the Hall-Petch relationship, the refined microstructure is directly responsible for an increase in strength and hardness of the friction stir welds [1.29,1.30]. In contrast to conventional fusion welding processes, the temperature of the welded steel is restricted in the solid phase. By avoiding the fusion and subsequent solidification of the metal, FSW can deliver welds free of typical arc welding defects like porosity, solidification cracking and embrittlement [1.14,1.31,1.32]. Additionally, the FSW process furnishes a number of technical and economic benefits:

- The substantially decreased distortion measured on welded plates translates into reduced re-work of the welded components, which can be a major cost in ship production [1.33,1.34].

- Minimal prior preparation of the plate surfaces and edges to be welded is required [1.2]; for instance, no grinding or brushing is generally necessary [1.35].

- Since melting temperatures are not reached, steel can be friction stir welded in any position [1.7,1.35], i.e. horizontal, vertical, inverted and even on the full circumference of pipes [1.36]; underwater FSW of structural steel has been successfully executed by Baillie *et al.* [1.17].

- The use of a non-consumable tool without the addition of filler material contributes to negligible chemical segregation of the weldment [1.3,1.21].

- Reduced health and safety and environmental risks as it produces no fumes, glare, sparks or noticeable spatter [1.15,1.35].

The feasibility of FSW on numerous steel grades has been established, for example on AISI 1018 mild steel [1.15], AISI 1080 high carbon steel [1.37], DH36 structural steel [1.21], high strength low alloy steel (HSLA-65) [1.38], API X80, L80 [1.39] and X100 grade high strength pipeline steels [1.20], and SAF 2507 super duplex stainless steel [1.14] to name but a few; there is no evidence yet that the process is unsuitable for welding a specific grade. In fact, studies demonstrate that FSW is capable of joining metals that are otherwise considered of low weldability or practically non-weldable by established fusion joining methods, such as particular

aluminium [1.40,1.41] and titanium alloys [1.42], or oxide dispersion strengthened (ODS) steels [1.43] where fusion welding results in decreased strength due to oxide particle accumulation towards the weld top surface [1.28,1.44].

In the case of high carbon steels, a study assesses the effectiveness of FSW on AISI 1080 (0.85 wt.% carbon) [1.37]. These steels exhibit appealing mechanical properties like high strength and wear resistance but their use as structural materials is restricted since they present low weldability in fusion welding, a consequence of the high carbon content. Therefore, welding of high carbon steels demonstrates significant challenges and is the subject of much research, mainly with respect to complex heat treating cycles in order to inhibit the formation of brittle phases. The study [1.37] concludes that welding of high carbon steels can be successfully attained by FSW; the process delivers joints with a martensite-free, homogeneous microstructure provided that suitable optimisation of the welding parameters is undertaken [1.37].

Moreover, FSW often presents a route for joining materials with desirable properties which would be lost if welded by fusion welding techniques, primarily by overcoming the harmful effects of melting and solidification on the properties of the parent material. One publication [1.45] argues that fusion welding of AISI 409M grade ferritic stainless steel has a detrimental effect on the beneficial properties of the wrought alloy; coarse grains form in the weld and heat affected zone, hence ductility, toughness and corrosion behaviour are seen to deteriorate. Such grain coarsening and the resultant deterioration in mechanical properties is observed even though this grade is specifically manufactured with very low carbon content (<0.03 wt.%) to promote its weldability compared to standard ferritic stainless steels. This type of stainless steel has seen limited industrial use due to the above complication in fusion welding, but the researchers find that FSW produces high quality welds of enhanced mechanical properties through the highly refined microstructure that is formed [1.45].

Sato *et al.* [1.14] discuss that duplex stainless steels are used in many industrial applications because of their satisfactory stress corrosion cracking resistance that derives from a balanced ratio of ferrite and austenite phases. Even though these steels are of acceptable weldability, fusion welding tends to break up the base material phase ratio by producing a grain coarsening effect on the dramatically increased ferritic phase, with intergranular and intragranular austenite. This results

in deterioration of the weld zone's fracture toughness and corrosion behaviour, thus creating the need for detailed monitoring and adjustment of diverse welding parameters. To mitigate these issues and the corresponding complexity related to fusion welding, the study assesses the potential of FSW; the process is seen to produce high quality joints, maintain this desirable ratio in the weld zone and refine its microstructure, hence developing welds of high strength and hardness [1.14].

FSW is discussed as the obvious solution to the challenges related to welding ultrafine grained alloys (average grain size below 1 µm) due to the lower peak temperature compared to fusion welding methods that is reached during the solid state joining process [1.46]. These materials are particularly appealing to many industrial sectors, e.g. aerospace, transportation and biomedical, thus the need for identifying suitable welding techniques. Nonetheless, conventional fusion welding of ultrafine grained materials is not feasible because it leads to significant grain coarsening after melting and solidification of the original favourable microstructure [1.46]. Elsewhere [1.39], it is concluded that FSW diminishes the grain coarsening effect in arc welded X80 grade steel, which is often observed towards the boundaries of the thermo-mechanically affected zone, hence the consequent decrease in hardness [1.39].

Joining of dissimilar materials is an important requirement for many industrial applications, in an attempt to benefit from the favourable properties of each parent material and reduce weight or production costs [1.26]. Significant problems generally arise from the different thermal and mechanical properties of the dissimilar materials to be welded. In steel to aluminium joints for instance, fusion welding is known to develop brittle intermetallic constituents which are highly detrimental to the weld quality [1.47]. It has been demonstrated that FSW is capable of welding diverse materials together, from different grades of aluminium or steel to greatly dissimilar materials, even ferrous to non-ferrous alloys [1.47], and the research on this subject is expanding rapidly [1.48]. Figure 1.4 provides an indicative macrograph of such a dissimilar joint between stainless steel (on the left side) and low alloy steel (etched).
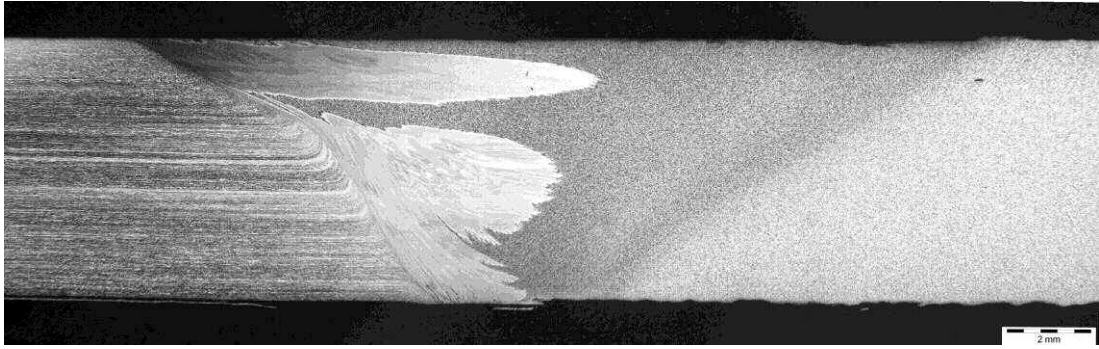
Figure 1.4. Macrograph of stainless steel to low alloy steel (right side, etched) dissimilar FSW (Courtesy of TWI Technology Centre)

Researchers investigate the FSW of 304 stainless steel to st37 structural steel [1.30]; dissimilar welding of these grades of steel is essential to the power and oil and gas industries among others. In these applications, stainless steel parts often function in high temperature environments whereas carbon steel ones are placed in less severe operating conditions. Fusion welding of such dissimilar steel parts is seen to produce a series of defects; development of brittle phases, hydrogen embrittlement or solidification cracking can be detrimental to their useful service life [1.30]. It is argued [1.30] that since separate studies have demonstrated the capability of the FSW process in dissimilar joints of high melting temperature metals, then it is worth investigating if FSW of stainless steel to structural steel will be equally successful in delivering high quality welds. Indeed, the study observed friction stir butt welds of st37 to 304 with a complex (but free of the above mentioned typical arc welding defects) microstructure which evolved through the intermixing of the two steels [1.30]. Additionally, tensile testing determined that the welds' tensile properties are improved compared to the structural steel parent plate.

FSW is proposed by Ishida *et al.* [1.49] as a suitable alternative to conventional joining methods for welding titanium to steel for the chemical industry. The main beneficial factor is the lower temperature reached within a friction stir weld than in other joining methods, which leads to considerable decrease in the formation of detrimental intermetallic phases. This work [1.49] examines the impact of the employed weld parameters upon the weld microstructure and mechanical properties of friction stir lap welds through a small scale optimisation study. The process is seen to successfully join the two metals; the tensile shear samples fractured in the parent material (Ti-side) irrespective of the parameter set used to produce the weld, and the optimum set of parameters is determined by the results of peel tests [1.49].

Marginally offsetting the tool into one of the two dissimilar materials to be butt welded instead of positioning it on the joint line is a promising technique to improve the weld quality and its visual appearance [1.50]; this is associated with the diverse thermo-mechanical properties of the two materials and specifically the different high temperature flow properties. The lateral shift of the FSW tool needs to be towards the softer metal that should be placed at the retreating side [1.51]. This metal will fill more readily the space left by the forward moving probe due to its enhanced flow behaviour [1.50]. Still, sufficient knowledge of the flow behaviour of the two materials is necessary to apply this method and avoid the formation of wormhole defects on the advancing side owing to incomplete plasticisation [1.30]. Joining of dissimilar materials through FSW remains a complex research subject where among other issues, the bimetallic (galvanic) corrosion performance of the welds requires more detailed investigation.

On the subject of process commercialisation, FSW was originally introduced for welding low melting point materials such as aluminium or magnesium alloys and has now reached a sufficient level of maturity and industrial acceptance as these materials are concerned [1.52]. However, the uptake of the process on steel for commercial applications is practically non-existent. Reynolds *et al.* [1.53] explain that FSW of aluminium has flourished commercially because it is a considerably improved welding process for most grades, delivering high quality welds, and joining alloys of poor weldability, hence the powerful incentives for its industrial use. In contrast, steels do not typically suffer from weldability issues, therefore slightly reducing the stimulus for introduction of new processes other than the established fusion welding techniques [1.53]. Most importantly, the process on steel is more complicated than on aluminium due to the extreme conditions experienced by the FSW tool for steel and the significantly higher flow stress of steel alloys at elevated temperatures coupled with their reduced thermal diffusion coefficient [1.53].

A major obstacle is the current tool technology, and more specifically the high requirements on the tool material [1.54]. The material from which tools for high melting point metals are manufactured needs to exhibit sufficient fracture toughness, wear resistance and chemical inertness with respect to the metal to be welded, all at high temperatures [1.15,1.54]. Adequate processing capability of the tool material is also required in order to develop distinct features and an intricate geometry on the tool shoulder and probe for enhanced heat generation and material mixing.

Research on possible FSW tool for steel materials has evaluated the use of refractory metals (e.g. Tungsten-based) and ceramics; the former though tend to exhibit poor wear resistance [1.15,1.32], whilst the latter suffer from erratic fracture behaviour and difficulties in fabricating complex features [1.55]. More recent developments in tool technology have yielded hybrid tools consisting of polycrystalline boron nitride (pcBN) particles in a refractory metal (WRe) binder, seeking to combine the favourable properties of the two materials. Still, pcBN tools are presently expensive and demonstrate cracking and reduced (with respect to WRe-based tools) yet considerable wear (Figure 1.5), thus are known to produce overall weld lengths that are too short (max. 40 m per tool) to be economically viable for any industry which may be assessing the introduction of the process [1.34].

In addition, the process on steel is sensitive to the tool material; researchers observe that tools produced from distinct materials are seen to develop different peak temperatures, consequently disparate microstructures are formed for a particular grade of steel [1.32]. Clearly, this reduces the repeatability and consistency of the process.

The FSW tool is required to generate appreciable thermal energy and substantial mechanical stirring while operating in extreme conditions (Figure 1.6). Combined with the above outlined restrictions in tool design and material, this presently allows for only two steel joint configurations to be welded, i.e. butt and lap joints. Still, a fundamental requirement for many industries such as shipbuilding is the capability to produce fillet welds (T-joints).

Publications note the current limitations of steel FSW, as outlined above, and conclude that new developments in tool design and material, and the identification of relevant niche applications which will decisively benefit from the introduction of FSW are the two critical factors for wider industrial uptake of the process on steel [1.15,1.32,1.53,1.56]. For the time being, the process remains overly immature and expensive for use outside experimental laboratories; it is far from becoming economically competitive to fusion welding methods, predominantly because of the issues associated with the FSW tool for steel [1.34], apart from very few cases that are insensitive to the high cost of the process when compared to the benefits involved, such as specific applications in the oil and gas industry [1.19].
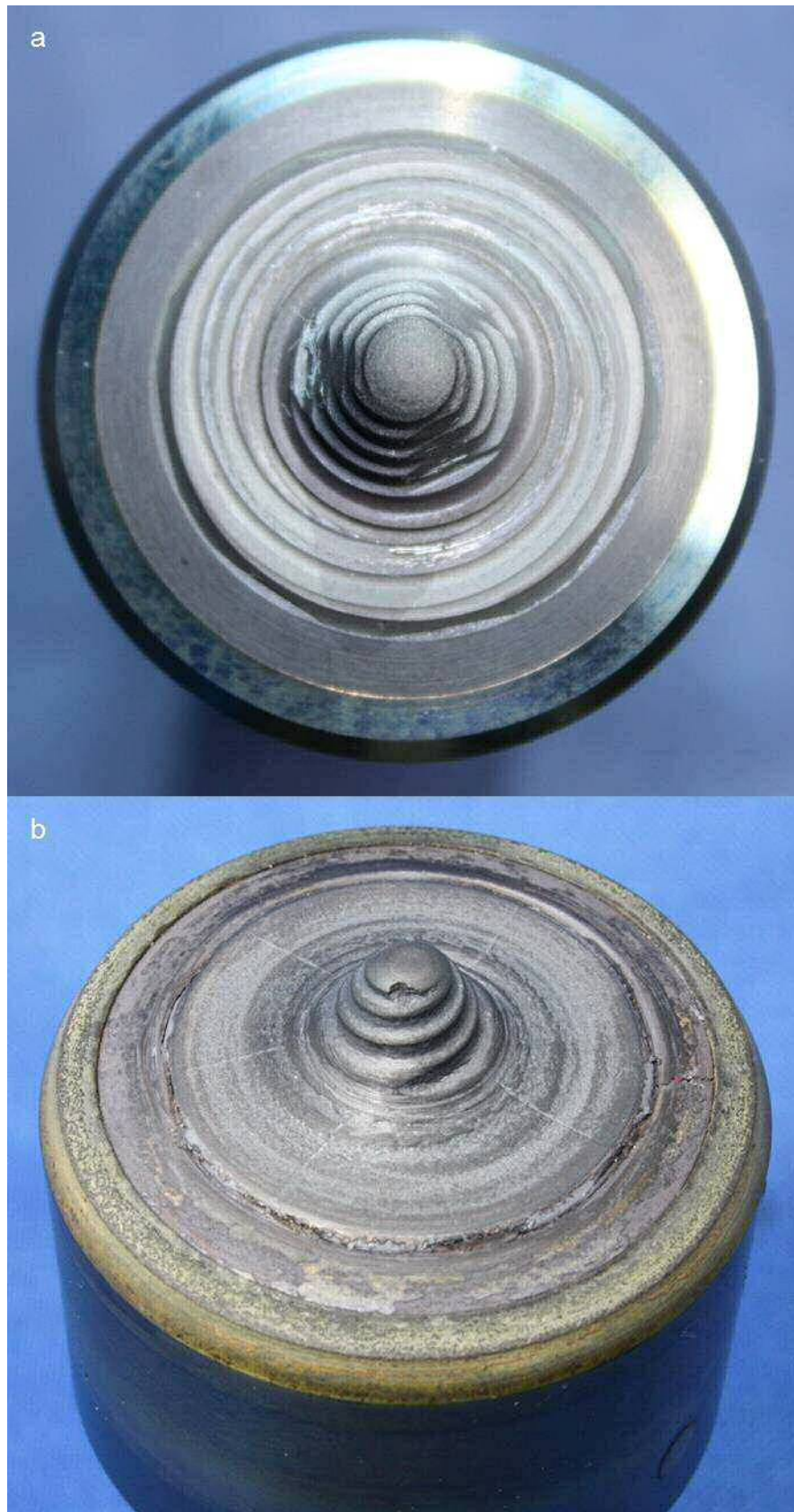
Figure 1.5. WRe-pcBN FSW tool for steel (a) brand new; (b) after welding approx. 20 m of DH36 steel [1.57]
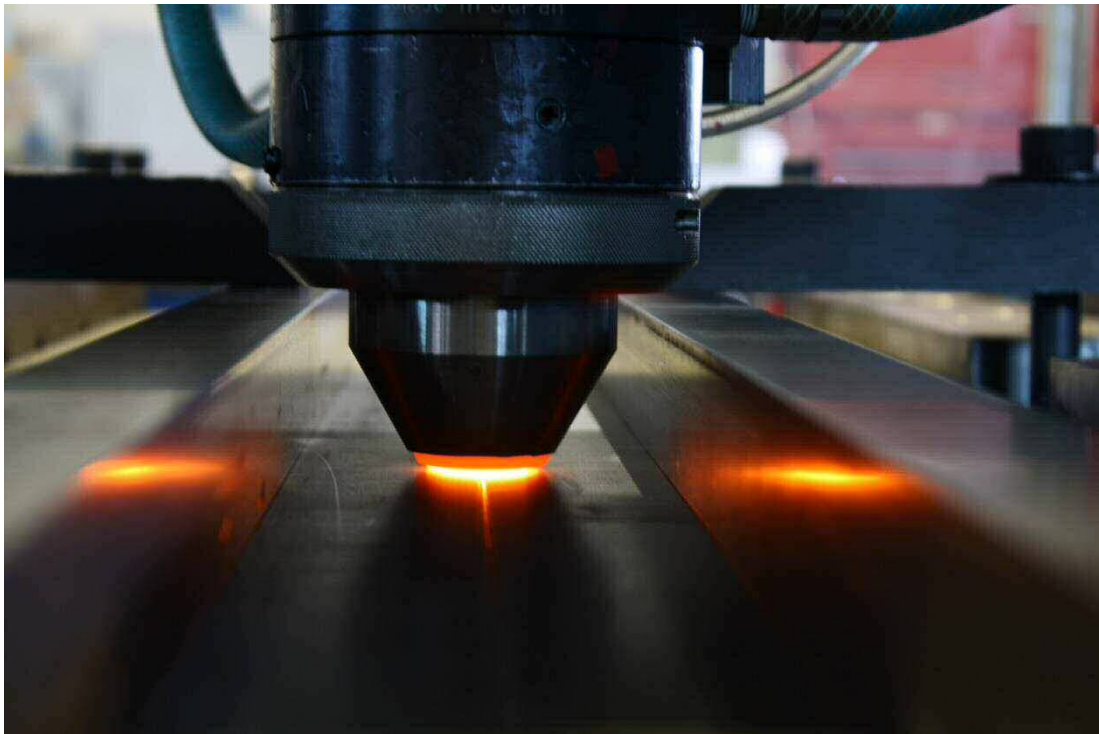
Figure 1.6. FSW tool for steel during operation (Courtesy of TWI Technology Centre)

The preceding discussion reveals a critical factor of fusion welding; re-solidification of the molten steel can develop entirely new and frequently undesirable microstructures, along with a range of defects. Moreover, corrective measures such as post-weld heat treatment or other complex processes are often required, aiming to essentially repair or restore some of the favourable properties of the deteriorated original microstructure. This harmful effect is generally eliminated with the use of FSW due to its solid state nature. Although still immature and with the tool issues currently unresolved, FSW of steel can deliver substantial merits when suitably optimised and if appropriately exploited in cost-insensitive niche applications which should drive developments forward [1.56].

As previously alluded to, earlier studies on steel FSW were primarily concerned with establishing the feasibility of the process on diverse steel grades. More recently, the relevant research is mostly involved in investigating the relationship between varying welding parameters and resultant weld properties. Fraser *et al.* [1.58] argue that many articles have been published which report on optimisation of the process in terms of specific mechanical properties such as tensile strength or fatigue performance for niche applications. However, optimal properties are not the primary requirement for many industrial applications, particularly for large scale manufacturing; the costs related to achieving properties above the minimum

acceptable are not justifiable in these applications. In contrast, FSW needs to be optimised with regard to high welding speed of defect-free and acceptable quality welds, within specifications or classification society rules in the case of shipbuilding and marine applications, rather than best possible mechanical properties for wider industrial introduction. This optimisation for high traverse speeds will be of interest to many industrial sectors where the highest possible welding speed is desirable in order to reduce production costs. Research studies have not been focusing enough on this aspect, which is closely associated with the technical and economic viability of the process [1.58].

Barnes *et al.* [1.32] discuss that the microstructural phases which evolve in steel friction stir welds could be predicted as analogous to the phases observed in fusion welds, solely as a result of comparable cooling rates which have been measured. In reality, more factors like the lower peak temperature and intense mechanical stirring play an important role on microstructural evolution during FSW. All these factors are governed by the applied process parameters, i.e. tool type, and rotational and traverse speed; this relation remains a weakly understood subject. Therefore, the need for methodical investigation of the link between varying welding parameters, resultant microstructure and mechanical properties of the welds becomes crucial in the development of steel FSW. Such research, in essence optimisation through experimental work, is necessary to advance the relevant technical knowledge on the attainable process parameters that deliver high quality low alloy steel friction stir welds [1.32]. Moreover, Ericsson & Sandstrom note that following optimisation, implementation of FSW can become a straightforward procedure delivering consistent results [1.59].

The current work is focusing on FSW of steel grade DH36, a low alloy steel utilised in the European shipbuilding industry among other sectors. For FSW of steel to become economically and technically viable for introduction in the shipbuilding industry, it should evolve into a process competitive with conventional fusion welding methods. In the shipbuilding sector, this requirement is typically encapsulated in high welding speeds (mm/min) which produce joints of acceptable quality, i.e. within classification society rules. Therefore, an optimisation study is a fundamental step towards this direction; that is, a study concerned with establishing the limits of the process (the process envelope) in terms of the two more significant parameters which can be directly controlled, tool traverse speed and tool rotational speed.

It will be discussed in more detail in Chapter 2 that there is significant grain refinement occurring during FSW of steel, from the parent material to the thermo-mechanically affected zone, primarily as a result of continuous dynamic recrystallization combined with the austenite to ferrite phase transformation in relatively high cooling rates and severe strains. As a result, more phases than the original ferrite / pearlite are commonly observed in the developed microstructure. Therefore, it is imperative that the process parameters are optimised for high welding speeds of acceptable quality welds, within the specifications of the application in focus, and in parallel, the weld quality is assessed by microstructural characterisation and mechanical property evaluation in order to improve the economic competitiveness of the process.

Few pertinent studies report on the effect of traverse speeds in the range of 200-300 mm/min on the developed microstructure and resultant mechanical properties of structural steels, much less on process optimisation at higher speeds. Nevertheless, their extent or thoroughness appears fairly restricted. Indicatively, Barnes *et al.* [1.32] assess the influence of varying process parameters on the FSW joints of a high strength low alloy steel. This work explores welding speeds in the range of 50-500 mm/min using a W-Re tool and 50-250 mm/min with a pcBN-based tool; however, the rotational speed is maintained constant for each range of speeds, 600 rpm and 400 rpm respectively. It is clarified elsewhere [1.58] that the ratio of traverse speed to rotational speed should fall within certain limits for quality welds to be achieved. As the rotational speed is not adjusted with respect to varying traverse speed, it generates high heat input, principally for the slower traverse speed welds [1.32]. Therefore, high temperatures above the upper transformation temperature (A_3) are reached during welding, and coupled with severe plastic deformation, result in high cooling rates. Thus, the thermo-mechanically affected zone being developed is a mixture of ferrite, bainite and martensite; the very high cooling rates promote martensite and bainite formation even in the inner heat affected zone [1.32]. Consequently, this otherwise comprehensive investigation is not a true evaluation of the manner in which welding parameters govern the weld microstructure in steel FSW. One more representative publication employs ten parameter sets, with a maximum traverse speed of 200 mm/min, in an optimisation study of the FSW of an advanced high strength steel (AHSS) [1.16]. Although the tensile shear test samples are seen to fracture in the heat affected zone, this research work does not seek to

enhance the tensile properties of this region through the evaluation of refined parameter sets.

There are diverse optimisation studies for FSW of aluminium alloys including modelling, statistical analysis or experimental work [1.60-1.64], but most seem rather small scale projects when compared to the present work, and therefore cannot be transferred into the FSW of steel. As an illustration, Kumar *et al.* [1.61] aim to optimise the FSW of two dissimilar aluminium alloys with respect to tensile properties and hardness of the weld by employing the Taguchi method. However, this approach leads to experimental examination of no more than nine sets of parameters; besides, there is no commentary on the microstructural evolution of the thermo-mechanically affected zone, hence this work's conclusions are limited [1.61]. In a similar investigation of dissimilar aluminium alloy friction stir welds relating to optimised strength, Ghosh *et al.* [1.64] assess the effect of merely four sets of parameters on the resultant microstructure and mechanical properties without discussing how these parameters were chosen.

In the present investigation and in contrast to previous process parameter development studies, 25 friction stir welds, the majority of which were produced with welding speeds rarely identified by other researchers, are thoroughly examined in order to determine a step change improvement to the current industrially accepted welding speeds. These are selected from a comprehensive and considerable spread of FSW DH36 butt joints in which slow, intermediate and fast welding speeds were trialled. This extensive work will assist in developing the fundamental knowledge on FSW of steel and is reported in this thesis.

1.2.   Development of process parameter envelope

The process parameter envelope for FSW of DH36 steel can be represented schematically by plotting the two more important welding parameters which can be directly controlled, tool rotational speed and traverse speed [1.11], as variables on the x and y axes of a graph (Figure 1.7). The development of the envelope begins with a set of parameters that are known to deliver acceptable quality welds on steel. It is then broadened outwards from these parameters, with varying rotational and traverse speeds, in order to establish the outer limits of the process envelope by producing and examining a series of welds. The envelope consists of the parameter

sets that produce welds of at least acceptable quality, and is divided in this case into three groups characterised by welding traverse speed. The shape of this envelope will vary with any further development and refinement of the process parameters. To generate the process envelope, extensive welding and considerable testing is required over a very large data set.
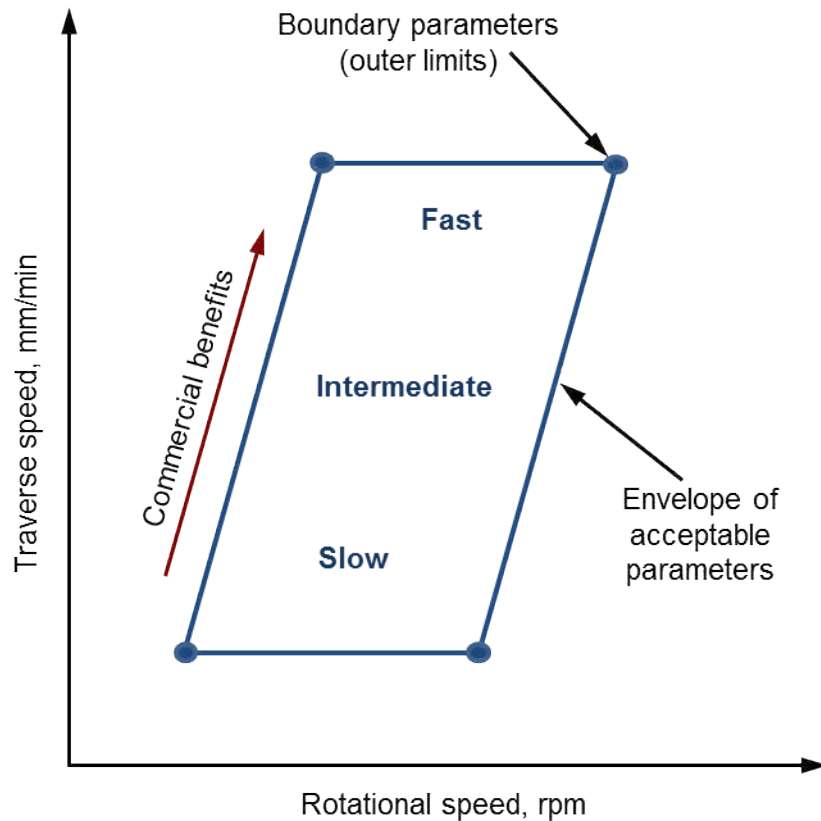
Figure 1.7. Schematic representation of the theoretical process parameter envelope

The process parameter envelope development in the present study commenced using the process parameters recommended by the FSW tool manufacturer. These are based upon a tool traverse speed of 100 mm/min and a tool rotational speed of 200 rpm. In simplistic terms, the tool rotational speed controls the frictional heat input to the weld zone which plasticises the steel whilst the tool traverse speed influences the weld cooling rate and thus has a significant effect on the evolving microstructure [1.16,1.32,1.65,1.66]. Other factors, for example the tool tilt, tool plunge depth, tool cooling, backing plate characteristics and clamping arrangement have a secondary but not insignificant effect upon the welding process.

The process parameters used cannot be considered in isolation from the tool itself. Whilst it is desirable to use process parameters that produce satisfactory welds in

terms of microstructure and mechanical properties, the current tool technology for FSW of steel is still relatively immature; on this account, attention must be paid to secure that the welding environment is not too aggressive that the tool's service life is shortened by the welding process. Therefore, a compromise is made between selecting parameters that deliver acceptable weld properties and parameters that extend the life of the tool and thereby improve the economic viability of the FSW process on steel. In the present study, a number of welds were initially produced using the previously stated process parameters to provide a baseline data set of the generated forces, torques and heat inputs resulting from these parameters. These data framed the basis for expanding the process envelope to higher traverse speeds.

It is desirable that FSW is competitive to conventional fusion welding techniques in terms of welding speed; hence the process parameters were extended to explore the potential to employ higher welding traverse speeds. Since the tool is to be traversed through the steel being welded faster, then it is necessary to establish that the steel ahead of the tool is sufficiently plasticised. This will ensure that the FSW tool experiences stable forces below the point where tool failure may occur and the steel continues to flow around the probe, hence can be consolidated behind it effectively.

To weld at higher traverse speeds, the tool rotational speed needs to be increased. Increasing the tool rotational speed raises the heat input towards the weld, but this effect does not occur in a linear manner; above a certain point, the friction couple between the tool and steel changes and the heat input into the weld can decrease, as a result of the complex process parameter interdependence [1.7,1.11,1.65]. Parameter selection is therefore an intricate process with many interdependent variables, many of which are currently poorly understood.

Since a baseline understanding of the welding process was achieved, the primary process parameters of tool rotational and traverse speed were expanded. The objective was to increase the traverse speed from 100 mm/min to approx. 350 mm/min, the point at which FSW would become competitive to fusion welding processes in terms of production speed of acceptable quality [1.57]. Evidently, further increases in welding speed beyond 350 mm/min are desirable to improve the competitiveness of FSW, thus faster traverse speeds were also trialled. Table 1.1 shows the welding speeds investigated in this initial process parameter

Table 1.1. List of welding parameters examined

Reference number	Rotational speed (rpm)	Traverse speed (mm/min)	Heat input (kJ/mm)	Traverse speed group
W01	200	100	3.44	
W02	200	110	3.07	
W03	200	120	2.68	
W04	200	130	2.61	Slow
W05	200	143	2.31	
W06	200	156	2.04	
W07	400	200	3.07	
W08	300	250	1.92	
W09	400	250	2.29	
W10	400	275	2.13	
W11	400	300	1.82	
W12	400	325	1.77	
W13	450	350	1.97	Intermediate
W14	500	350	2.37	
W15	400	375	1.45	
W16	450	400	1.61	
W17	500	400	2.02	
W18	550	400	1.91	
W19	575	450	1.92	
W20	700	450	1.78	
W21	600	500	1.77	
W22	650	500	2.12	Fast
W23	575	500	1.35	
W24	700	500	2.23	
W25	675	500	2.01	

development work. The heat input calculations are based on the equation presented by McPherson *et al.* [1.21] such that: $H = \varepsilon 2\pi R \tau / 1000V$, where ε dimensionless factor of FSW process efficiency, R rotational speed in rpm, τ average steady state torque on the tool in Nm, and V traverse speed in mm/min. In practice, the contact conditions, thus friction coefficient, between tool and material may vary during welding [1.11] for a number of reasons like imbalance in plunging force [1.7,1.65], or variations in plate thickness. Hence, the actual heat input may also slightly differ from the calculated value.

There are other methods which have additionally been proposed to evaluate the heat input apart from the above outlined. Indicatively, Schmidt *et al.* [1.66] point out that thermal energy (Q) during FSW is predominantly generated by the tool shoulder and this energy is proportional to the tool rotational speed (ω). Following from this, a separate publication [1.67] argues that since the tool advances at a constant traverse speed (s), the specific heat input to the weld zone can be described as Q/s. Thus, it is proposed that the ratio of rotational to traverse speed (ω/s) is a valid indicator of the heat input that is transferred to the weld per unit length [1.67].

Through this process parameter development programme, the state of the art has been increased from the conventionally adopted welding traverse speed of 100 mm/min to more commercially attractive speeds in the region of 400–500 mm/min. However, welding is known to substantially affect the microstructure and mechanical properties of components and structures [1.68]. Although a step change in the welding speed has been identified, the purpose of the research work presented in the following chapters is to assess the impact of this increase on the microstructural evolution and mechanical properties of each friction stir weld.

1.3. Preliminary observations

FSW is discussed as an advanced and versatile solid state joining method, delivering an array of advantages in welding of steel and other high temperature metals, including the capability to join metals of low weldability and the dissimilar welding of alloys of very different families. The process is also proposed as the appropriate welding technique for overcoming issues related to conventional fusion welding, mainly the harmful effects on the microstructure and properties of the parent material as a result of melting and solidification.

To deliver these beneficial effects however, the process needs to be suitably optimised. Envisaging that the complexities surrounding the FSW tool for steel will eventually be solved, this optimisation should be undertaken in terms of high speed welding of acceptable quality joints, within application-specific requirements, in order to achieve wider industrial acceptance.

A comprehensive process parameter development programme consisting of 25 friction stir welds of 2000 x 200 x 6 mm DH36 steel plates has been implemented with the intention of establishing a step change improvement to the current industrially accepted welding speeds for this process. An extensive data set has been generated to account for a wide range of typical and atypical process parameters. The welding traverse speed on DH36 steel has been increased to a great extent compared to the conventionally recommended speed of 100 mm/min. This represents considerable potential economic advantages in terms of the competitiveness of FSW to conventional fusion welding processes.

Still, the quality of the produced welds needs to be assessed through comprehensive microstructural examination and mechanical testing; this investigation is required to develop a preliminary DH36 steel FSW parameter envelope, provide an understanding of the relation between welding parameters and their effect on weld microstructures and mechanical properties, and confirm any enhancements to the techno-economic competitiveness of the process. These essential testing programmes are reported in the following chapters.

1.4. References

[1.1]   Thomas WM, Nicholas ED, Needham JC, Murch MG, Temple-Smith P, Dawes CJ. Friction welding. PCT/GB92/02203, 1991.

[1.2]   Thomas WM, Threadgill PL, Nicholas ED. Feasibility of friction stir welding steel. Sci Technol Weld Join 1999;4:365–72.

[1.3]   Nandan R, DebRoy T, Bhadeshia HKDH. Recent advances in friction-stir welding - Process, weldment structure and properties. Prog Mater Sci 2008;53:980–1023.

[1.4]   Fonda RW, Lambrakos SG. Analysis of friction stir welds using an inverse problem approach. Sci Technol Weld Join 2002;7:177–81.

[1.5] Peel M, Steuwer A, Preuss M, Withers PJ. Microstructure, mechanical properties and residual stresses as a function of welding speed in aluminium AA5083 friction stir welds. Acta Mater 2003;51:4791–801.

[1.6] Azevedo J, Infante V, Quintino L, dos Santos J. Fatigue Behaviour of Friction Stir Welded Steel Joints. Adv Mater Res 2014;891-892:1488–93.

[1.7] Threadgill PL, Leonard AJ, Shercliff HR, Withers PJ. Friction stir welding of aluminium alloys. Int Mater Rev 2009;54:49–93.

[1.8] Scialpi A, De Filippis LAC, Cavaliere P. Influence of shoulder geometry on microstructure and mechanical properties of friction stir welded 6082 aluminium alloy. Mater Des 2007;28:1124–9.

[1.9] Marzoli LM, Strombeck A v., Dos Santos JF, Gambaro C, Volpone LM. Friction stir welding of an AA6061/Al2O3/20p reinforced alloy. Compos Sci Technol 2006;66:363–71.

[1.10] He X, Gu F, Ball A. A review of numerical analysis of friction stir welding. Prog Mater Sci 2014;65:1–66.

[1.11] Mishra RS, Ma ZY. Friction stir welding and processing. Mater Sci Eng R Reports 2005;50:1–78.

[1.12] Reynolds AP, Lockwood WD, Seidel TU. Processing-Property Correlation in Friction Stir Welds. Mater Sci Forum 2000;331-337:1719–24.

[1.13] Elbanhawy A, Chevallier E, Domin K. Numerical investigations of friction stir welding of high temperature materials. NAFEMS World Congr. 2013, Salzburg, Austria: 2013.

[1.14] Sato YS, Nelson TW, Sterling CJ, Steel RJ, Pettersson CO. Microstructure and mechanical properties of friction stir welded SAF 2507 super duplex stainless steel. Mater Sci Eng A 2005;397:376–84.

[1.15] Lienert T, Stellwag W, Grimmett B, Warke R. Friction stir welding studies on mild steel. Weld J Res Suppl 2003:1–9.

[1.16] Ghosh M, Kumar K, Mishra RS. Process Optimization for Friction-Stir-Welded Martensitic Steel. Metall Mater Trans A 2012;43:1966–75.

[1.17] Baillie P, Campbell S, Galloway A, Cater S, McPherson N. A Comparison of Double Sided Friction Stir Welding in Air and Underwater for 6mm S275

Steel Plate. Int J Chem Nucl Metall Mater Eng 2014;8:651–5.

[1.18]   Cater S, Martin J, Galloway A, McPherson N. Comparison between friction stir and submerged arc welding applied to joining DH36 and E36 shipbuilding steel. In: Mishra R, Mahoney MW, Sato Y, Hovanski Y, Verma R, editors. Frict. Stir Weld. Process. VII, Hoboken, NJ: Wiley; 2013, p. 49–58.

[1.19]   Kumar A, Fairchild DP, Macia ML, Anderson TD, Jin HW, Ayer R, et al. Evaluation of Economic Incentives and Weld Properties for Welding Steel Pipelines Using Friction Stir Welding. Proc. Twenty-first Int. Offshore Polar Eng. Conf., vol. 8, Maui, Hawaii: The International Society of Offshore and Polar Engineers (ISOPE); 2011, p. 460–7.

[1.20]   Cho H-H, Kang SH, Kim S-H, Oh KH, Kim HJ, Chang W-S, et al. Microstructural evolution in friction stir welding of high-strength linepipe steel. Mater Des 2012;34:258–67.

[1.21]   McPherson N, Galloway A, Cater S, Hambling S. Friction stir welding of thin DH36 steel plate. Sci Technol Weld Join 2013;18:441–50.

[1.22]   McPherson N, Galloway A, Wood J, Cater SR. A comparison between single sided friction stir welded and submerged arc welded DH36 steel thin plate. 9th Int. Conf. Trends Weld. Res., 2012.

[1.23]   Reynolds AP, Tang W, Posada M, Deloach J. Friction stir welding of DH36 steel. Sci Technol Weld Join 2003;8:455–60.

[1.24]   Toumpis A, Galloway A, Cater S, McPherson N. Development of a process envelope for friction stir welding of DH36 steel – A step change. Mater Des 2014;62:64–75.

[1.25]   Uzun H, Dalle Donne C, Argagnotto A, Ghidini T, Gambaro C. Friction stir welding of dissimilar Al 6013-T4 To X5CrNi18-10 stainless steel. Mater Des 2005;26:41–6.

[1.26]   Satyanarayana VV, Reddy GM, Mohandas T. Dissimilar metal friction welding of austenitic-ferritic stainless steels. J Mater Process Technol 2005;160:128–37.

[1.27]   Han J, Li H, Zhu Z, Barbaro F, Jiang L, Xu H, et al. Microstructure and mechanical properties of friction stir welded 18Cr–2Mo ferritic stainless steel thick plate. Mater Des 2014;63:238–46.

[1.28] Han W, Ukai S, Wan F, Sato Y, Leng B, Numata H, et al. Hardness and Micro-Texture in Friction Stir Welds of a Nanostructured Oxide Dispersion Strengthened Ferritic Steel. Mater Trans 2012;53:390–4.

[1.29] Hansen N. Hall–Petch relation and boundary strengthening. Scr Mater 2004;51:801–6.

[1.30] Jafarzadegan M, Feng AH, Abdollah-zadeh A, Saeid T, Shen J, Assadi H. Microstructural characterization in dissimilar friction stir welding between 304 stainless steel and st37 steel. Mater Charact 2012;74:28–41.

[1.31] Gibson BT, Lammlein DH, Prater TJ, Longhurst WR, Cox CD, Ballun MC, et al. Friction stir welding: Process, automation, and control. J Manuf Process 2014;16:56–73.

[1.32] Barnes SJ, Bhatti AR, Steuwer A, Johnson R, Altenkirch J, Withers PJ. Friction Stir Welding in HSLA-65 Steel: Part I. Influence of Weld Speed and Tool Material on Microstructural Development. Metall Mater Trans A 2012;43:2342–55.

[1.33] McPherson N. Thin Plate Distortion - The Ongoing Problem in Shipbuilding. J Sh Prod 2007;23:94–117.

[1.34] Toumpis A, Galloway A, Cater S, Molter L. A techno-economic evaluation of friction stir welding of DH36 steel. 10th Int. Frict. Stir Weld. Symp., Beijing, China: 2014.

[1.35] Amini A, Asadi P, Zolghadr P. Friction stir welding applications in industry. Adv. Frict. Weld. Process., Cambridge: Woodhead Publishing; 2014, p. 671–722.

[1.36] Fairchild D, Kumar A, Ford S, Nissley N, Ayer R, Jin H, et al. Research Concerning the Friction Stir Welding of Linepipe Steels. Trends Weld. Res. Proc. 8th Int. Conf., Pine Mountain, Georgia: ASM International; 2009, p. 371–80.

[1.37] Chung YD, Fujii H, Ueji R, Tsuji N. Friction stir welding of high carbon steel with excellent toughness and ductility. Scr Mater 2010;63:223–6.

[1.38] Konkol P, Mathers J, Johnson R, Pickens J. Friction stir welding of HSLA-65 steel for shipbuilding. J Sh Prod 2003;19:159–64.

[1.39] Ozekcin A, Jin HW, Koo JY, Bangaru N V, Ayer R, Vaughn G, et al. A microstructural study of friction stir welded joints of carbon steels. Int J Offshore Polar Eng 2004;14:284–8.

[1.40] Williams JC, Starke EA. Progress in structural materials for aerospace systems. Acta Mater 2003;51:5775–99.

[1.41] Pedemonte M, Gambaro C, Lertora E, Mandolfino C. Fatigue assessment of AA 8090 friction stir butt welds after surface finishing treatment. Aerosp Sci Technol 2013;27:188–92.

[1.42] Buffa G, Ducato A, Fratini L. FEM based prediction of phase transformations during Friction Stir Welding of Ti6Al4V titanium alloy. Mater Sci Eng A 2013;581:56–65.

[1.43] Baker BW, Brewer LN. Joining of Oxide Dispersion Strengthened Steels for Advanced Reactors. Jom 2014;66:2442–57.

[1.44] Chen CL, Tatlock GJ, Jones AR. Microstructural evolution in friction stir welding of nanostructured ODS alloys. J Alloys Compd 2010;504:S460–6.

[1.45] Lakshminarayanan AK, Balasubramanian V. Assessment of fatigue life and crack growth resistance of friction stir welded AISI 409M ferritic stainless steel joints. Mater Sci Eng A 2012;539:143–53.

[1.46] Sun YF, Fujii H, Tsuji N. Microstructure and mechanical properties of spot friction stir welded ultrafine grained 1050 Al and conventional grained 6061-T6 Al alloys. Mater Sci Eng A 2013;585:17–24.

[1.47] Watanabe T, Takayama H, Yanagisawa A. Joining of aluminum alloy to steel by friction stir welding. J Mater Process Technol 2006;178:342–9.

[1.48] Bhadeshia HKDH. Editorial. Sci Technol Weld Join 2010;15:646–7.

[1.49] Ishida K, Gao Y, Nagatsuka K, Takahashi M, Nakata K. Microstructures and mechanical properties of friction stir welded lap joints of commercially pure titanium and 304 stainless steel. J Alloys Compd 2015;630:172–7.

[1.50] Beygi R, Kazeminezhad M, Kokabi A. Microstructural evolution and fracture behavior of friction-stir-welded Al-Cu laminated composites. Metall Mater Trans A 2014;45:361–70.

[1.51] Al-Roubaiy AO, Nabat SM, Batako ADL. Experimental and theoretical analysis of friction stir welding of Al–Cu joints. Int J Adv Manuf Technol 2014;71:1631–42.

[1.52] DebRoy T, Bhadeshia HKDH. Friction stir welding of dissimilar alloys – a perspective. Sci Technol Weld Join 2010;15:266–70.

[1.53] Reynolds A., Tang W, Gnaupel-Herold T, Prask H. Structure, properties, and residual stress of 304L stainless steel friction stir welds. Scr Mater 2003;48:1289–94.

[1.54] Wang J, Su J, Mishra RS, Xu R, Baumann J a. Tool wear mechanisms in friction stir welding of Ti–6Al–4V alloy. Wear 2014;321:25–32.

[1.55] Rai R, De A, Bhadeshia HKDH, DebRoy T. Review: friction stir welding tools. Sci Technol Weld Join 2011;16:325–42.

[1.56] Bhadeshia HKDH, DebRoy T. Critical assessment: friction stir welding of steels. Sci Technol Weld Join 2009;14:193–6.

[1.57] Collaborative Research Project HILDA (High Integrity Low Distortion Assembly), E.U. Seventh Framework Programme (SCP2-GA-2012-314534-HILDA).

[1.58] Fraser K, St-Georges L, Kiss L. Optimization of Friction Stir Welding Tool Advance Speed via Monte-Carlo Simulation of the Friction Stir Welding Process. Materials (Basel) 2014;7:3435–52.

[1.59] Ericsson M, Sandstrom R. Influence of welding speed on the fatigue of friction stir welds, and comparison with MIG and TIG. Int J Fatigue 2003;25:1379–87.

[1.60] Lakshminarayanan A, Balasubramanian V. Process parameters optimization for friction stir welding of RDE-40 aluminium alloy using Taguchi technique. Trans Nonferrous Met Soc China 2008;18:548–54.

[1.61] Kumar S, Kumar A. Optimization of process parameters for friction stir welding of joining A6061 and A6082 alloys by Taguchi method. Proc Inst Mech Eng Part C J Mech Eng Sci 2012;227:1150–63.

[1.62] Zhang H, Liu H. Mathematical model and optimization for underwater friction stir welding of a heat-treatable aluminum alloy. Mater Des 2013;45:206–11.

[1.63] Kasman S. Optimisation of dissimilar friction stir welding parameters with grey relational analysis. Proc Inst Mech Eng Part B J Eng Manuf 2013;227:1317–24.

[1.64] Ghosh M, Kumar K, Kailas SV, Ray A. Optimization of friction stir welding parameters for dissimilar aluminum alloys. Mater Des 2010;31:3033–7.

[1.65] Mishra RS, De PS, Kumar N. Friction Stir Welding and Processing: Science and Engineering. Cham: Springer; 2014.

[1.66] Schmidt H, Hattel J, Wert J. An analytical model for the heat generation in friction stir welding. Model Simul Mater Sci Eng 2004;12:143–57.

[1.67] Jamshidi Aval H, Serajzadeh S. A study on natural aging behavior and mechanical properties of friction stir-welded AA6061-T6 plates. Int J Adv Manuf Technol 2014;71:933–41.

[1.68] Schaumann P, Collmann M. Influence of Weld Defects on the Fatigue Resistance of Thick Steel Plates. Procedia Eng 2013;66:62–72.

2. Microstructural characterisation of DH36 steel friction stir welds

2.1. Introduction

The process parameter development programme discussed in Chapter 1 has generated a substantial number of 2000 mm long welds of varying parameter sets, expanding the process envelope and trialling welding traverse speeds rarely attempted before. This is highly desirable in order to improve the techno-economic competitiveness of the process for use in large scale manufacturing applications as an alternative to traditional fusion welding techniques.

Nevertheless, the impact of these diverse FSW parameters and particularly of high speed welding on the weld quality, i.e. on the process's technical competence, remains to be evaluated. In addition, establishing a relation between varying process parameters and resultant weld microstructure of DH36 steel joints is critical for advancing the fundamental understanding on this solid state joining process and supporting the optimisation work undertaken herein.

The technical literature on FSW of structural steel remains relatively limited, principally for high welding speeds, when compared to the research output on other metals. Earlier studies on structural steel FSW routinely discussed the effects of slow traverse speeds during welding in heavily controlled laboratory conditions. Representatively, Konkol *et al.* [2.1] assess process parameters for FSW of HSLA-65 steel in the context of shipbuilding applications, with traverse speeds in the region of 100-140 mm/min. The plates to be welded are prepared to a great extent by milling and grinding; an initial entry hole is drilled in the interface of the butted plates and these are preheated to 300°C along with the Tungsten-based tool, primarily to protect the latter from fracture [2.1]. The parent material microstructure is seen as equiaxed ferrite with slightly banded pearlite. The heat affected zone (HAZ) consists of refined ferrite grains with randomly dispersed pearlite, a product of phase transformation from austenite in low cooling rate; the thermo-mechanically affected zone (TMAZ) comprises coarser blocky ferrite and Widmanstätten ferrite with carbide precipitation [2.1]. The tool rotational speed is not disclosed but the above two observations, i.e. the HAZ heated above the lower transformation

temperature (A_1) and the suggestion of grain growth in the TMAZ indicate that the heat input to the weld region is likely to be excessively high.

A separate study employs even slower traverse speeds in the range of 25-100 mm/min with rotational speed of 450–650 rpm for FSW of AISI 1018 mild steel [2.2]; welds free of defects are produced using these slow parameter sets. The parent material is of the typical equiaxed ferrite and refined pearlite microstructure. As in the previous research [2.1], grain refinement is observed in the outer and mid HAZ, and attributed to slow cooling rates developed. However, the inner HAZ displays a grain coarsening effect; it is explained that for the particular alloy, such grain growth implies peak temperatures exceeding 1100°C during welding, i.e. higher than the steel's upper transformation temperature (A_3), thus resulting in the formation of coarser austenite grains [2.2]. Microstructural characterisation and experimental temperature measurements with thermocouples indicate that the TMAZ experienced peak temperatures of at least 1200°C, therefore substantial grain growth is observed in the evolved ferrite rich microstructure. As discussed, full austenitization of the steel due to the extreme peak temperatures combined with slow cooling rates developed after welding are responsible for grain coarsening of the TMAZ [2.2]. This is a recurring trend reported by preliminary studies on steel FSW [2.1-2.3], where the welding parameters were clearly not optimised. Compared to the process parameters assessed herein (see Table 1.1), the very high rotational speeds linked to the slow traverse speeds that are applied by Lienert *et al.* [2.2] produce considerable amounts of heat which raises the weld zone temperature to an undesirably high level.

Early in the development of FSW for steel alloys, the oil and gas industry discerned and thus assessed the process's benefits. As an illustration, one publication investigates the microstructural evolution of friction stir welded API X80 steel grade [2.3]. Ferrite, granular bainite and martensite, along with fine niobium and titanium precipitates are seen in the X80 parent material. The HAZ is very similar to the parent material, only of slightly finer grains. As suggested previously [2.1], it is established that this zone has been heated above A_1 [2.3]; this is not an unexpected observation considering that the employed traverse speed of 100 mm/min is distinctly slow for the applied rotational speed of 550 rpm (suboptimal parameter set producing an overly high peak temperature weld). The TMAZ is characterised as principally granular bainite and lath martensite; in an analogous observation to Konkol *et al.* [2.1], the grains are seen to be much coarser than the parent material

and HAZ [2.3]. Grain growth is most likely a consequence of this weld region being subjected to extreme thermal energy conditions (generated by the high rotational speed) for substantial time (due to slow traverse speed) [2.2,2.4]. The study concludes by summarising the identified benefits of FSW compared to fusion welding; negligible softening of the HAZ which is routinely the weak link in fusion welding and the fact that coarser grains in the TMAZ do not form on an uninterrupted region such as the problematic fusion line in fusion welding [2.3]. Hence, reduced tendency for failure in these FSW zones is anticipated. However, the grain coarsening in the TMAZ is distinguished as one area requiring improvement through process optimisation.

Reynolds *et al.* [2.5] examine friction stir single sided welds of hot rolled, 6.4 mm thick DH36 steel, produced by four different welding speeds in an inert gas environment, to assess the relationship between varying weld parameters and resultant weld properties. A bainitic and martensitic microstructure is observed in the bulk of the TMAZ of the fast weld (450 mm/min) [2.5], clearly a product of austenite transformation in high cooling rates; this developed microstructure is seen to substantially improve the weld tensile properties. Still, only this weld's microstructural features are reported therefore no comparison can be made to the intermediate and slower welds.

More recent work [2.6] on the same grade of steel, DH36, extends the assessment of friction stir welded plates, also examining three different thicknesses (4, 6, and 8 mm) and comparing to submerged arc welded (SAW) plates of the same thickness in order to evaluate the potential of FSW as a shipbuilding welding process. The parent material is seen to consist of bands of ferrite and pearlite, as expected for rolled low alloy steel plates. An acicular shaped ferrite microstructure is detected in the TMAZ, consistent over the mid-thickness of all weld samples, with a finer unspecified structure seemingly increasing with decreasing plate thickness [2.6]; the welding traverse speed and hence the developed cooling rate is significantly lower than in Reynolds *et al.* [2.5], therefore the latter is postulated to be a form of bainite.

Ghosh *et al.* [2.7] study the friction stir lap welding of high strength martensitic M190 steel thin plates. The objective is to optimise the FSW of M190 steel in the automotive industry by assessing the resultant microstructure and mechanical properties produced by ten different sets of welding parameters, 600-1200 rpm rotational speed and 51-203 mm/min traverse speed, also applying forced air

cooling. The study [2.7] finds that the microstructure of the weld nugget becomes predominantly martensitic with increasing traverse and rotational speed, due to very high cooling rate. Bainite is seen to appear and gradually increase with the same rotational speed but slower traverse speeds, hence marginally lower cooling rates. It is concluded that the temperature of the inner HAZ exceeds the steel's A_1 temperature during welding thus austenite transformed into ferrite and pearlite during cooling [2.7]. This is an indication that the process parameters are not suitably optimised, i.e. the tool rotational speed is too high for the traverse speed employed, therefore generating excessive heat towards the weld region. Still, the outer HAZ temperature remains below A_1 therefore exhibiting tempered martensite because of the martensitic parent material and the amount of heat dissipating through this region [2.7].

In an investigation into the possible use of FSW as an alternative to electric resistance welding of API X100 grade high strength linepipe steel, Cho *et al.* [2.8] examine its microstructural evolution during friction stir butt welding after significant prior preparation of the plates. Their work is mainly focused on the grain structure development in a single set of process parameters, 127 mm/min and 450 rpm, using optical microscopy, scanning electron microscopy with electron backscatter diffraction and transmission electron microscopy. Originating from the parent material microstructure of dual phase ferrite and bainite, the TMAZ is reported as having a very fine, homogeneous microstructure whilst the stir zone (central TMAZ) is acicular shaped bainitic ferrite rich. The former is attributed to continuous dynamic recrystallization, while the latter occurs because of the particular to this region austenite to ferrite phase transformation under high cooling rate and high strain [2.8]. Possible heterogeneity of the weld is not discussed however, as the microstructural assessment is confined only on the retreating side of the weld zone.

In the context of shipbuilding once again, a separate article reports on an in-depth examination of the influence of varying welding traverse speed and FSW tool material on the resultant microstructure of a high strength low alloy steel (HSLA-65) [2.9]. The HSLA-65 parent material is described as the characteristic equiaxed ferrite and pearlite microstructure with refined niobium carbides. Bead-on-plate FSW is performed using W-Re tools at traverse speeds of 50-500 mm/min whereas pcBN tools produce butt welds in the range of 50-250 mm/min. It is explained that the process parameters are chosen such that both tool types generate similar specific heat input distribution [2.9]. Interestingly, higher traverse speeds are not explored

with the pcBN tool since it has exhibited probe fracture during trials. Weld temperatures are approximated through an evaluation of the forces exerted on each tool type during FSW; higher forces correspond to less plasticisation of the steel due to lower weld zone peak temperature. The examined FSW tool materials, pcBN and W-Re, develop varying peak temperatures in the weld, thus different cooling rates because of the diverse thermal properties of each tool. From this analysis [2.9], use of pcBN tools is seen to result in lower temperatures than the W-Re tools for comparable specific thermal energy produced. The lower weld peak temperature measured for the pcBN tool leads to smaller prior austenite grain size, which gives rise to the evolution of a more polygonal and less acicular microstructure. However, the same temperature is found to develop high cooling rates, therefore a higher ratio of harder phases such as bainite and martensite. Thus, it is argued that microstructural evolution during FSW is directed by the combination of peak temperature, which affects austenite grain size hence the tendency for acicular grain formation, and consequent cooling rate [2.9]. Apart from the tool material, the weld microstructure is particularly affected by increasing welding speed; the TMAZ and HAZ are seen to reduce in size with increasing traverse speed and constant rotational speed because less heat is gradually generated per unit length. As the welding parameters employed are not suitably optimised (see the relevant discussion in Chapter 1), mechanical stirring of the alloy is combined with excessively high thermal energy which is generated and dissipated towards the weld. Therefore, the weld zone peak temperature during FSW is found to considerably exceed the steel's A_3 temperature. The consequent high cooling rates develop a TMAZ consisting of ferrite and harder phases such as bainite and martensite. These hard phases are also observed in the inner HAZ. The weld material experiences the high peak temperatures for long periods due to tool traverse speeds not optimised, i.e. not high enough with respect to the rotational speed. Hence, larger austenite grain size is promoted which in turn favours the formation of acicular shaped grains of ferrite, bainite and martensite [2.9].

The above discussed publications disclose that FSW parameters and welding conditions have a dominant effect on the peak temperature and cooling rate, hence the resultant microstructure. Equally, the multi-physics nature of FSW is an important factor in the microstructural evolution; thermo-mechanical processing of the parent material in severe conditions of high strain, strain rate and peak temperatures during FSW of steel [2.10] commonly leads to dynamic

recrystallization in the TMAZ [2.2] and to complex microstructures which are substantially different from the ones predicted by equilibrium diagrams or the current knowledge on fusion welding [2.2,2.9].

For this purpose, a detailed microstructural characterisation study of the produced welds is implemented towards assessing the weld quality and supporting the step change improvement in welding traverse speeds, i.e. the optimisation work described in Chapter 1. One outcome of this microstructural assessment is generating important information regarding the mechanical properties that are likely to be attained in the weld zone. A secondary outcome is detecting undesirable process induced flaws or defects that could compromise the integrity of the weld, the absence of which provides reassurance that the process parameters outlined in Table 1.1 will lead to an acceptable level of quality. The microstructural evolution and its possible variations throughout the weld region are thoroughly examined and reported herein.

2.2. Experimental procedures

2.2.1. Material and welding details

A substantial number of single sided friction stir butt welds in 6 mm thick DH36 steel were produced using a PowerStir FSW machine operated in position control. The PowerStir welding machine is a moving gantry assembly with a moveable welding head on which the FSW tool is mounted (Figure 2.1). It has a sizeable operating bed (6 m x 4 m) on which large scale components can be friction stir welded. This FSW machine is fully equipped with data capture capability that enables real time monitoring of the welding operation to assist with post process analysis of many process parameters to be studied. Of these, the tool traverse speed and the tool rotational speed play a significant role in terms of productivity and quality whereas the tool spindle torque, induced tool forces, and plunging force (F_z) provide information about the onset and consistency of steady state conditions; a typical operational condition plot is presented in Figure 2.2.
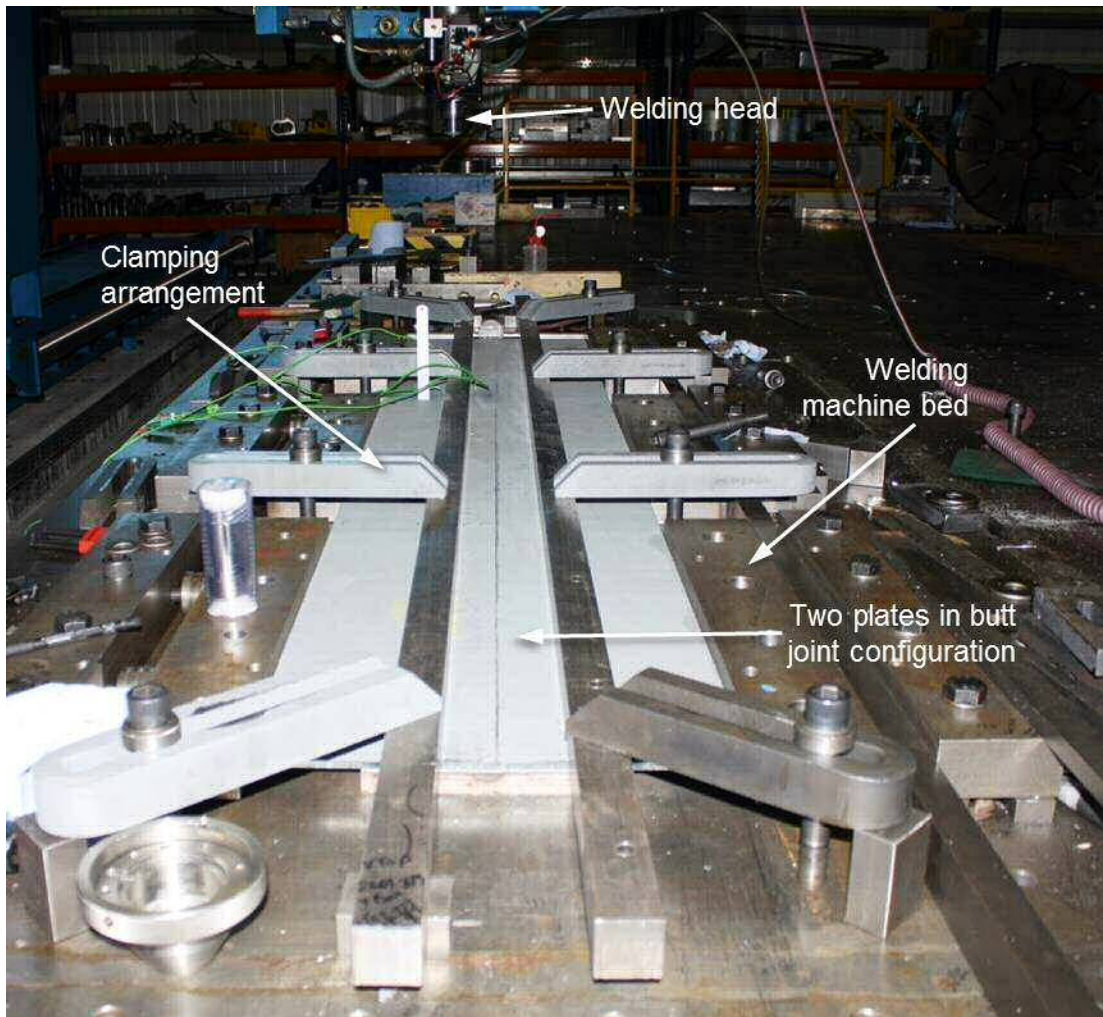
Figure 2.1. General view of the FSW machine and experimental setup prior to welding
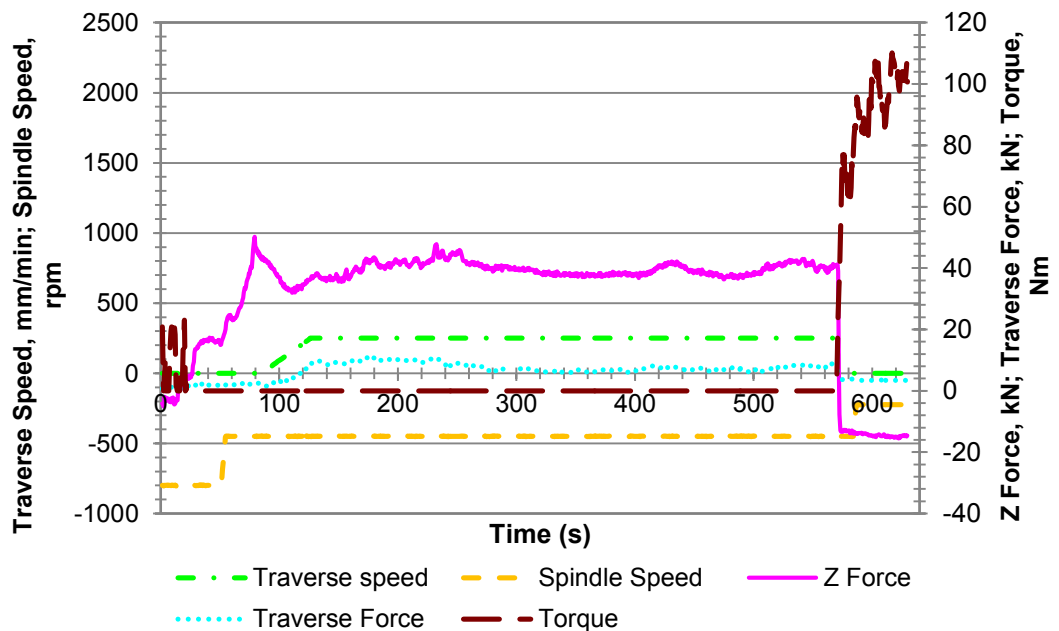

Figure 2.2. Typical chart of tool position, process parameters & force data during FSW

All plates were 2000 mm in length and 200 mm in width, therefore fabricating a welded component of 400 mm in width. The rolled plates were securely clamped to the machine bed in a square edge butt joint configuration (Figure 2.1) and welded in the as received condition without any prior surface preparation. A separate study argues that the latter provides a measure of the process's sturdiness for use in industrial environments [2.11]. The nominal chemical composition of the low alloy steel grade DH36 that was examined in this study is presented in Table 2.1, as provided by the steel supplier. Lloyd's Register rules [2.12] specify grade DH36 as a high strength steel for shipbuilding and other structural applications with the mechanical properties outlined in Table 2.2.

Table 2.1. Chemical composition of 6 mm thick DH36 steel (wt.%)

C	Si	Mn	P	S	Al	Nb	N
0.11	0.37	1.48	0.014	0.004	0.02	0.02	0.002

Table 2.2. Mechanical properties of grade DH36 [2.12]

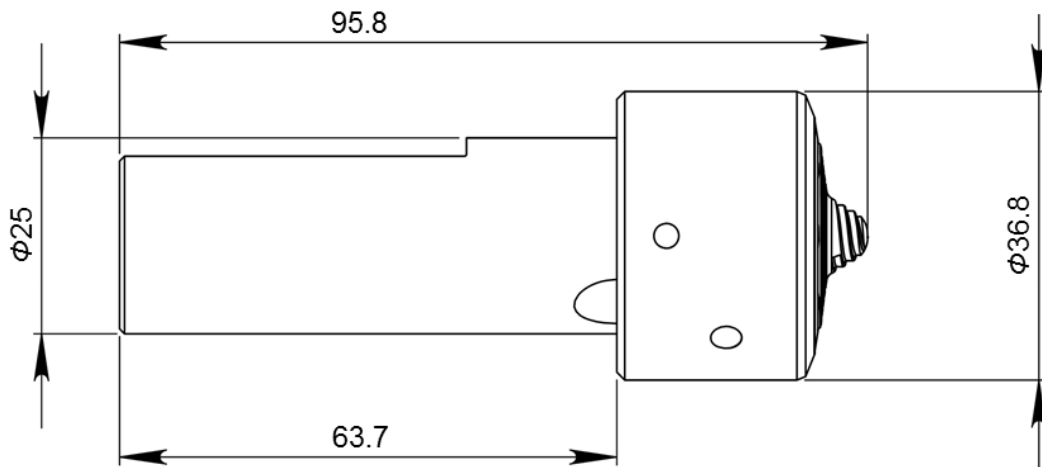| Yield strength (min), MPa	Tensile strength, MPa	Charpy V-notch impact tests average energy (min), J*	
		Longitudinal	Transverse
355	490-630	34	24

*For thickness t ≤ 50 mm, at -20°C.

Figure 2.3. Basic dimensions of the FSW tool employed for all welds [2.13]

FSW was performed using hybrid WRe-pcBN stepped spiral tools (also see Chapter 1) developed by MegaStir (designation Q70, Figure 2.3). This type of tool is equipped with a scrolled shoulder, having a probe length of 5.7 mm and rotating

anti-clockwise. The tool is protected by an inert gas environment against oxidation due to the high temperatures of the FSW process [2.11].

2.2.2. Microstructure evaluation

One metallographic sample was transversely sectioned from a random position within the steady state condition region of each of the 25 welds. In the steady state region, the forces that the FSW tool sustains stabilise (Figure 2.2) and the weld quality is improved; hence, any sample removed from any position within the steady state region is expected to be representative of the properties of the entire weld. The region of steady state conditions is commonly identified by visual observation of the welded plates (a good quality surface without excessive flash formation, voids or cracks), and confirmed by analysis of the forces (on the longitudinal and vertical direction) on the tool; this is typically established beyond the first 50-150 mm of welding [2.13].

A consistent metallographic preparation process was applied on each sample examined and this process made use of the normal metallographic preparation equipment and consumables. This consisted of hot mounting, grinding and polishing on a semi-automatic preparation machine, followed by etching with Nital 2%. The samples were then positioned on a stage and macrographic images of the weld zone were captured. A more detailed examination of areas of interest within the weld region identified on the macrographs was performed with the aid of an Olympus GX51 light optical microscope that involved taking several micrographic images from each sample being studied. Furthermore, a Hitachi S-3700 tungsten filament scanning electron microscope (SEM) with a large chamber of 150 x 110 mm and energy dispersive spectroscopy (EDS) capability (Oxford Inca 350 with 80 mm X-Max detector) was used for chemical characterisation.

2.3.   Results and discussion

To maintain a consistent approach, the following nomenclature is adopted in the present thesis in accordance with the terminology proposed by Threadgill [2.14]; the main regions of the weld zone are illustrated in Figure 2.4 where:

- AD: Advancing side, the side where the rotating FSW tool pushes the metal towards the weld direction, i.e. forwards. The convention employed for the entire

thesis is that samples are prepared so that the advancing side is presented on the left side of all images.

- RT: Retreating side, the side where the rotating tool pushes the metal in a direction opposite to the weld direction, i.e. backwards.

- TMAZ: Thermo-mechanically affected zone in which the material has been thermo-mechanically stirred by the FSW tool.

- Weld root: part of TMAZ, around and below the tip of the FSW tool's probe.

- HAZ: Heat affected zone, a region typically observed in microstructures developed by any welding process, where the metal has been affected by heat as it dissipates from the TMAZ, but not mechanically stirred.

- PM: Parent material, metal not affected by the process. The characteristic equiaxed ferrite / pearlite banded microstructure of DH36 steel [2.5] is displayed in Figure 2.5; although rarely discernible at this magnification (x1000), the lamellar structure of pearlite is faintly visible in Figure 2.5b.
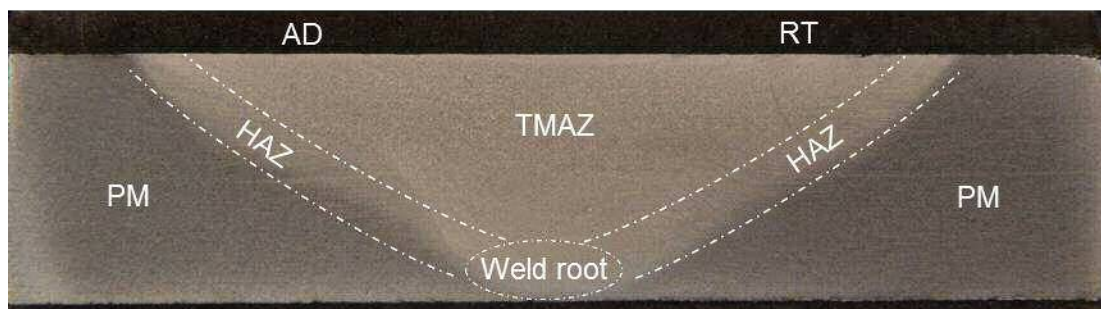

Figure 2.4. Typical macrograph of the friction stir weld region [Etched]

Referring to the classification in Table 1.1, the group of slow welds presents a very homogeneous microstructure without any flaws. These exhibit a ferrite rich microstructure with highly refined grains of random geometry. The suitably optimised FSW parameters employed in this work have not generated excessive amounts of thermal energy, hence TMAZ grain coarsening as in earlier research on steel FSW [2.1-2.3] is not observed herein (also see relevant discussion in section 2.1). A very small content of what is expected to be acicular shaped bainitic ferrite is found in W03 (Figure 2.6), the content of which is seen to steadily increase with increasing traverse speed and constant rotational speed (200 rpm). This observation confirms that the cooling rate is increasing with increasing traverse speed. Previous work [2.9] has also established this relation of higher ratio of acicular shaped phases with
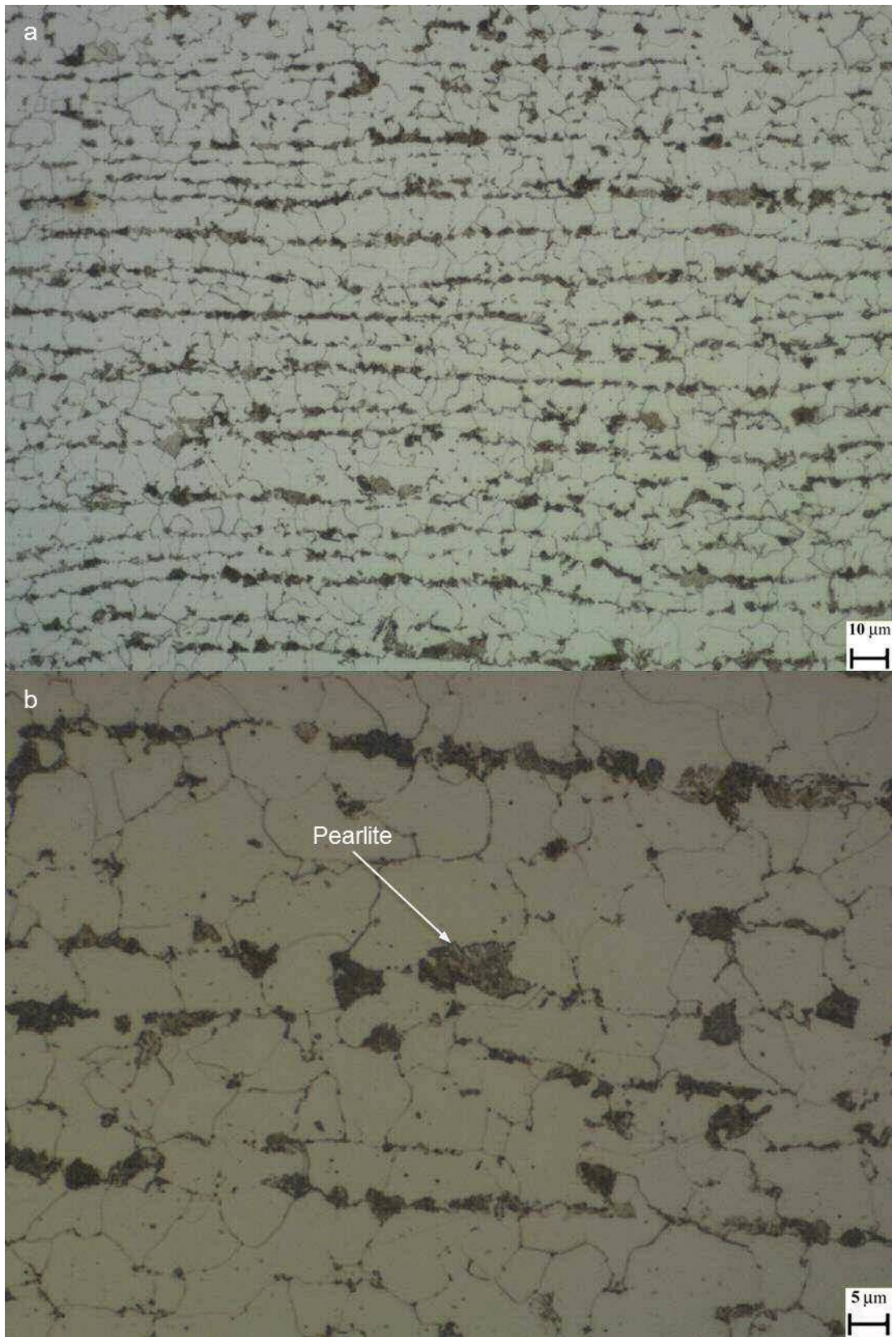
Figure 2.5. Steel grade DH36 parent material microstructure (a) [x500, Etched]; (b) [x1000, Etched]

decreasing heat input per unit length, i.e. increasing traverse speed.

Additionally, there is a threshold value of approx. 130 mm/min above which this apparently acicular bainitic ferrite microstructure occurs at a small ratio relative to the above described ferrite rich microstructure. The parameters of W01, W02 and W03 resulted in welds being produced with a large and symmetrical tool footprint on the weld surface. Using a similar traverse speed of 127 mm/min, Cho *et al.* [2.8] observe a predominantly acicular bainitic ferrite stir zone microstructure developed as acicular bainitic ferrites nucleate mainly on the austenite grain boundaries. It is noted that this is a product of the phase transformation of austenite, in the supercritical stir zone, to ferrite at a high cooling rate. Still, the cause of the high cooling rate remains unclear since the stated rotational speed (450 rpm) [2.8] is
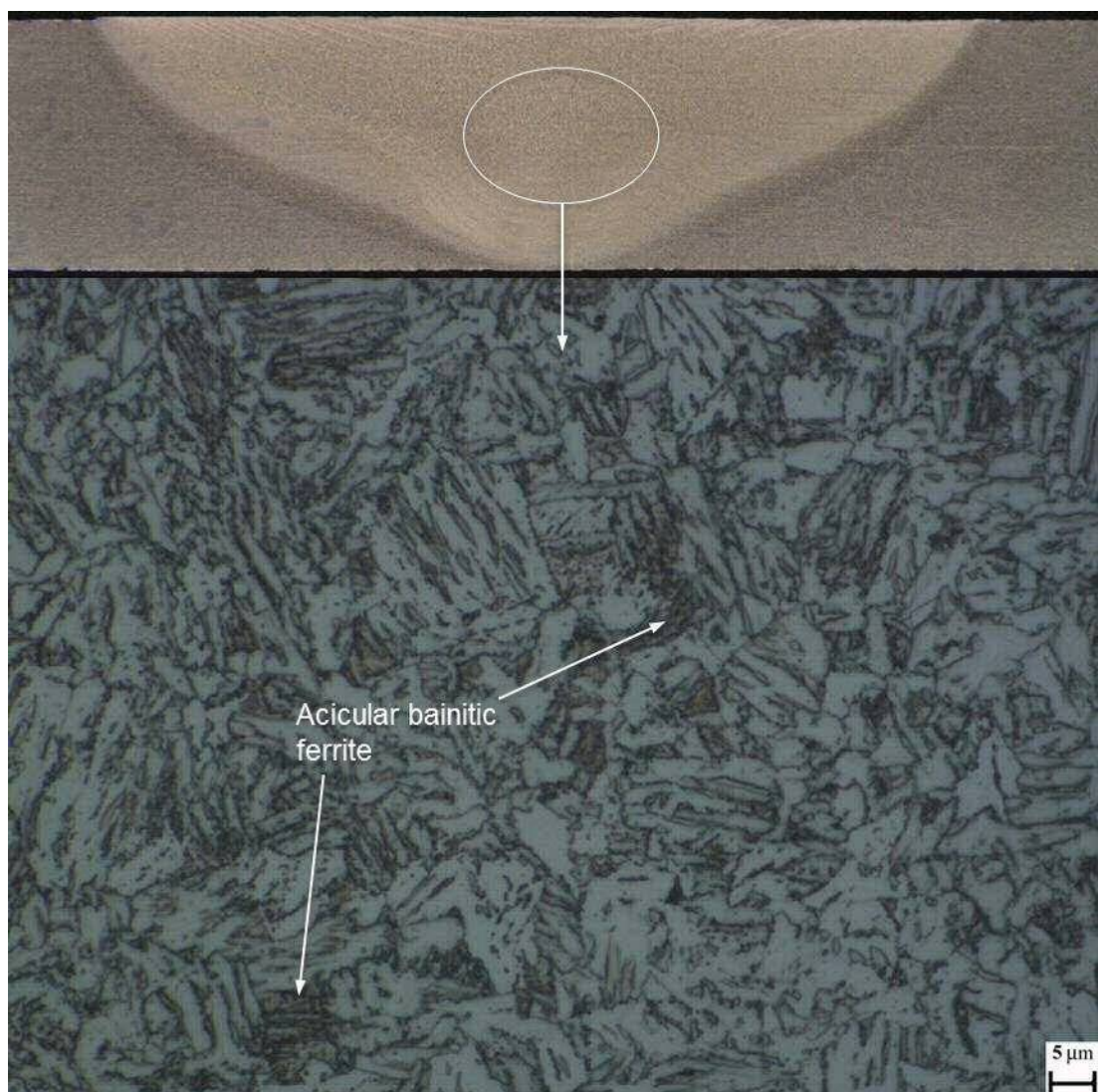

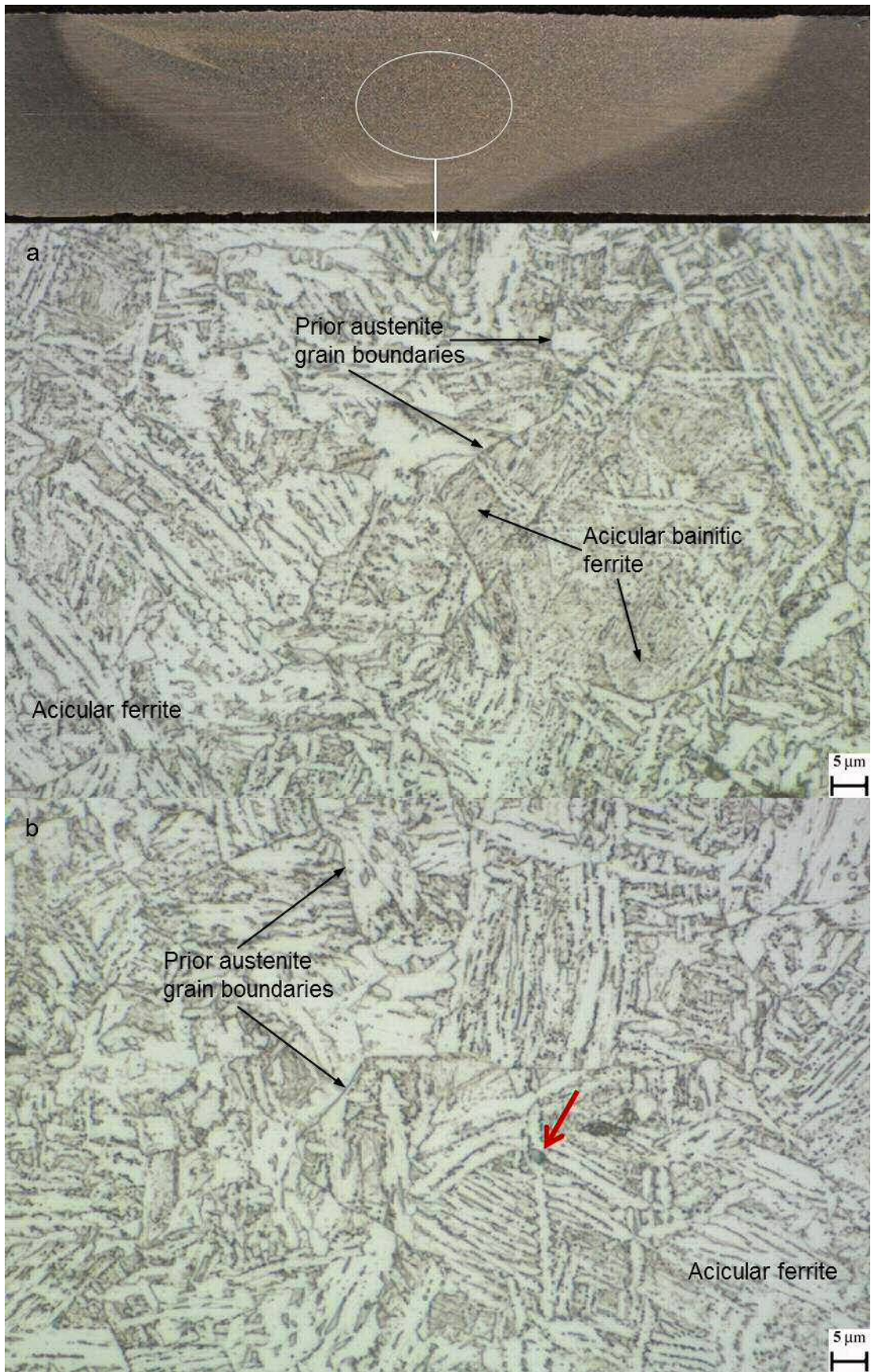**Figure 2.6. W03, microstructure of mid-TMAZ [x1000, Etched]**

Figure 2.7. W07, microstructure of mid-TMAZ [x1000, Etched]

quite high for the above mentioned traverse speed when compared to the parameter sets employed herein. This high rotational speed is expected to lead to high heat input, which in turn would lower the cooling rate after welding. Thus, it is conceivable that the bainitic ferrite microstructure is the outcome of an undisclosed applied forced cooling method and the steel's different thermal properties to DH36.

W07 has been classified in the group of slow weld parameters; contrary to other welds of this group however, it exhibits an acicular ferrite predominant microstructure (Figure 2.7). Prior austenite grain boundaries are observed to some extent mainly on smaller, more randomly mixed, bainite-rich regions (Figure 2.7a). A number of acicular ferrite platelets are seen to nucleate from non-metallic inclusions (one such example is marked with a red arrow in Figure 2.7b) and emanate in
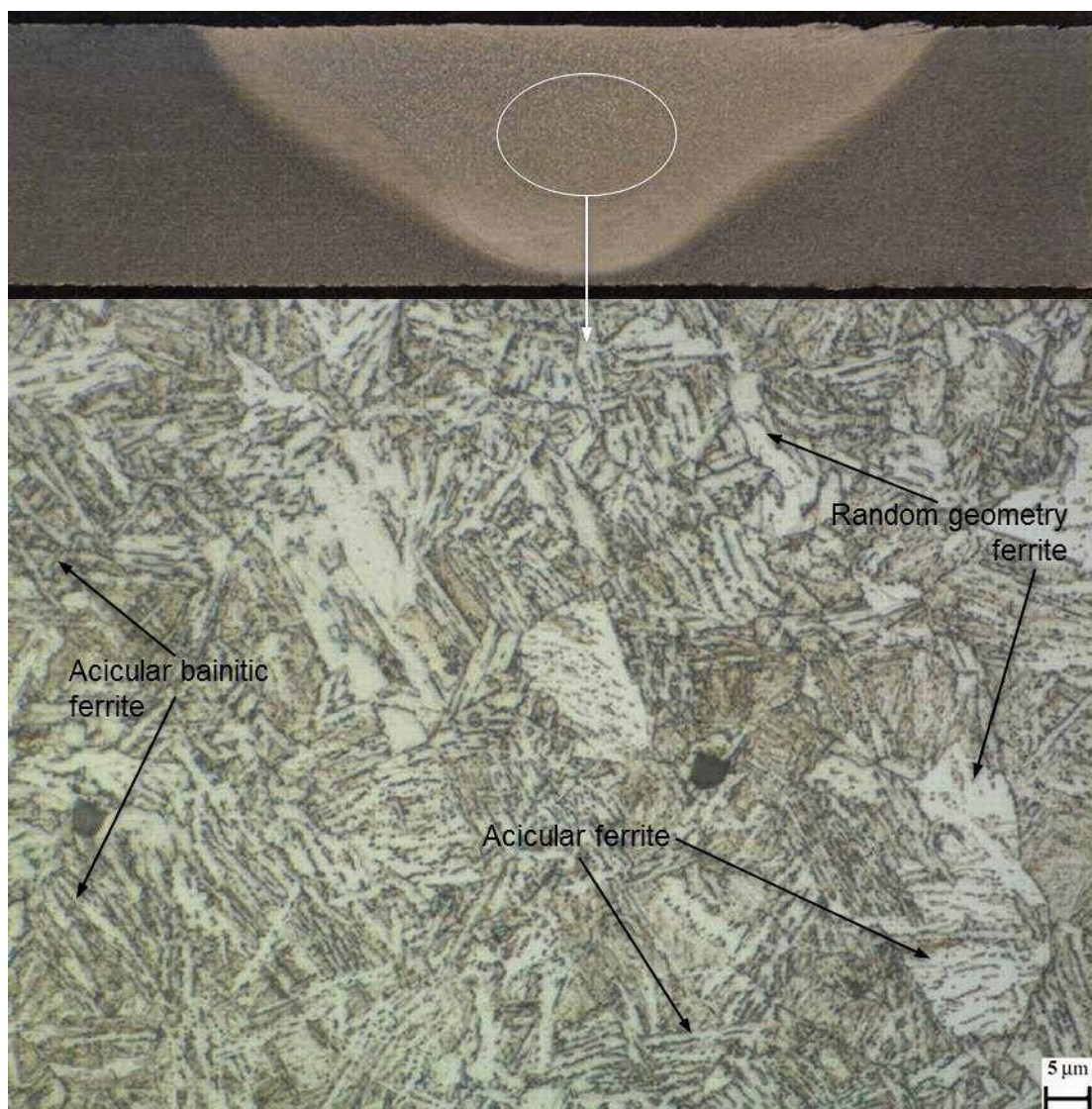

Figure 2.8. W10, microstructure of mid-TMAZ [x1000, Etched]

random directions, as discussed by other researchers [2.15-2.17]. In all, this group of welds is expected to have acceptable mechanical properties. As discussed earlier, another study [2.6] reports mainly acicular ferrite microstructure in the TMAZ of DH36 welds; thus, it can be concluded that the welding conditions have produced a comparable cooling rate to the one occurring in weld W07.
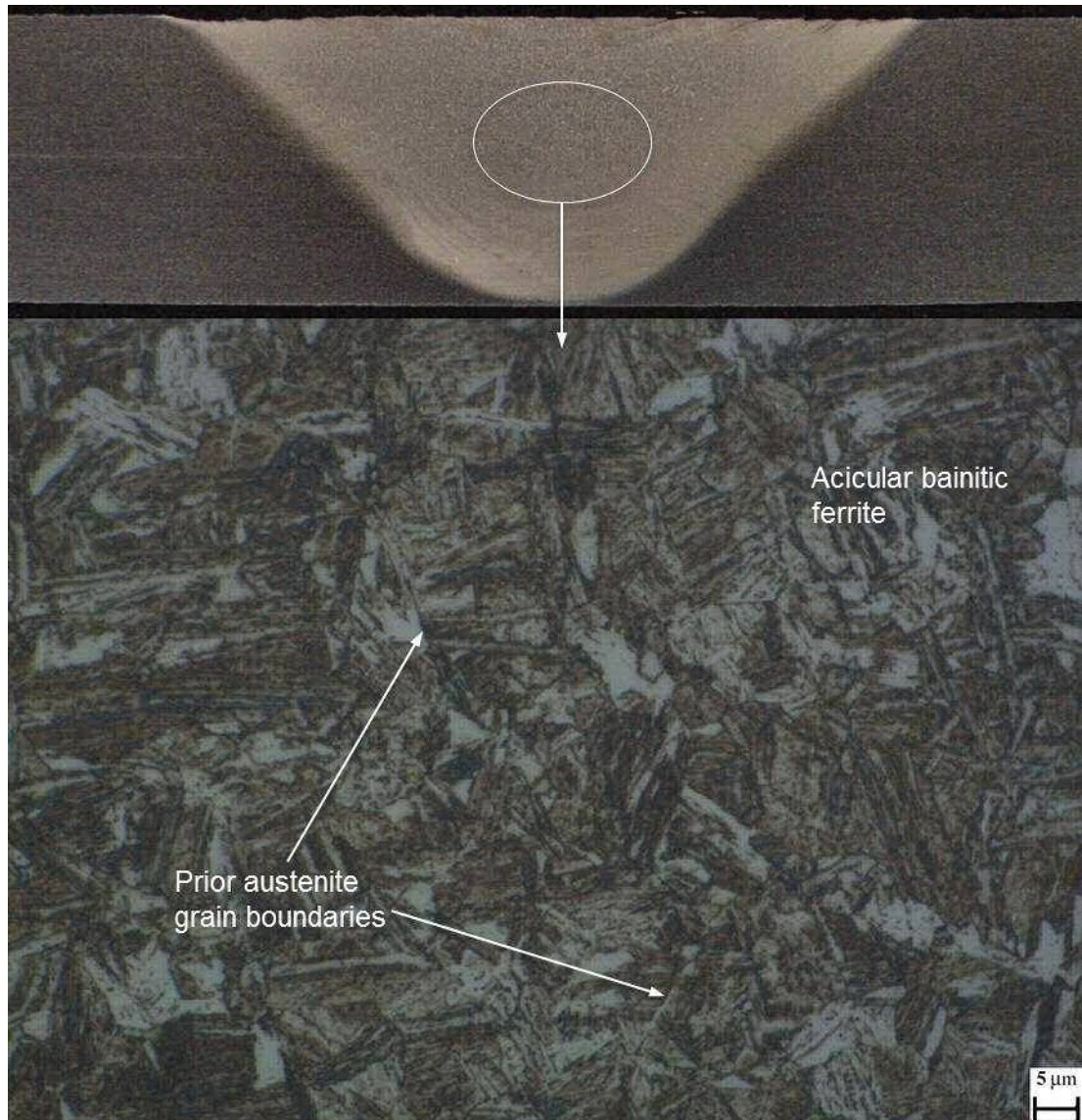
Figure 2.9. W15, microstructure of mid-TMAZ [x1000, Etched]

In the intermediate group of welds with rotational speed of 400 rpm and as traverse speed is seen to increase, the microstructure becomes more heterogeneous (Figure 2.8) with regions of increasing bainite content (suggesting increased cooling rates). However, this heterogeneous microstructure does not seem to have a significant effect on the mechanical properties (see Chapters 3 & 4). Nevertheless, weld W15

features a reasonably homogeneous acicular bainitic ferrite microstructure (Figure 2.9); this suggests that a good balance of rotational and traverse speed has been achieved. In addition, prior austenite grain boundaries can narrowly be observed on the light optical microscope (Figure 2.9), only on the bainite predominant regions.
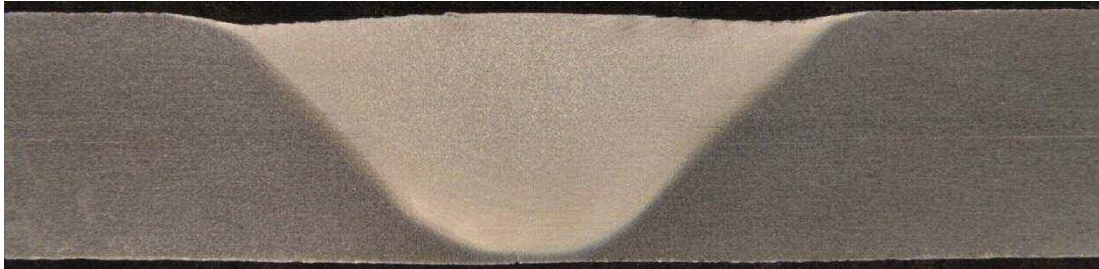

Figure 2.10. W16, macrograph disclosing a narrower TMAZ and HAZ compared to W13 (Figure 2.11) [Etched]
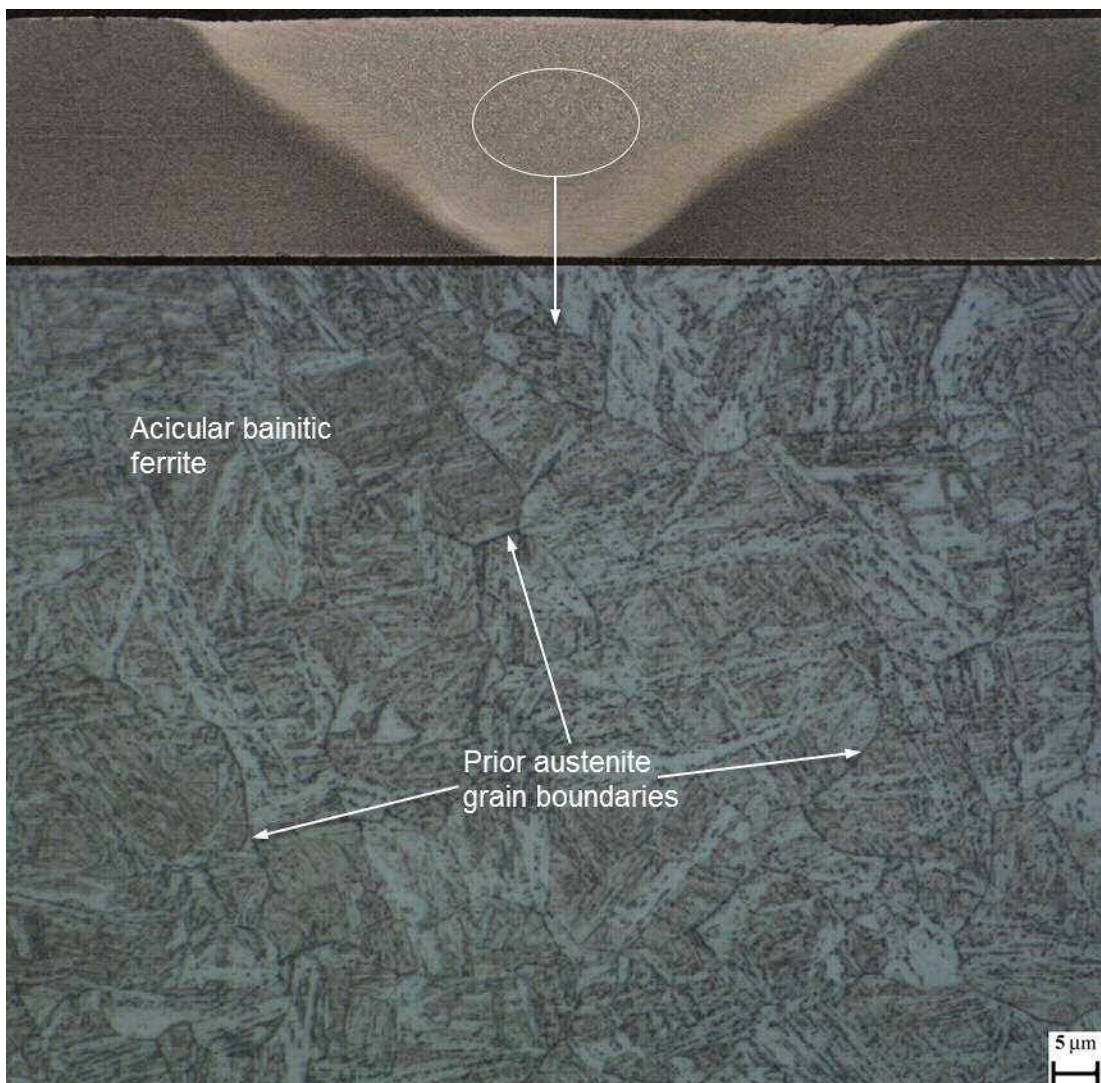

Figure 2.11. W13, microstructure of mid-TMAZ [x1000, Etched]

The FSW process is tolerant to welding speed variations at the 450 rpm rotational speed. Both welds in this intermediate group exhibit a homogeneous, fully acicular bainitic ferrite microstructure with prior austenite grain boundaries. Due to marginally lower heat input (refer to Table 1.1), W16 presents a rather small HAZ (note Figure 2.10 as compared to the macrograph of Figure 2.11); weld W13 however seems to be the product of an excellent intermediate set of parameters (Figure 2.11).

At the high welding speed of 500 mm/min, the microstructure of all five welds becomes heterogeneous, with poorly mixed regions of acicular ferrite and varying bainite content; Figure 2.12 presents two characteristic examples. The presence of bainite has increased considerably in this group due to the even higher cooling rate that is occurring. Prior austenite grain boundaries are detected on the regions of bainite predominant microstructure (Figure 2.12). The arrows in the same figure indicate acicular bainitic ferrites growing from these boundaries; this observation is also reported elsewhere [2.8,2.15,2.18].

Two distinct microstructures co-exist within the TMAZ of weld W24 (Figure 2.13); the sharp transition from acicular ferrite to acicular bainitic ferrite is expected to act as stress concentration region. Stress concentration, i.e. a localised site of stresses above average, is the reason for fatigue crack initiation even though the applied stress is lower than the yield strength of the material [2.19]. Stress concentration occurs by discontinuities of any type in a component under stress [2.19]. Clearly, the discontinuity can be a notch of any shape (e.g. weld root flaw [2.20]), change in the component geometry (such as the weld toe in fusion welding [2.21]), or an abrupt change in local microstructure resulting in material property variations [2.22].

This latter issue is often discussed in the technical literature; one characteristic study finds that the zone of microstructural transition from parent material to HAZ is the critical site for fracture during tensile testing of tungsten inert gas (TIG) welded AISI 4130 high strength steel instead of the commonly problematic region of the weld toe [2.23]. Elsewhere, it is noted that the heterogeneity in the microstructure between weld zone and HAZ, as a result of phase transformations, is commonly linked to material property variations in the micro scale [2.24]. Caballero *et al.* [2.25] record a substantial decrease in impact toughness of bainitic steels due to the banded microstructure which evolves by manganese segregation during solidification. The study argues that stress concentration generated by the disparity in this heterogeneous microstructure's local hardness distribution is partly
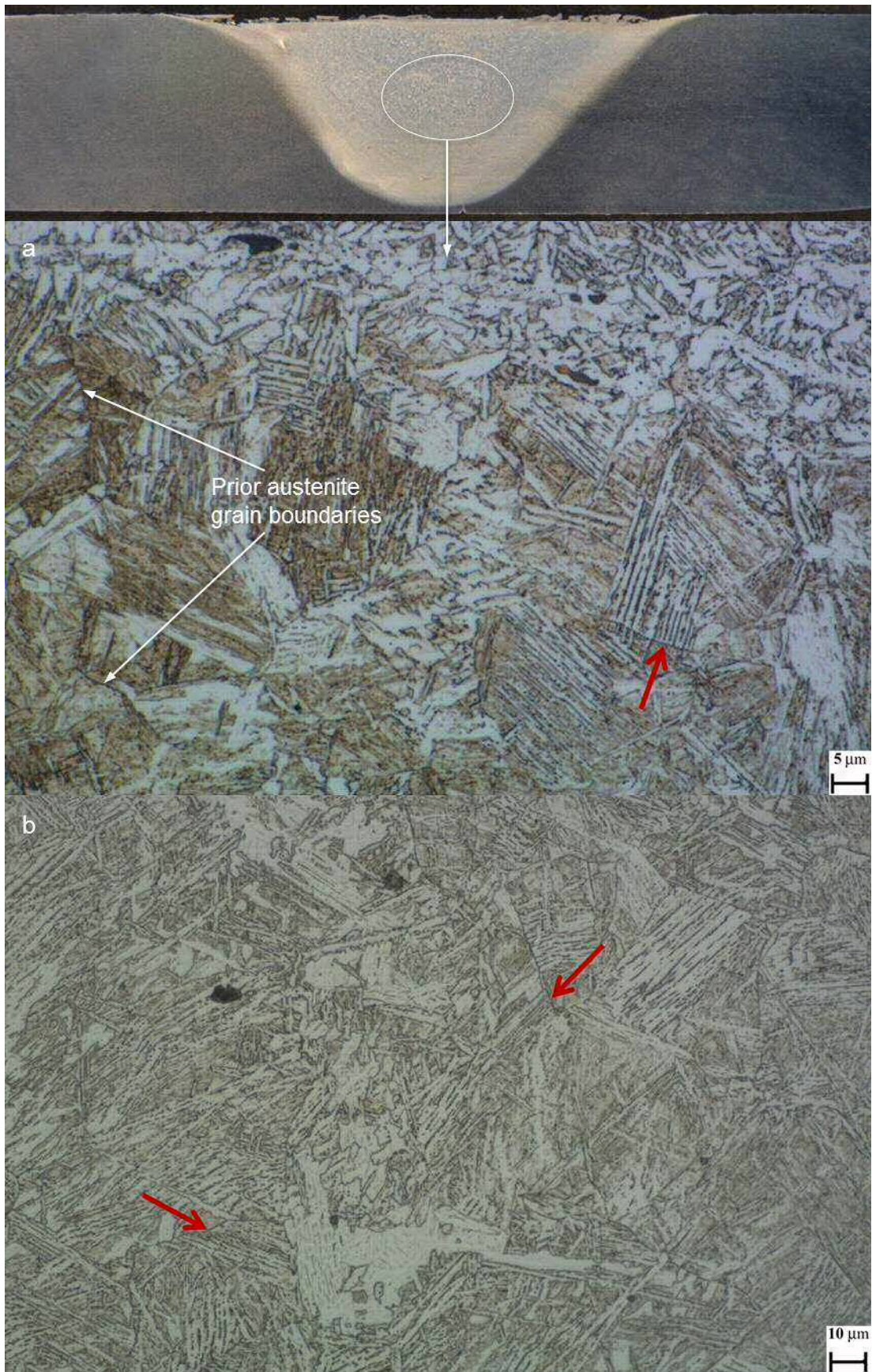
Figure 2.12. Mid-TMAZ microstructure (a) W21 [x1000, Etched]; (b) W24 [x500, Etched]

responsible for the reduced toughness of these alloys [2.25]. Moreover, Mochizuki *et al.* [2.26] propose a model which evaluates the impact of stress concentration developed by the small-scale microstructural heterogeneity on the mechanical properties of fusion welded structural steels and primarily on fracture initiation.

The microstructural heterogeneity of weld W24 in the macro and micro scale is better displayed in Figure 2.14a & b respectively. As in the preceding discussion, the rapid microstructural transition should produce substantial hardness variations which create stress concentration regions, from a highly localised level (Figure 2.14b) to the weldment's thickness (Figure 2.14a). Yet, this weld's parameters have achieved a good balance of rotational speed (sufficient heat input for proper thermo-
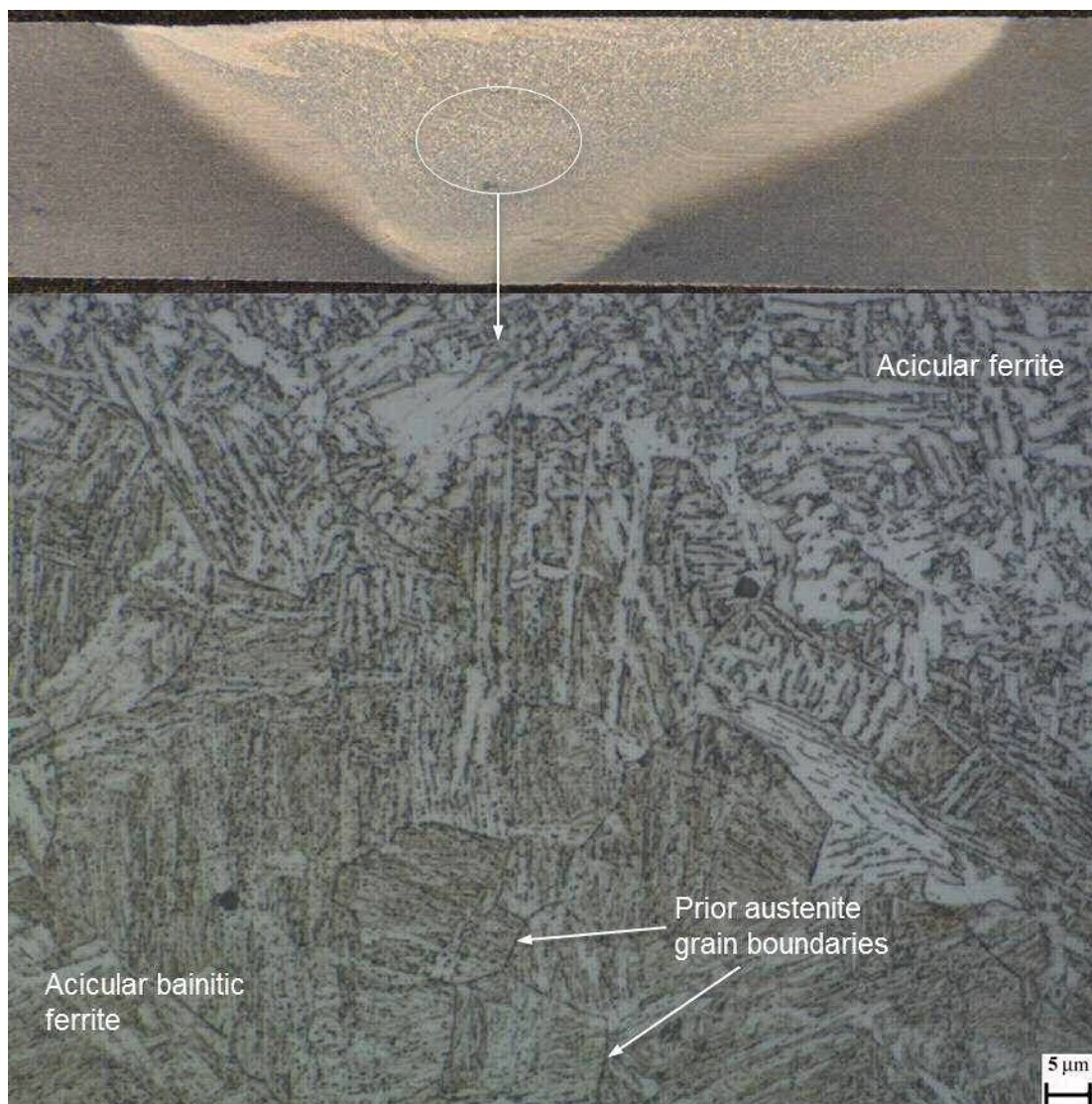

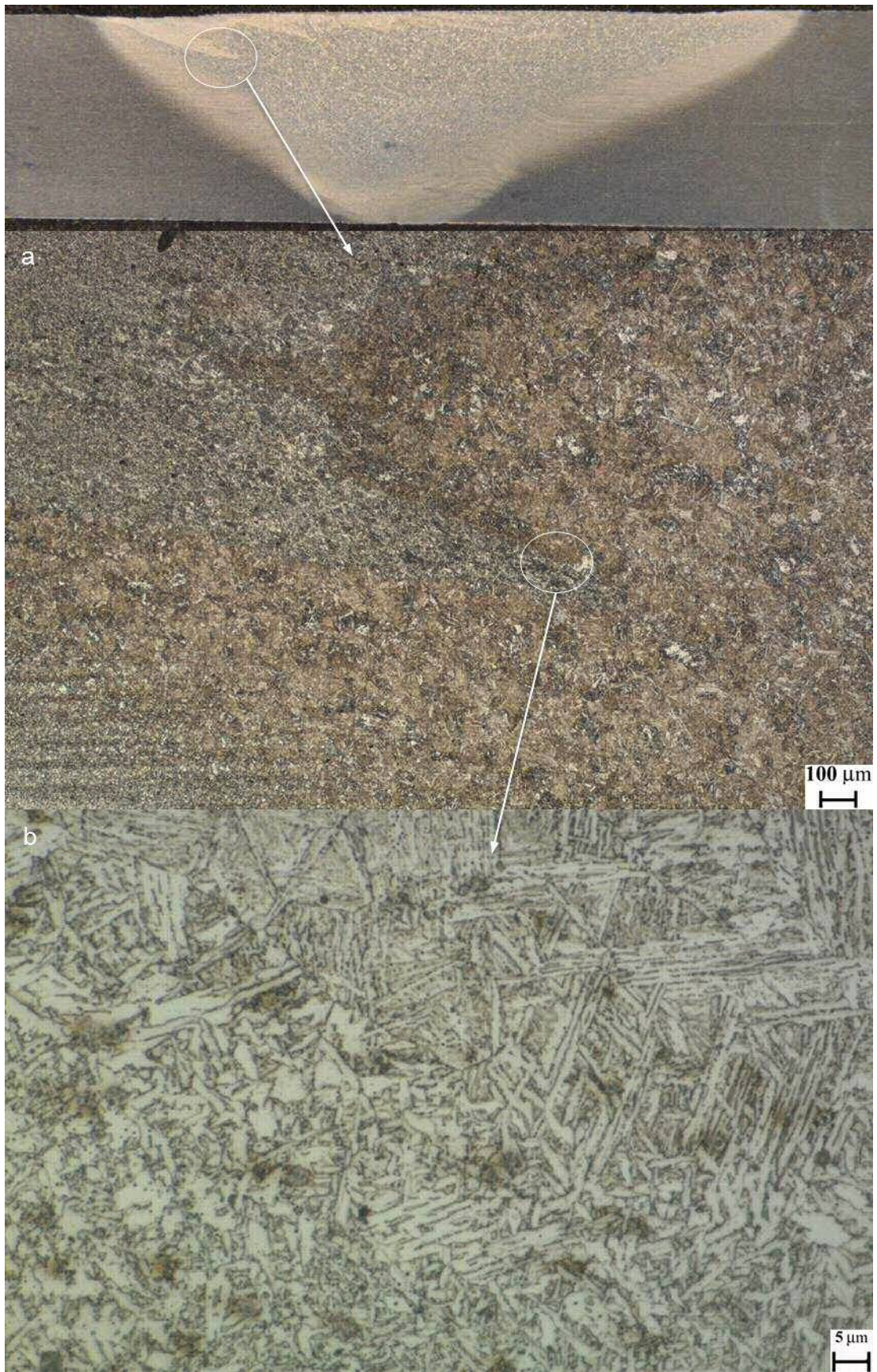**Figure 2.13. W24, microstructure of mid-TMAZ [x1000, Etched]**

Figure 2.14. W24 AD side TMAZ (a) [x50, Etched]; (b) [x1000, Etched]

mechanical stirring) and traverse speed (affecting the cooling rate which governs the ratio of phases) to produce acceptable quality welds (see Chapter 3).

Reynolds *et al.* [2.5] report that a bainitic and martensitic (therefore acicular by definition) microstructure has evolved in the TMAZ using the same grade of steel and a marginally lower traverse speed of 450 mm/min. The study concludes that this is a consequence of the phase transformation of austenite during fast cooling, and since no ferrite is observed in this region, evidence of FSW elevating the steel's temperature above the A_3 [2.5]. The rotational speed of this weld is not made clear in order to allow comparisons with the current welds. Still, the formation of martensite suggests that the cooling rate developed during their welding process is higher than the rate occurring herein.

The process becomes very sensitive to parameter change, i.e. variations in rotational speed in the group of fast welds (at 500 mm/min). Evidence for this is drawn from two observations; firstly, welds W24 and W25 only differ by 25 rpm in rotational speed but in view of its mechanical property assessment (see related discussion in Chapter 3), W25 is rather unstable, as if steady state conditions have not been achieved. Secondly, incomplete fusion appears on the top AD side in two of the five welds in this group (W21 and W22), within which interconnected non-metallic inclusions are detected (Figure 2.15). These flaws have a significant length with secondary paths and are clearly expected to affect the mechanical properties of the welds (Chapter 3), particularly their fatigue performance (Chapter 4).

SEM-EDS analysis of several sites containing non-metallic inclusions (one representative case is provided in Figure 2.16) recorded high concentration (wt.%) of silicon (6.5%) and zinc (36%), both of which are indicators of paint primer [2.27]. Furthermore, up to 48% oxygen and 44% iron was identified demonstrating the presence of oxide scale. Since the steel plates used herein have not received any preparation prior to welding (section 2.2.1), the results of the EDS analysis suggest that the non-metallic inclusions are a mixture of oxide scale and paint primer from the plate surfaces. Correspondingly, a separate publication [2.27] has established through EDS analysis that the non-metallic inclusions which have been drawn into the weld zone (considerably more pronounced than in the current work) during FSW of S275 structural steel are in fact oxides from the steel plate surfaces which also remained untreated prior to welding; minor traces of primer are also recorded [2.27].
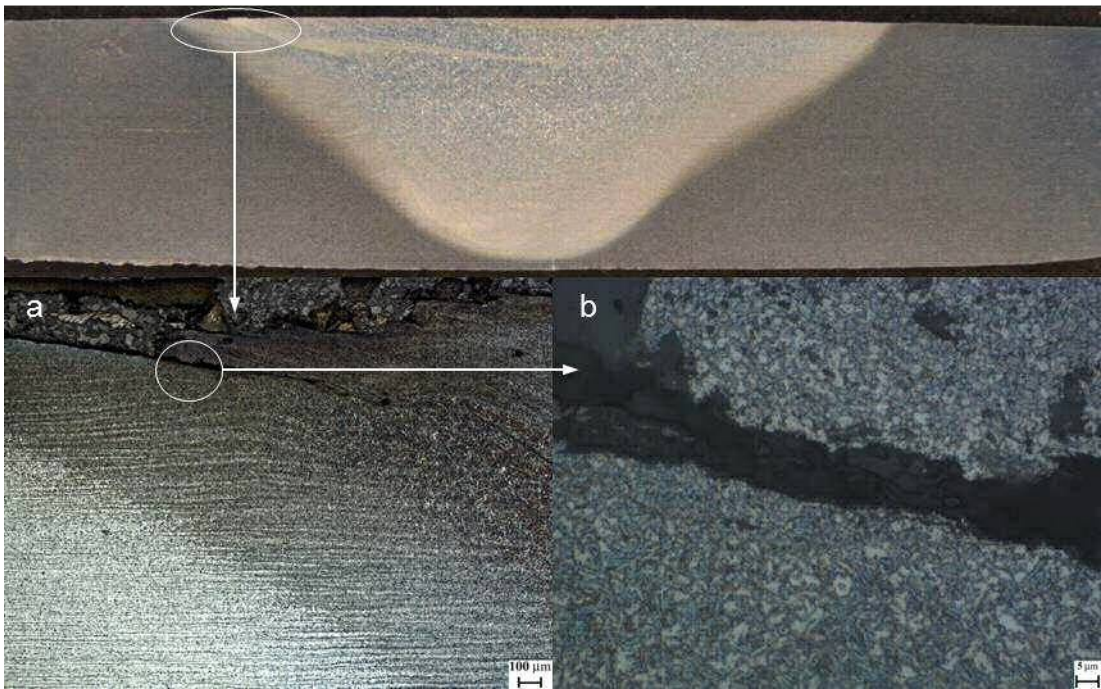
Figure 2.15. W22 AD top surface (a) [x50, Etched]; (b) [x1000, Etched]

Figure 2.16. W22 AD top TMAZ, region of SEM-EDS analysis

There is evidence of a minor weld root flaw in most of the examined welds (Figure 2.17); regions of insufficient or no welding of the original interface between the two plates. It has been noted that this is a common issue [2.28] which requires tackling through process optimisation [2.29], since such a flaw is difficult to eliminate entirely during FSW of single sided butt joints outside laboratory conditions [2.30,2.31]. Moreover, some samples present a poor quality top surface with fissures, or surface breaking flaws [2.32], introducing non-metallic inclusions in the TMAZ [2.33] which have been classified above as primer and oxides (Figure 2.18). Similar poor top surface with grooves is reported in a previous study and is attributed to the tool shoulder [2.1]. Nevertheless, both types of flaws are regarded as processing features [2.30,2.34] and are expected to be resolved as the technical expertise on FSW of steel gradually develops. As a general note, no embedded or surface breaking flaws (except those mentioned above for welds W21 and W22) are detected in the bulk of the weld zone (TMAZ) and especially in the mid AD side where the shear forces on the alloy are expected to be the highest. Thus, high speed FSW of steel grade DH36 is feasible; the process is tolerant to parameter variation in low and intermediate speeds but less tolerant at the highest speed (500 mm/min).
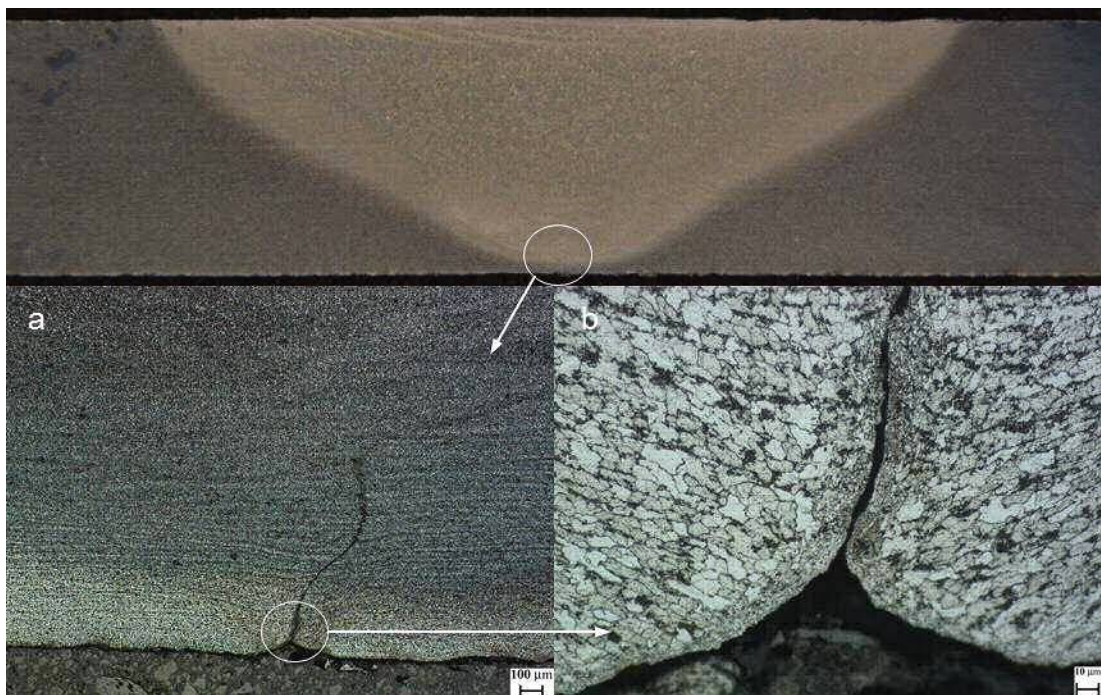
Figure 2.17. Weld root flaw in W09 (a) [x50, Etched]; (b) [x500, Etched]
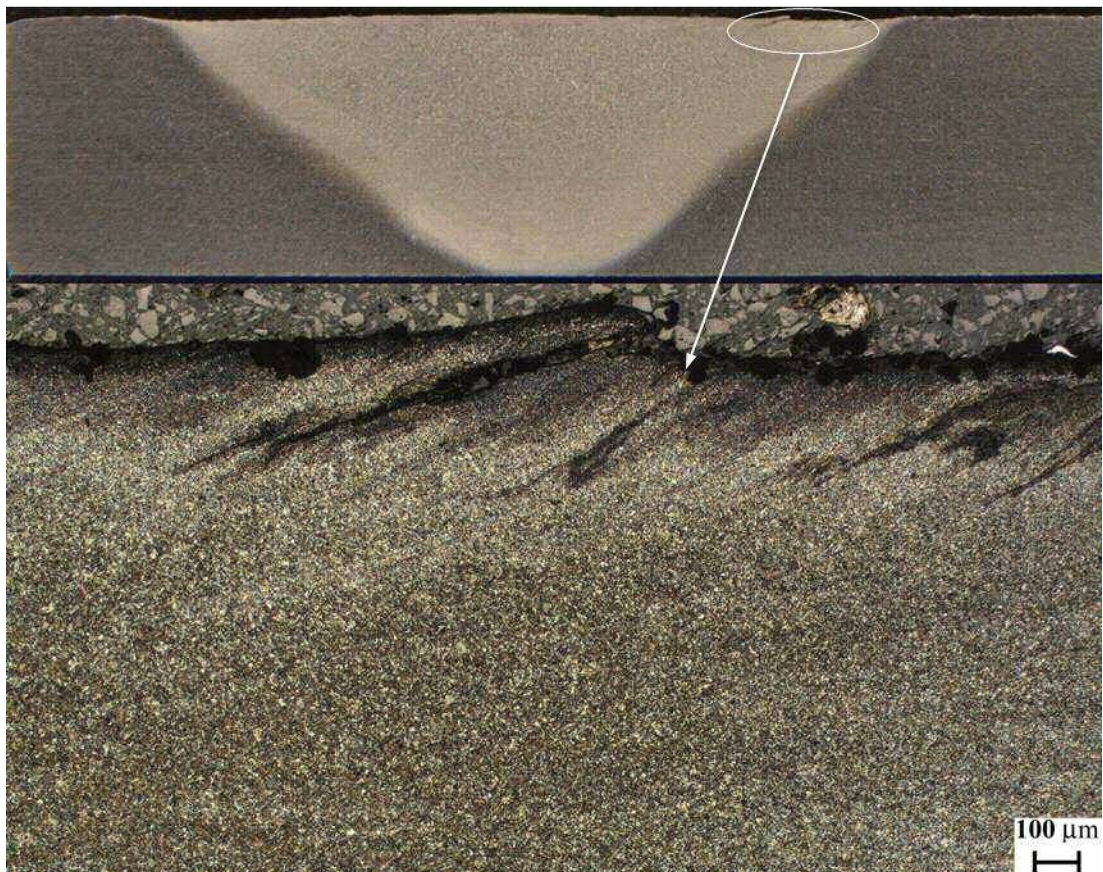
Figure 2.18. W12 RT top surface, [x50, Etched]

2.4. Conclusions

A detailed microstructural characterisation study of the 25 welds produced through the process envelope development programme has been undertaken with the intention of assessing the weld zone quality and consequently confirming the technical capacity for high traverse speed FSW. Furthermore, the link between welding parameters and evolved weld microstructures has been explored.

From this investigation, it is evident that the two more important process parameters, tool traverse and rotational speed impact heavily on the resultant microstructure. The study has demonstrated that FSW of steel grade DH36 generates a complex metallurgical system in which slow traverse speeds in the region of 100-200 mm/min result in a highly refined, ferrite rich microstructure, the intermediate traverse speeds of 250-400 mm/min produce predominantly acicular bainitic ferrites, and the fast traverse speeds (450-500 mm/min) develop

heterogeneous microstructures with distinct regions of acicular ferrite and acicular bainitic ferrite.

Moreover, the 25 parameter sets have been found to produce sound and defect-free welds, primarily in the bulk of the TMAZ; this provides further supporting evidence on the feasibility of high speed FSW in the range of 400-500 mm/min. Additionally, a number of parameters in this speed group have been identified as generating an attractive combination of acceptable quality level and economically competitive processing conditions.

Two recurrent process-related flaws have been identified in the majority of the examined welds. The weld root flaw, a routine problem in single sided friction stir butt welding and the top surface breaking flaws are expected to be addressed through new developments in the process and the FSW tool for steel.

The intricate microstructural system of steel FSW is anticipated to affect the mechanical properties of the weldments; this relation is evaluated in Chapters 3 and 4.

2.5. References

[2.1] Konkol P, Mathers J, Johnson R, Pickens J. Friction stir welding of HSLA-65 steel for shipbuilding. J Sh Prod 2003;19:159–64.

[2.2] Lienert T, Stellwag W, Grimmett B, Warke R. Friction stir welding studies on mild steel. Weld J Res Suppl 2003:1–9.

[2.3] Ozekcin A, Jin HW, Koo JY, Bangaru N V, Ayer R, Vaughn G, et al. A microstructural study of friction stir welded joints of carbon steels. Int J Offshore Polar Eng 2004;14:284–8.

[2.4] ASM International Handbook Committee. ASM Handbook Volume 4: Heat Treating. Materials Park, OH: ASM International; 2002.

[2.5] Reynolds AP, Tang W, Posada M, Deloach J. Friction stir welding of DH36 steel. Sci Technol Weld Join 2003;8:455–60.

[2.6] McPherson N, Galloway A, Cater S, Hambling S. Friction stir welding of thin DH36 steel plate. Sci Technol Weld Join 2013;18:441–50.

[2.7]   Ghosh M, Kumar K, Mishra RS. Process Optimization for Friction-Stir-Welded Martensitic Steel. Metall Mater Trans A 2012;43:1966–75.

[2.8]   Cho H-H, Kang SH, Kim S-H, Oh KH, Kim HJ, Chang W-S, et al. Microstructural evolution in friction stir welding of high-strength linepipe steel. Mater Des 2012;34:258–67.

[2.9]   Barnes SJ, Bhatti AR, Steuwer A, Johnson R, Altenkirch J, Withers PJ. Friction Stir Welding in HSLA-65 Steel: Part I. Influence of Weld Speed and Tool Material on Microstructural Development. Metall Mater Trans A 2012;43:2342–55.

[2.10] Toumpis AI, Galloway AM, Arbaoui L, Poletz N. Thermomechanical deformation behaviour of DH36 steel during friction stir welding by experimental validation and modelling. Sci Technol Weld Join 2014;19:653–63.

[2.11] Cater S, Martin J, Galloway A, McPherson N. Comparison between friction stir and submerged arc welding applied to joining DH36 and E36 shipbuilding steel. In: Mishra R, Mahoney MW, Sato Y, Hovanski Y, Verma R, editors. Frict. Stir Weld. Process. VII, Hoboken, NJ: Wiley; 2013, p. 49–58.

[2.12] Lloyd's Register. Rules for the Manufacture, Testing and Certification of Materials. London: 2014.

[2.13] Collaborative Research Project HILDA (High Integrity Low Distortion Assembly), E.U. Seventh Framework Programme (SCP2-GA-2012-314534-HILDA).

[2.14] Threadgill PL. Terminology in friction stir welding. Sci Technol Weld Join 2007;12:357–60.

[2.15] Bhadeshia HKDH. Bainite in Steels. 2nd ed. London: IOM Communications; 2001.

[2.16] Yokomizo T, Enomoto M, Umezawa O, Spanos G, Rosenberg R. Three-dimensional distribution, morphology, and nucleation site of intragranular ferrite formed in association with inclusions. Mater Sci Eng A 2003;344:261–7.

[2.17] Byun JS, Shim JH, Cho YW. Influence of Mn on microstructural evolution in Ti-killed C–Mn steel. Scr Mater 2003;48:449–54.

[2.18] Shim J-H, Byun J-S, Cho YW, Oh Y-J, Shim J-D, Lee DN. Mn absorption characteristics of Ti2O3 inclusions in low carbon steels. Scr Mater 2001;44:49–54.

[2.19] Maddox SJ. Fatigue Strength of Welded Structures. 2nd ed. Cambridge: Woodhead Publishing; 2002.

[2.20] Le Jolu T, Morgeneyer TF, Denquin A, Gourgues-Lorenzon AF. Fatigue lifetime and tearing resistance of AA2198 Al–Cu–Li alloy friction stir welds: Effect of defects. Int J Fatigue 2015;70:463–72.

[2.21] Parunov J, Ćorak M, Gilja I. Calculated and prescribed stress concentration factors of ship side longitudinal connections. Eng Struct 2013;52:629–41.

[2.22] Romanova V, Balokhonov R, Schmauder S. Three-dimensional analysis of mesoscale deformation phenomena in welded low-carbon steel. Mater Sci Eng A 2011;528:5271–7.

[2.23] Nascimento MP, Ribeiro RB, Voorwald HJC. Fatigue Crack Growth in Re-welded AISI 4130 High Strength Steel. 14th Eur. Congr. Fatigue, Cracow, Poland: 2002.

[2.24] Tattoli F, Pierron F, Rotinat R, Casavola C, Pappalettere C. Full-field strain measurement on titanium welds and local elasto-plastic identification with the virtual fields method. AIP Conf. Proc., vol. 1315, 2010, p. 860–5.

[2.25] Caballero FG, Chao J, Cornide J, García-Mateo C, Santofimia MJ, Capdevila C. Toughness deterioration in advanced high strength bainitic steels. Mater Sci Eng A 2009;525:87–95.

[2.26] Mochizuki M, Higuchi R, Katsuyama J, Toyoda M. Evaluation of Strength Characteristics Considering Microscopic Heterogeneity of Structural Steels and Weld Zone by Using FEM-MD Coupling Method. Proc. ASME Press. Vessel. Pip. Conf., vol. 6, San Antonio, TX: ASME; 2007, p. 117–24.

[2.27] Baillie P, Campbell SW, Galloway AM, Cater SR, McPherson NA. Friction stir welding of 6 mm thick carbon steel underwater and in air. Sci Technol Weld Join 2015;20:585–93.

[2.28] Ji S, Xing J, Yue Y, Ma Y, Zhang L, Gao S. Design of friction stir welding tool for avoiding root flaws. Materials (Basel) 2013;6:5870–7.

[2.29] Dickerson T, Przydatek J. Fatigue of friction stir welds in aluminium alloys that contain root flaws. Int J Fatigue 2003;25:1399–409.

[2.30] Kadlec M, Růžek R, Nováková L. Mechanical Behaviour of AA 7475 Friction Stir Welds with the Kissing Bond Defect. Int J Fatigue 2014;74:7–19.

[2.31] Santos TG, Miranda RM, Vilaça P. Friction Stir Welding assisted by electrical Joule effect. J Mater Process Technol 2014;214:2127–33.

[2.32] British Standards Institution. BS 7910. Guide to methods for assessing the acceptability of flaws in metallic structures. London: 2013.

[2.33] Toumpis A, Galloway A, Cater S, McPherson N. Development of a process envelope for friction stir welding of DH36 steel – A step change. Mater Des 2014;62:64–75.

[2.34] Zhou C, Yang X, Luan G. Effect of root flaws on the fatigue property of friction stir welds in 2024-T3 aluminum alloys. Mater Sci Eng A 2006;418:155–60.

3. Mechanical property evaluation of friction stir welded steel grade DH36

3.1. Introduction

Through the process parameter development programme detailed in Chapter 1, the state of the art in FSW of steel grade DH36 has been increased from the conventionally adopted traverse speed of 100 mm/min to a more commercially attractive speed of 400 mm/min and potentially up to 500 mm/min. Microstructural characterisation of the extensive set of produced welds has shown that the developed microstructure is highly dependent upon the newly trialled parameter sets of increasing traverse speed, from refined ferrite grains in slow speeds to acicular ferrite and acicular bainitic ferrite in the fast. Hence, FSW of structural steel at high speeds is feasible but the impact of this complex microstructural system on weld mechanical properties needs to be assessed.

A number of pertinent studies [3.1–3.8] on FSW of various steel grades have been produced in recent years, developing the fundamental knowledge on this joining process. Yet, publications specific to welding of structural steel remain sparse. An earlier mechanical property evaluation of DH36 steel welds with regard to FSW parameters utilised notes that the weld hardness demonstrates a continuous increase from parent material to nugget, with a variation of approximately 190 HV up to the peak hardness of the fast weld [3.1]. The tensile tests reveal significant overmatching of all welds; longitudinal tensile tests show that the yield strength (YS) of the welds is higher than the parent plate's ultimate tensile strength (UTS), and this is attributed to the developed bainite / martensite weld microstructure being very different to the original ferrite / pearlite. In all, weld hardness and strength are seen to increase with increasing welding speed. However, the effect of increasing rotational speed on weld properties is not considered in this study [3.1].

A separate study explores the FSW of X80 and L80, two grades of steel which are mainly employed in the oil and gas industry [3.2]. As above [3.1], the hardness of the L80 friction stir welds is seen to gradually rise from base material to heat affected zone (HAZ) and substantially increase in the thermo-mechanically affected zone (TMAZ). It is observed that the rotational speed greatly affects the weld

hardness; therefore, the study proposes that the weld hardness distribution can be tailored by the appropriate use of welding parameters like traverse and rotational speed, and tool plunging force [3.2]. Likewise, the X80 steel welds present higher hardness than the parent plate, with a notable peak in the advancing (AD) side of the TMAZ [3.2].

Two prior studies on FSW of mild steel (AISI 1018) [3.3] and high strength structural steel (HSLA-65) [3.4] reach comparable results while welding at traverse speeds in the range of 25-140 mm/min (characterised as slow traverse speeds herein). In contrast to the previously discussed papers [3.1,3.2], both research groups find minor hardness variations from parent material to stir zone (central TMAZ) in the mid-thickness of welds, ranging from 20 to 40 HV. Actually, Konkol *et al.* [3.4] report that the TMAZ is mildly harder than the parent material, with a peak on the retreating (RT) side, whereas the HAZ is marginally softer. The latter could be attributed to HAZ grain coarsening to some extent, as a result of high heat input and low cooling rate due to a combination of slow welding speed and possible high rotational speed; yet, the applied rotational speed is not disclosed. As in most relevant testing programmes, the transverse tensile samples in both studies fractured in the base material, denoting welds of better tensile properties than the parent plate [3.3,3.4].

McPherson *et al.* [3.5] investigate the potential introduction of FSW in the shipbuilding industry through mechanical property assessment of DH36 steel joints and comparison to submerged arc welding (SAW). Variations in hardness distribution of friction stir welds are considered minor and certainly not expected to produce adverse effects. Likewise, impact toughness levels for FSW and SAW samples are reported to be similar and within classification society (class) impact requirements. The welds' tensile behaviour is not discussed in detail, however all transverse tensile samples fractured in the parent material. The positive findings of a small scale fatigue testing programme are discussed in Chapter 4; still, this study [3.5] concludes that there is sufficient evidence to establish FSW as a process that can deliver DH36 steel joints within shipbuilding specifications.

More publications [3.6,3.7] assess the possible introduction of FSW of steel in other sectors. Research work relevant to the automotive industry aims to optimise the friction stir lap welding of martensitic M190 steel by employing ten varying parameter sets [3.6]. It is observed that the hardness distribution of each weld varies substantially, from parent plate to HAZ to weld nugget (central TMAZ), with

pronounced drops at the inner HAZ. The results of the tensile shear tests show that all samples fractured in the vicinity of the inner HAZ that seems to be the weakest region due to the developed ferrite / pearlite microstructure. Ghosh *et al.* [3.6] however do not proceed in developing new sets of parameters which will improve the mechanical properties of the weld zone, consequently weakening their case for an optimisation study. The capacity of FSW to potentially substitute electric arc welding of API X100 linepipe steel is explored by Cho *et al.* [3.7]. Micro-hardness measurements show that the stir zone hardness is considerably increased compared to all other weld regions, mainly due to its developed acicular bainitic ferrite microstructure. The minimum hardness, even lower than the base material, is detected in the HAZ [3.7]; this may be a consequence of possible grain coarsening due to high heat input by the parameter set employed (450 rpm – 127 mm/min). Still, no other mechanical properties of the weldments are assessed to confirm the inferior (as anticipated by the reduced hardness) strength of this region as previously [3.6]. Quite similarly, Barnes *et al.* [3.8] find appreciably harder weld nuggets than the HSLA-65 base metal, an observation aligned with the microstructure of principally hard phases which is formed. Again, the minimum hardness is recorded in the over-tempered outer HAZ of the slowest traverse speed used, where coarser grains are seen [3.8].

Above review of the relevant literature reveals contrasting observations on hardness distribution of steel friction stir welds, varying with grade of steel being examined and processing parameters employed, mainly traverse speed. In addition, impact toughness data with regard to differing weld parameters are especially rare in publications. However, there is general agreement in mechanical property evaluation; consistently better transverse tensile properties of the welds compared to the parent material are established.

Although a step change in the welding traverse speed has been achieved (Chapter 1), particularly within the context of marine applications, the purpose of the present study is to assess the effect of this increase on the mechanical properties of the joint. The objective is to establish an initial interpretation of the relation between resultant microstructure and developed mechanical properties through transverse tensile testing, micro-hardness measurements and Charpy impact pendulum testing of the 25 DH36 structural steel friction stir butt welds (2000 mm long) which were trialled.

3.2. Experimental procedures

3.2.1. Tensile testing

Transverse tensile tests were conducted in parallel to the microstructural examination study (Chapter 2) to further support the development of the process envelope, in that the tensile properties were assessed using a consistent testing programme. This testing programme enabled the determination of the YS and UTS that the applied sets of weld parameters produce on the welded plates, along with the position of fracture (parent plate or weld metal).

All transverse tensile tests were performed on a calibrated Instron 8802 servo-hydraulic uniaxial tensile testing system in accordance with ISO Standards [3.9]. Three samples were sectioned from each weld presented in Table 1.1 in line with the same specifications in order to maintain the repeatability of results (Figure 3.1). In addition, three samples were sectioned and tested from the base material of three randomly selected welded plates but in parallel to the weld direction. Thus, the mechanical properties of DH36 in the longitudinal direction were established and provided values for comparison. The consistent control method used was an extension rate of 0.5 mm/min up to extension of 1.25 mm, then 5 mm/min up to fracture.
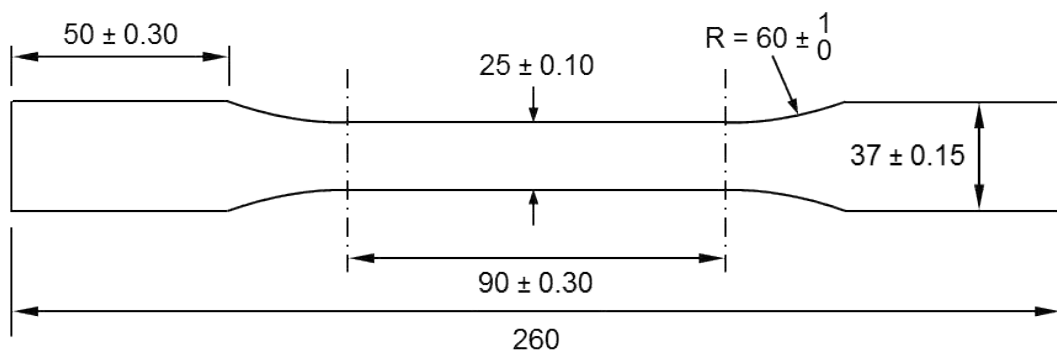
Figure 3.1. Transverse tensile sample of rectangular cross section (thickness 6 mm)

3.2.2. Hardness and impact toughness

Micro-hardness measurements were taken across the entire weld zone using a Mitutoyo hardness tester (Figure 3.2). The instrument was calibrated by employing a sample of known and uniform hardness; the measuring accuracy is ±5 HV. The measurements were performed by applying a load of 200 gf and using a grid

spacing of 1 mm (for both x and y directions) (Figure 3.3).
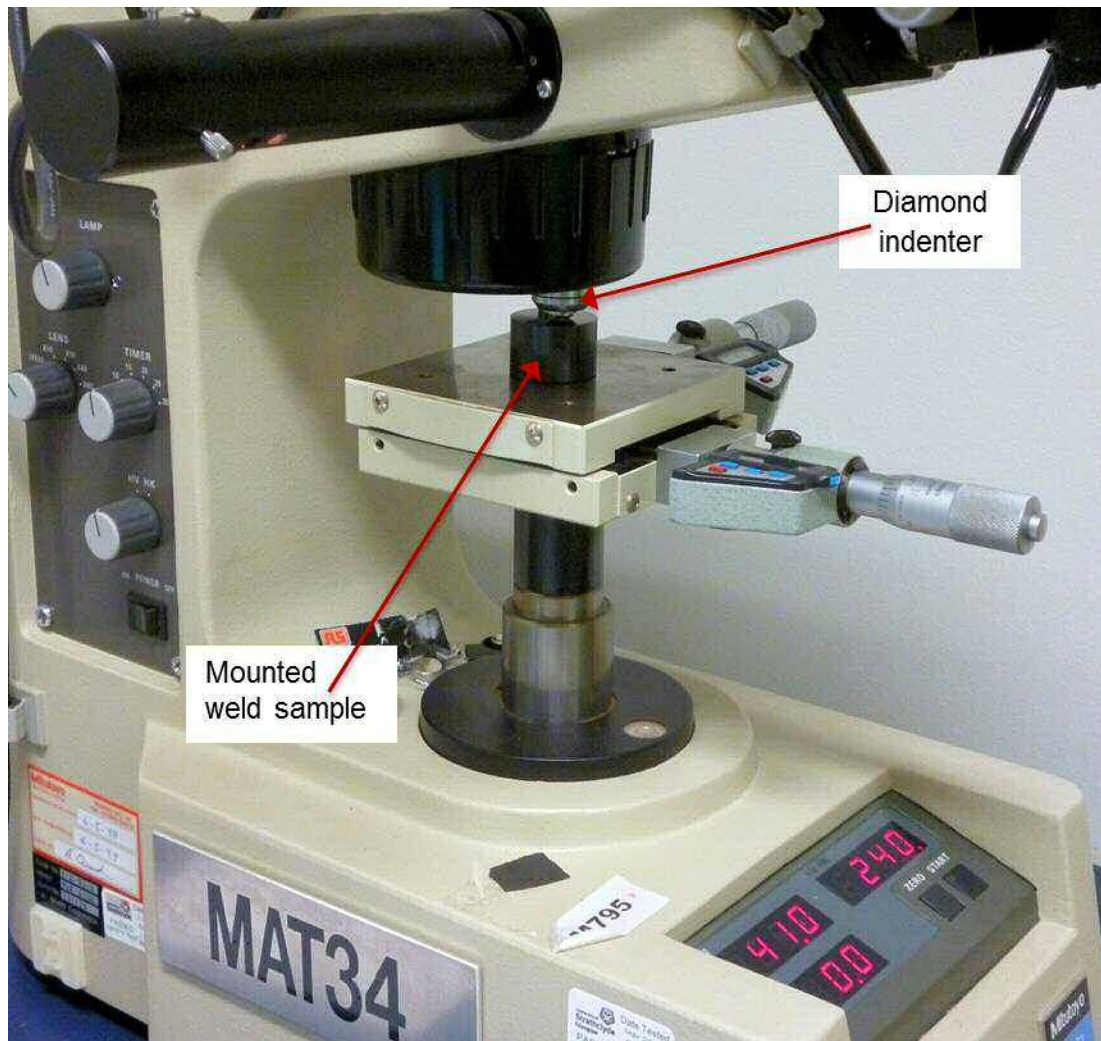
Figure 3.2. Mitutoyo hardness tester

Charpy impact tests with the standard V-notch were performed according to ISO Standards [3.10] in order to evaluate the toughness of the weld region in relation to the welding parameters used. Samples were sectioned perpendicular to the weld centreline and transverse to the weld direction (Figure 3.4). One sample was sectioned with the notch axis of symmetry on the weld centreline. To examine the full width of the weld region, three additional samples were sectioned towards both sides of the weld in 1.5 mm increments (Figure 3.5). In this configuration, each sample with the notch axis at 4.5 mm from the weld centreline included a small percentage of parent material which was essentially the same for either side. All other samples fully consisted of thermo-mechanically stirred material.

Reduced-section samples of 5 mm width were used due to the plate thickness of 6

mm [3.10]. In total, three sets of seven tests were performed in room temperature (~20°C) for each set of parameters to improve the accuracy of the results.
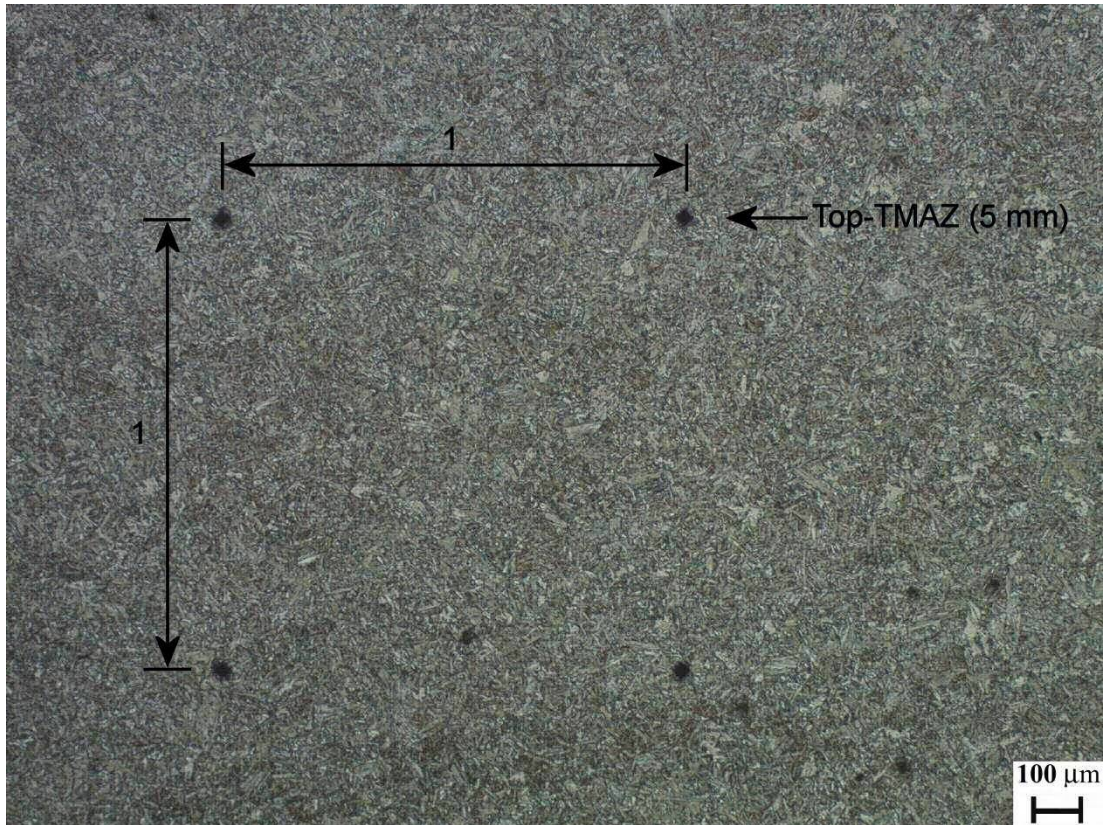

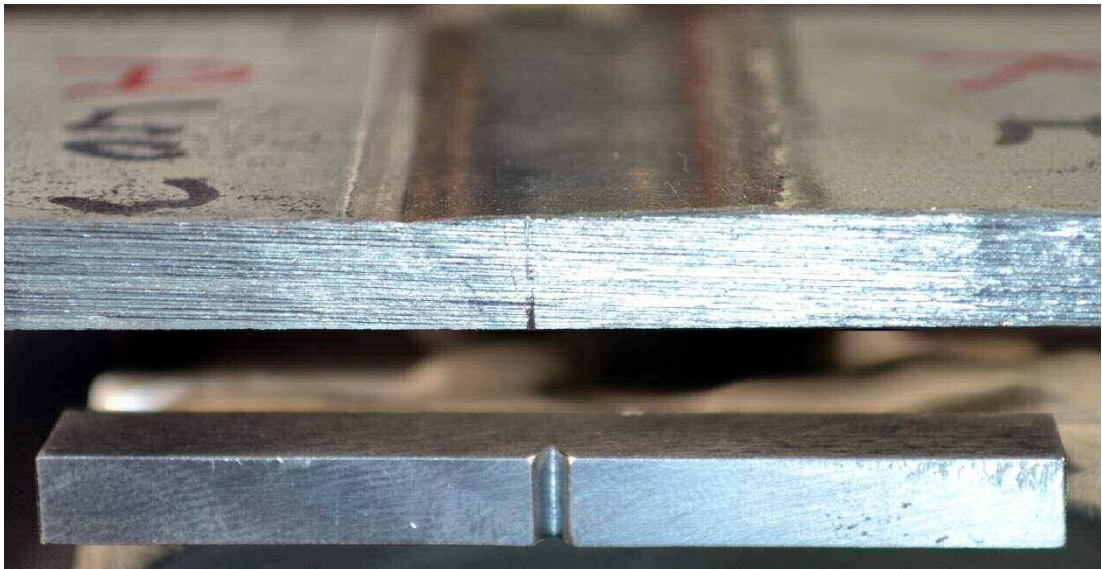**Figure 3.3. Grid spacing for micro-hardness measurements, image from weld W07 [x50, Etched]**

Figure 3.4. Charpy sample and notch orientation (bottom) relative to welded plate section (top)
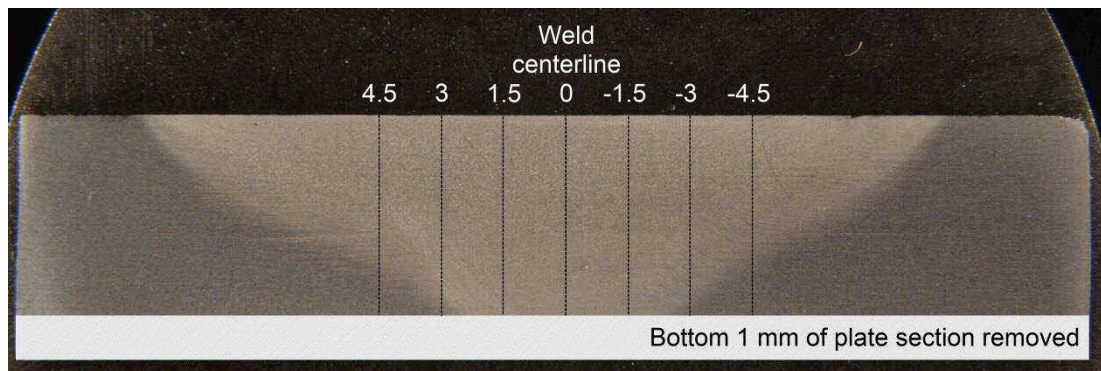
Figure 3.5. Typical macrograph showing the position of the notch axis of symmetry of the seven Charpy samples examined from each weld [Etched]

3.3. Results and discussion

3.3.1. Tensile properties

Stress vs. strain charts were plotted for each transverse tensile test to evaluate the consistency of the generated data and to determine the YS and UTS of each sample. The calculated tensile properties are outlined in Table 3.1.

The samples of 19 out of the 25 welds fractured in the parent material rather than the weld. This demonstrates that these 19 sets of welding parameters produced welds of higher strength than the parent material. All samples prepared from the 18 slow and intermediate welds (as classified in Table 1.1) fractured in the parent material. Even welds which consist of high acicular bainitic ferrite phase ratio and therefore could be expected to show brittle behaviour proved to be stronger than the parent material. Identical tensile behaviour is reported in other studies [3.1,3.3-3.5,3.11], where all transverse tensile samples produced from welds of similar sets of parameters fractured in the parent material, well away from the HAZ. Equally, welds with a heterogeneous microstructure (e.g. W08), i.e. containing stress concentration regions which may act as crack initiation sites (as detailed in Chapter 2), or welds with minor process related flaws such as weld root flaw or fissures on the top surface fractured in the parent material; the latter has also been underlined in another investigation [3.11].

The group of fast welds (450 & 500 mm/min) demonstrated a different behaviour. All samples from welds W19, W21, W22 and W23 fractured in the weld, and specifically in a brittle-like manner on the outer boundary of the advancing side. This fracture

site corresponds to the AD outer top TMAZ region where non-metallic inclusions were found to be interconnected in an incomplete fusion characteristic (Figure 3.6), also described as lap [3.12]. This feature was mainly observed in welds W21 and W22 (Chapter 2). It is worthy of note that the YS of these welds is not reduced compared to the range of values exhibited by all other weldments (Table 3.1); this is explained by the highly refined microstructure of the TMAZ, discussed in Chapter 2, which develops high strength weld zone. Fracture occurred in the AD TMAZ because these incomplete fusion paths acted as preferential sites for crack initiation and propagation.

Table 3.1. Summary of DH36 FSW transverse tensile test results (PM: parent material)

| Reference number | Weld details | | Transverse tensile testing at room temperature | | | |
	Rotational speed, rpm	Traverse speed, mm/min	Yield strength (0.2%), MPa	UTS, MPa	Fracture region	Fracture mode
Slow						
W01	200	100	395 408 398	530 540 536	PM	Ductile
W02	200	110	390 394 386	530 536 535	PM	Ductile
W03	200	120	401 396 392	536 529 527	PM	Ductile
W04	200	130	406 407 401	535 536 533	PM	Ductile
W05	200	143	398 400 409	521 527 529	PM	Ductile
W06	200	156	405 396 397	531 523 525	PM	Ductile
W07	400	200	320 380 391	512 516 528	PM	Ductile
Intermediate						
W08	300	250	382 385 386	519 514 522	PM	Ductile
W09	400	250	384 384 381	525 523 519	PM	Ductile
W10	400	275	383 384 378	522 521 525	PM	Ductile

|						
W11	400	300	406 401 406	516 509 517	PM	Ductile
W12	400	325	387 387 388	526 525 524	PM	Ductile
W13	450	350	399 405 396	539 544 534	PM	Ductile
W14	500	350	412 400 407	522 520 518	PM	Ductile
W15	400	375	390 390 392	528 530 525	PM	Ductile
W16	450	400	397 396 393	540 534 532	PM	Ductile
W17	500	400	402 400 411	523 523 521	PM	Ductile
W18	550	400	408 409 411	521 521 523	PM	Ductile
Fast						
W19	575	450	403 416 409	487 461 471	Weld, AD side	Brittle
W20	700	450	388 384 387	528 499 521	PM Weld, AD side	Ductile Brittle
W21	600	500	383 384 400	457 458 488	Weld, AD side	Brittle
W22	650	500	412 408 417	526 563 534	Weld, AD side	Brittle
W23	575	500	423 429 442	433 462 480	Weld, AD side	Brittle
W24	700	500	382 388 401	519 523 546	PM	Ductile
W25	675	500	397 390 394	514 458 532	Weld, AD side PM	Brittle Ductile
PM – 1 **PM – 2** **PM – 3**	Longitudinal direction		339 340 340	521 525 526	PM	Ductile
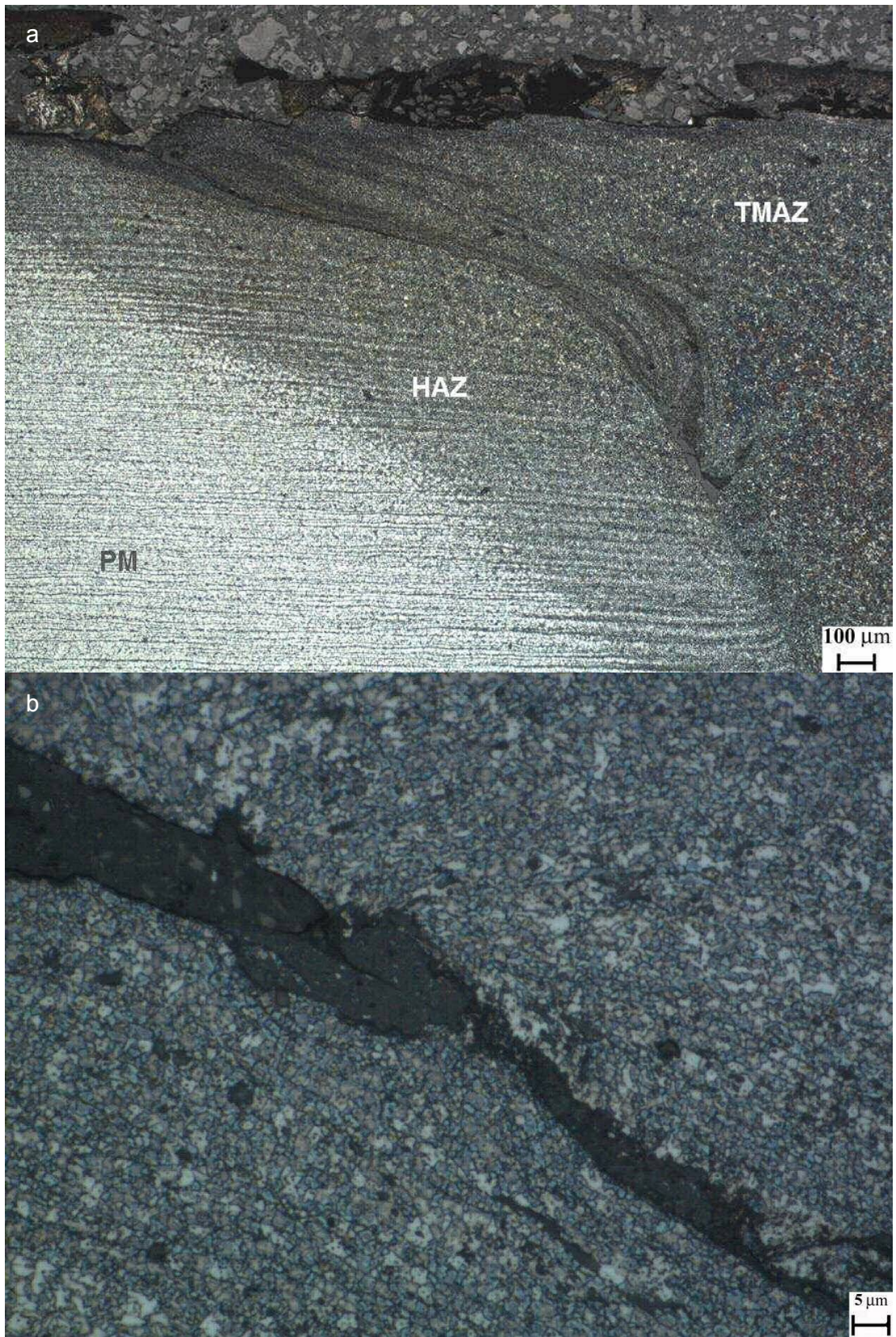
Figure 3.6. W21 (600 rpm – 500 mm/min) AD outer top TMAZ (a) [x50, Etched]; (b) [x1000, Etched]

Two samples from weld W25 fractured inside the weld (brittle fracture on outer AD side) and one fractured in the parent material in a ductile manner (Figure 3.7). In fact, there is a noteworthy difference in the fracture surfaces of the first two samples; one sample's fracture surface has the FSW tool's features imprinted on it (on the mid-AD TMAZ, Figure 3.7a). This denotes that the metal was mechanically worked (similar to forging) by the FSW tool in this region rather than thermo-mechanically stirred, perhaps due to lower heat input.
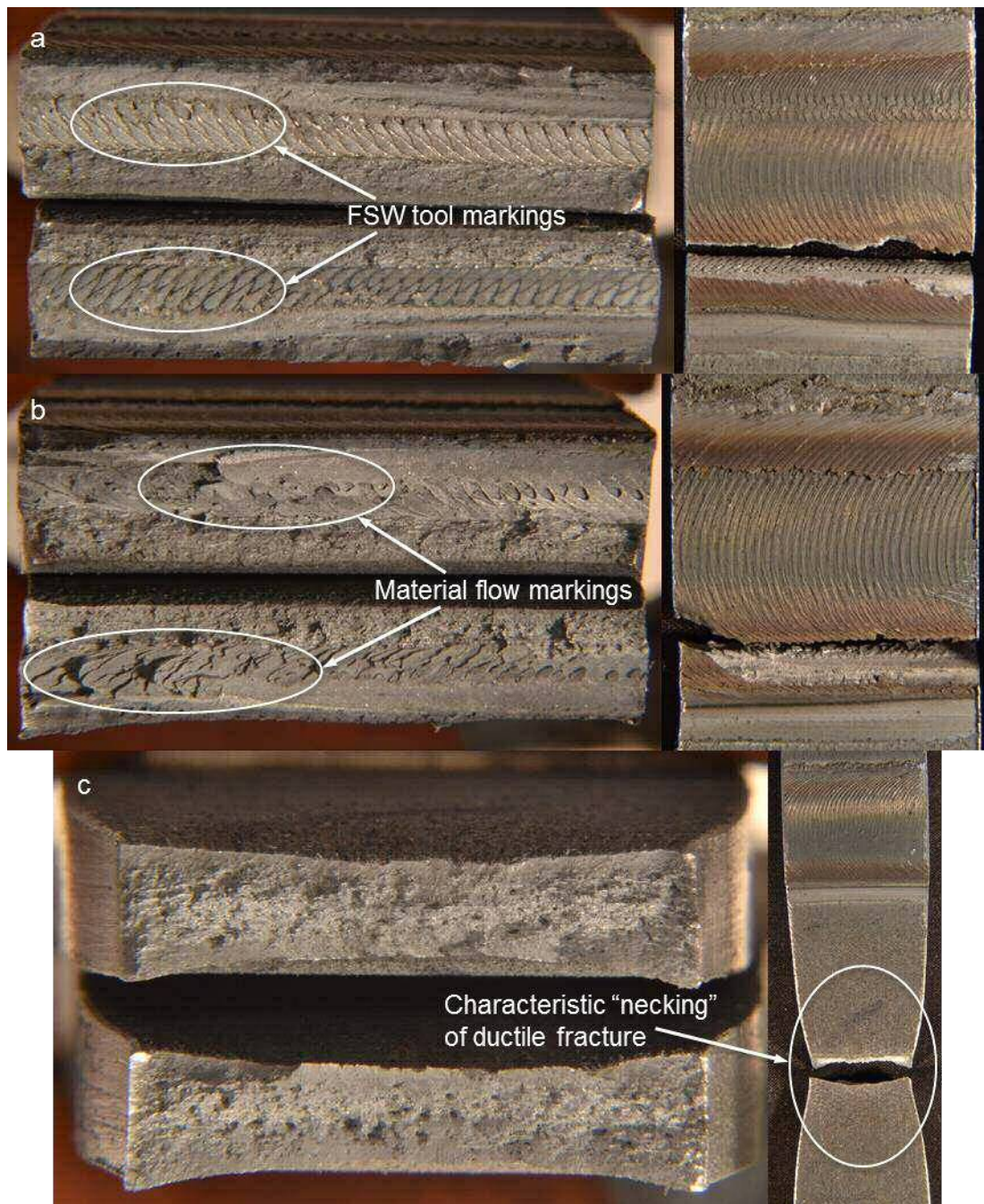

Figure 3.7. Three samples of W25 exhibiting different fracture behaviour

The second sample reveals markings consistent with lower (than required) temperature material flow patterns, suggesting lower heat input in this region (Figure 3.7b). Figure 3.7c presents the third sample examined from weld W25, with a typical ductile fracture. As briefly alluded to in Chapter 2, such observations indicate that this set of parameters is on a threshold value producing welds where steady state conditions have not been reached (an "unstable" weld). Comparable unstable behaviour was displayed by the tensile samples of weld W20.

W24 is the only one of the fast weld category that fractured in the parent material with a typically ductile fracture. Although a very heterogeneous microstructure (with possible stress concentration regions associated with this heterogeneity) has been observed (Chapter 2), all three samples proved to be stronger than the DH36 base material. It would appear that this set of parameters delivered a suitable ratio of traverse and rotational speed that is translated into acceptable tensile behaviour. This is attributed to the grain refinement and a satisfactory balance of microstructures overtaking the negative effects of heterogeneity.

3.3.2. Hardness distribution

For reporting purposes, two representative welds from each group of slow, intermediate and fast welds will be discussed herein with reference to the weld region hardness. In addition, all hardness values presented in Figure 3.8 refer to the top-TMAZ of each weld sample, i.e. 1 mm below the top surface (Figure 3.3). The hardness of the slow and intermediate welds (Figure 3.8a & b) is higher than that of the parent material, a finding also reported elsewhere [3.2,3.8]. Class rules for fusion welding require that the maximum hardness does not exceed 350 HV for steel grades with a nominal minimum yield strength up to 420 MPa (as is the case with DH36) [3.13]. All slow and intermediate welds apart from W15, which displays marginally higher hardness values across the weld zone, would be deemed acceptable should they were assessed by fusion welding rules [3.13], also considering their satisfactory transverse tensile test results (section 3.3.1). The hardness of each weld is symmetrical across the weld region, with a relatively even distribution from advancing to retreating side of the TMAZ. Hardness data recorded by Lienert *et al.* [3.3] for FSW of mild steel with a traverse speed comparable to W01 demonstrate such a small degree of variability. In the current study, the hardness of the weld region in both groups is seen to increase with increasing cooling rate of the weld. In absolute terms, both intermediate welds have produced

higher hardness values compared to the group of slow welds, as a result of their lower heat input (Table 1.1) which has generated higher cooling rates hence increasing bainite content. This relationship of increasing hardness with higher traverse speed is also highlighted by Reynolds *et al.* [3.1].

In the group of fast welds (Figure 3.8c), W24 exhibits high hardness values but narrowly within the above mentioned class rules [3.13], with minor variations across the weld region. As discussed in Chapter 2, evenly distributed weld material hardness, i.e. the absence of a discontinuity, should not develop stress concentration regions; hence, this partly explains the excellent behaviour of this specific weld's samples in the transverse tensile tests. As expected due to its higher cooling rate, W25 is seen to produce higher hardness values particularly on the advancing side, and with more pronounced variations (Figure 3.8c). This reflects the microstructural heterogeneity of this weld with regions of varying bainite concentration, thus suggests that different regions of the welded material, as it is stirred from the advancing to the retreating side, are experiencing different cooling rates. The very high hardness value on the outer advancing side should correlate with the same weld's tensile samples fracturing at the same position. In absolute terms again, the fast welds have produced similar hardness levels to the intermediate group indicating similar cooling rates.

Such variations in the hardness distribution within the TMAZ of most welds currently examined are often reported by other researchers. Ghosh *et al.* [3.6] note that the significant variations of hardness within the weld zone of all welding parameters examined occur due to the heterogeneity of the resultant microstructure, from weld nugget to HAZ. Further, the differences in peak hardness between weld nugget regions depend on the weld parameters used hence the subsequent cooling rate of each weld [3.6]. A separate study [3.7] argues that the substantially higher hardness found in the stir zone is caused by the acicular shaped bainitic ferrite microstructure. Similar microstructure is observed in most of the intermediate and high speed welds of this study but with smaller variations in the hardness of the TMAZ, suggesting a reasonably homogeneous microstructural distribution.
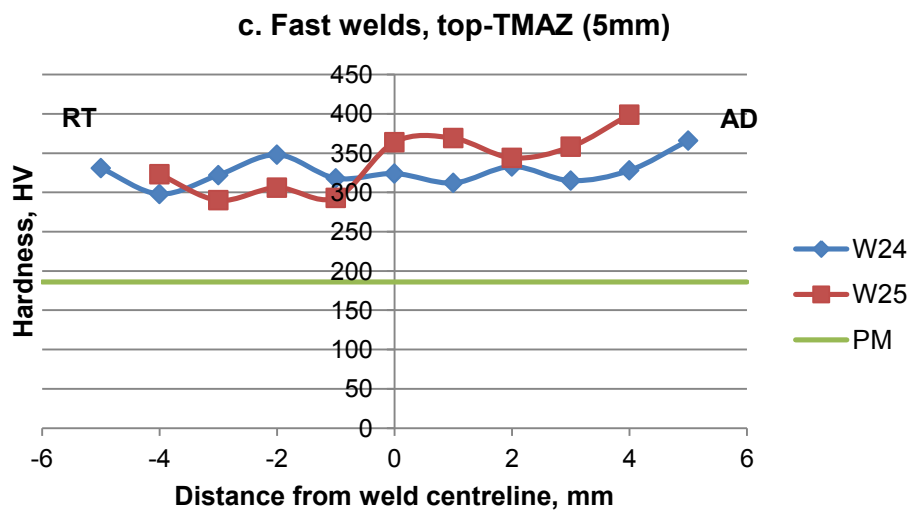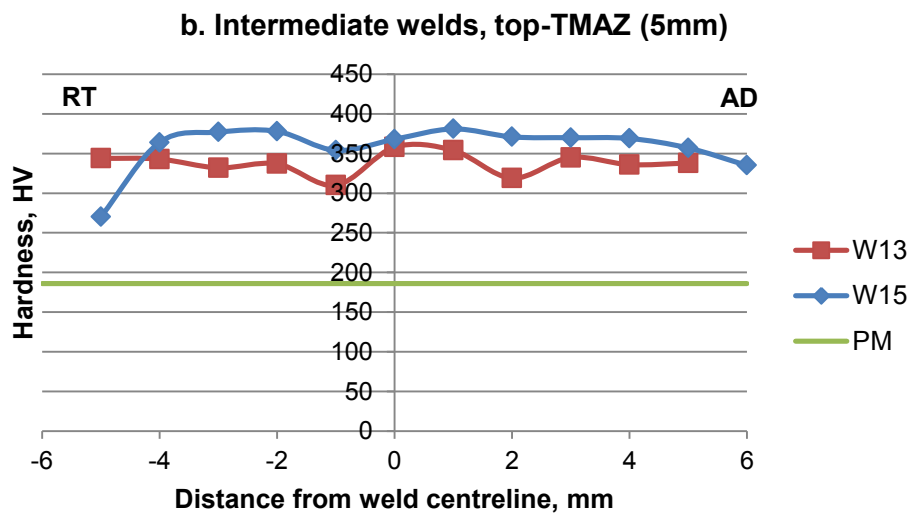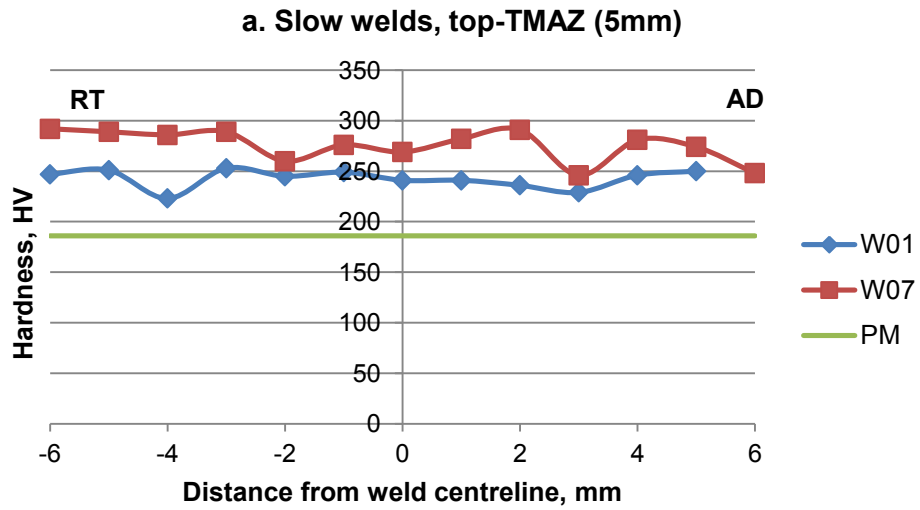
Figure 3.8. Hardness distribution of the weld region for three groups of weld parameters

3.3.3. Impact toughness measurements

The impact toughness data presented in Figures 3.8 & 3.9 have been normalised to a 10 x 10 mm equivalent by a scaling factor of 3/2 in accordance with class rules [3.13], also discussed by McPherson *et al.* [3.5]. The impact toughness of most welds at 20°C is seen to be reduced compared to the parent material (Figure 3.9). The slow welds follow a similar pattern of peak values on the weld centreline and lowest values nearing both sides of the TMAZ. Impact toughness data generated by Cater *et al.* [3.11] present an analogous distribution for slow traverse speed FSW of E36, a grade of steel that is close to DH36 in terms of chemical composition and shipbuilding applications. Herein, the presence of acicular ferrite in W07 should have a detrimental effect on the impact toughness when compared to the ferrite-rich (with refined grains of random geometry) microstructure in W01. This issue of acicular ferrite possibly resulting in lower weld toughness is outlined in one more study [3.5]. An earlier publication [3.4] reports even more reduced impact toughness for the mid-TMAZ of HSLA-65 FSW at the same range of traverse speeds. Still, it is argued that the recorded low toughness could be considered adequate for this grade of steel in shipbuilding applications [3.4].
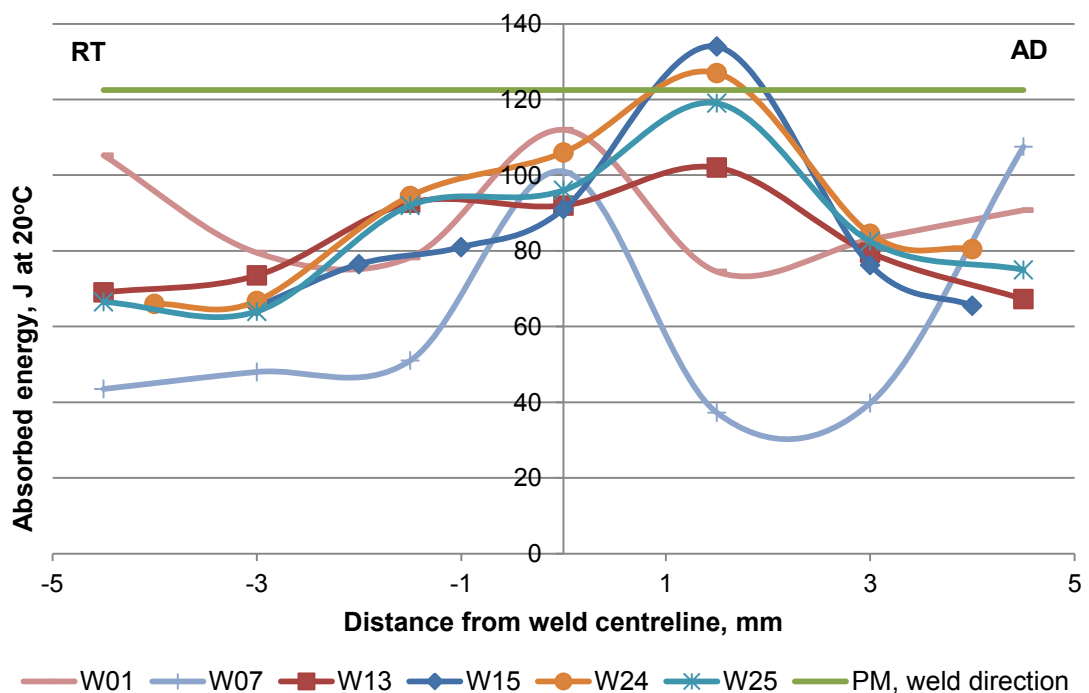

Figure 3.9. Impact toughness distribution in the weld region for six indicative sets of weld parameters

All intermediate and fast welds exhibit a similar trend in impact toughness distribution, with a peak observed in the inner TMAZ of the advancing side and gradual decrease towards the outer boundaries of the TMAZ on both sides. The homogeneous acicular bainitic ferrite microstructure observed in W15 has produced marginally higher impact toughness in the AD TMAZ than the heterogeneous microstructure of W24. The latter has been characterised as having two distinct structures, acicular bainitic ferrite and acicular ferrite (Chapter 2); as with weld W07 discussed above, the presence of acicular ferrite seems to be responsible for the slightly reduced impact toughness of W24. Considerable variation between the impact toughness of the advancing and retreating sides is apparent in the intermediate and fast welds. It should be highlighted that two sets of parameters which were previously identified as being well balanced, W15 and W24, overmatch the parent plate's impact toughness in the inner AD TMAZ.

The data in Figure 3.9 reveal that increasing the traverse speed from 100 mm/min to 375 mm/min and 500 mm/min delivers a significant effect of improving the impact toughness on the advancing side, although having a lesser improvement on the retreating side. The impact toughness on both sides of the outer TMAZ however is seen to decrease to some extent with the intermediate and fast traverse speed. Still, the improvement in impact toughness offers a level of confidence in increasing the FSW traverse speed.

A closer inspection of the 500 mm/min traverse speed welds (Figure 3.10) discloses an impact toughness pattern which is in agreement with their tensile test results. The five welds are essentially separated into two distinct categories; the impact toughness of W21, W22 and W23 is seen to be reduced with respect to the parent material, with a peak on the mid or inner AD TMAZ. The same three welds exhibited consistent brittle fracture in the weld zone in the transverse tensile tests. As anticipated, the observed decline in ductility, from originally ductile parent material to brittle weld, has been detrimental to the toughness of the material [3.14]. In contrast, the two welds of this group which showed different behaviour in tensile testing, W24 with higher strength than the parent plate and W25 with mixed tensile results, demonstrate better impact toughness and analogous distribution, which matches the parent material on the inner AD TMAZ.
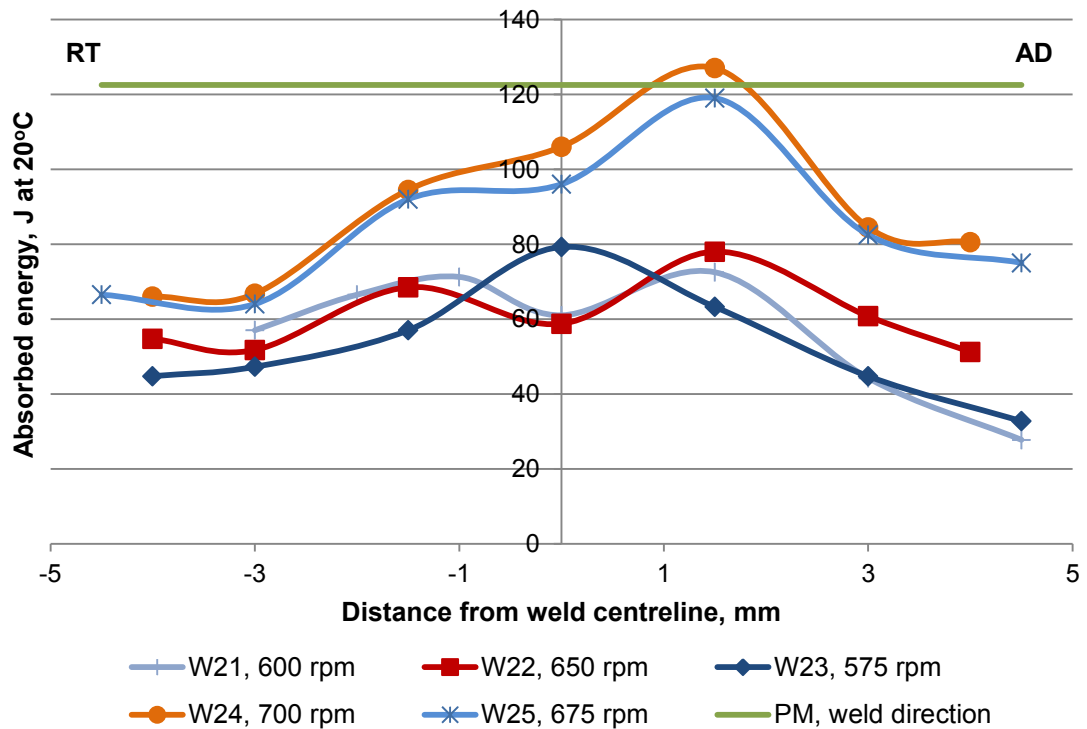
Figure 3.10. Impact toughness distribution in the weld region for the 500 mm/min traverse speed welds

3.4. Conclusions

The range of widely acceptable FSW traverse speeds in steel has been substantially expanded through the process parameter development programme reported in Chapter 1. These newly established FSW parameters are seen to generate a complex metallurgical system, and this diverse microstructure is expected to influence the mechanical properties of the weldments. Therefore, this study has assessed the quality of the produced welds by means of mechanical testing to provide an initial understanding of the relationship between weld microstructures and mechanical properties.

The slow and intermediate group welds demonstrate higher strength than the parent material in transverse tensile testing. This behaviour is exhibited irrespective of possible stress concentration regions due to heterogeneous microstructure which has been observed in certain welds, or sporadic appearances of surface breaking flaws such as weld root flaws and top surface laps. A number of weld parameters have been identified in tensile testing which may produce fast (in the region of 400

mm/min) or very fast (potentially up to 500 mm/min) welds of acceptable quality that are technically competitive to conventional fusion welding techniques, particularly in the shipbuilding industry. However, this remains to be confirmed through extensive fatigue testing. The process has shown to be less tolerant to parameter variations at these high welding traverse speeds, where most tensile samples fractured in the weld zone or displayed unstable behaviour. Hence, there is considerable scope for further refinement via additional examination of high speed welds.

Moreover, this step change in the potential competitiveness of FSW of steel through increased welding traverse speeds is seen to improve the impact toughness of the weld without compromising strength and hardness as shown by the Charpy impact testing results and micro-hardness measurements.

The fatigue performance of steel welds is of critical importance in marine applications; thus, a comprehensive and detailed fatigue testing programme of steel FSW has been undertaken and is presented as a separate study in Chapter 4.

3.5. References

[3.1] Reynolds AP, Tang W, Posada M, Deloach J. Friction stir welding of DH36 steel. Sci Technol Weld Join 2003;8:455–60.

[3.2] Ozekcin A, Jin HW, Koo JY, Bangaru NV, Ayer R, Vaughn G, et al. A microstructural study of friction stir welded joints of carbon steels. Int J Offshore Polar Eng 2004;14:284–8.

[3.3] Lienert T, Stellwag W, Grimmett B, Warke R. Friction stir welding studies on mild steel. Weld J Res Suppl 2003:1–9.

[3.4] Konkol P, Mathers J, Johnson R, Pickens J. Friction stir welding of HSLA-65 steel for shipbuilding. J Sh Prod 2003;19:159–64.

[3.5] McPherson N, Galloway A, Cater S, Hambling S. Friction stir welding of thin DH36 steel plate. Sci Technol Weld Join 2013;18:441–50.

[3.6] Ghosh M, Kumar K, Mishra RS. Process Optimization for Friction-Stir-Welded Martensitic Steel. Metall Mater Trans A 2012;43:1966–75.

[3.7] Cho H-H, Kang SH, Kim S-H, Oh KH, Kim HJ, Chang W-S, et al. Microstructural evolution in friction stir welding of high-strength linepipe steel.

Mater Des 2012;34:258–67.

[3.8]   Barnes SJ, Bhatti AR, Steuwer A, Johnson R, Altenkirch J, Withers PJ. Friction Stir Welding in HSLA-65 Steel: Part I. Influence of Weld Speed and Tool Material on Microstructural Development. Metall Mater Trans A 2012;43:2342–55.

[3.9]   British Standards Institution. BS EN ISO 6892-1. Metallic materials – Tensile testing – Part 1: Method of test at room temperature. London: 2009.

[3.10]   British Standards Institution. BS EN ISO 148-1. Metallic materials – Charpy pendulum impact test – Part 1: Test method. London: 2010.

[3.11]   Cater S, Martin J, Galloway A, McPherson N. Comparison between friction stir and submerged arc welding applied to joining DH36 and E36 shipbuilding steel. In: Mishra R, Mahoney MW, Sato Y, Hovanski Y, Verma R, editors. Frict. Stir Weld. Process. VII, Hoboken, NJ: Wiley; 2013, p. 49–58.

[3.12]   Becker W, Shipley R, editors. ASM Handbook Volume 11: Failure Analysis and Prevention. Materials Park, OH: ASM International; 2002.

[3.13]   Lloyd's Register. Rules for the Manufacture, Testing and Certification of Materials. London: 2014.

[3.14]   Totten GE, editor. Steel Heat Treatment: Metallurgy and Technologies. 2nd ed. Boca Raton, FL: CRC Press; 2007.

4. Fatigue performance investigation of DH36 steel friction stir welds

4.1. Introduction

As outlined in Chapter 1, there has been a growing number of studies demonstrating the feasibility of FSW on steel, producing defect-free welds, examining the microstructure and associated mechanical properties of the welds and concluding on the beneficial impact of this solid state joining process on the properties of welded steel components [4.1-4.8]. The extensive examination of DH36 steel FSW implemented herein has appreciably expanded on the commonly applied welding speeds through the process parameter development work in Chapter 1. The microstructural characterisation study in Chapter 2 reports on a complex metallurgical system which is highly influenced by the FSW process parameters. This work is complemented by the mechanical property evaluation in Chapter 3 which has identified a number of fast weld parameter sets that are technically and potentially economically competitive to fusion welding methods. Moreover, an understanding of the link between the evolved microstructures in steel FSW and the resultant mechanical properties has been established.

There remains however one important mechanical property of steel friction stir welds, fatigue, which requires investigation and reporting. Fatigue of metals is a particularly significant property for numerous applications such as aerospace and marine [4.7], and is considered to be the most important failure mechanism for steels [4.9]. It is commonly quoted for example that fatigue is responsible for almost 90% of all mechanical service failures [4.10]. In welded components, the weld itself contains process related flaws from which cracks can rapidly propagate [4.11]. Thus, welding has been demonstrated as an undermining factor to the mechanical properties of such components; specifically under cyclic loading, welds are generally the dominant factor for fracture [4.12], also characterised as the critical design factor in shipbuilding [4.7]. In fusion welding, solidification cracking, i.e. minor inner cracks which can act as crack propagation sites during fatigue loads are considered unacceptable by international standards, hence need to be avoided [4.12]. Undercut and lack of weld penetration are other examples of intolerable defects which are

widely reported as highly detrimental features in terms of fatigue life [4.11]. Therefore, fatigue life of welded components is commonly much reduced when compared to components that are unwelded. The efforts in extending the fatigue life of components are primarily concentrated on improvements in design [4.13]. International rules have been developed to implement specifications in the design of structural details, thus reducing the applied stresses particularly by minimising possible stress concentration regions [4.14].

The research on FSW of aluminium and other low melting point metals is quite extensive, with the process achieving a level of maturity [4.6] (also see Chapter 1). It has been demonstrated that FSW is a viable option for joining aluminium alloys in a number of industrial applications where welded components need to operate in extreme conditions and therefore high fatigue strength is a fundamental requirement [4.15,4.16]. Many publications on FSW of aluminium examine the weldments' fatigue behaviour; indicatively, Ericsson and Sandstrom [4.17] investigate the effect of varying welding speed on the fatigue performance of friction stir butt welded high strength Al6082 and compare this to MIG and TIG fusion welding. The fatigue life of the friction stir welded samples is found to be practically unaffected by speed increasing within the industrially acceptable range; FSW exhibits higher fatigue strength than the two examined fusion welding methods in the same stress range [4.17]. Other studies assess the process's defect tolerance and fatigue behaviour with regard to the weld root flaw [4.18] and the post welding top surface finishing [4.16]. Kadlec *et al.* [4.18] evaluate the effect of the weld root flaw ("kissing bond") on the FSW fatigue performance of a high strength aluminium alloy and attempt a quantitative analysis concerning this flaw's length. A critical weld root flaw length of approx. 300 μm is established; the welds' fatigue performance is seen to significantly decline when a longer flaw is detected, hence becoming an unacceptable defect [4.18].

Although material property data are gradually being generated for FSW of high melting point alloys, the process has been slow to transfer to steel due to the more extreme conditions, mainly high flow stress and temperature that are developed [4.6] and the associated heavy requirements on the tool material (see Chapter 1). The relevant publications evaluating its behaviour in fatigue loading are few [4.7] and seemingly small scale investigations.

A comprehensive study [4.5] evaluating the technical capacity of FSW as a

shipbuilding welding process of DH36 steel in relation to submerged arc welding (SAW), a well-established technique in the shipbuilding sector, reports on a predominantly acicular ferrite microstructure in the thermo-mechanically affected zone (TMAZ). SAW samples present a typical acicular ferrite microstructure defined around proeutectoid ferrite grains. The study concludes that FSW of DH36 steel is feasible and moreover carries significant improvements in the mechanical properties of the welded components; specifically, a fatigue testing programme of limited extent demonstrates that FSW samples exhibit better fatigue performance than the SAW samples of equivalent thickness [4.5]. In addition, analysis of the chemical composition of all welds reveals that SAW produces considerably different composition than the parent material due to the addition of filler material, whilst FSW results in no chemical segregation of the parent material [4.5]. A further publication from the same research group compares double sided FSW of S275 structural steel in air and underwater in terms of the evolved microstructure and resultant mechanical properties [4.6]. It is detailed that the TMAZ in both cases comprises refined ferrite grains produced by dynamic recrystallisation (DRX), smaller in air welding where slower cooling rate is expected, and dissociated pearlite. Fatigue testing (revealing comparable fatigue strength for air and underwater welds), tensile testing and hardness measurements show that underwater FSW, an indispensable application for the marine sector, is not detrimental to the welds' mechanical properties apart from decreased impact toughness [4.6].

High quality welds of steel grade A36 are produced with pcBN and Tantalum-based FSW tools in a study assessing the mechanical properties and particularly the welds' fatigue performance with a focus on the shipbuilding sector [4.7]. Virtually no deterioration of the parent plate properties due to FSW is observed; tensile testing of the welds produced with the Tantalum fabricated tool reveals higher yield strength (YS) than the corresponding of the pcBN tool. The fatigue life of both groups of welds has not declined compared to the parent plate behaviour, with the Tantalum tool welded samples performing slightly better. The latter is attributed to the improved efficiency of this type of tool linked with suitably optimised welding parameters delivering an even hardness distribution throughout the weld zone [4.7]. On the relevant subject of fatigue crack growth rate, Pandey and Gupta [4.8] investigate friction stir butt welds of 3 mm thick mild steel. The weld YS is found to be moderately increased compared to the base material, 310 MPa and 286 MPa respectively, but the elongation to fracture is reduced due to the harder weld zone. It

is concluded that the fatigue crack growth rates for FSW and base material are almost identical when using stress ratio (R) of 0.1, whereas the latter's crack growth rate is higher for R=0.2 [4.8].

A study on the FSW of AISI 409M ferritic stainless steel researches the welds' fatigue behaviour with regard to the parent material properties [4.19]. FSW is seen to transform the original coarse parent material grains into a refined ferrite / martensite banded structure of significantly higher hardness. The resultant dual phase microstructure is responsible for an improvement in the fatigue life compared to the parent material; notably, friction stir welded samples present higher fatigue life than the base material and improved resistance to crack propagation [4.19]. Despite being quite comprehensive, the examination of only 300 mm long welds at a noticeably slow welding speed (90 mm/min) weakens this study's merit. It is worthy of note that fusion welding reduces the desirable mechanical properties (ductility, toughness, etc.) of this alloy because of significant grain growth, whereas FSW can prevent these issues and achieve high integrity welds by developing a highly refined microstructure [4.19]; this represents an infrequently discussed positive effect of FSW, also detailed in Chapter 1.

Due to the significance of a solid understanding of the fatigue behaviour in supporting the acceptance of the process on steel within a wider industrial environment, the considerable potential of FSW in delivering high fatigue performance welds as concluded in the above discussed publications and the lack of pertinent studies on low alloy steel, a detailed and extensive fatigue testing programme of steel grade DH36 FSW is undertaken. This novel programme assesses the welds' fatigue behaviour by testing samples in constant amplitude uniaxial tensile loading, generating the stress-life *(S-N)* data and comparing to international recommendations for fusion welding, also characterising the weld microstructure and analysing the fatigue samples' fracture surfaces; the experimental procedures and findings are reported herein.

4.2. Experimental procedures

There are no internationally accepted standards for the testing and assessment of welded components under fatigue [4.7], apart from guidelines. The lack of such standards is even more evident with regard to investigating the FSW of steel [4.19],

a novel process. Thus, this study has formulated and observed a new standard operating procedure, i.e. a comprehensive set of guidelines for the fatigue assessment of steel friction stir welds. This allows for a fully compliant fatigue testing programme to be performed, and the various experimental stages are described below.

4.2.1. Material and welding details

The material under examination is steel grade DH36 (6 mm thick) with the nominal chemical composition and steel plate dimensions outlined in Chapter 2. Equally, welding was performed on the FSW machine described in Chapter 2, using identical FSW tools for steel in analogous process conditions and joint configuration.

Three new 2000 mm long friction stir welds were produced for the fatigue testing programme using welding parameters selected as representative of the three traverse speed groups (Table 1.1) which are comprehensively examined in Chapter 2 and 3; these are provided in Table 4.1. The three welds are henceforth referred to as "slow", "intermediate" and "fast" weld. All other welding parameters (including backing plate and clamping procedure) were maintained constant to enhance the consistency of the results.

Table 4.1. FSW parameters employed in the fatigue testing programme

Welding speed group	Slow	Intermediate	Fast
Traverse speed (mm/min)	100	250	500
Rotational speed (rpm)	200	300	700

4.2.2. Sample preparation

All fatigue and tensile samples were manufactured from the above outlined DH36 steel welds; their position and sequence with regard to the start of the weld was consistently marked before sectioning (Figure 4.1). The specific preparation stages, i.e. sectioning, machining and polishing adhered strictly to BS 7270 [4.20]. To this end, sectioning and subsequent machining were performed with gradually decreasing depths of removed material to diminish any work hardening or residual stress effects on the surfaces. In addition, liquid coolant was used in order to prevent any modifications to the samples' microstructure by heat treatment. The

samples' sides were polished longitudinally to minimise the contribution of any transverse machining marks to the fatigue performance, particularly from the parallel length, up to a surface finish of at least 0.2 μm R_a [4.20]. To ensure that the required surface roughness was achieved, a large number of randomly chosen samples were validated using a Mitutoyo surface roughness measuring system (Figure 4.2). In contrast, the samples' top and bottom surfaces were tested in the "as-welded" condition. Fatigue and transverse tensile samples were prepared with the same basic dimensions, which are outlined in Figure 3.1 (Chapter 3).
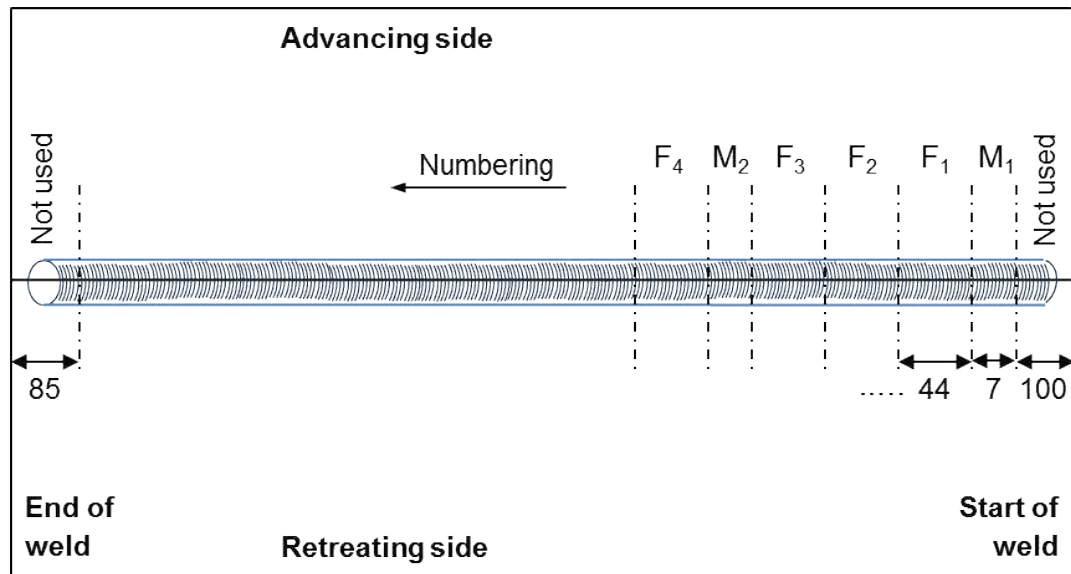

Figure 4.1. Schematic of the samples' position on a FSW; Fx: fatigue sample, Mx: metallography sample

The measurement of weld misalignments and other irregularities of the fatigue samples' geometry is an influential factor which is often overlooked in fatigue testing programmes. Clamping on the fatigue testing machine and consequent axial loading will certainly re-align a sample incorporating possible weld misalignment or distortion. This will induce tensile or compressive stresses on any surface breaking and even embedded flaws, hence accelerating or hindering any cracks which may initiate from these [4.11]. For this purpose, contact scans of all samples' top surface geometry (Figure 4.3) were performed using a Mitutoyo Crysta Apex C 121210 coordinate measuring machine (CMM) of 0.1 μm resolution and 3.5 μm measuring accuracy.

Analysis of the recorded CMM data revealed insignificant secondary bending due to axial or angular misalignment acting upon the samples during testing; few samples

displayed maximum distortion of 0.72 mm. Hence, the effect of possible weld misalignment on the fatigue performance was considered negligible in this study.
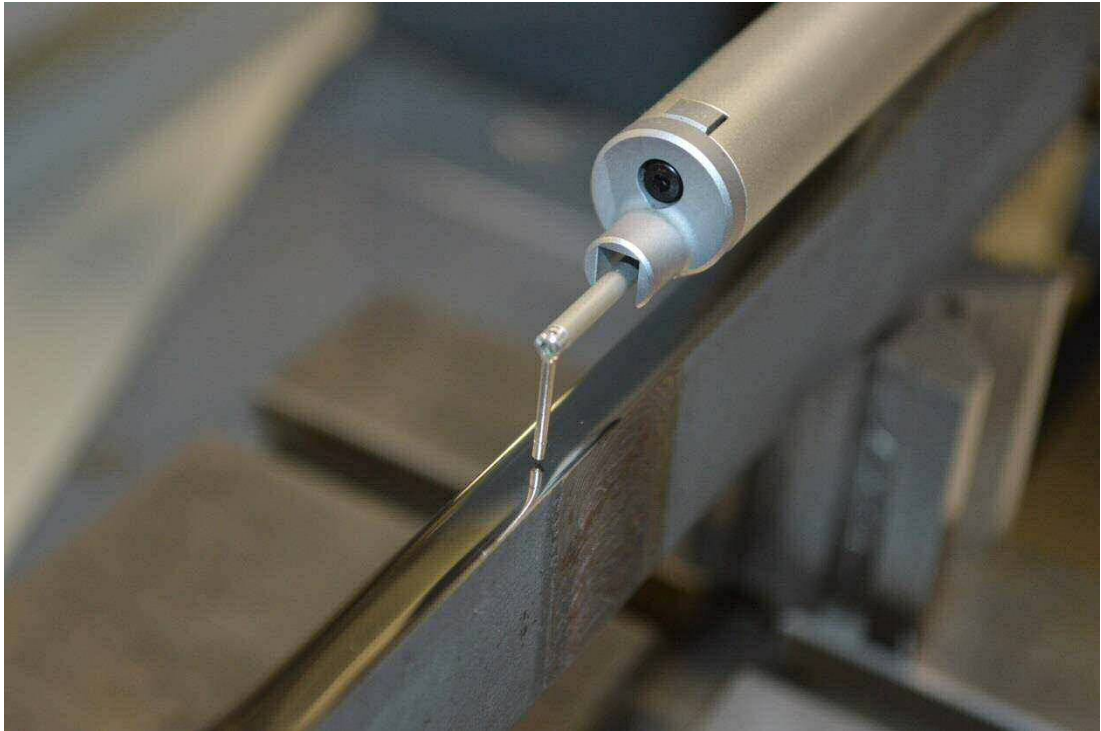

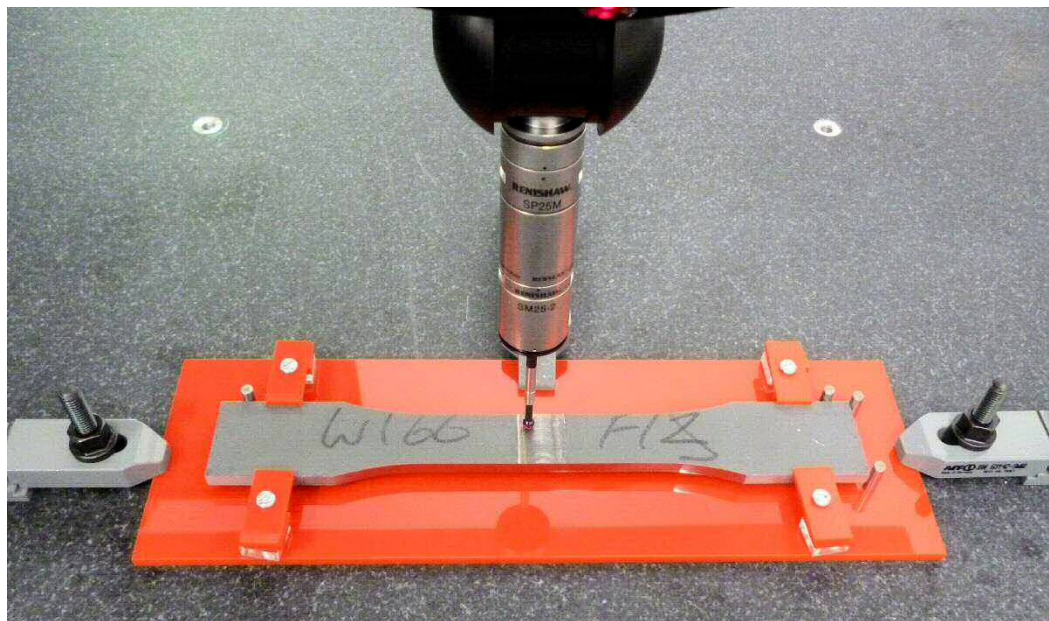**Figure 4.2. Fatigue sample on the surface roughness tester**

Figure 4.3. CMM contact measurements on a typical fatigue sample

4.2.3. Metallographic examination and hardness measurements

A detailed microstructural characterisation of the three welds was performed in order to correlate their microstructure to the mechanical properties which are expected to exhibit, particularly their performance under fatigue, and to assess the quality of the welds by identifying possible flaws or defects induced by the FSW process. Metallographic samples were sectioned from the positions in between the fatigue samples for each weld. This allowed the examination of a specific section of the weld microstructure should the adjacent fatigue samples reveal an irregular behaviour and provided a sufficient understanding of the microstructure along the entire length of each weld. The metallographic preparation and examination of all samples was performed in a method identical to the one specified in Chapter 2, also making use of the same nomenclature; again, the advancing (AD) side is seen on the left side of the images. Equally, the scanning electron microscope (SEM) with energy dispersive spectroscopy (EDS) described in Chapter 2 was employed for additional fracture surface examination and chemical analysis of top surface non-metallic inclusions.

Micro-hardness measurements were recorded for several positions which were deemed representative of the weld zone, consistently for all three welds (Figure 4.4), to provide an understanding of the hardness distribution of the weld zones, hence information relevant to the behaviour during mechanical testing. Measurements were recorded using the Mitutoyo hardness tester introduced in Chapter 3 and by applying a load of 200 gf.
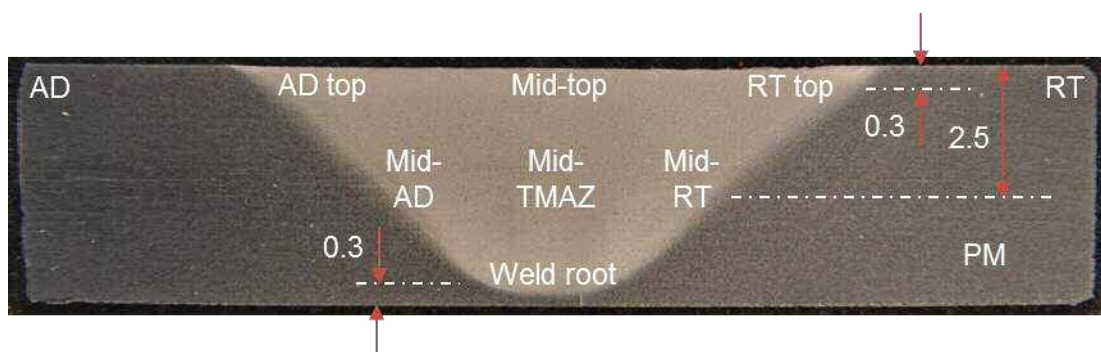

Figure 4.4. Typical FSW macrograph with the positions of hardness measurements [Etched]

4.2.4. Transverse tensile testing

Three samples per weld were subjected to transverse tensile testing in line with the procedure outlined in Chapter 3 and with the purpose of determining the YS of the

weldments. The trend reported in Chapter 3 and in the relevant technical literature [4.1-4.6] was confirmed in this study; all slow and intermediate weld samples fractured in the parent material, denoting welds of higher tensile strength. Still, the fast weld samples fractured in the AD side of the weld exactly as detailed in Chapter 3 for weld W25 (Figure 3.6a). The average YS value from the three intermediate samples is 382 MPa (Table 4.2); this was used for calculating the fatigue testing parameters of all three welds, therefore offering consistency and comparable results.

Table 4.2. Transverse tensile test results of the intermediate weld

Tensile sample	Traverse speed (mm/min)	Rotational speed (rpm)	Yield strength, 0.2% (MPa)	Region of fracture	Fracture mode
Inter-1			385		
Inter-2	250	300	382	Parent material	Ductile
Inter-3			378		
Average YS			**382**		

4.2.5. Transverse fatigue testing

As in the case of the transverse tensile testing, fatigue testing was carried out on an Instron 8802 fatigue testing system. The number of tested samples per weld and stress range is provided in Table 4.3. Emphasis was placed on the intermediate welding speed, where more samples were tested and in three stress ranges to enhance the statistical validity of the recorded data. This investigation has aimed to perform high cycle fatigue (HCF) testing, i.e. loading cycles to fracture above 10^5 [4.21]. The *S-N* approach was employed since it is considered appropriate for components subjected to HCF, with mostly elastic stresses and negligible plastic deformation [4.21,4.22]. The selection of applicable stress ranges was informed by trial tests which were initially performed, commencing with stress range of 80% of YS. Additionally, the effect of varying FSW parameters on the fatigue behaviour was established by testing samples from the slow and fast welds at one stress range and comparing these results with the basic *S-N* data of the intermediate weld.

The calculated stress levels of all stress ranges which were used for programming the Instron 8802 fatigue testing system, principally mean stress and amplitude, are

summarised in Table 4.4. The stress ratio was maintained approx. equal to 0.1 and the stress frequency constant at 10 Hz during the testing programme. The actual stresses attained by the testing machine vary insignificantly from the calculated values (no more than 0.1%).

Table 4.3. Number of tested fatigue samples per welding speed

Welding speed	Stress range (% of YS)	Number of tested samples
Intermediate	90	10
	80	10
	70	5
Slow	80	8
Fast	80	8

Table 4.4. Summary of the fatigue testing nominal stresses

Welding speed	Stress range	Maximum stress	Minimum stress	Mean stress	Amplitude
	% of YS	σ_{max} (MPa)	σ_{min} (MPa)	σ_m (MPa)	σ_a (MPa)
Intermediate	90	343.80	34.38	189.09	154.71
	80	305.60	30.56	168.08	137.52
	70	267.40	26.74	147.07	120.33
Slow	80	305.60	30.56	168.08	137.52
Fast	80	305.60	30.56	168.08	137.52

4.3. Results and discussion

4.3.1. Microstructural characterisation

The slow traverse speed weld (100 mm/min – 200 rpm) presents a ferrite predominant, homogeneous microstructure with significant grain refinement in comparison to the parent material (Figure 4.5). The formation of highly refined ferrite grains has been reported previously whilst examining the FSW of steel grade E36

[4.3], a shipbuilding steel comparable to DH36 in terms of chemical composition and mechanical properties, and of a mild steel where it is associated with DRX [4.8]. The ferrite grains are of random geometry, with minor traces of acicular shaped grains (Figure 4.5). This observation is in good agreement with the findings on the slow welds discussed in Chapter 2 and in a published work [4.4].
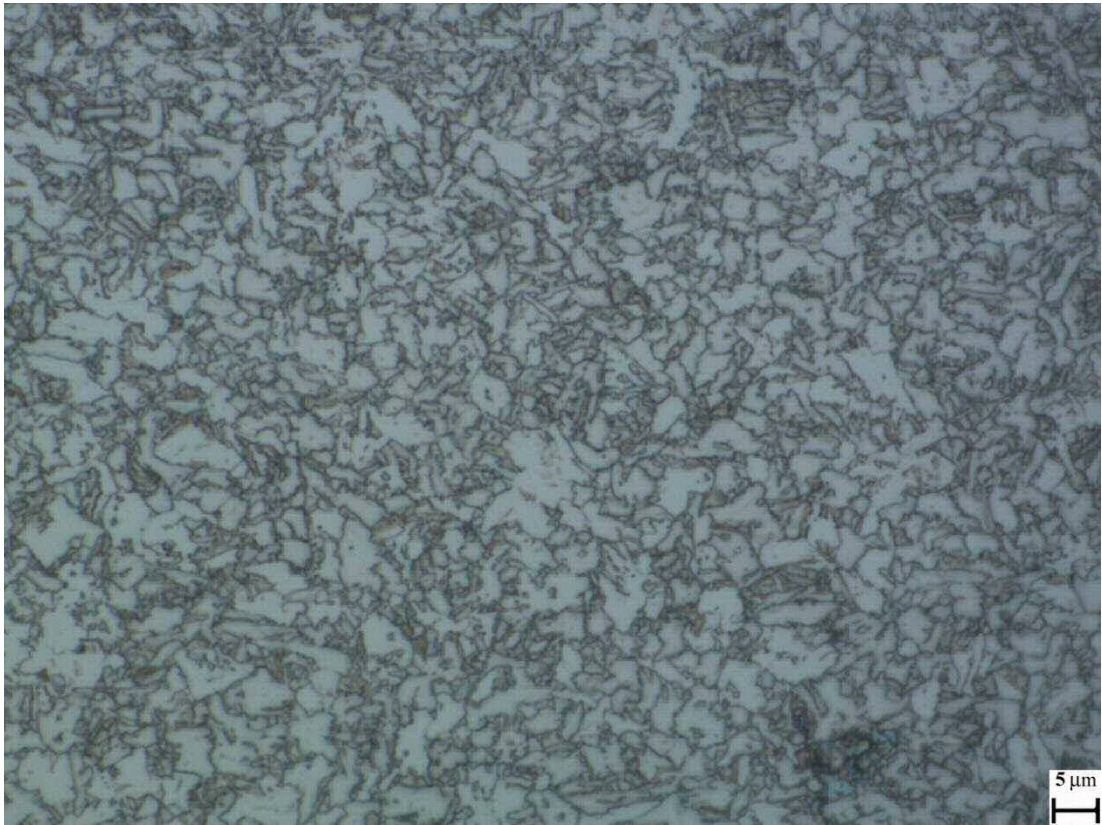

Figure 4.5. Slow weld, microstructure of mid-TMAZ [x1000, Etched]

As expected for this mild set of welding parameters, no flaws are visible in the bulk of the TMAZ, the transition from the heat affected zone (HAZ) to the TMAZ is smooth (Figure 4.6a showing the retreating (RT) side), and the non-metallic inclusions introduced in the weld from the plates' side surfaces are not completely mixed but remain interconnected. The weld's top surface is slightly uneven but gradually improving towards the end of the weld length. Both sides of the top surface present signs of non-metallic inclusions interconnected in sporadic incomplete fusion regions, however insignificant in size (Figure 4.6b). SEM-EDS examination of these non-metallic inclusions (Figure 4.7) in line with the relevant analysis in Chapter 2 revealed high concentration (wt.%) of zinc (9%) and silicon (20%), denoting the presence of paint primer as discussed elsewhere [4.23]. The same sites are also seen to contain high percentage of oxygen (36% – 43%), thus
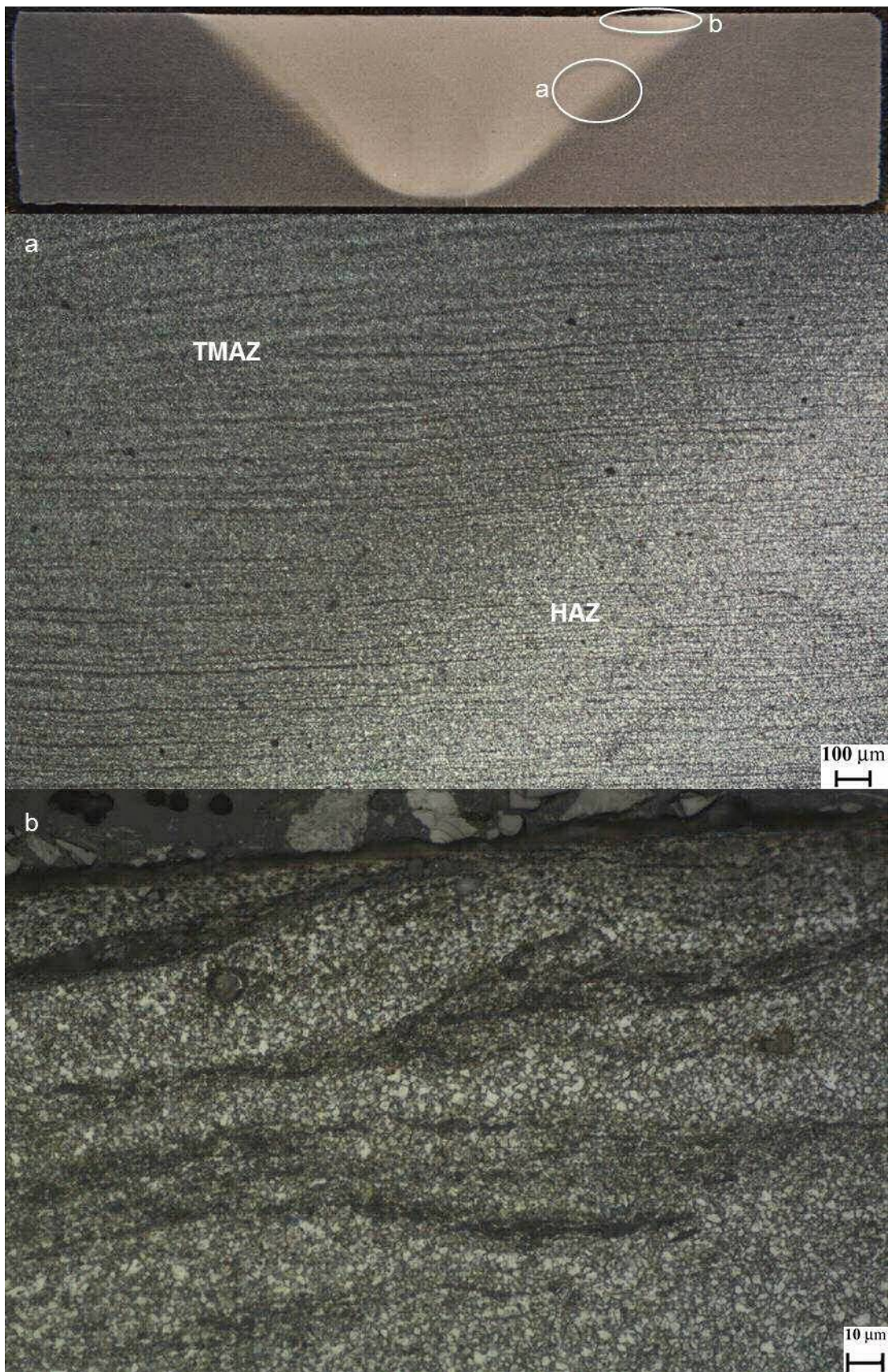
Figure 4.6. Slow weld, RT side (a) transition from HAZ to TMAZ [x50, Etched]; (b) top surface [x500, Etched]

providing evidence of oxide scale. This has arisen from the lack of any substantial plate preparation prior to FSW, which is standard practice during the current work as outlined in Chapter 2. The same issue of steel plate top surface oxides being drawn into the weld zone due to the stirring action of the tool has been explored previously [4.23].
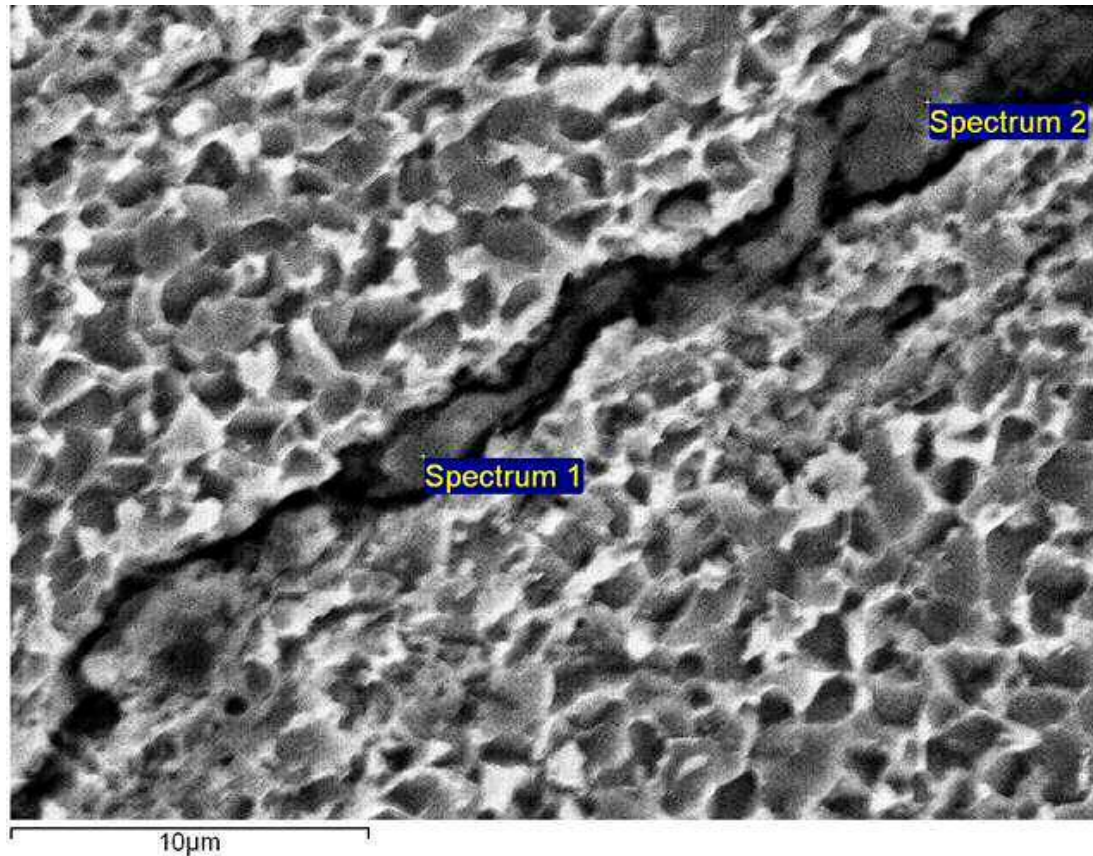

Figure 4.7. SEM-EDS analysis of slow weld top surface

A heterogeneous microstructure is exhibited by the weld at 250 mm/min – 300 rpm (intermediate traverse speed); this consists of acicular shaped bainitic ferrite rich regions and ferrite predominant regions of either acicular shape or of random geometry (Figure 4.8a & b). Prior austenite grain boundaries are faintly observable in the bainite rich areas of the TMAZ (Figure 4.8b). The evolved acicular ferrite and acicular bainitic ferrite phases have been disclosed in previous studies on the same grade of steel [4.5] and for identical welding parameters [4.4], also coinciding with the corresponding examination in Chapter 2. The microstructure differs towards the bottom and outer sides of the weld, shifting to predominantly refined ferrite grains of random geometry (Figure 4.8c). This latter image also features a discontinuity in the surrounding structure, i.e. a cavity, created by a non-metallic inclusion.

The top surface of the intermediate weld is mildly uneven, indented by the FSW tool shoulder's threads. There is a small number of incomplete fusion paths, or laps [4.24] observed particularly on the outer top RT side (Figure 4.9), with entrapped and interconnected non-metallic inclusions in various stages of oxidation (seen in different shades of grey). These laps are seen to provide crack initiation sites during fatigue testing (section 4.3.3). SEM-EDS analysis of the laps on several metallographic samples (one such site is presented in Figure 4.10) recorded concentrations (wt.%) of zinc (max. 27%), silicon (max. 20%) and oxygen (max.
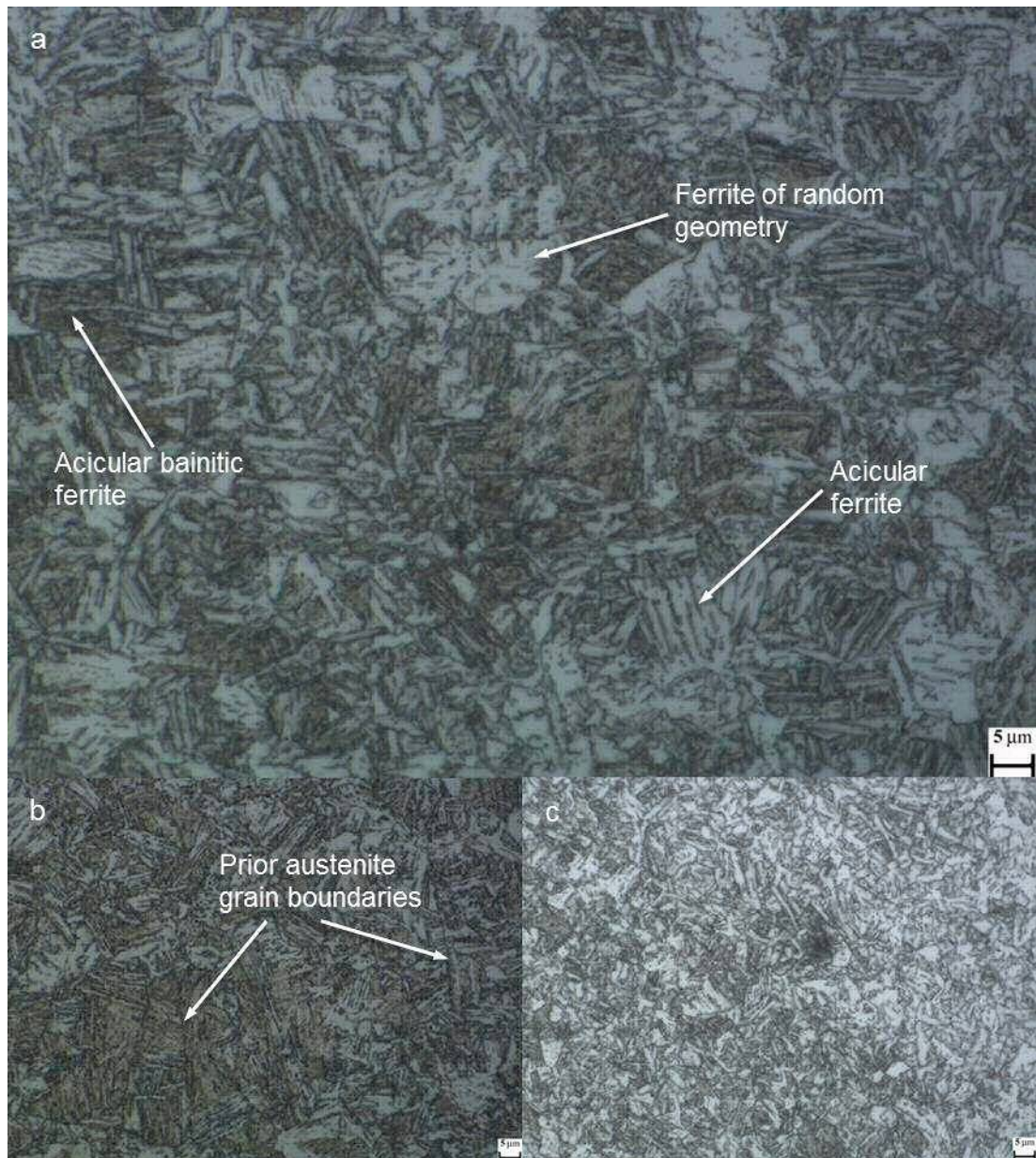

Figure 4.8. Intermediate weld [x1000, Etched] (a) & (b) microstructure of mid-TMAZ; (c) microstructure of outer AD TMAZ
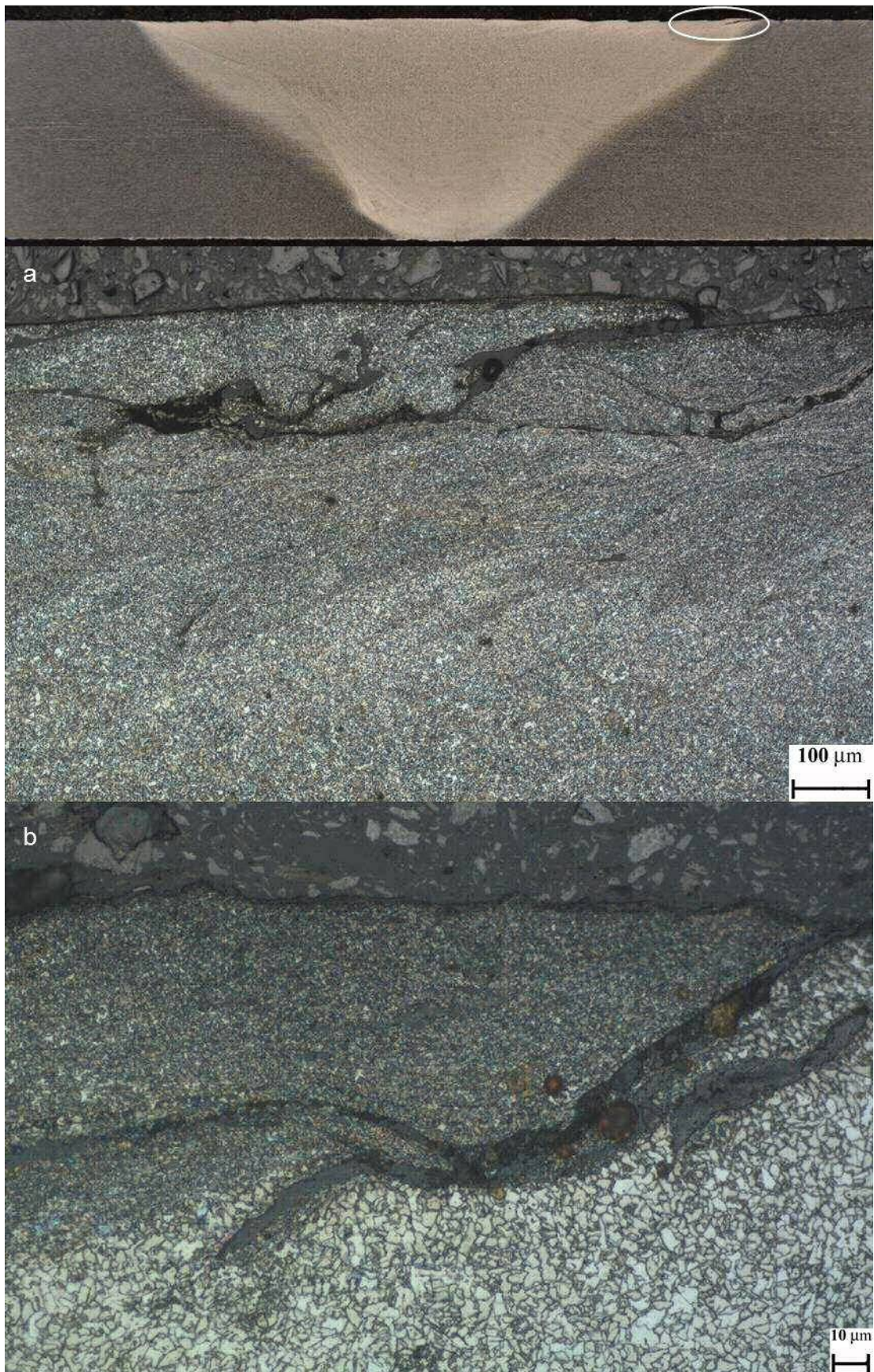
Figure 4.9. Intermediate weld, RT side top surface (a) [x100, Etched]; (b) [x500, Etched]
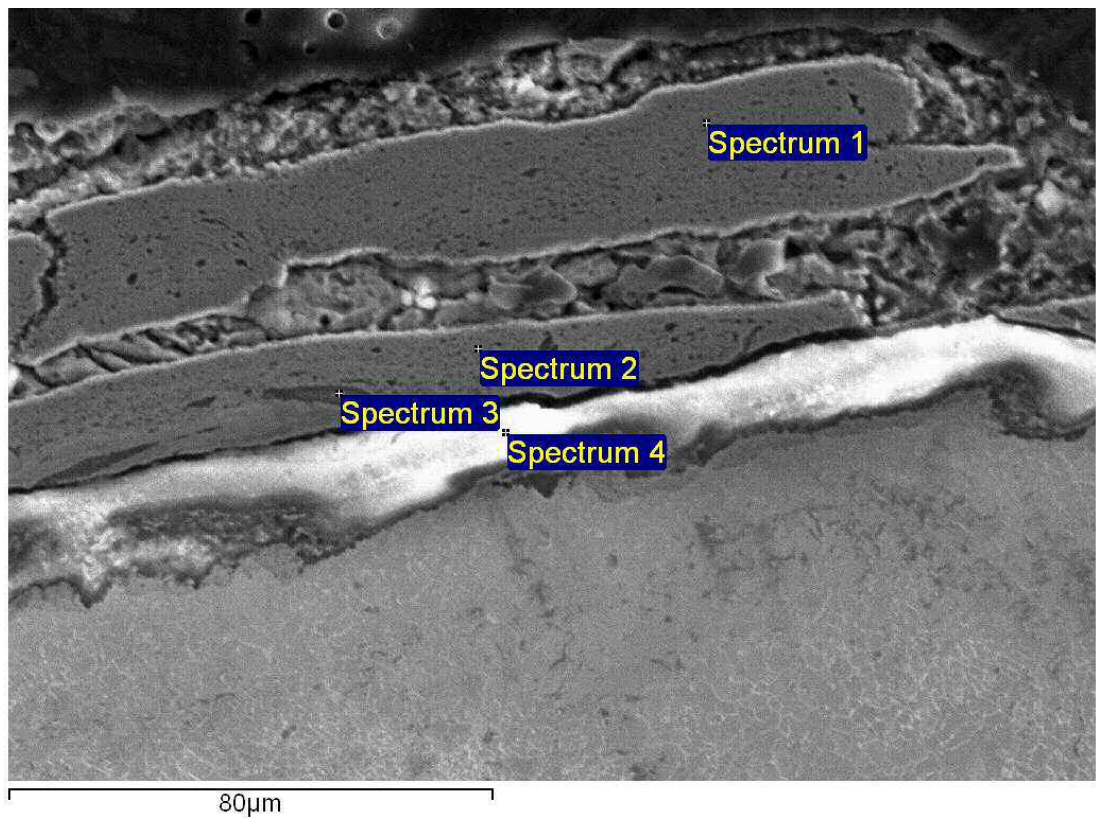
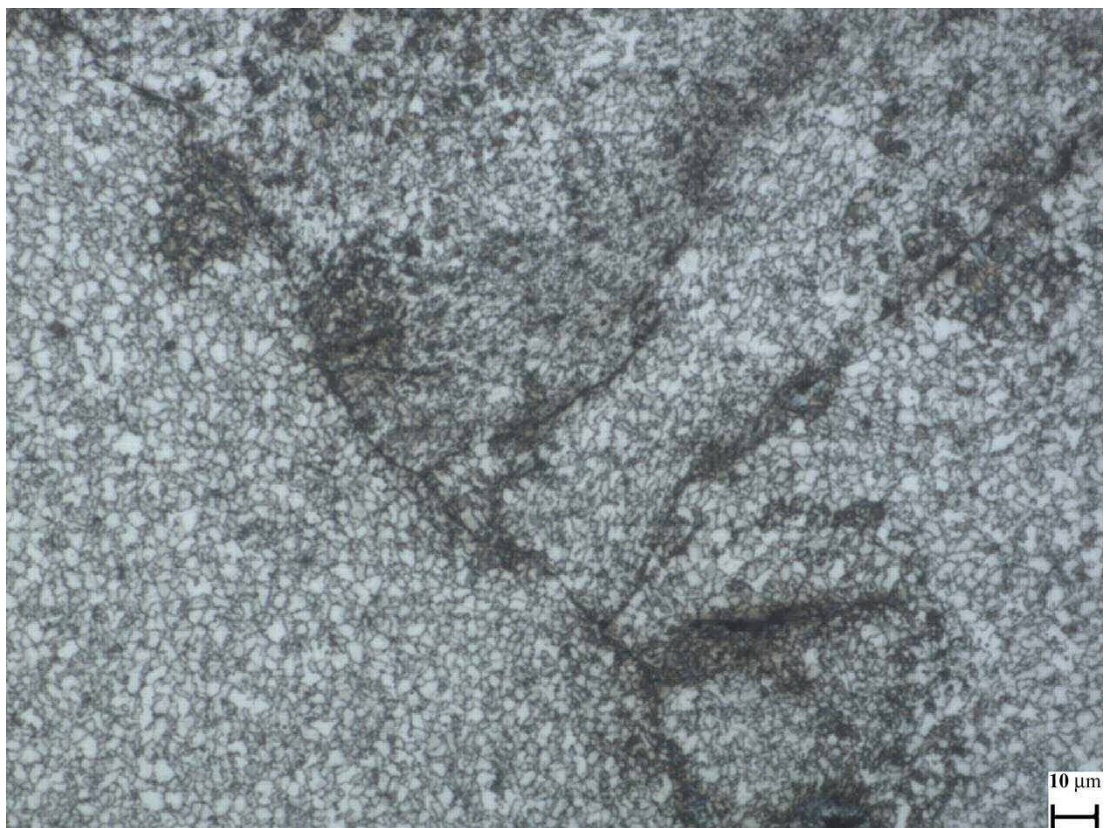**Figure 4.10. SEM-EDS analysis of intermediate weld top surface**

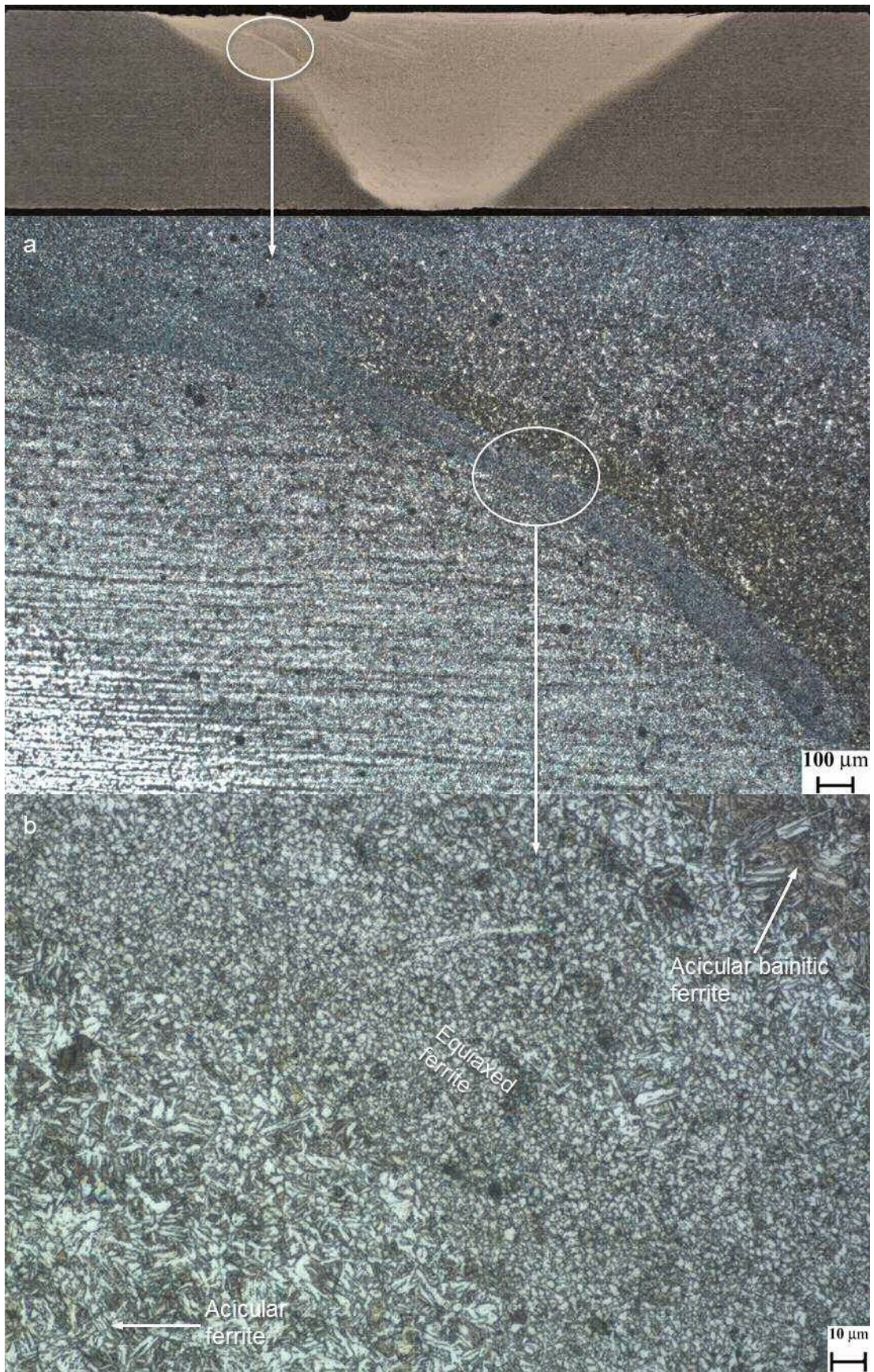**Figure 4.11. Intermediate weld, AD side [x500, Etched]**

Figure 4.12. Intermediate weld, top AD side (a) [x50, Etched]; (b) [x500, Etched]

42%) similar to the slow weld; hence, the non-metallic inclusions are again identified as a mixture of paint primer and oxide scale. In addition, a number of separate sites within the laps were found to contain oxygen and iron in approx. the stoichiometric concentration (30.1 – 69.9 wt.% respectively) of haematite (Fe_2O_3) [4.25], an oxide phase known to form on low alloy steels in high temperature environments [4.26] (as is the case with FSW of steel).

Moreover, there is strong indication of a recurrent region of insufficient fusion, also labelled cold shut [4.24], observed at the mid-AD side of the intermediate weld (Figure 4.11). The weld root has been fully fused and the microstructure of this region comprises recrystallized ferrite and pearlite. There has been no substantial mechanical stirring of the steel in this area; therefore, the driving force for the transformation by DRX is the thermal energy which has dissipated from the bulk of the weld zone.

A microstructural feature of one of the examined samples from the intermediate weld is of particular interest. There is one material flow line in the outer top AD side with a microstructure quite distinct from the surrounding regions (Figure 4.12a). This is a predominantly ferrite phase of refined and nearly equiaxed grains inside the previously discussed acicular bainitic ferrite and acicular ferrite of the TMAZ (Figure 4.12b). Thus, this distinctly heterogeneous area has evolved by steel having been transported from another region (e.g. the outer bottom side where slower cooling rates occurred) due to the powerful stirring action of the tool during FSW.

The fast traverse speed weld (500 mm/min – 700 rpm) displays a heterogeneous but predominantly acicular shaped bainitic ferrite microstructure with minor regions of acicular ferrite (Figure 4.13). The increased bainitic content is a direct consequence of the high cooling rate due to the higher traverse speed of this weld. More, prior austenite grain boundaries are clearly detected (Figure 4.13); acicular shaped grains are seen to nucleate perpendicular to these boundaries. These observations conform with the microstructural characterisation in Chapter 2 and in a separate publication [4.4] for corresponding welding parameters.

The weld demonstrates poor quality top surface with laps introducing non-metallic inclusions in the TMAZ which emerge in post-weld oxidation (Figure 4.14a) and marks on both sides corresponding to the tool shoulder's features (Figure 4.14b); these are all stress concentration regions which are expected to provide crack initiation sites hence influence the weld's fatigue performance. As in the case of the

slow and intermediate welds earlier, SEM-EDS analysis (Figure 4.15) established that these non-metallic inclusions are a combination of paint primer (max. 22% zinc, max. 24% silicon) and oxide scale (max 51% oxygen). Similar poor top surface with fissures has been identified in Chapter 2 and is also confirmed by optical microscopy on the HSLA-65 shipbuilding steel friction stir welds of an earlier publication [4.2]. Konkol *et al.* [4.2] attribute this process related flaw to the tool shoulder and clarify that it could compromise the weld's fatigue performance.

The FSW tool has deviated marginally off centre as it traverses through the original plate interface developing evidently intermittent insufficient fusion at the weld root, i.e. a weld root flaw (Figure 4.16a). Since there is almost no stirring action of the tool's probe on the steel in this region of reduced peak temperature, the thin film of non-metallic inclusions on the surface of the two plates being welded is not fully dispersed, thus forming a joint line remnant [4.27] as an extension of the weld root flaw (Figure 4.16a). For the same reason of diminished mechanical deformation, the microstructure of this region is appreciably different from the bulk of the weld (TMAZ). This consists of highly refined, roughly equiaxed ferrite grains, where the
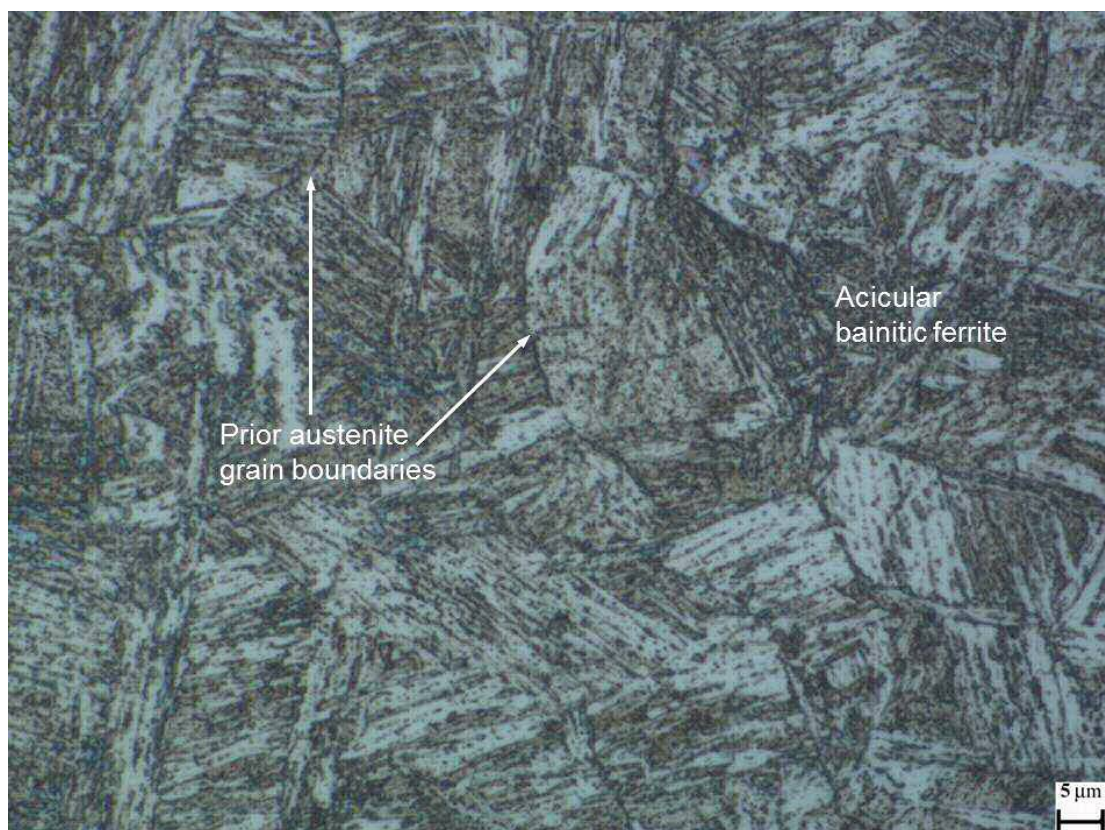

Figure 4.13. Fast weld, microstructure of mid-TMAZ [x1000, Etched]
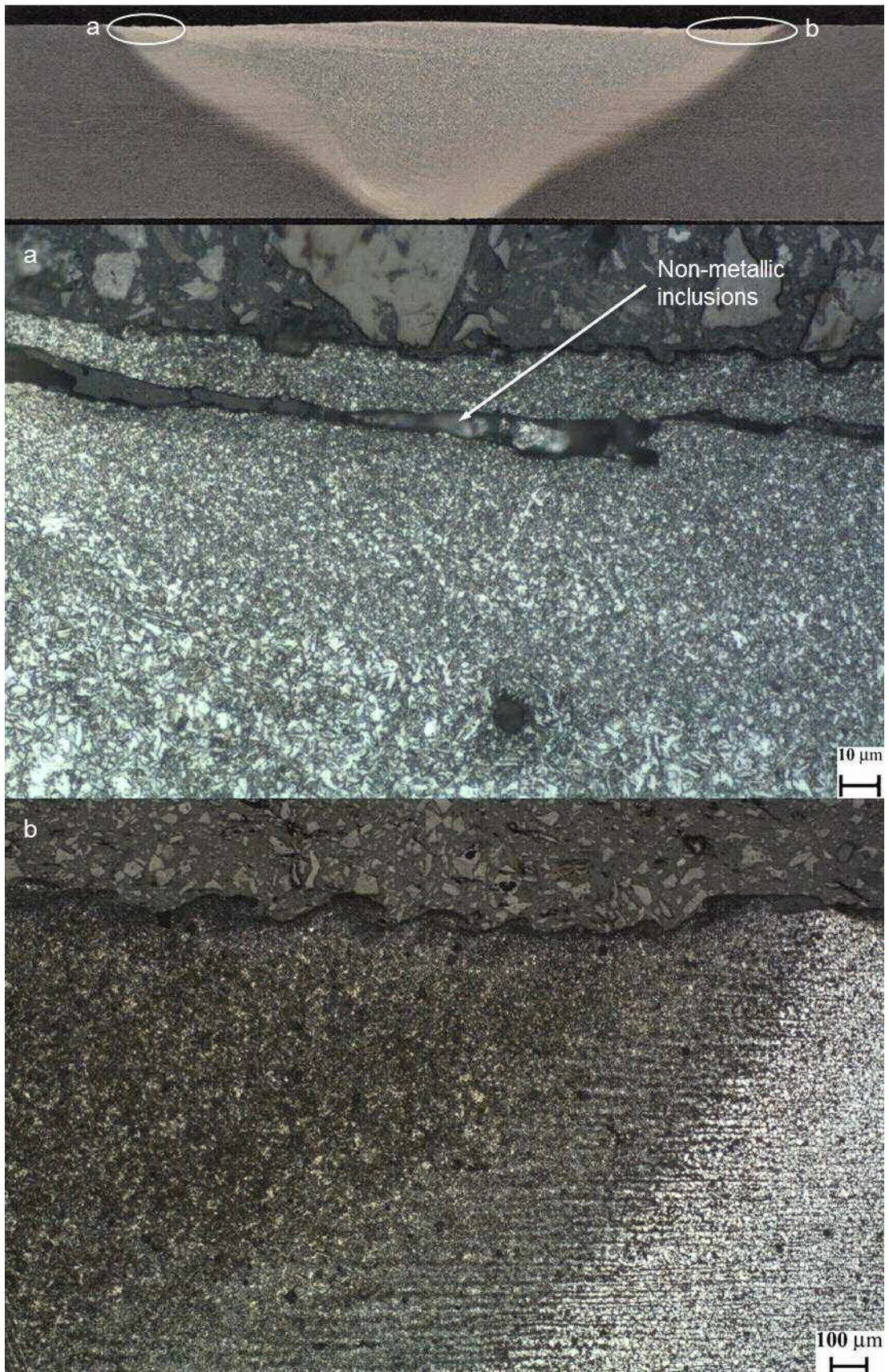
Figure 4.14. Fast weld, top surface (a) AD side [x500, Etched]; (b) RT side [x50, Etched]

original ferrite / pearlite grain structure is still barely visible (Figure 4.16b). This transformation is attributed to the thermal energy dissipating towards the bottom of the plate.
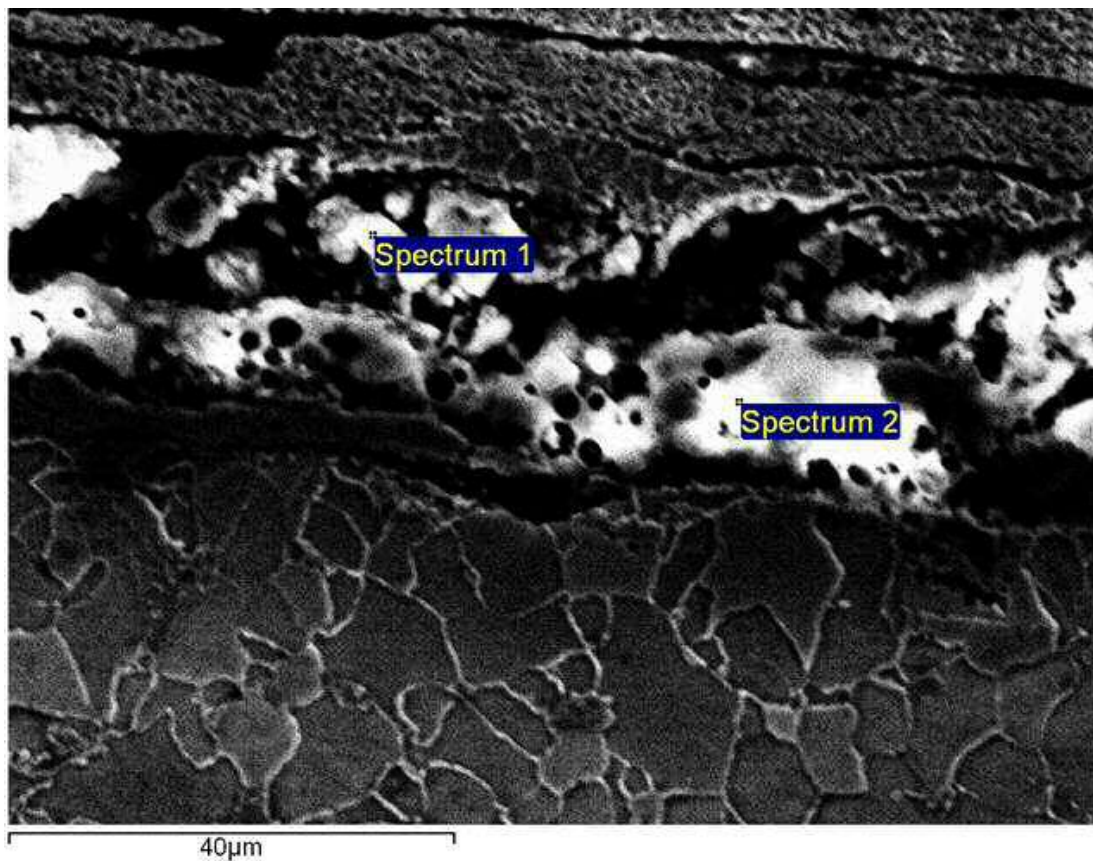
Figure 4.15. SEM-EDS analysis of fast weld top surface

The boundary between HAZ-TMAZ on the mid-AD side of the fast weld contains few discontinuous cavities or voids (Figure 4.17) with directionality identical to the flow of material (downwards and inwards). This is an issue related to insufficient plasticisation and subsequent irregular material flow [4.28]; the abrupt change in the poorly plasticised steel's direction of flow during FSW [4.29], i.e. nearly horizontal motion under the influence of the tool's shoulder shifting to practically vertical due to the effect of the probe's features [4.30], and the associated high shear forces [4.28] are primarily responsible for developing these flaws [4.29].
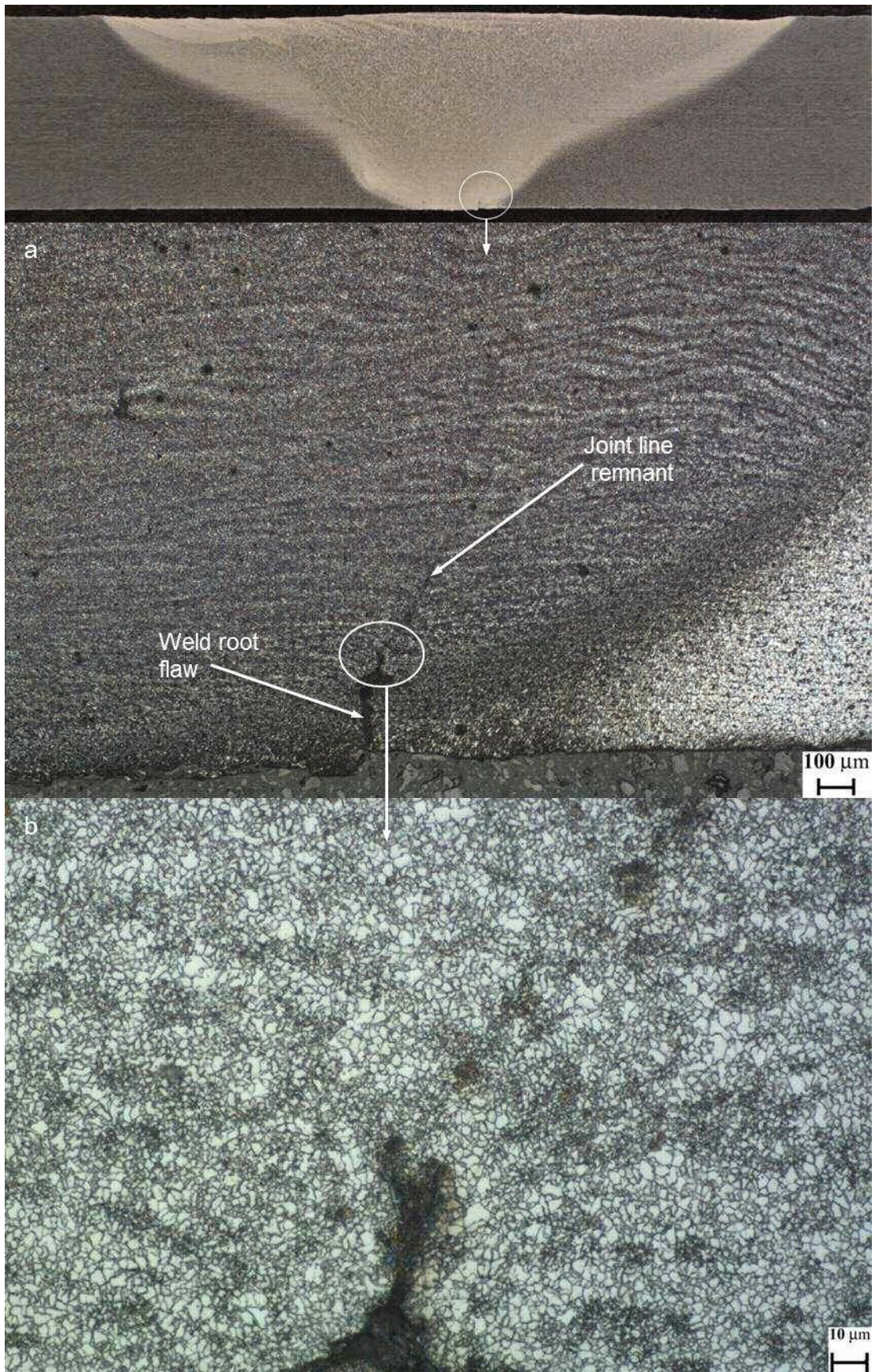
Figure 4.16. Fast weld, root (a) [x50, Etched]; (b) [x500, Etched]
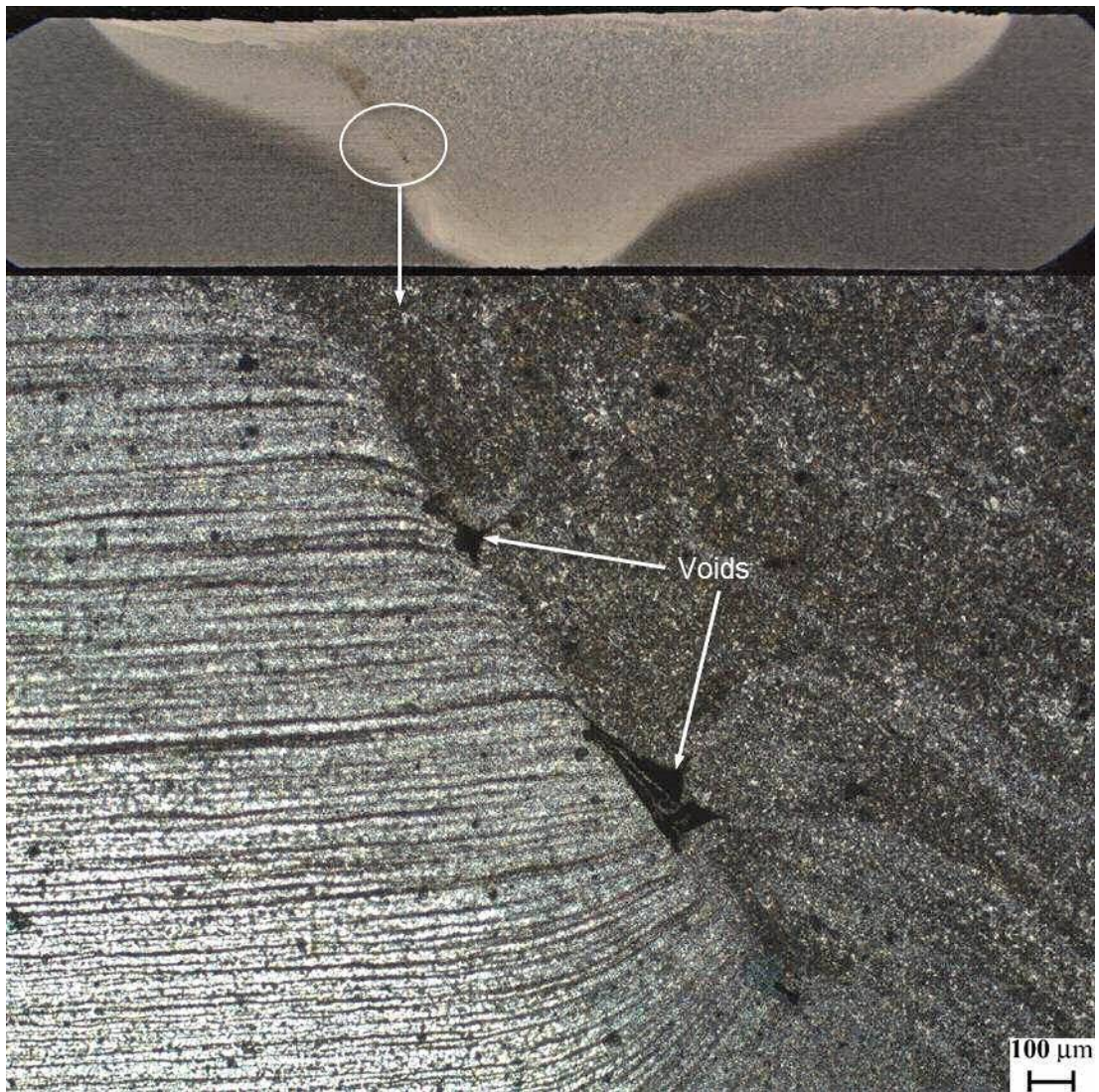
Figure 4.17. Fast weld, boundary of HAZ-TMAZ, AD side [x50, Etched]

4.3.2. Hardness distribution

The micro-hardness measurements for the three welds are presented in Table 4.5, where the values are supplied as the average of two measurements per position marked in Figure 4.4. Since the current testing programme has been concentrating on the intermediate welding speed, two samples from this weld were measured for improved accuracy. The hardness values follow the anticipated order, in line with the relevant discussion in Chapter 3; the hardness of the weld is seen to increase as the welding speed is increased. This is attributed to the increasing cooling rate which develops harder phases such as bainite. The microstructural examination above (section 4.3.1) and the corresponding in Chapter 2 have noted the rise in the bainite content with each speed increment. Broadly, all welds are harder than the parent

material but still within classification society (class) requirements [4.31]. The gradual increase from parent material hardness to a peak in the middle of the TMAZ is also identified by Azevedo *et al.* [4.7] using the same type of FSW tool for steel and similar welding speeds (to the slow and fast). Pandey and Gupta [4.8] record smaller increase in the TMAZ hardness compared to the base material; this is connected to the application of a very slow welding speed (80 mm/min) for the given rotational speed (700 rpm) which develops lower cooling rates.

Table 4.5. Micro-hardness (Vickers) measurements for the three welds (PM: parent material)

Weld	AD top	Mid-top	RT top	Mid-AD	Mid-TMAZ	Mid-RT	Weld root	PM
Slow	225	247	244	230	226	222	225	189
Inter-1	302	257	247	266	265	247	240	169
Inter-2	316	241	254	259	279	233	254	191
Fast	320	303	318	306	355	356	250	184

4.3.3. Fatigue assessment

The experimental *S-N* data of the intermediate (250 mm/min) speed samples for the three stress ranges are plotted as fatigue life (in number of cycles to fracture) vs. nominal stress range value for each sample ($\Delta\sigma$, in MPa) in double logarithmic scale (Figure 4.18). The details of each test are provided in Table A.1 of Appendix A. The ultimate fracture position for 24 out of the 25 tested samples of the intermediate weld was the weld's RT side (Figure 4.19). The fracture initiation sites are pinpointed as the lap defects observed on this side's top surface; minor embedded flaws detected on the AD side did not offer crack initiation sites (also refer to section 4.3.6). In addition, the transverse tensile samples of the same weld fracturing in the DH36 base material substantiates that, except for the yield strength, static loading does not carry important information on the material's performance in real environments where cyclic loading is the dominant stress mechanism.

The original objective of this investigation has been the recording of fatigue lives in HCF testing, i.e. within the range of $10^5 - 2.5 \times 10^6$ cycles (section 4.2.5). This testing programme reveals an excellent picture of FSW of low alloy steel, with all tests reaching well above 10^5 cycles. One intermediate weld test at 70% of YS was

terminated before fracture since it reached a number of cycles (2.6×10^6) beyond the predetermined objective. The surface breaking flaws are less pronounced in this region of the weld, thus no fracture occurred within the duration of the particular test (further examined in section 4.3.6).

The fatigue test data for the slow and fast weld at 80% of YS are plotted in Figure 4.20 together with the intermediate weld results of the same stress range for comparison. Table A.1 (Appendix A) outlines the relevant test details. Six samples of the slow (100 mm/min) weld exhibited excellent fatigue behaviour; the tests were terminated at or above 2.5×10^6 cycles without fracture. One sample fractured prematurely at 4.2×10^5 cycles and a second at 1.1×10^6 cycles (although both higher than the lower limit of cycles that was set) on the AD side of the weld, and this is attributed to the incomplete fusion paths observed in this segment of the weld (section 4.3.6).
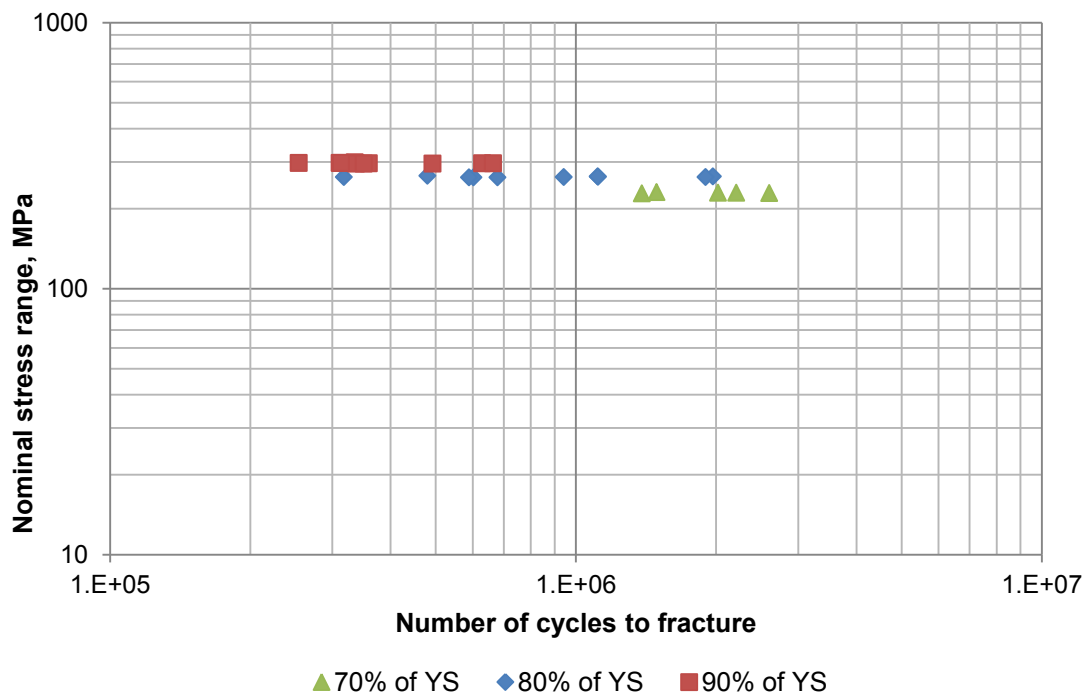
Figure 4.18. *S-N* data for the intermediate weld

The fast (500 mm/min) weld demonstrated a rather mixed fatigue behaviour; the eight samples recorded fatigue lives higher than 10^5 cycles but with some scatter of the results, from 1.3×10^5 to 7.3×10^5, and contrasting fracture regions. The varying intensity of the flaws observed in this weld is responsible for this phenomenon. In five samples, fracture propagated from the weld root flaw which has been documented earlier (Figure 4.16). The fracture location of the remaining three
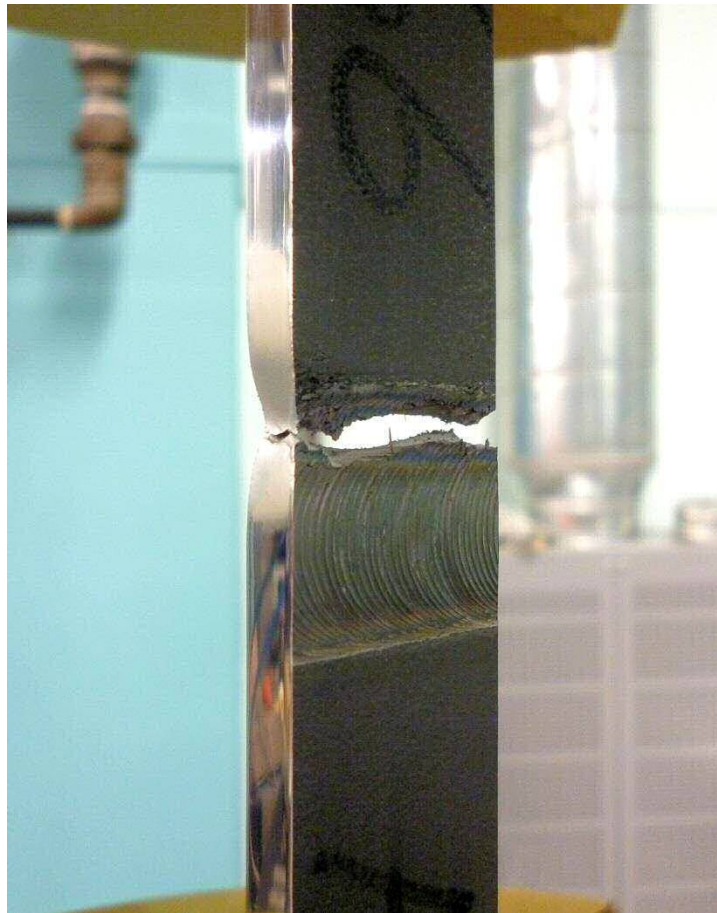
Figure 4.19. Typical fracture position of intermediate weld sample
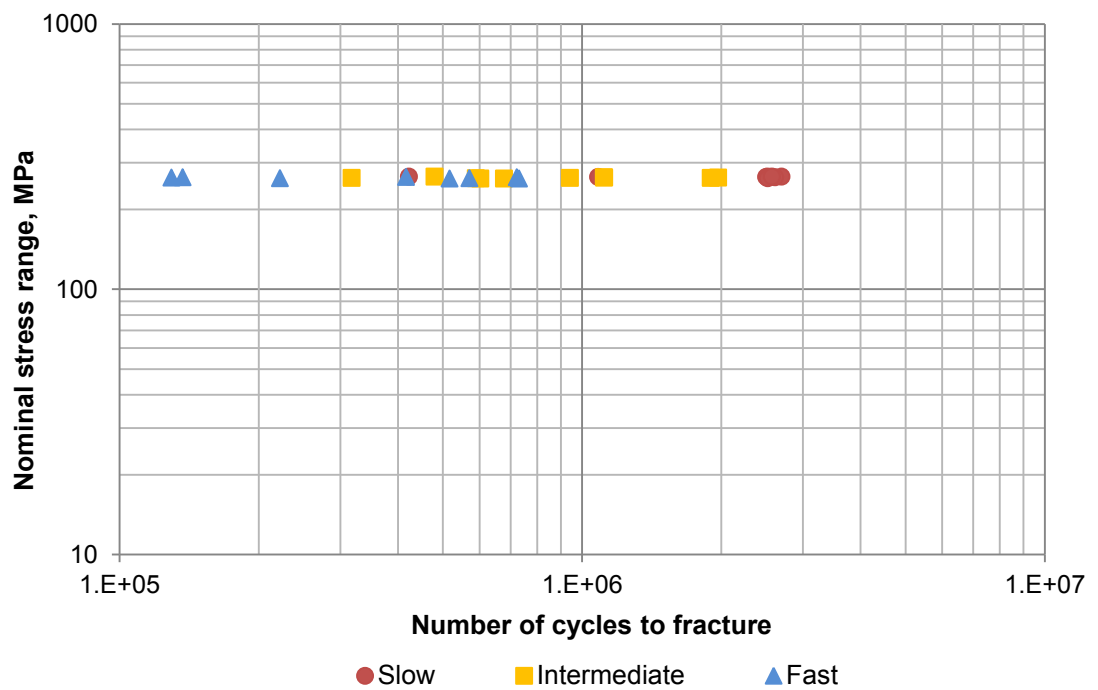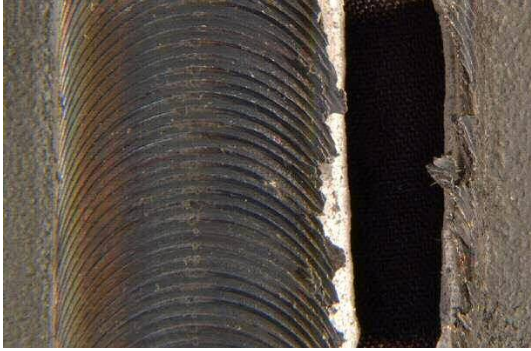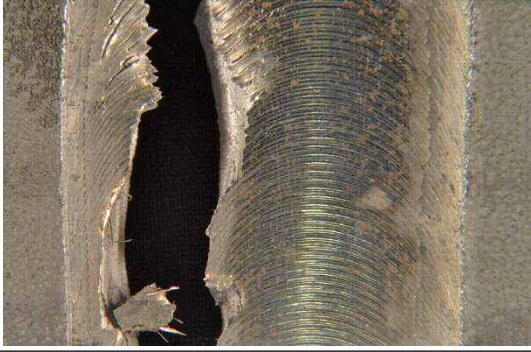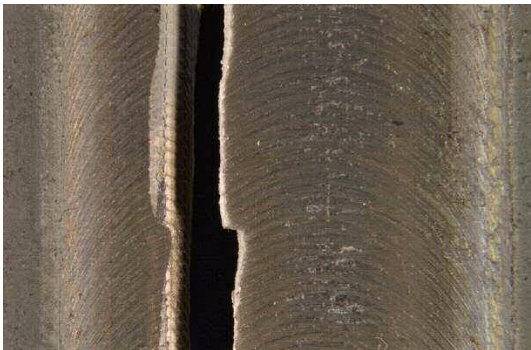
Figure 4.20. Fatigue test results for 3 welding speeds at 80% of YS

samples corresponds to the AD side laps and embedded flaws discussed in section 4.3.1. Table 4.6 outlines the fracture location of each welding speed sample that was tested in fatigue loading.

Table 4.6. Fracture location of each welding speed sample

Welding speed	Fracture location	Number of fractured samples	Top fracture surface (AD side on the left)
Inter-mediate	Outer RT side	24	
Slow	AD side	2	
Fast	Weld root	5	
	Inner AD side	3	

4.3.4. Comparison to IIW recommendations

In order to understand the relevance of the above reported results, mainly for the intermediate weld, these need to be placed in the context of international regulations and specifications. In the maritime sector for instance, the fatigue performance of welded joints is of critical importance as components are subjected to repeated cyclic loading conditions [4.7]. Most pertinent class rules are based on the recommendations of the International Institute of Welding (IIW) for fusion welds [4.32]. A series of design related fatigue classes (FAT classes) have been established to ensure safe operation of the welded joints during their effective service life and enable the streamlined and reliable design of welded structural details. The FAT classes define the cyclic stress range that will not result in fracture within 2×10^6 cycles at a 97.7% probability for various structural details (e.g. butt welding in flat position with backing strip). All values within these FAT classes are based on experimental data and refer to certain boundary conditions, specifically weld geometry, defect limits and material properties (e.g. hardness) that are stated in the IIW recommendations [4.32] and class rules.

Figure 4.21. *S-N curve of the three welds compared to the IIW FAT 80 class*

Although seemingly different from conventional fusion welds in weld geometry and metallurgical features, the fatigue loading mechanism and related design aspects of
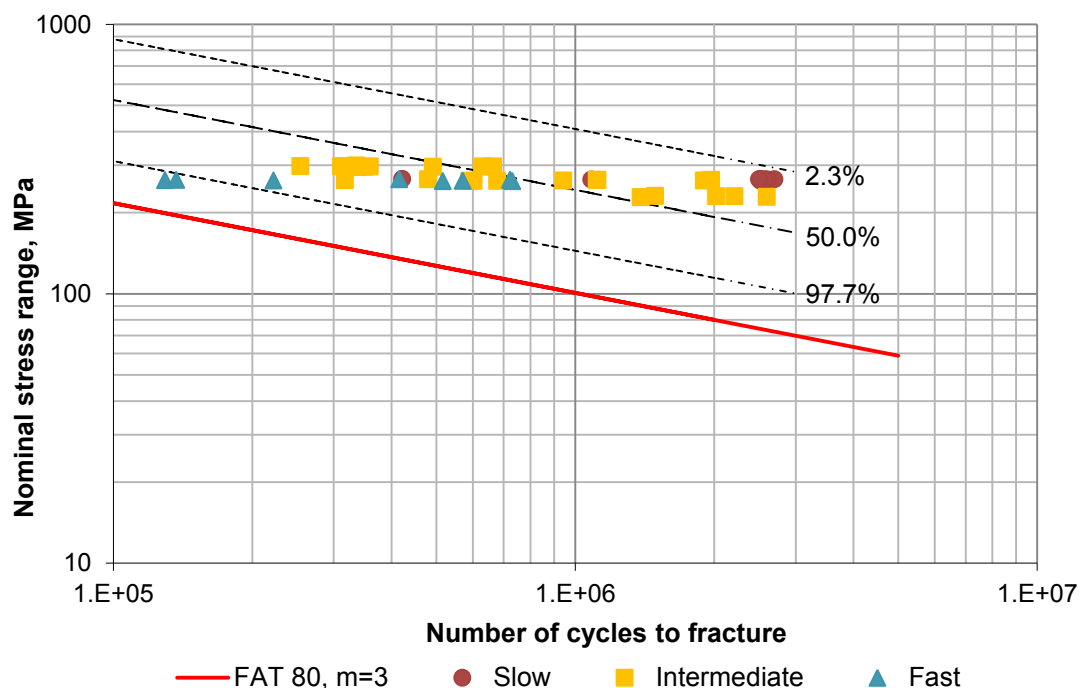
friction stir butt welds are essentially equivalent. Thus, FSW needs to be initially evaluated and compared to the established class rules for fusion welding for the process to be introduced in marine applications. Figure 4.21 displays the *S-N* curve for the three welds; the slope of the curve is m=3 according to the IIW recommendations. The dotted lines represent the probability of survival at 97.7%, 50.0% (mean) and 2.3%. The solid line indicates the IIW FAT 80 weld detail class for single sided butt welded joints at 97.7% probability of survival (detail depicted in Table 4.7) [4.32].

Table 4.7. IIW butt weld structural detail and FAT class; adapted from [4.32]

No.	Structural detail	Description	FAT Steel	Requirements and remarks
214		Transverse butt weld, welded on non-fusible temporary backing, root crack.	80	Backing removed, root visually inspected. Misalignment <10% of plate thickness.

There is a degree of scatter in the *S-N* data (Figure 4.21) due to the diverse fatigue performance of the slow and fast welds. Nonetheless, the results demonstrate higher fatigue strength for all samples of the three welds in comparison to the FAT 80 class. The fatigue strength of the FAT 80 class at 2×10^6 cycles is 80 MPa for 97.7% probability of survival. The FSW samples' fatigue strength is calculated at 114.5 MPa (again evaluated at 2×10^6 cycles for 97.7% probability of survival); this is 43% higher than the strength stated in the IIW recommendations for fusion welding. Since no standards for assessing the fatigue behaviour of steel FSW exist, analogous comparison to IIW-recommended fatigue design classes is employed by one more publication, in which the FSW fatigue data are contrasted to the FAT 112 class [4.19]. The examined welds' fatigue performance is higher than this class, which is the most demanding in fusion welding of steel [4.19].

Figure 4.22 provides a point of reference for the intermediate weld's fatigue test results when compared to the results of high quality laser welded (LW) butt joints (3 mm thick DH36 steel welds in transverse cyclic loading at 10 Hz) generated in a prior investigation [4.33]. Both sets of results display similar fatigue strengths for comparable stress ranges; in fact, FSW is seen to produce marginally longer fatigue life at the highest stress range.

As a general note, the fatigue performance of the tested samples illustrates a considerable potential of steel FSW; the welds show better overall fatigue strength in comparison to the IIW recommendations for corresponding fusion welds and comparable to laser welding, irrespective of any minor surface breaking and embedded flaws that have been detected. It is argued elsewhere [4.34] that the improved mechanical properties (predominantly higher fatigue strength) of friction stir welded steel components could conceivably lead to the use of reduced plate thicknesses, thus delivering substantial weight and cost savings for many industries such as shipbuilding.
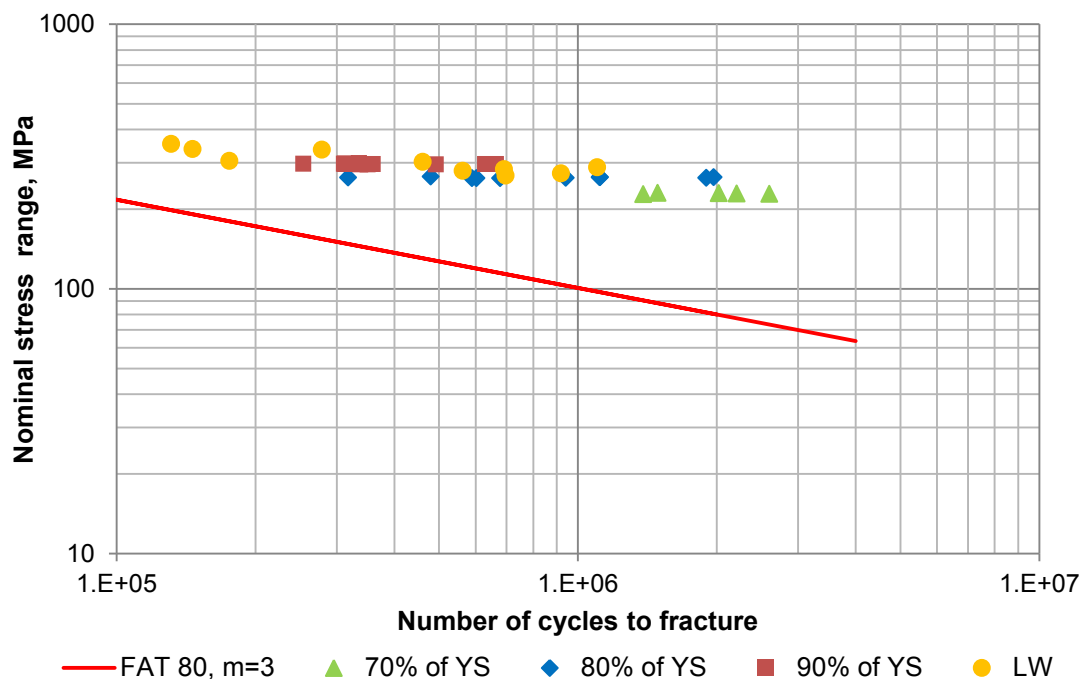
Figure 4.22. Intermediate weld fatigue test results vs. laser welding and FAT 80 class

4.3.5. Lap defect removal

Microstructural observations and subsequent measurements on the captured micrographs (Figure 4.9 is such an example) with suitable software have shown that the deepest top surface lap defect found in the intermediate speed weld is approx. 0.45 mm. Since this defect has been the decisive factor in fracture initiation, it is fitting to assess the weld's fatigue behaviour should this process related feature had been avoided, perhaps by more rigorous but costly in industrial applications prior surface preparation [4.35]. For this purpose, three supplementary fatigue tests were performed at a stress range of 90% of YS employing intermediate weld samples

from which the top 0.5 mm had been removed by fine grinding up to 800-grit SiC paper. The three tests were terminated at $3.2×10^6$ cycles or above; the samples revealed no visible evidence of fracture initiation features post-testing.
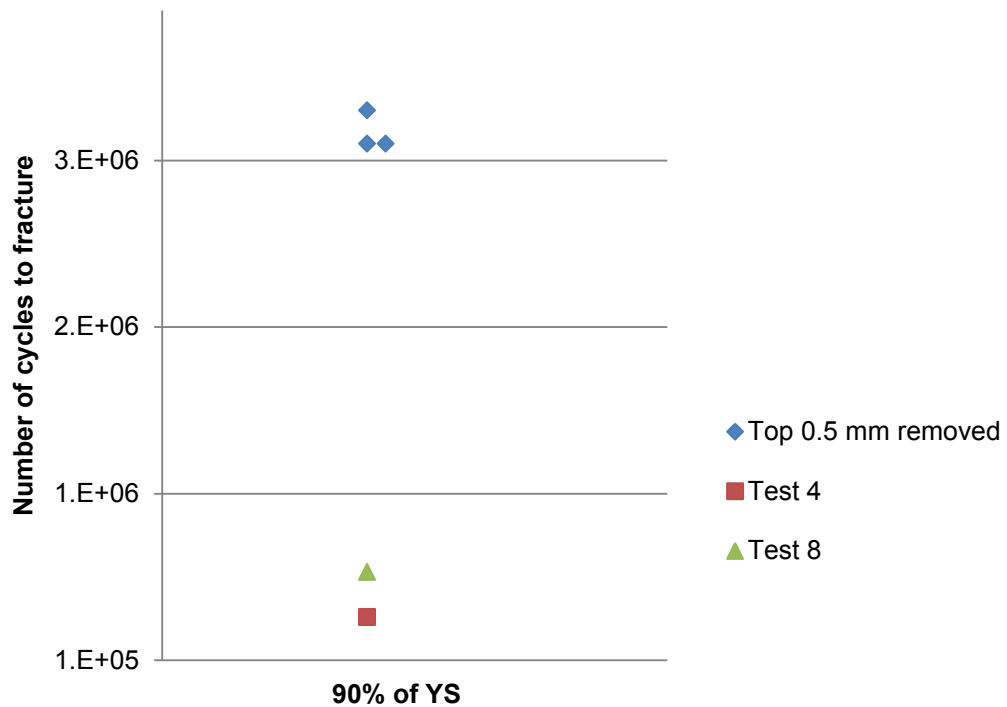
Figure 4.23. Additional tests with samples' top 0.5 mm removed vs. two standard tests

The additional samples' *S-N* data are plotted with the corresponding of two standard fatigue samples also tested at 90% of YS and sectioned from neighbouring (to the additional) sites of the intermediate weld (Figure 4.23). The supplementary samples with the top 0.5 mm removed are seen to substantially outperform the standard fatigue samples for the same stress range. This comparison offers further confirmation of a considerable improvement in fatigue life by the simple removal of the lap defect and an indication of the potentially impressive fatigue performance of the process when an acceptable quality weld (specifically, without surface breaking defects) has been achieved. A comparable approach is followed by a separate study evaluating the influence of the post-welding top surface condition on the fatigue performance of friction stir butt welded AA8090 [4.16]. As-welded samples are tested opposite to top surface treated ones by grinding which removed any weld irregularities. The surface treated samples reveal higher fatigue life than the corresponding as-welded, principally for lower stress ranges; fracture is found to initiate for the former in the base material or HAZ whereas for the latter in the weld

nugget. Thus, the research concludes that post-weld surface finishing can offer clear improvement to the fatigue behaviour because it eliminates process related flaws which serve as crack initiation sites [4.16].

4.3.6. Fracture surface analysis

Post-failure fracture surface analysis of all samples tested in fatigue loading is performed to provide information on the crack initiation sites, the crack propagation paths and the mode of fracture. To this end, the samples were positioned on a stage and high quality macrographs of their fracture surfaces were captured in a consistent manner.

A recurrent pattern of fracture is observed in the intermediate weld samples; principally brittle fracture occurred on the outer RT side, with cracks initiating from this side's lap defect (introduced in section 4.3.1, Figure 4.9) and fracture surfaces revealing the typical semi-elliptical crack propagation front [4.36]. For reporting purposes, two samples' typical fracture surfaces are presented herein as all the surfaces are almost identical. Figure 4.24 features the two extreme cases in terms of number of cycles to fracture (lowest and highest) for the intermediate group tested at 80% of YS in order to enhance the fine differences from one sample to another. Figure 4.24a presents the sample that reached 317,472 cycles to fracture; uniform crack initiation from multiple sites corresponding to the FSW tool shoulder's markings on the weld's top surface is indicated with the arrows. Each of these sites includes many secondary which are seen as light of dark shaded hairline cracks. As a result, numerous cracks propagate faster through the sample leading to reduced number of cycles hence poorer fatigue performance. The other extreme, a sample from the same weld and fatigue testing group with 1,967,444 cycles until fracture is observed in Figure 4.24b; here, crack initiation concentrated in one site. Fewer secondary hairline cracks are detected to initiate from this area. Therefore, such localised crack initiation has taken significantly longer to propagate through the entire cross-section of the sample. In contrast, the minor embedded flaw (cold shut) which has been mentioned in section 4.3.1 as seen principally in the AD side of the intermediate weld did not contribute in the fracture behaviour of the fatigue samples.

The typical shape of a friction stir butt weld is curved towards the bottom surface of the two welded plates (e.g. macrograph of Figure 4.12). The fracture plane of all intermediate fatigue samples is practically perpendicular to the weld top surface

(Figure 4.25). Thus, cracks have initiated at the outer RT side of the top surface (lap defect upper "lip" marked in Figure 4.25), propagated for a short part of the cross-section in the outer TMAZ and then advanced in the parent material. The highly refined microstructure of the weld has diverted the crack propagation path away from the weld zone and into the coarser-grained parent material. Consequently, the bottom layer of all samples' fracture surfaces (both samples in Figure 4.24), the final fracture region [4.18], is the parent plate which exhibits mainly ductile fracture as anticipated. Furthermore, examination of the regions which appear to be better welded thus exhibiting ductile fracture (right side regions of both samples' fracture surfaces in Figure 4.24) reveals less pronounced crack initiation sites on the top surface; the periodicity of these sites as they correlate to the tool shoulder's markings on the weld's surface is displayed in Figure 4.26a. The lap defect is
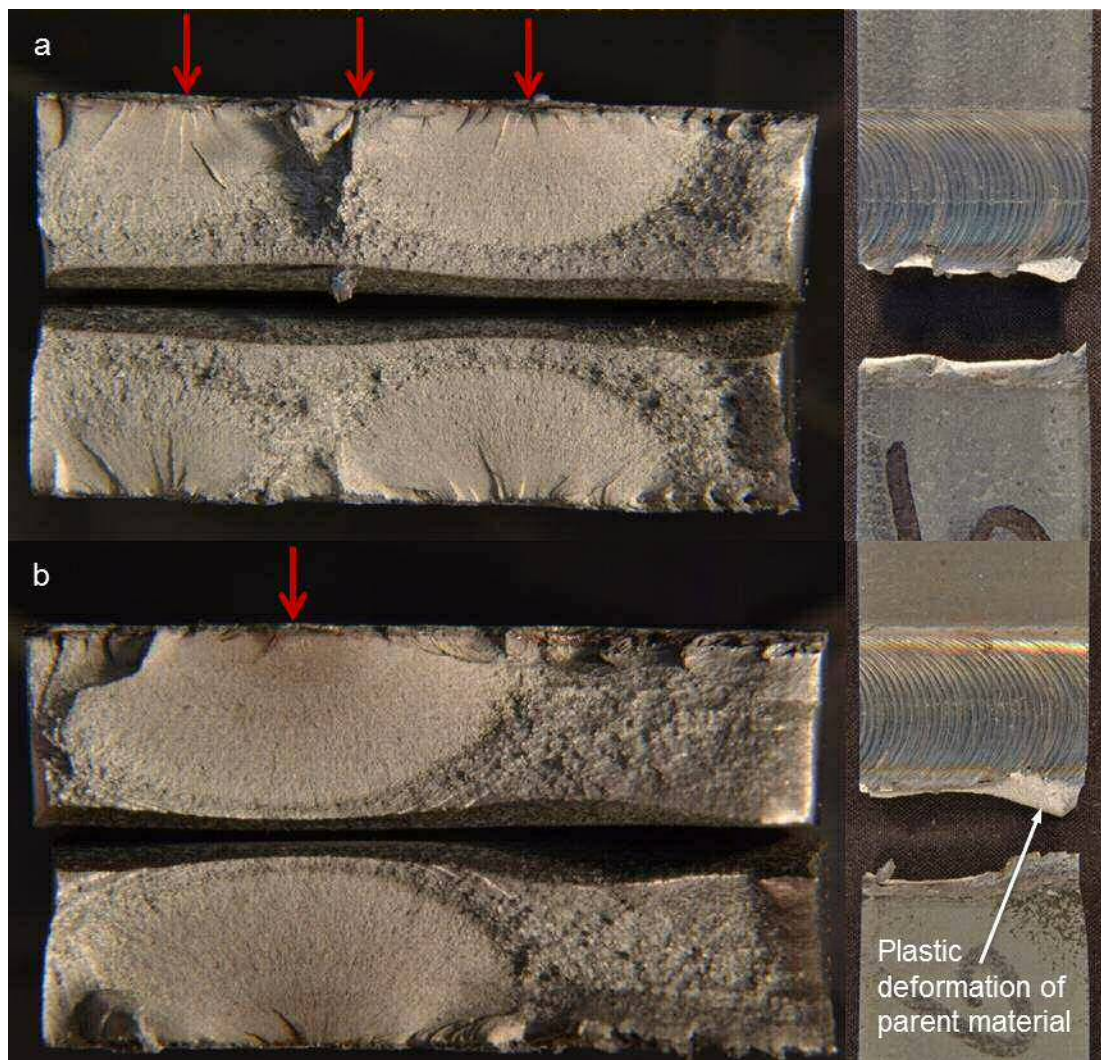
Figure 4.24. Intermediate weld samples tested at 80% of YS (a) 317,472 cycles; (b) 1,967,444 cycles

observed almost continuously along the weld length but with varying intensity and depth. Therefore, some weld regions (e.g. these marked with arrows in Figure 4.24 where the lap defect is more pronounced) have been more convenient in developing initiated cracks (Figure 4.26b demonstrates such a major crack propagation site) than others (the cracks in Figure 4.26a are seen to tail off within approx. 1 mm from the top surface).
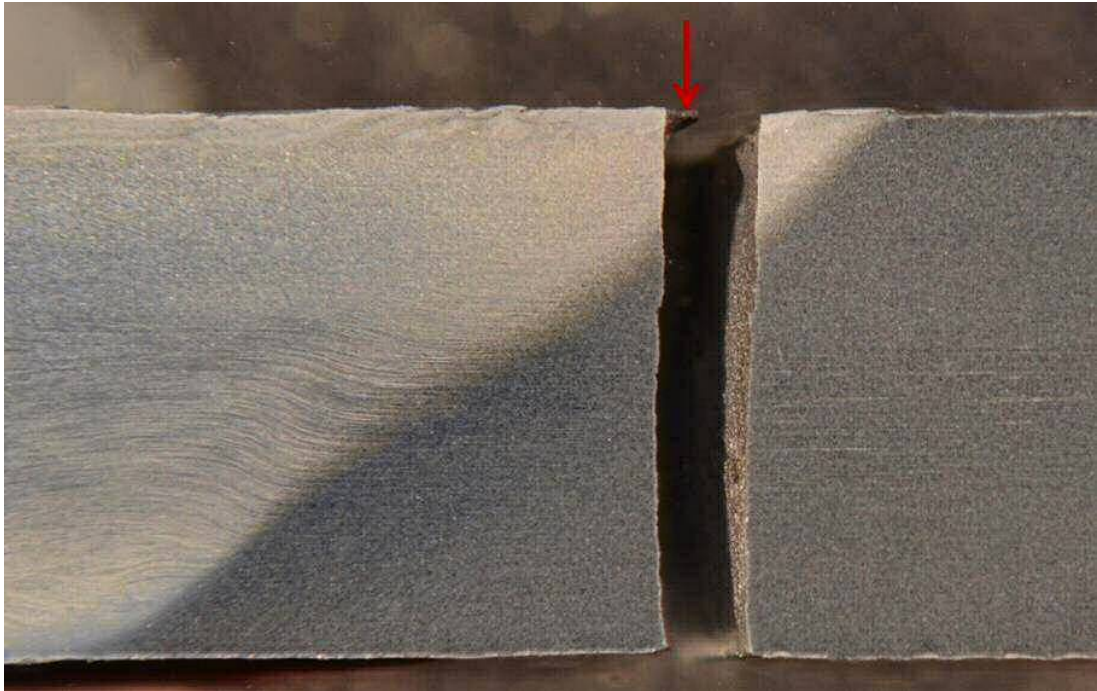
Figure 4.25. Macrograph of intermediate weld sample's fracture path (side view) [Etched]
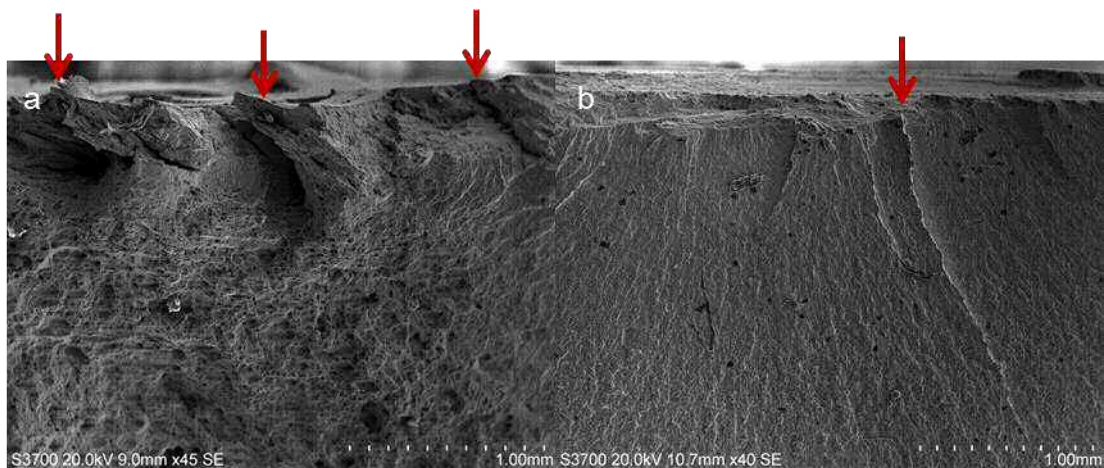
Figure 4.26. SEM examination of intermediate weld sample's crack initiation sites from top surface (RT side)
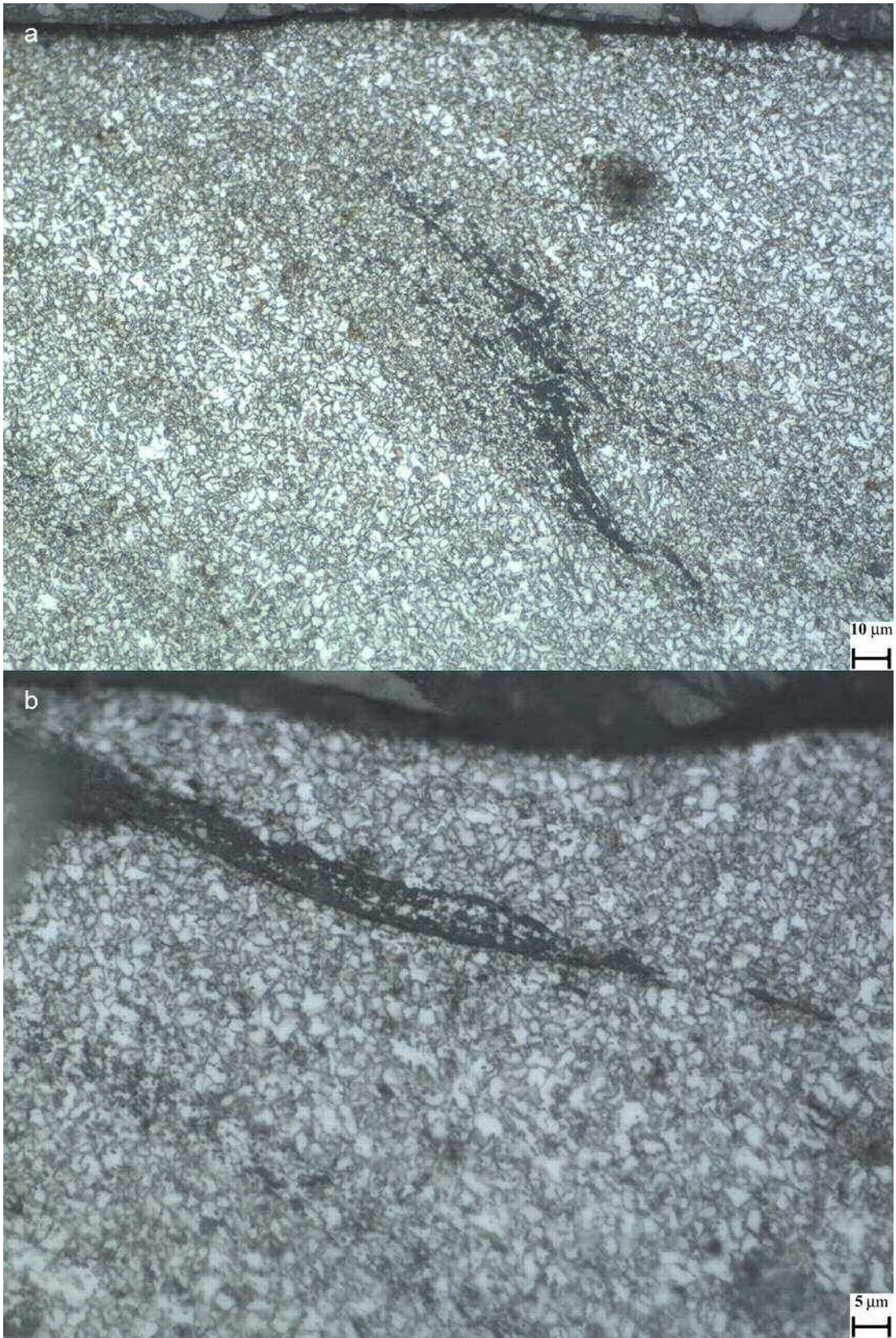
Figure 4.27. Slow weld, AD side top surface (a) [x500, Etched]; (b) [x1000, Etched]

In the case of two slow weld samples which actually fractured, the crack initiation sites have originated from incomplete fusion paths (laps) on the top AD side (Figure 4.27). These paths, which have formed in the direction of material flow, contain interconnected non-metallic inclusions (characterised as oxide scale and paint primer in section 4.3.1) and are quite steep; hence, excessive concentration of stresses must have been present. Again, the fracture path is seen to have propagated through the TMAZ and finally into the parent material in a plane nearly perpendicular to the top surface (Figure 4.28); two more pronounced of the laps from which cracks did not propagate are marked in Figure 4.28. The two fatigue samples under consideration were sectioned from immediately adjacent positions of the slow weld. Therefore, incomplete fusion paths have developed solely on this particular short section of the weld length. The fracture surfaces of these samples are analogous to the surfaces of the intermediate weld samples (Figure 4.24b).
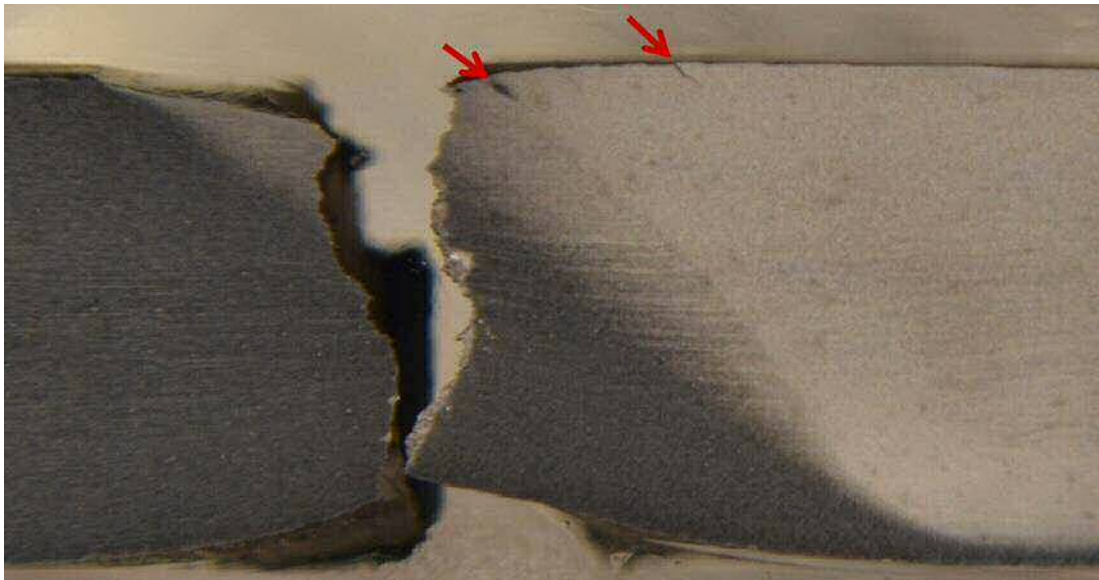
Figure 4.28. Macrograph of slow weld sample's fracture path (side view) [Etched]

Similarly to the intermediate and slow samples examined above, the five fast weld samples where cracks progressed from the weld root flaw display fracture surfaces (Figure 4.29) comparable to Figure 4.24b and a fracture plane perpendicular to the plate thickness. The crack propagated in the middle of the weld zone, almost exactly in the path of the original plate interface (Figure 4.30). The importance of the weld root flaw as a limiting factor in the fatigue performance of FSW and the difficulties in eradicating it have been established in prior studies [4.16,4.18].
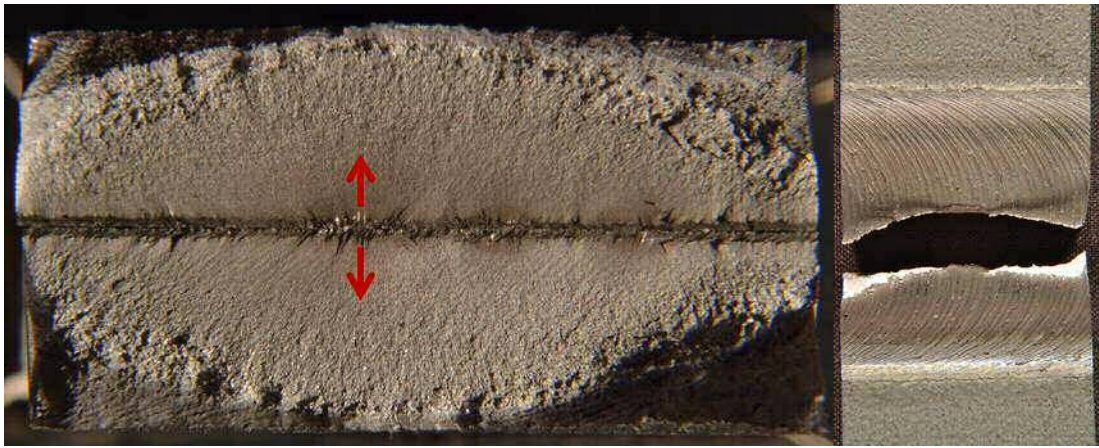
Figure 4.29. Fast weld sample tested at 80% of YS (731,208 cycles to fracture)
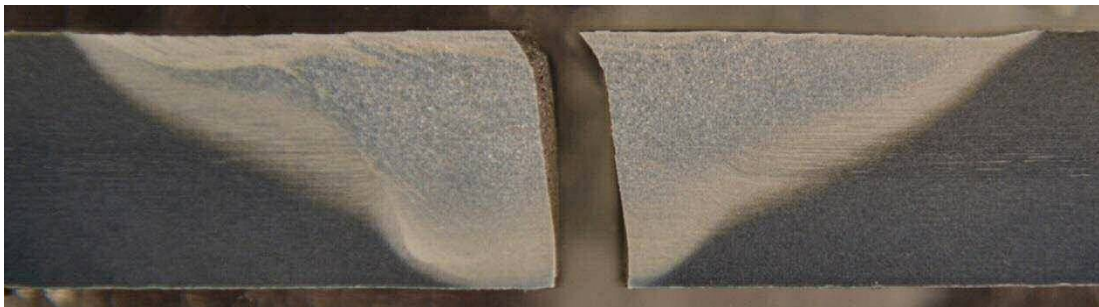
Figure 4.30. Macrograph of fast weld sample's fracture path (side view) [Etched]

However, three more fatigue samples of the fast weld reveal fracture surfaces identical to one tensile sample of the high speed welds discussed in Chapter 3 and in an earlier publication [4.4]. It was then argued that these surfaces are product of the FSW tool probe's features, indication that lower than required heat input was provided in this region, leading to insufficient plasticisation of the alloy which was ultimately mechanically worked rather than thermo-mechanically stirred by the tool [4.4]; this description is fitting in illustrating these samples' fracture surfaces (Figure 4.31). The incomplete fusion between HAZ and TMAZ (AD side) and the related voids have already been exhibited in Figure 4.17. Additionally, Figure 4.31 offers evidence of uniform crack initiation from the tool shoulder's markings on the weld top surface (as indicated on the figure).

Further investigation of the fracture mechanism in these three fast weld fatigue samples is performed by the macrograph of one sample's fracture path (side view) combined with the weld zone's macrograph (Figure 4.32) and SEM examination of the fracture surfaces (Figure 4.33). The fracture path is seen to commence at the top surface lap defect (its regular occurrence is marked with arrows in Figure 4.33a), follow the fastest route in merging with the incomplete fusion region of the AD side
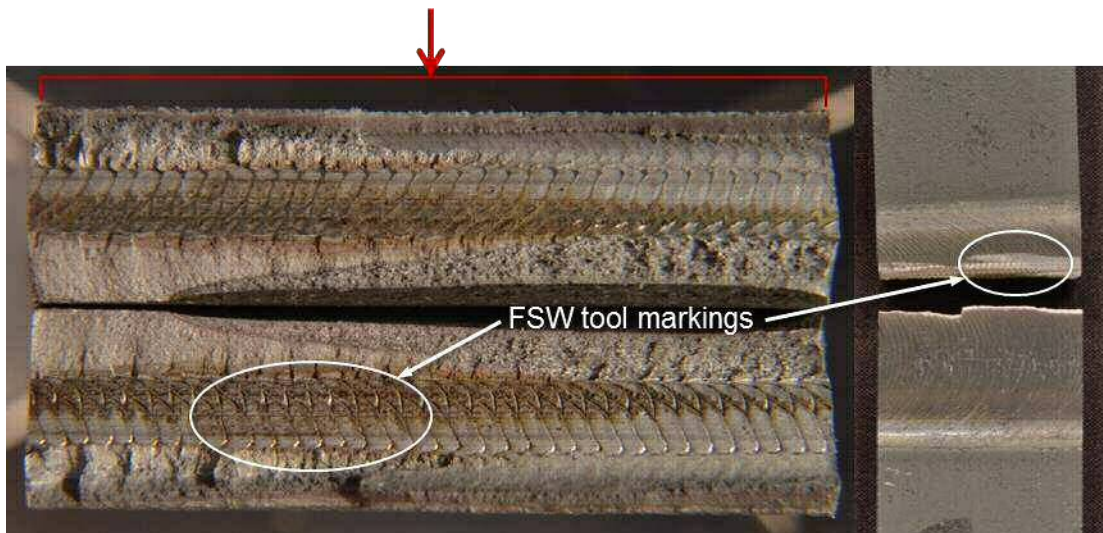
Figure 4.31. Fast weld sample tested at 80% of YS (222,272 cycles to fracture)
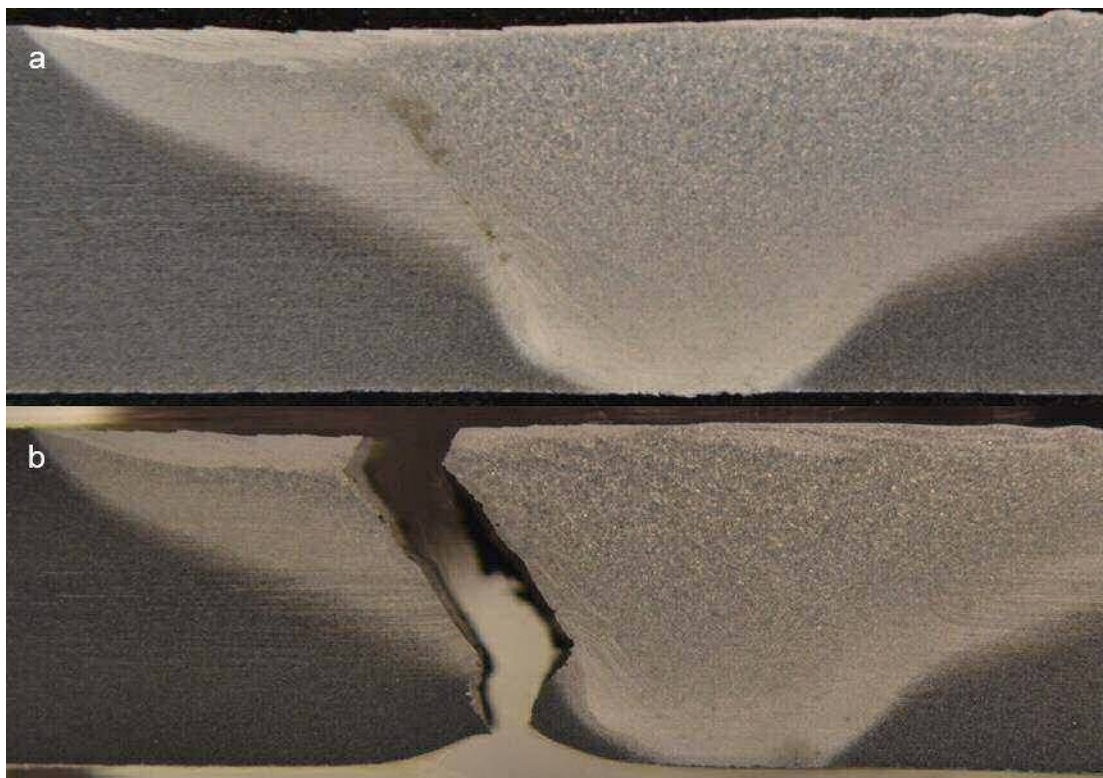
Figure 4.32. Macrograph of fast weld [Etched] (a) weld zone; (b) fatigue sample's fracture path (side view)

(i.e. the path requiring the least effort through the material) and conclude outside the weld zone when a region of adequate fusion is reached (diverted in a comparable way to the intermediate and slow weld fracture paths presented above). Furthermore, the periodicity of the embedded flaw (incomplete fusion region in which voids have developed) as it relates to the rotating FSW tool (through

correlation to the tool shoulder's top surface markings) is observed in Figure 4.33 and even clearer in Figure 4.34. The weld root flaw did not participate in the fracture path in this case.
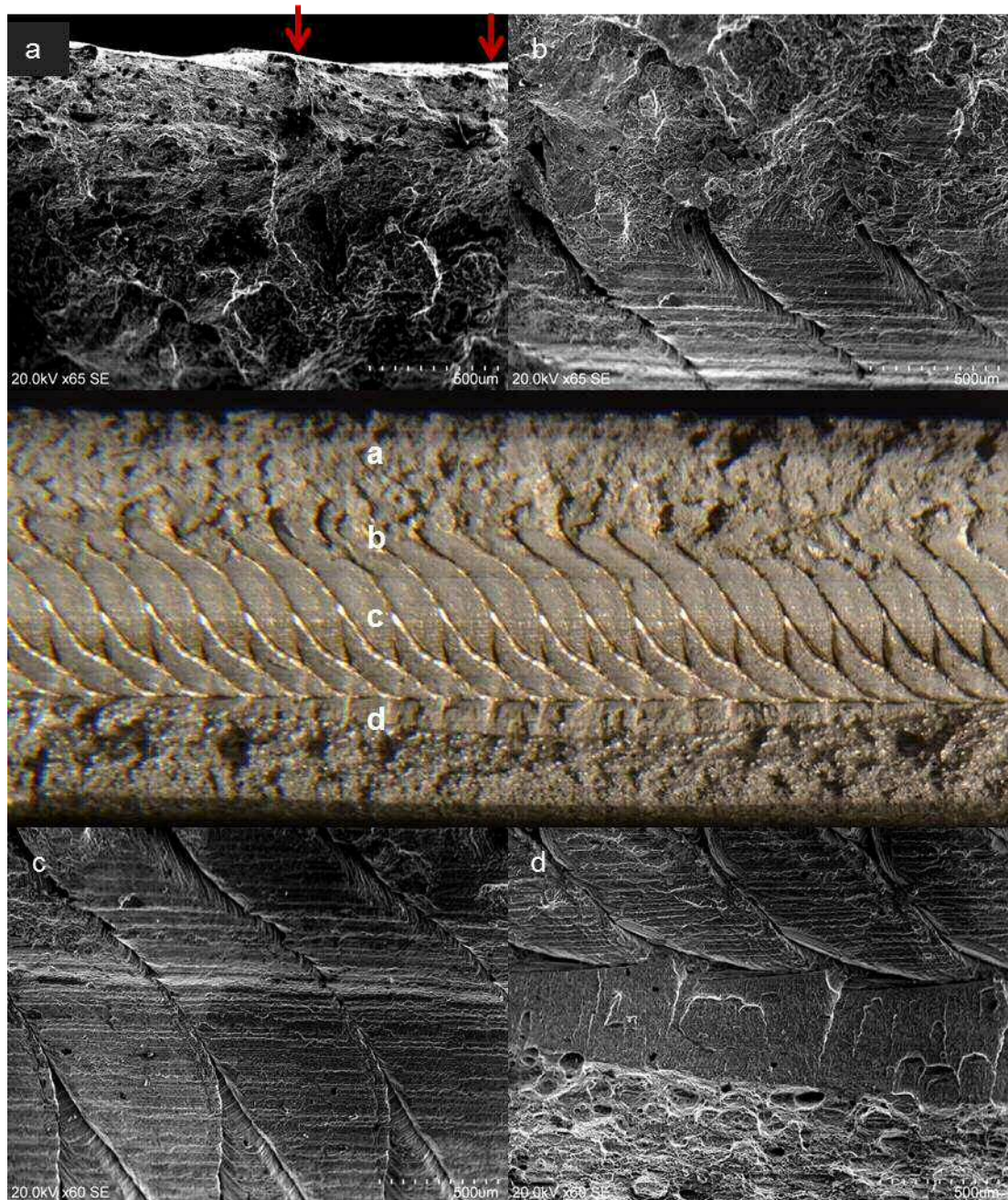
Figure 4.33. SEM examination of fast weld fatigue sample's fracture path (AD side)

The fatigue performance of the fast weld samples is inconsistent. Seven of the eight samples can roughly be classified into two groups with respect to the recorded number of cycles to fracture. One group is composed of the samples that fractured from the weld root flaw, with a range of cycles to fracture between 5.2×10^5 –
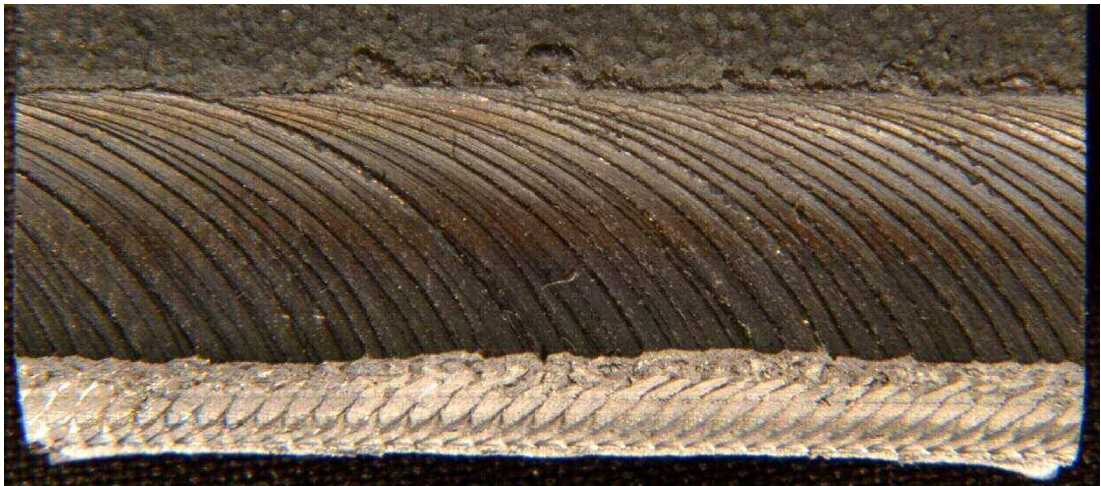
Figure 4.34. Fast weld sample tested at 80% of YS (129,490 cycles to fracture)
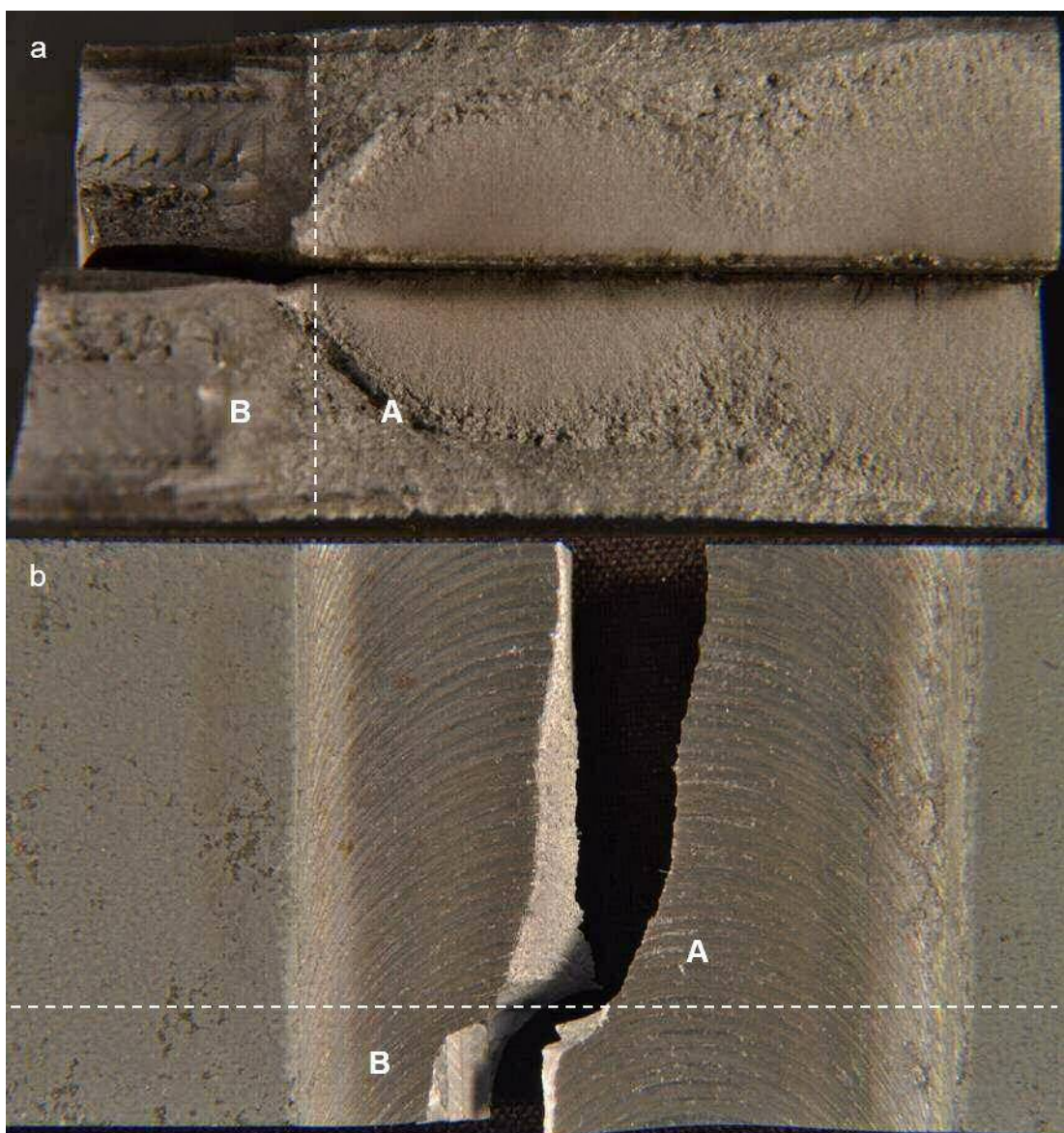
Figure 4.35. Fast weld sample tested at 80% of YS (416,112 cycles to fracture)

Chapter 4. Fatigue performance investigation   112

7.3×10^5. The second is formed by the three samples that fractured in the inner AD side; their fatigue performance is substantially poorer, in the range of 1.3×10^5 – 2.2×10^5. This signifies that the combined effect of the top surface laps and the incomplete fusion in the mid-AD side has been more detrimental to the fatigue behaviour than the weld root flaw. Interestingly, the eighth fatigue sample registered a number of cycles to fracture which is approx. in the mid-range of the two groups above, i.e. 4.2×10^5. The explanation for this behaviour is provided by examination of the fracture surfaces (Figure 4.35). The particular sample has been sectioned from a weld region which contains one occurrence of the fracture mode transition, from weld root fracture (noted as segment A in the figure) to AD side fracture (segment B); this has been captured in its fatigue performance and fracture surfaces.

4.4. Conclusions

A fully developed programme of fatigue performance assessment of 6 mm thick DH36 steel friction stir butt welds has been undertaken by adopting a comprehensive set of experimental procedures to build on the fundamental knowledge of the process and address the lack of pertinent studies for fatigue testing of friction stir welded low alloy steel. This has examined the weld microstructure and hardness distribution, geometry and possible misalignments, tensile properties and fatigue behaviour, also accounting for the effect of varying welding speed.

The observed microstructure that evolved in the three welds, their hardness distribution and the associated transverse tensile test results are in excellent agreement with the findings of the corresponding analyses in Chapter 2 and 3 respectively. The transverse tensile samples of the slow and intermediate weld which fractured in the parent material demonstrate that apart from the yield strength, static loading does not inform on the alloy's performance in real environments where cyclic loading is the dominant stress mechanism.

Extensive fatigue testing has established that friction stir welds of steel grade DH36 exhibit satisfactory fatigue life, even at a stress range of 90% of yield strength, above the weld detail class of the International Institute of Welding for single side fusion welded butt joints. The slow welding speed which produces a highly refined, homogeneous and free of embedded flaws microstructure demonstrates the best

fatigue performance of the three welding speeds which have been investigated. Notwithstanding any minor surface breaking flaws developed in the intermediate weld, high fatigue strength was recorded for three stress ranges, therefore displaying excellent fatigue performance (better than relevant international recommendations for fusion welding and equal to high quality laser welding). The fatigue strength of the high speed weld samples is reduced to a certain degree compared to the two slower welds; still, the weld achieved fatigue life above 10^5 cycles at a stress range of 80% of yield strength and this is anticipated to improve dramatically when various process related flaws are addressed.

An understanding of the relationship between weld flaws and their influence on the fatigue performance has been established. Microstructural examination, post testing fracture surface analysis identifying consistent fracture position and the complementary assessment of samples without top surface defects have demonstrated that minor embedded flaws do not offer crack initiation sites whilst surface breaking flaws such as the markings produced by the FSW tool shoulder's features on the top surface of the weld deliver a significant impact on the fatigue life. These lap defects need to be tackled by optimisation of the process parameters and improvements in the design and material of the FSW tool for steel. This investigation further justifies the need for full penetration welds and to carefully address the tool shoulder's markings which in many cases serve as the critical fracture initiation site in the absence of a weld root flaw.

4.5. References

[4.1]   Reynolds AP, Tang W, Posada M, Deloach J. Friction stir welding of DH36 steel. Sci Technol Weld Join 2003;8:455–60.

[4.2]   Konkol P, Mathers J, Johnson R, Pickens J. Friction stir welding of HSLA-65 steel for shipbuilding. J Sh Prod 2003;19:159–64.

[4.3]   Cater S, Martin J, Galloway A, McPherson N. Comparison between friction stir and submerged arc welding applied to joining DH36 and E36 shipbuilding steel. In: Mishra R, Mahoney MW, Sato Y, Hovanski Y, Verma R, editors. Frict. Stir Weld. Process. VII, Hoboken, NJ: Wiley; 2013, p. 49–58.

[4.4]   Toumpis A, Galloway A, Cater S, McPherson N. Development of a process envelope for friction stir welding of DH36 steel – A step change. Mater Des 2014;62:64–75.

[4.5]   McPherson N, Galloway A, Cater S, Hambling S. Friction stir welding of thin DH36 steel plate. Sci Technol Weld Join 2013;18:441–50.

[4.6]   Baillie P, Campbell S, Galloway A, Cater S, McPherson N. A Comparison of Double Sided Friction Stir Welding in Air and Underwater for 6mm S275 Steel Plate. Int J Chem Nucl Metall Mater Eng 2014;8:651–5.

[4.7]   Azevedo J, Infante V, Quintino L, dos Santos J. Fatigue Behaviour of Friction Stir Welded Steel Joints. Adv Mater Res 2014;891-892:1488–93.

[4.8]   Pandey K, Gupta S. Fatigue Crack Growth Analysis of Mild Steel Plate Welded by Friction Stir Welding. ASME 2013 Int. Mech. Eng. Congr. Expo., San Diego, CA: ASME; 2013, p. V009T10A013.

[4.9]   Sohar C. Lifetime Controlling Defects in Tool Steels. Berlin: Springer-Verlag; 2011.

[4.10]   Campbell F, editor. Elements of Metallurgy and Engineering Alloys. Materials Park, OH: ASM International; 2008.

[4.11]   Maddox SJ. Fatigue Strength of Welded Structures. 2nd ed. Cambridge: Woodhead Publishing; 2002.

[4.12]   Schaumann P, Collmann M. Influence of Weld Defects on the Fatigue Resistance of Thick Steel Plates. Procedia Eng 2013;66:62–72.

[4.13]   Kirkhope K, Bell R, Caron L, Basu R, Ma K-T. Weld detail fatigue life improvement techniques. Part 1: review. Mar Struct 1999;12:447–74.

[4.14]   Pilkey W. Formulas for Stress, Strain, and Structural Matrices. 2nd ed. Hoboken, NJ: Wiley; 2005.

[4.15]   Lomolino S, Tovo R, dos Santos J. On the fatigue behaviour and design curves of friction stir butt-welded Al alloys. Int J Fatigue 2005;27:305–16.

[4.16]   Pedemonte M, Gambaro C, Lertora E, Mandolfino C. Fatigue assessment of AA 8090 friction stir butt welds after surface finishing treatment. Aerosp Sci Technol 2013;27:188–92.

[4.17] Ericsson M, Sandstrom R. Influence of welding speed on the fatigue of friction stir welds, and comparison with MIG and TIG. Int J Fatigue 2003;25:1379–87.

[4.18] Kadlec M, Růžek R, Nováková L. Influence of the Kissing Bond Defect to the Fatigue Life in Friction Stir Welds of 7475 Aluminium Alloy. 10th Int. Frict. Stir Weld. Symp., Beijing, China: 2014.

[4.19] Lakshminarayanan AK, Balasubramanian V. Assessment of fatigue life and crack growth resistance of friction stir welded AISI 409M ferritic stainless steel joints. Mater Sci Eng A 2012;539:143–53.

[4.20] British Standards Institution. BS 7270. Metallic materials – Constant amplitude strain controlled axial fatigue – Method of test. London: 2006.

[4.21] Devlukia J, Bargmann H, Rüstenberg I. Fatigue Assessment of an Automotive Suspension Component using Deterministic and Probabilistic Approaches. In: Marquis G, Solin J, editors. Eur. Struct. Integr. Soc., vol. 22, Elsevier; 1997, p. 1–16.

[4.22] Lee Y-L, Taylor D. Stress-Based Fatigue Analysis and Design. In: Lee Y-L, Pan J, Hathaway R, Barkey M, editors. Fatigue Test. Anal., Burlington: Butterworth-Heinemann; 2005, p. 103–80.

[4.23] Baillie P, Campbell SW, Galloway AM, Cater SR, McPherson NA. Friction stir welding of 6 mm thick carbon steel underwater and in air. Sci Technol Weld Join 2015;20:585–93.

[4.24] Becker W, Shipley R, editors. ASM Handbook Volume 11: Failure Analysis and Prevention. Materials Park, OH: ASM International; 2002.

[4.25] King W, Hay M. Alternative and Enhanced Chemical Cleaning: Basic Studies Results FY2010. Aiken, SC: 2011.

[4.26] West GD, Birosca S, Higginson RL. Phase determination and microstructure of oxide scales formed on steel at high temperature. J Microsc 2005;217:122–9.

[4.27] Threadgill PL. Terminology in friction stir welding. Sci Technol Weld Join 2007;12:357–60.

[4.28] Chen ZW, Pasang T, Qi Y. Shear flow and formation of Nugget zone during friction stir welding of aluminium alloy 5083-O. Mater Sci Eng A 2008;474:312–6.

[4.29] He X, Gu F, Ball A. A review of numerical analysis of friction stir welding. Prog Mater Sci 2014;65:1–66.

[4.30] Seidel TU, Reynolds AP. Visualization of the material flow in AA2195 friction-stir welds using a marker insert technique. Metall Mater Trans A 2001;32:2879–84.

[4.31] Lloyd's Register. Rules for the Manufacture, Testing and Certification of Materials. London: 2014.

[4.32] Hobbacher A. Recommendations for Fatigue Design of Welded Joints and Components. International Institute of Welding, doc. IIW-1823-07. Paris: 2008.

[4.33] Collaborative Research Project BESST (Breakthrough in European Ship and Shipbuilding Technologies), E.U. Seventh Framework Programme (FP7/2007–2013), grant agreement 233980.

[4.34] Barnes SJ, Bhatti AR, Steuwer A, Johnson R, Altenkirch J, Withers PJ. Friction Stir Welding in HSLA-65 Steel: Part I. Influence of Weld Speed and Tool Material on Microstructural Development. Metall Mater Trans A 2012;43:2342–55.

[4.35] Lohwasser D, Chen Z, editors. Friction stir welding. From basics to applications. Cambridge: Woodhead Publishing; 2010.

[4.36] Pook LP. Some implications of corner point singularities. Eng Fract Mech 1994;48:367–78.

5. Thermo-mechanical deformation behaviour of DH36 steel during friction stir welding

5.1. Introduction

The newly developed process parameters (presented in Chapter 1) for the FSW of steel grade DH36 have been thoroughly assessed in terms of microstructural evolution (Chapter 2) and resultant mechanical properties (Chapter 3); since the fatigue performance of the welds is of high priority for marine applications, this has been evaluated separately in Chapter 4. For a comprehensive examination of DH36 steel FSW however, it is equally important to explore the thermo-mechanical response of the material during the welding process.

The behaviour of an alloy under thermo-mechanical deformation, as in the case of FSW, can be accurately represented by determining the evolution of flow stress as a function of test temperature and strain rate [5.1]. The flow stress of a material, the stress that yields the material as a function of strain, is an important consideration when deciding on the basic parameters of a metalworking process [5.2-5.4]. It is influenced by many factors; material properties such as grain size, crystal structure, existing phases, and process requirements including temperature and strain rate [5.1,5.3]. FSW is developed by thermo-mechanical stirring hence can be viewed as one such metalworking process [5.5]. Therefore, it is critical that an understanding of the flow stress generated over a range of temperatures and strain rates is achieved such that improvements in process parameters and in the accuracy of any predictive modelling being undertaken will be more robust as a result of these experimental data.

Clearly, the experimental conditions to be adopted, i.e. test temperature and rate of deformation need to closely match the actual conditions occurring during FSW. Moreover, knowledge of the thermal cycle alone is not enough to understand and consequently simulate the FSW process; the severe mechanical work, a major part of the process, is recognised as paramount in microstructural evolution and one of the differentiating factors from the corresponding microstructures which evolve in fusion welding along with the lower peak temperatures reached in FSW [5.6].

There are diverse thermo-mechanical deformation data on steels [5.4,5.7-5.15] and other alloys [5.16-5.19] available in the relevant technical literature, none of which is on steel grade DH36 and in conditions that simulate FSW. One publication [5.4] discusses the effect of temperature and strain rate on the high temperature (850°C–1150°C) deformation behaviour of 42CrMo medium carbon low alloy steel by hot compression testing on a Gleeble thermo-mechanical simulator. It is reported that in high temperature and low strain rate deformation conditions, flow stress curves consist of four diverse stages which are governed by two opposing phenomena, work hardening and thermally induced flow softening, specifically dynamic recrystallisation (DRX) and dynamic recovery (DRV) [5.4]. In conditions of lower temperature and higher strain rate however, the last two stages, i.e. the rapid decrease of flow stress due to DRX and high dislocation annihilation followed by a steady state flow stress are less discrete as DRV becomes the principal phenomenon. The same work [5.4] notes that the alloy's flow stress is greatly influenced by test temperature and strain rate. Deformation by hot compression occurs primarily by thermally induced phenomena, mainly DRX which is dependent on temperature and duration of deformation; that is, increased temperature and decreased strain rate, i.e. longer deformation duration, offer more time for thermal energy accretion hence induce higher mobility at grain boundaries for DRX and dislocation annihilation to develop, both of which effectively decrease the flow stress. As explained [5.4], flow softening is frequently exhibited by steel alloys in such thermo-mechanical deformation conditions associated with common metalworking processes.

Abbasi and Momeni [5.8] assess the hot workability of Fe-29Ni-17Co, the properties of which are highly affected in high temperature deformation processes, by hot compression tests in the temperature range of 900°C–1200°C and strain rates from 10^{-3}/s to 10/s, and a fairly limited microstructural examination of the deformed samples. Discussing the flow stress curves of the alloy [5.8], it is noted that DRX with a single peak stress is exhibited in the high temperature / low strain rate conditions, i.e. a grain refinement method. In low temperature / high strain rate testing conditions, the flow stress curves demonstrate a steady rise, without one distinctive peak, to the end of the deformation. In comparable terms to the above explanation [5.4], the latter indicates that the extent of DRX is reduced because these conditions do not bear enough thermal activation energy; work hardening is the leading process in this case [5.8]. The alloy's processing map, a map for

identifying the processing conditions where the desirable effects of DRX occur, is also developed; the study [5.8] concludes that the processing map, mechanical testing and microstructural examination confirm that the most appropriate temperature range for hot deformation of the specific alloy is 1000°C–1200°C due to its improved workability because of enhanced DRX.

Another study [5.12] is conducted in similar testing conditions, hot compression tests at 850°C–1150°C in strain rates of 10^{-4}/s to 3/s, to evaluate the flow stress and the effect of DRX on the deformation behaviour of a medium carbon microalloyed steel. The presented analysis [5.12] is in agreement with the observations of the previous study [5.8]; nearly all flow stress curves for high test temperatures reveal a single peak stress and subsequent progressive decrease to a steady state stress, hence the occurrence of DRX. Again, the single peak stress is difficult to identify with increasing strain rate or decreasing test temperature, thus the impact of DRX is limited while at the lowest examined test temperature (850°C), no DRX but DRV takes place [5.12].

In the present thermo-mechanical deformation study, hot axisymmetric compression testing is undertaken in order to assess the behaviour of low alloy steel grade DH36 at elevated temperatures and generate flow stress data reproducing the deformation which is developed during the actual FSW process. The intention is to validate any relevant modelling work on FSW and in particular, modelling focused on the material flow around the tool and the resultant process forces that develop, advance the fundamental understanding of the process, assist in establishing process parameters and finally, improve the tooling and machine specifications during future FSW developments, e.g. pre-heat assisted FSW.

A key objective of the current testing programme is the physical simulation of steel FSW, since the alloy is being deformed in conditions which approximate the process. This research work will generate important data to support developments in FSW of steel. Nevertheless, equally valuable information will be derived from a microstructural examination of the deformed samples. To this end, the processed samples are cooled in a specific cooling rate for each test temperature to closely match the entire thermal cycle inside the welded steel. In parallel, a second testing programme which investigates the effect of the same thermal cycles on identical samples but without deformation is carried out. Subsequent metallographic preparation, microstructural characterisation and comparison to actual DH36 steel

FSW samples is performed to allow for a detailed evaluation of the influence of temperature and strain rate (independently) on the evolved microstructure; such a study is the first of this type on DH36 steel and its results will further strengthen the understanding of the FSW process.

5.2. Experimental procedures

5.2.1. Testing details

Solid cylindrical samples (9 mm diameter, 18 mm length) were produced from a 10 mm thick rolled plate of steel grade DH36 in the as received condition (details provided in Chapter 2). The flow stress of the material was recorded for 25 diverse sets of temperature and medium to high strain rate (Table 5.1) by performing 58 uniaxial hot compression tests on a Gleeble 3800 thermo-mechanical testing system. This testing method has been previously discussed as appropriate for deformation studies that establish the true stress / true strain curve of a material [5.20], as in the current work.

Table 5.1. Number of thermo-mechanical deformation tests performed per set of test temperature and strain rate

Test parameters	10^{-3}/s	10^{-2}/s	10^{-1}/s	1/s	10/s	50/s	10^2/s
700°C	3	2					
750°C	2	2	2				
800°C	2	3	3				
850°C		3	2	3			
900°C			2	2	3	2	
950°C				2	3	2	2
1000°C					3	2	2
1100°C					2	2	2

The deformation parameters of Table 5.1 and the thermal cycle of the simulation are based on an analysis of data generated by thermocouples that were accurately positioned in various regions within the weld zone of 6 mm DH36 plates subjected to FSW [5.21]. The combined temperature distribution map of Figure 5.1 was produced by this comprehensive study; the map is composed of temperature measurements

during multiple experiments, therefore these values should be considered as representative of each weld region rather than of a specific position [5.21]. In this analysis, material flow occurring below 700°C and with low strain rate is found to be essentially insignificant. Conversely, the metal under the shoulder and around the probe of the tool is found to be experiencing temperatures close to or above 1100°C and high strain rates (10/s–10^2/s) [5.21]; strain rates of 10^2/s have also been reported elsewhere [5.5]. These conditions are therefore the processing envelope of FSW and are appropriate for a simulation of the process. Barnes et $al.$ [5.6] predict a comparable temperature gradient, a decrease in peak temperature with increasing weld depth, since the influence of the thermal energy produced by the tool shoulder on the evolved microstructure is seen to decline. An earlier study [5.5] has also employed thermocouples placed in short channels inside the steel plate and on the top surface in order to improve the understanding of the processing conditions. It is explained [5.5] that there are challenges involved in this approach, especially with regard to the correct positioning of the thermocouples during welding. The study has recorded peak surface temperatures of approx. 1000°C close to the tool shoulder / plate contact area but with suboptimal process parameters [5.5] (see relevant discussion in Chapter 2).
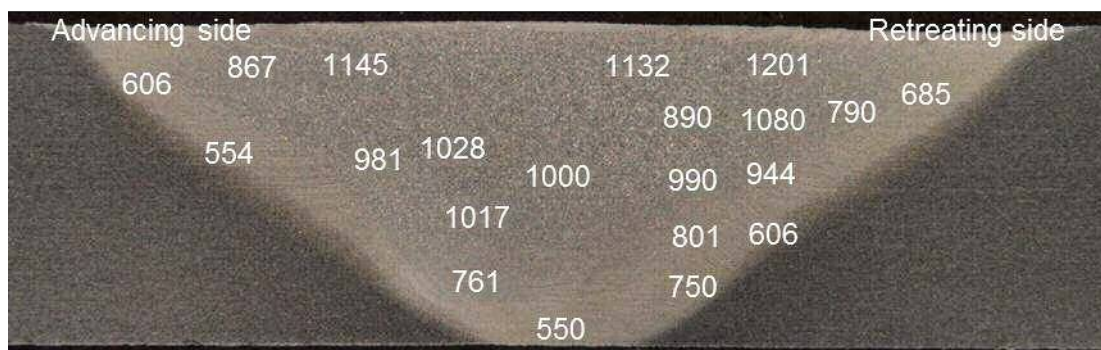
Figure 5.1. Temperature distribution map of a typical friction stir weld in DH36 [5.21]

The testing programme has been implemented according to the guidelines set by Roebuck et $al.$ [5.22]. The consistent experimental procedure which was followed throughout this programme is outlined below:

1. Spot welding thermocouples onto the sample,

2. Applying conductive paste and fixing small graphite plates on the two faces of the steel sample to prevent it from bonding with the anvils of the machine. Samples

used at the very high test temperatures (above 1000°C), where graphite will react with steel, were fitted with thin pieces of tantalum foil.

3. Inserting and securing the sample in the pre-calibrated Gleeble (Figure 5.2),

4. Heating each sample at a heating rate of 80°C/s using direct resistance heating,

5. Equalising the temperature for 60 s in order to ensure that the compressive test occurs when the required test temperature is homogenous in the entire sample,

6. Performing the compressive test in vacuum, at the homogenous temperature (isothermal) and up to 0.693 strain (standard 50% deformation),

7. Ending compressive test and air cooling each sample at a predetermined cooling rate for each test temperature, as per Table 5.2.
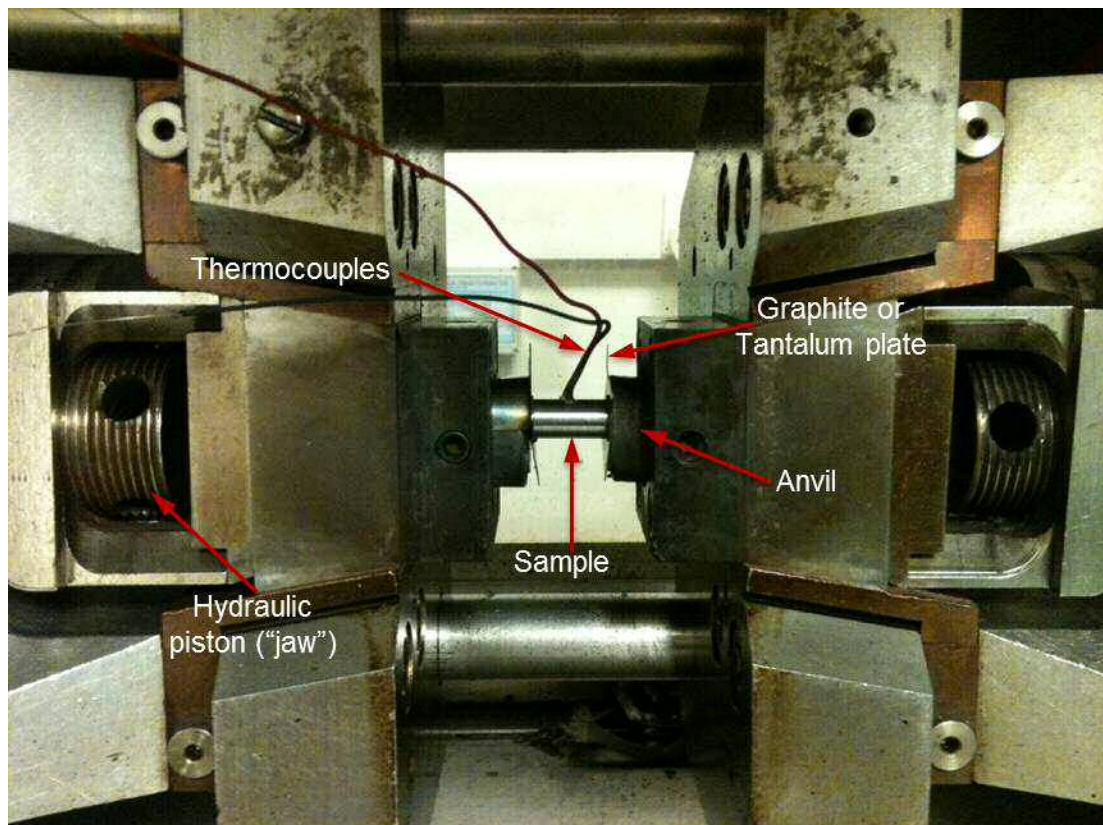
Figure 5.2. The Gleeble testing chamber

Cooling rates in the range of 5-10°C/s are calculated in a prior research work on steel FSW in which traverse speeds between 25 mm/min and 100 mm/min are evaluated [5.5]. Welding in higher traverse speeds, as the intermediate and fast group explored in this thesis (Table 1.1) has developed faster cooling rates and this is reflected in Table 5.2. Lienert *et al.* [5.5] argue that it is usually more suitable to

use the cooling rate for the temperature region of 800°C to 500°C than the average rate of the entire cooling cycle (from peak to room temperature); the same approach has been followed in the current work. Although the cooling rate of each test is maintained constant for this part (800°C-500°C) as specified in Table 5.2, this is seen to slow down as cooling progresses below approx. 450°C. Nevertheless, analysis of thermocouple data has confirmed that this effect closely simulates the actual FSW process; natural air cooling of the welded plates proceeds with decreasing rate as the temperature approach the ambient [5.21].

Table 5.2. Cooling rate per test temperature

Test temperature	Cooling rate
700°C	10°C/s
750°C	15°C/s
800°C	10°C/s
850°C	15°C/s
900°C	15°C/s
950°C	20°C/s
1000°C	15°C/s
1100°C	20°C/s

In parallel, a second testing programme for thermally treated samples was also undertaken to isolate the effect of strain energy on the microstructural evolution (Table 5.3). To improve the consistency of the results and to allow for more reliable comparison with the hot compressed samples, this second programme involved the use of DH36 steel samples of identical dimensions to the above thermo-mechanical deformation programme, sectioned from the same steel plate, tested on the same Gleeble 3800 thermo-mechanical testing system and in an analogous experimental procedure, particularly with respect to an equivalent thermal cycle, namely:

1. Spot welding thermocouples onto the sample and securing it in the Gleeble as detailed above,

2. Applying the same heating rate of 80°C/s, temperature equalising time of 60 s and subsequently cooling rates as in Table 5.2,

3. Ending test without exerting any compressive deformation on the sample.

Table 5.3. Number of thermal treatment tests performed per test temperature

Test temperature	Number of tests
700°C	2
750°C	2
800°C	2
850°C	2
900°C	2
950°C	2
1000°C	2
1100°C	2

5.2.2. Microstructural characterisation

Publications [5.20,5.23] explain that in hot axisymmetric compression testing, friction between the compressed sample and the testing machine's anvils needs to be contained through the use of lubrication and thin platens; these two methods have been employed herein (see step 2 in the thermo-mechanical deformation testing procedure above). Reduced friction results in decreased barrelling effect, thus enabling the sample to deform uniformly. This also minimises the development of a dead zone [5.20,5.23], i.e. a region outside the sample's centre and towards its circumference that remains essentially undeformed during hot compression testing [5.24]. As an illustration, a separate study reports on uneven barrelling and dead zone in hot compressed 1035 steel samples and this is partly attributed to variations in lubrication [5.24].

To provide a high level of confidence in the examination of the experimentally generated microstructures, thermo-mechanically deformed and thermally treated samples were transversely sectioned approximately at the midpoint of their longitudinal axis; the subsequent optical microscopy focused on the microstructure at the centre of this transverse section, hence away of any dead zone which might have emerged. Furthermore, an effort was made to section each sample exactly where the thermocouples had been spot welded, thus establishing that the recorded thermal cycle had been experienced by the particular steel section. One sample from each set of conditions of both testing programmes was sectioned as defined above and metallographically prepared by adhering to the process described in Chapter 2. Characterisation of the evolved microstructures was performed using the

light optical microscope also introduced in Chapter 2. Energy dispersive spectroscopy (EDS) on the Hitachi scanning electron microscope (SEM) which is first presented in Chapter 2 was employed for chemical characterisation of the elemental segregation on the steel plate centreline.

5.3.   Results and discussion

5.3.1. Flow stress analysis

Thermo-mechanical deformation data were generated for each set of conditions outlined in Table 5.1 and these data were plotted in stress – strain charts to evaluate their consistency. Each plotted curve is the flow stress of DH36 parent material within specific boundary conditions (test temperature, strain rate and strain). Two tests were conducted for each set of conditions and in most cases, the consistency of the results was found to be very good or excellent (Figure 5.3). Where the repeatability of the data was deemed inadequate due to minor deviations in the flow stress curves, a third test was performed. The temperature profile for each test was also plotted in order to provide confirmation that the required thermal cycle was
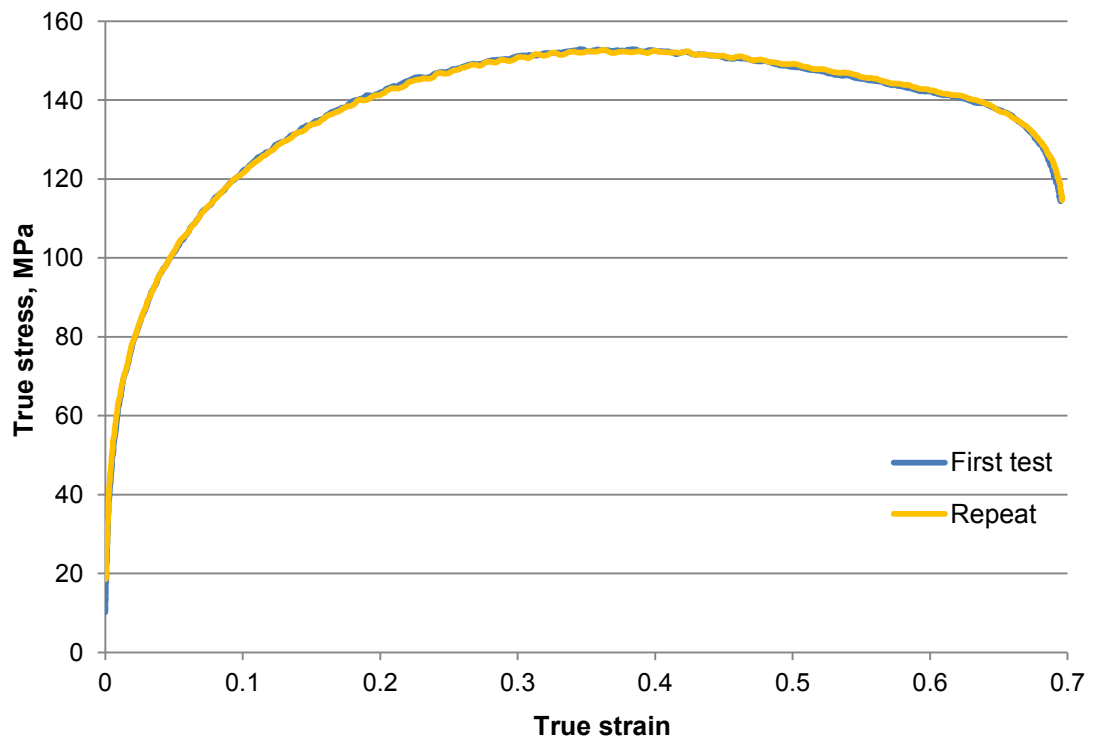
Figure 5.3. Flow stress chart for 2 tests at 10/s – 1100°C
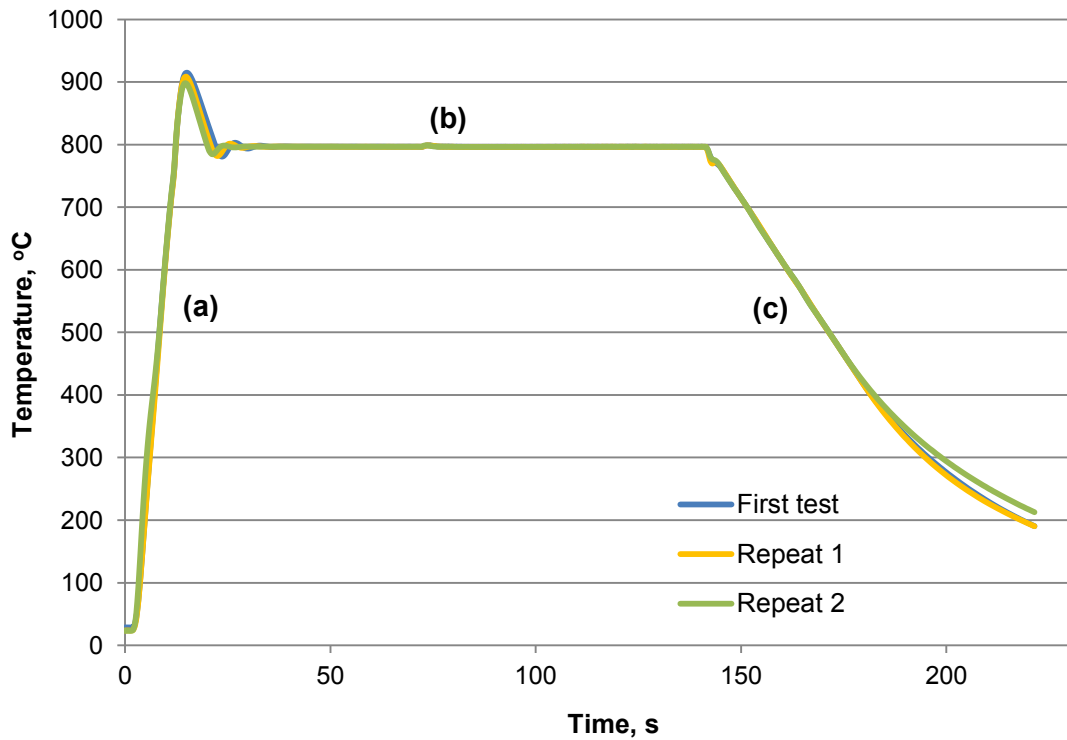
Figure 5.4. Temperature profile for the 3 tests at 10⁻¹/s – 800°C (a) heating stage; (b) equalising and deformation stage; (c) cooling stage
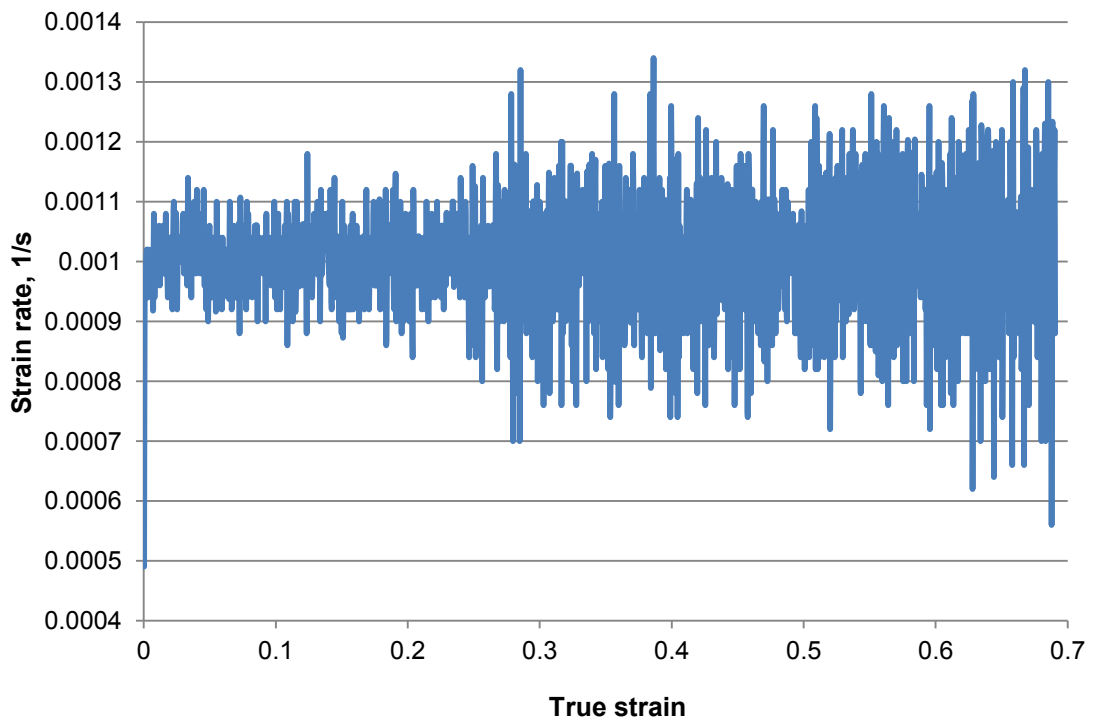
Figure 5.5. Strain rate profile for test "Repeat 2" at 10⁻³/s – 700°C

followed and that the test temperature was kept constant during the equalising and deformation stage. One such plotted temperature profile is presented in Figure 5.4.

Further, the strain rate profile (strain rate vs. strain) was plotted for the deformation stage of each test to verify that the prescribed strain rate was exerted on the sample during the majority of the deformation (Figure 5.5).

The evolution of flow stress in steel alloys follows two patterns [5.1,5.3,5.4,5.8,5.12] and these were verified in DH36. First, the flow stress is seen to increase with increasing strain rate. This is represented in Figure 5.6 where the flow stress curves of four tests with increasing strain rate and constant temperature have been superimposed. Second, the flow stress is seen to decrease with increasing temperature. This relation is exhibited in Figure 5.7 where four tests of increasing temperature and constant strain rate of 10^{-2}/s have been plotted. Hence, the flow softening phenomenon is found to be more pronounced as the strain rate is seen to decrease for a fixed temperature (Figure 5.6) and as the deformation temperature is seen to increase at a constant strain rate (Figure 5.7). It has been confirmed by previous studies [5.4,5.8] that there is either more deformation time or higher temperature respectively for thermal energy build-up which promotes DRX. On this account, the flow stress is seen to increase but at a decreasing rate in both figures.
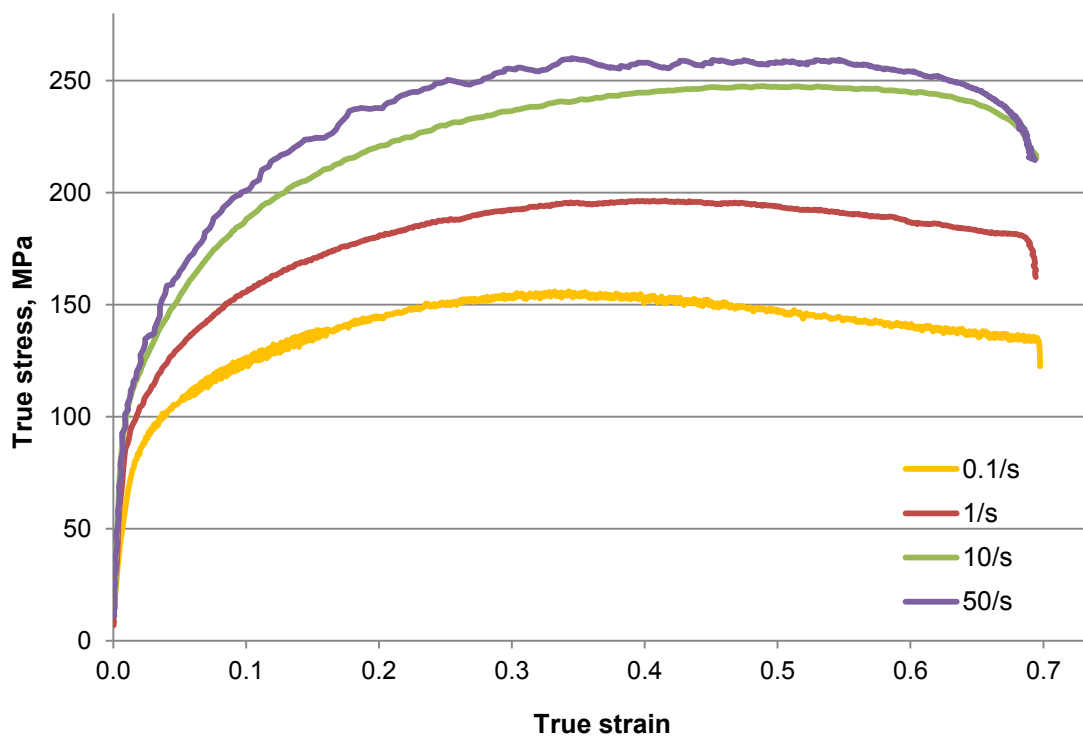
Figure 5.6. Evolution of flow stress with increasing strain rate (at 900°C)
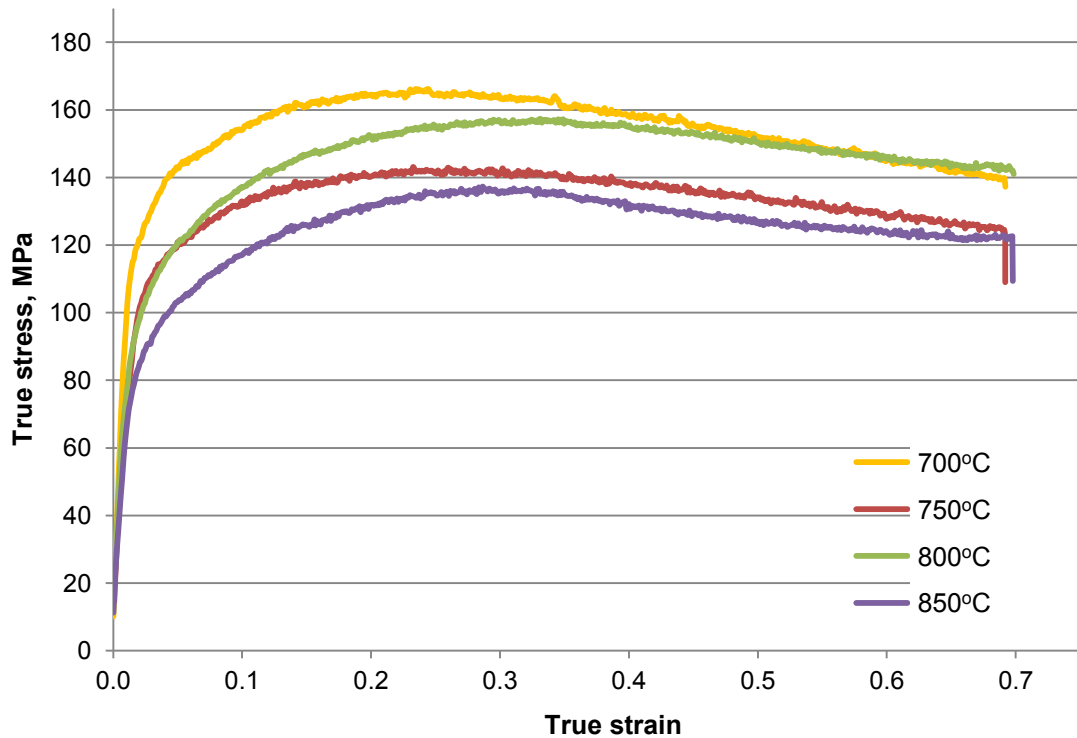
Figure 5.7. Evolution of flow stress with increasing temperature (at 10^{-2}/s)

This deformation behaviour of DH36 steel indicates that FSW parameters which produce regions of high strain rate and lower temperature within the weld zone may develop embedded flaws as a consequence of insufficient material flow; such conditions can occur when welding with inadequate heat input generation in high traverse speeds (suggesting high rate of deformation), for instance in suboptimal process parameters. Nevertheless, the same behaviour offers an explanation for the fact that slow welding speeds (normally producing high heat input and lower strain rates) rarely give rise to any embedded flaws; the latter has been consistently demonstrated in Chapter 2 and 4 and in earlier publications [5.5,5.25].

Two of the four flow stress curves in Figure 5.6 (strain rate of 10^{-1}/s and 1/s), i.e. low strain rates at a high temperature, and all curves of Figure 5.7, i.e. flow stress at a very low strain rate (10^{-2}/s) exhibit the common DRX behaviour with a relatively distinct single peak also reported by a previous study [5.8]. Thus, extensive grain refinement is expected to be occurring in such deformation conditions which simulate regions of a typical friction stir weld. One peak stress becomes difficult to determine as the strain rate is seen to increase for the constant deformation temperature of 900°C (Figure 5.6), particularly for the tests in strain rate of 10/s and 50/s. This suggests that the influence of DRX is reduced similarly to the relevant

discussion in another publication [5.12]. Table 5.4 presents the average value of the recorded flow stress for each set of deformation parameters that were tested and for 0.3 strain. The values in the table verify the previously mentioned effect of increasing temperature and strain rate on flow stress.

Table 5.4. Average flow stress (in MPa) for each set of parameters at 0.3 strain

Test parameters	10^{-3}/s	10^{-2}/s	10^{-1}/s	1/s	10/s	50/s	10^2/s
700°C	109	163.5					
750°C	95	144	202				
800°C	103	156	204				
850°C		137	180	214			
900°C			154	190	236	257	
950°C				163	209.5	237	227
1000°C					188.5	215	205
1100°C					151	163	165

There are however three anomalous datasets in Table 5.4 (highlighted in the table), all at the same test temperature of 800°C (strain rate of 10^{-3}/s, 10^{-2}/s and 10^{-1}/s) which contradict the relation of increasing temperature / decreasing flow stress. In these three cases, the flow stress is higher than the one recorded for 750°C and constant strain rate; this is also visible in Figure 5.7. This atypical behaviour of DH36 steel at 800°C has been established from 8 tests in total (Table 5.1), therefore is well validated. It is argued that this irregularity is caused by an abrupt change in the deformation behaviour of the alloy due to its dual phase of ferrite and austenite at that temperature. Indeed, the test temperature of 800°C is the only one examined which is well within the intercritical temperature range of steel. Nevertheless, metallographic examination of the samples at 800°C notes the extensive similarities to the microstructure of the hot compressed samples at 750°C, mainly the ferrite grain refinement through DRX (see section 5.3.2).

Comparable irregular behaviour has been previously identified during deformation of a plain carbon steel; Essadiqi and Jonas [5.26] evaluate the impact of strain and strain rate on the austenite to ferrite transformation by hot compression testing in temperatures between 790°C – 840°C (all tests in the intercritical temperature range of the examined steel alloy). An analogous deformation mechanism to the one

determined herein is initially exhibited in all tests, with work hardening being the leading mode and then gradually surpassed by the development of flow softening [5.26]. Still, a relation of flow stress with temperature which is contradictory to the conventional in steels (as previously analysed) is observed after the peak stress; the lowest test temperature is seen to produce the lowest flow stress [5.26]. It is explained that in high strains (similar to the anomalous flow stress data for the 800°C above), flow softening is found to increase with decreasing temperature because first, the flow stress of austenite is higher than that of ferrite at the same (intercritical) temperature and second, the content of stable ferrite is continuously increasing with decreasing temperature [5.26].

It is worth noting here that hot compression testing in the majority of the corresponding deformation studies on steel alloys [5.4,5.8,5.12,5.27] is conducted above 850°C (i.e. close to fully austenitic microstructure in most cases) because these studies are concerned with establishing the flow stress in conditions appropriate for metalworking processes. For this reason, the atypical behaviour of DH36 steel at 800°C has not been reported previously to the best knowledge of the author. With respect to FSW, the increased flow stress of DH36 steel signifies that welding in the vicinity of 800°C should be avoided as it will expose the FSW tool to substantially higher forces than those in 850°C for instance. Clearly, the results of Table 5.4 suggest that DH36 steel FSW is more suitably performed at temperatures above 1000°C if the tool is to sustain decreased forces from the plasticised alloy; however, this will also result in a more demanding environment for the tool material as peak temperatures are concerned, therefore a balance between these two factors needs to be achieved.

5.3.2. *Microstructural characterisation of thermo-mechanically deformed and thermally treated samples*

The following microstructural characterisation investigates a wide number of representative samples, outlines their important features and consistently compares samples that were subjected to thermo-mechanical deformation by hot compression testing with samples which experienced the same thermal cycle but without any applied strain. The boundary conditions which have been employed to establish the alloy's flow stress in section 5.3.1, i.e. temperature, strain and strain rate are known to be the critical factors in terms of microstructural development during FSW [5.5].

Thus, a correlation to the above flow stress analysis and to actual welds discussed in Chapter 2 is also provided.

The original parent material banding (see Chapter 2) is still noticeable in the thermo-mechanically deformed sample at 10^{-2}/s – 700°C (Figure 5.8a); the ferrite grains present evidence of DRX to a certain extent, as predicted by the analysis of this sample's flow stress behaviour (section 5.3.1). There is apparent precipitation of carbides on ferrite due to the cooling rate applied (10°C/s) whilst the pearlite sites exhibit a tendency for dissociation (Figure 5.8a). The considerably longer duration of deformation of the 10^{-3}/s – 700°C sample (11.55 minutes vs 1.16 minutes of the 10^{-2}/s strain rate) has resulted in pronounced spheroidisation of pearlite (Figure 5.8b). Since comparable features (banding and equiaxed ferrite grains) are observed in both cases (Figure 5.8a & b), it is the longer test duration and consequently more thermal energy provided that are responsible for the transformation rather than the applied strain.

Dissociation and even spheroidisation of pearlite is frequently reported by FSW studies as observed in the heat affected zone (HAZ) of slow speed (up to approx. 100 mm/min) steel friction stir welds, for example in st37 steel [5.28], DH36 low alloy steel [5.29] and AISI 1018 mild steel [5.5]; in the latter study, partial cementite spheroidisation is attributed to the alloy being exposed to a temperature below the lower transformation temperature (A_1) for considerable time [5.5]. Evidence of pearlite degeneration is also detected in the thermo-mechanically affected zone (TMAZ) of S275 underwater FSW [5.30]. Moreover, this metallurgical feature is seen in the highly refined overlap region of double sided DH36 steel FSW [5.31]. A microstructure consisting of dissociated fine pearlite and highly refined (recrystallized), equiaxed ferrite is also identified in the overlap region of double sided S275 structural steel friction stir welds [5.30]; as above, these studies [5.30,5.31] are employing slow traverse speeds of 125 mm/min and 100 mm/min respectively. The overlap region of double sided FSW is a zone where the material has been thermo-mechanically stirred twice [5.21], i.e. heated and deformed during the first and second pass of the FSW tool. Combined with the slow traverse speed, the processing conditions in this region of double sided FSW [5.30,5.31] are very similar to the ones (substantial time at a medium temperature and slow deformation) developed in the 10^{-3}/s – 700°C compressive test.

It is argued herein that the particular thermo-mechanical deformation test, due to the longer time period spent at 700°C is unintentionally simulating the spheroidising (soft) annealing as a heat treating process of steels. Spheroidising annealing is performed at a temperature slightly below A$_1$ (as in the test under consideration) on a number of ferrous alloys such as hypoeutectoid steels of ferrite / pearlite microstructure and tool steels in order to reduce the alloy's hardness [5.32]. Indeed, micro-hardness measurements on this sample (using the equipment and method defined in Chapter 3) record average hardness of 168 HV, i.e. marginally lower than the parent material of 186 HV (Chapter 3). The developed microstructure is often described as spheroidised carbides (or cementite) in a ferrite matrix [5.32,5.33]. In thermodynamic terms, spheroidal pearlite is more stable than in any other form, even in the lamellar structure which is observed at room temperature [5.33]. Still, activation of the transformation to spheroidise the pearlitic regions requires thermal energy. Spheroidisation can take place at temperatures up to approx. 700°C, if sufficient time in that temperature is provided, by transformation of cementite into carbides which diffuse and subsequently evolve in a thermodynamically stable spheroidal form [5.33]. As a result, microstructures comparable to the one in Figure 5.8b are found in numerous low alloy steels and tool steels for which spheroidising annealing is a common heat treatment [5.33].

The appropriate annealing temperature for DH36 steel is calculated at 692°C [5.32], hence attained in the 700°C test. According to Liscic [5.32], the minimum required time at this temperature is 9 minutes for the specific samples' dimensions; this is also exceeded by the test at 10^{-3}/s strain rate. However, only partial spheroidisation of the sample's microstructure has occurred because of the faster cooling rate (10°C/s) compared to the rate necessary to develop fully globular particles (approx. 25°C/h) [5.32].

The thermally treated sample is entirely unaffected by the thermal cycle (Figure 5.8c), therefore appears identical to the DH36 parent material's images of Chapter 2; this was expected since the test temperature did not exceed the A$_1$ of approx. 727°C and no strain was applied either. Thus, the effect of strain energy is significant in this comparison; although the thermo-mechanically deformed sample at 10^{-2}/s was also heated below A$_1$, minor recrystallisation of ferrite and partial dissociation of pearlite is observed.
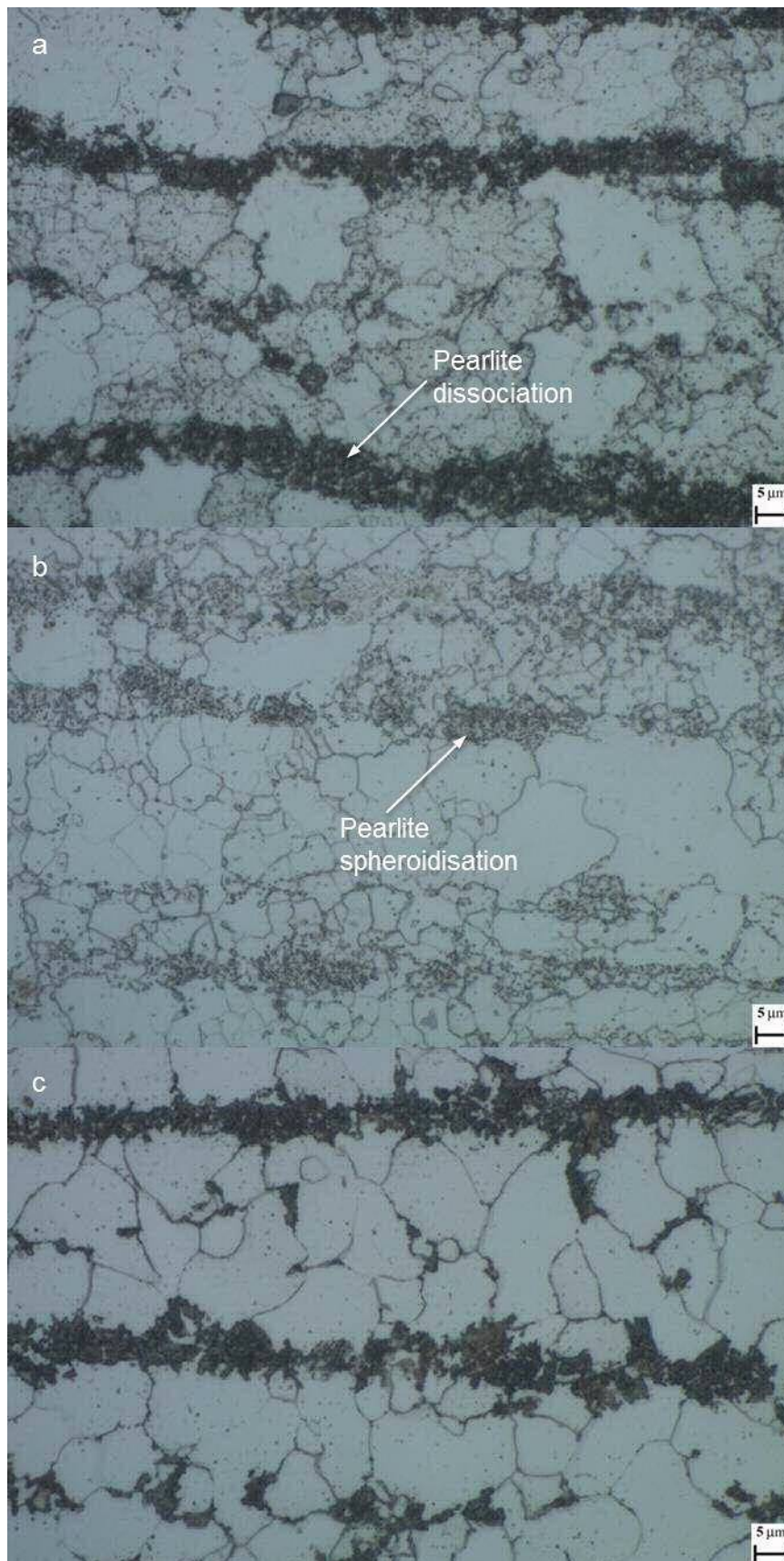
Figure 5.8. Microstructure [x1000, Etched] of thermo-mechanically deformed at (a) 10^{-2}/s – 700°C; (b) 10^{-3}/s – 700°C; (c) thermally treated at 700°C

The microstructure in the centre of the deformed sample at 10^{-1}/s – 750°C displays increased refinement of ferrite grains through DRX (estimated in section 5.3.1), when compared to the previous test at 10^{-2}/s – 700°C, and partial dissociation of pearlite (Figure 5.9a). The parent material banding is barely discerned. Figure 5.9 is captured in the centre of the samples (as detailed in section 5.2.2), which is also the middle of the DH36 steel plate. Hence, the differently shaded, thin layered structure in the middle of the image is generated by the centreline segregation; this is attributed to elements with a higher propensity to segregate such as S, P and Mn and is generally considered undesirable in steel production [5.34,5.35]. Manganese sulphides (MnS) are also noted in the centre of the thermally treated sample (Figure 5.9b), elongated and deformed (but with continuous outline) by the manufacture process [5.35,5.36]. MnS inclusions are known to develop in the Mn-rich centreline segregation zone during solidification of steel [5.34,5.35]. SEM-EDS analysis of several centreline segregation regions (one instance is seen in Figure 5.10) confirms the greatly increased concentration (wt.%) of P (0.18%), S (6.83%) and Mn (11.10%). To provide a point of reference, the corresponding maximum allowable values for the bulk of the examined steel grade DH36 as specified by Lloyd's Register rules [5.37] are 0.035%, 0.035% and 1.60%.

The thermally treated sample at 750°C exhibits less parent material banding than the corresponding thermo-mechanically deformed, thus more random distribution of ferrite but (qualitatively) less ferrite grain refinement (Figure 5.9b). In both samples, the temperature has barely exceeded A_1. The pearlite regions are dissociated and more randomly dispersed (Figure 5.9b); this is comparable to the degenerated pearlite which is discerned in the HAZ of DH36 friction stir welds employing a slow traverse speed of 125 mm/min [5.31]. Although its strain rate is not too severe, the effect of the compressive deformation and specifically its contribution to DRX is identifiable but less significant than in the previous comparison (at 700°C). The deformed and thermally treated samples at 800°C feature microstructures which are remarkably similar to the ones at 750°C, i.e. comparable recrystallisation of ferrite and dissociation of pearlite.

Figure 5.9. Microstructure [x1000, Etched] of (a) thermo-mechanically deformed at 10^{-1}/s – 750°C; (b) thermally treated at 750°C
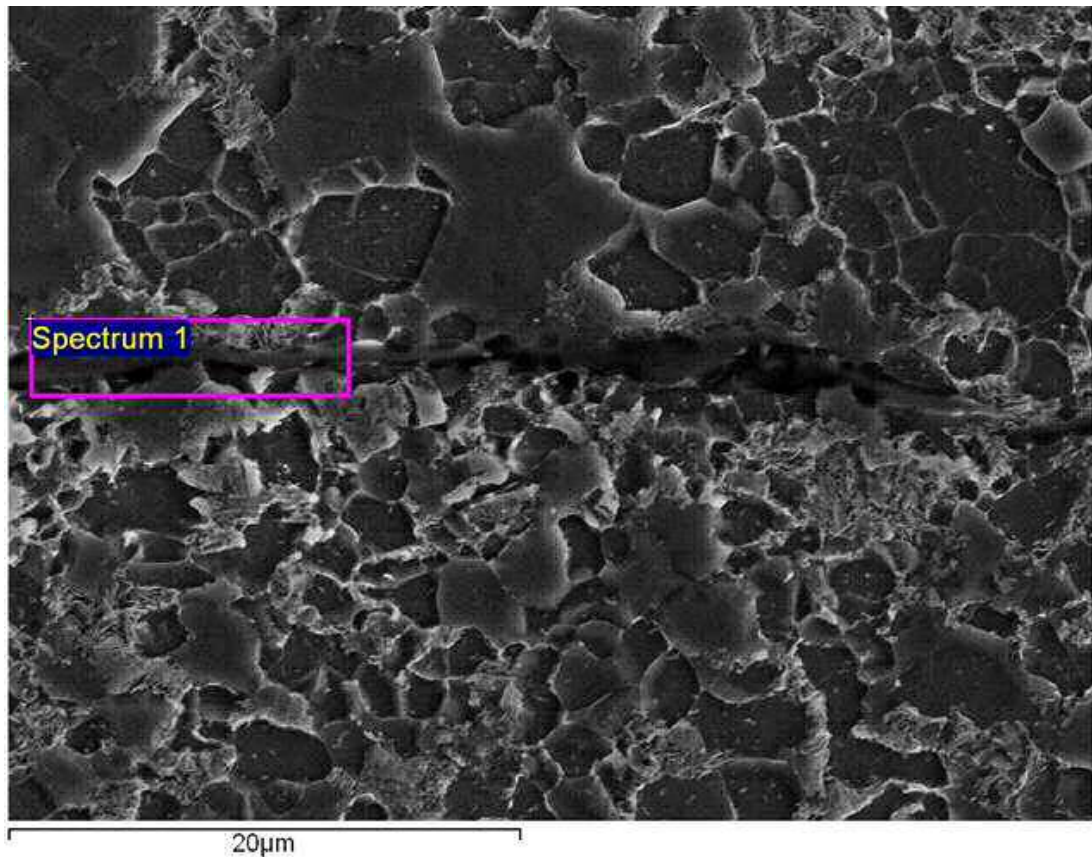
Figure 5.10. SEM-EDS analysis of steel plate centreline

Refined ferrite grains of random geometry have formed in the thermo-mechanically deformed sample at 10^{-1}/s – 850°C (Figure 5.11a). Recrystallisation has been promoted further as a consequence of the increased peak temperature which is close to the upper transformation temperature of steel (A_3). This is the first set of conditions where traces of acicular shaped grains with suggestion of acicular bainitic ferrites have evolved (Figure 5.11a), an outcome of the increase in cooling rate (15°C/s). The microstructure of the thermally treated sample is similar in terms of ferrite grain refinement and analogous dissociation of pearlite but with fewer traces of acicular shaped grains (Figure 5.11b). Therefore, the effect of the increased compressive strain rate is still recognisable to a certain degree.
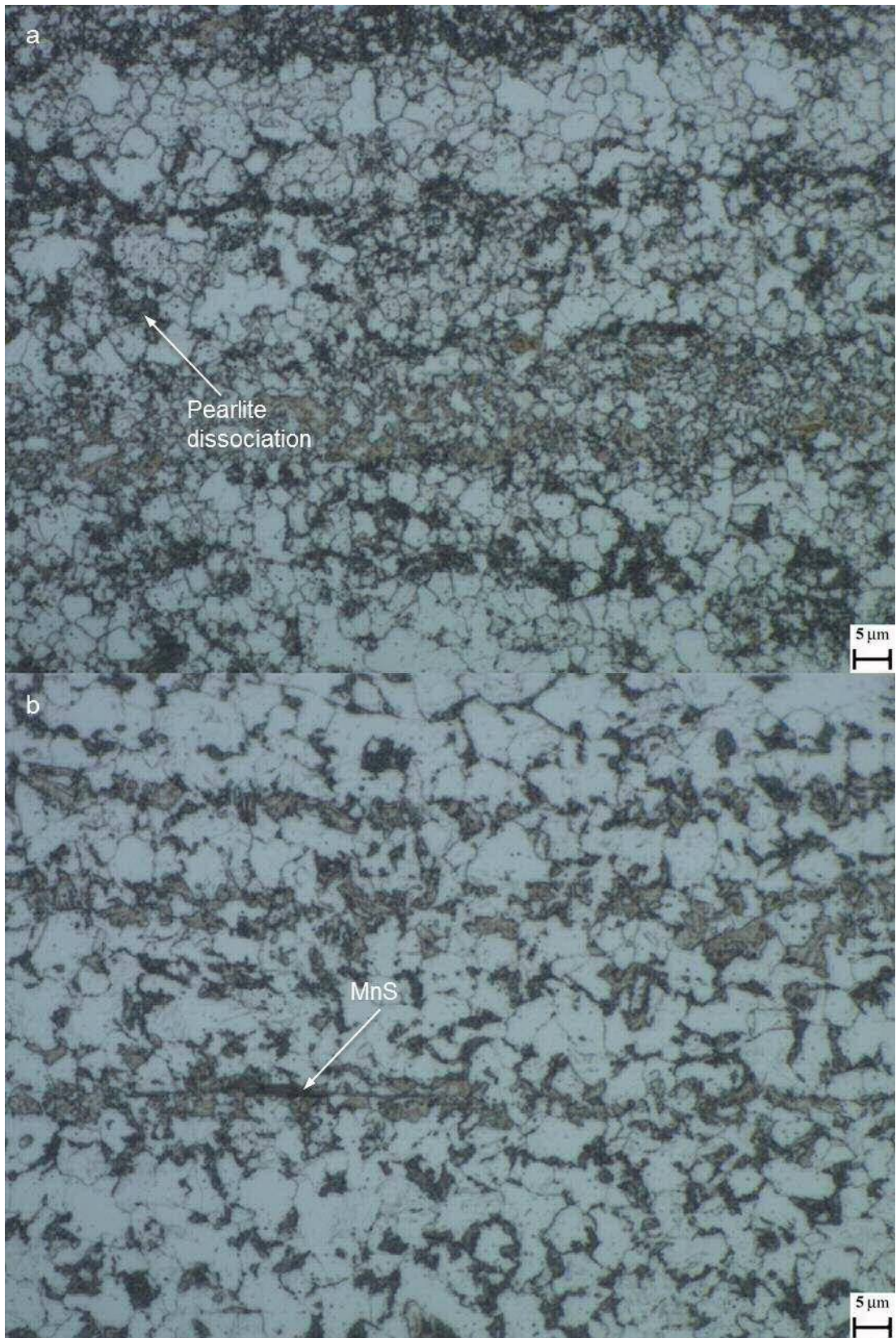
Figure 5.11. Microstructure [x1000, Etched] of (a) thermo-mechanically deformed at 10^{-1}/s – 850°C; (b) thermally treated at 850°C
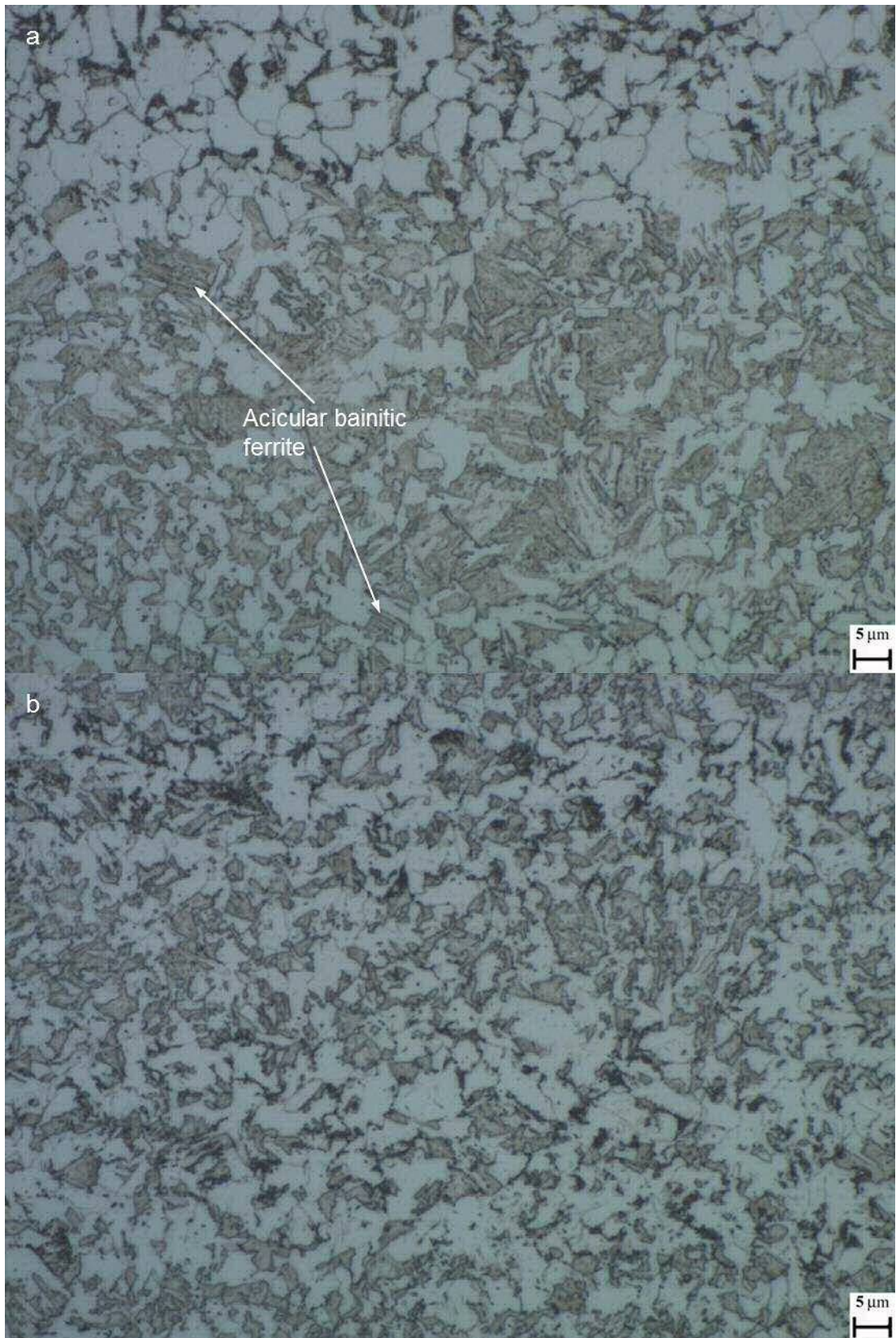
Equally to the previous set of testing parameters, ferrite grains of random geometry and increased traces of acicular shaped grains are exhibited in the centre of the thermo-mechanically deformed sample at 50/s – 900°C (Figure 5.12a). The microstructure of the thermally treated sample at the same test temperature matches the above description (Figure 5.12b). Although not observed in the corresponding sample at 850°C (Figure 5.11b), fine acicular bainitic ferrites have now nucleated. Thus, the thermal cycle has become the principal driving force for the evolved microstructure in both samples of the 900°C test temperature; despite the application of a high strain rate (50/s), the deformation-related effect is almost negligible. Minor traces of Widmanstätten ferrite delineating a prior austenite grain boundary are also identified in Figure 5.12b. Widmanstätten ferrite is noted to nucleate either from prior austenite grain boundary allotriomorphic ferrite or exactly on these boundaries and in temperatures close to A$_3$ [5.38,5.39], as is the specific test temperature (900°C). Importantly, it has been found to develop in the TMAZ of low alloy steel FSW after recrystallisation of the austenite grains [5.28,5.40].

A significant transition from the previously examined microstructures is observed in the 950°C test samples (Figure 5.13). The microstructure has become heterogeneous in the centre of the thermo-mechanically deformed sample at 10^2/s – 950°C (peak temperature well above A$_3$) since the content of fine acicular bainitic ferrites is seen as increased (Figure 5.13a); the latter is attributed to the faster cooling rate of 20°C/s that has been employed in this test. Additionally, the acicular and random geometry ferrite grains are more refined than in the previous test. An identical commentary can be used for the thermally treated sample at the same temperature and cooling rate (Figure 5.13b). Almost no pearlitic sites are observed whilst there is evidence of Widmanstätten ferrite. The increased test temperature and higher cooling rate are responsible for developing such similar microstructures in the two samples. In contrast, the influence of the compressive deformation is even less distinguishable.
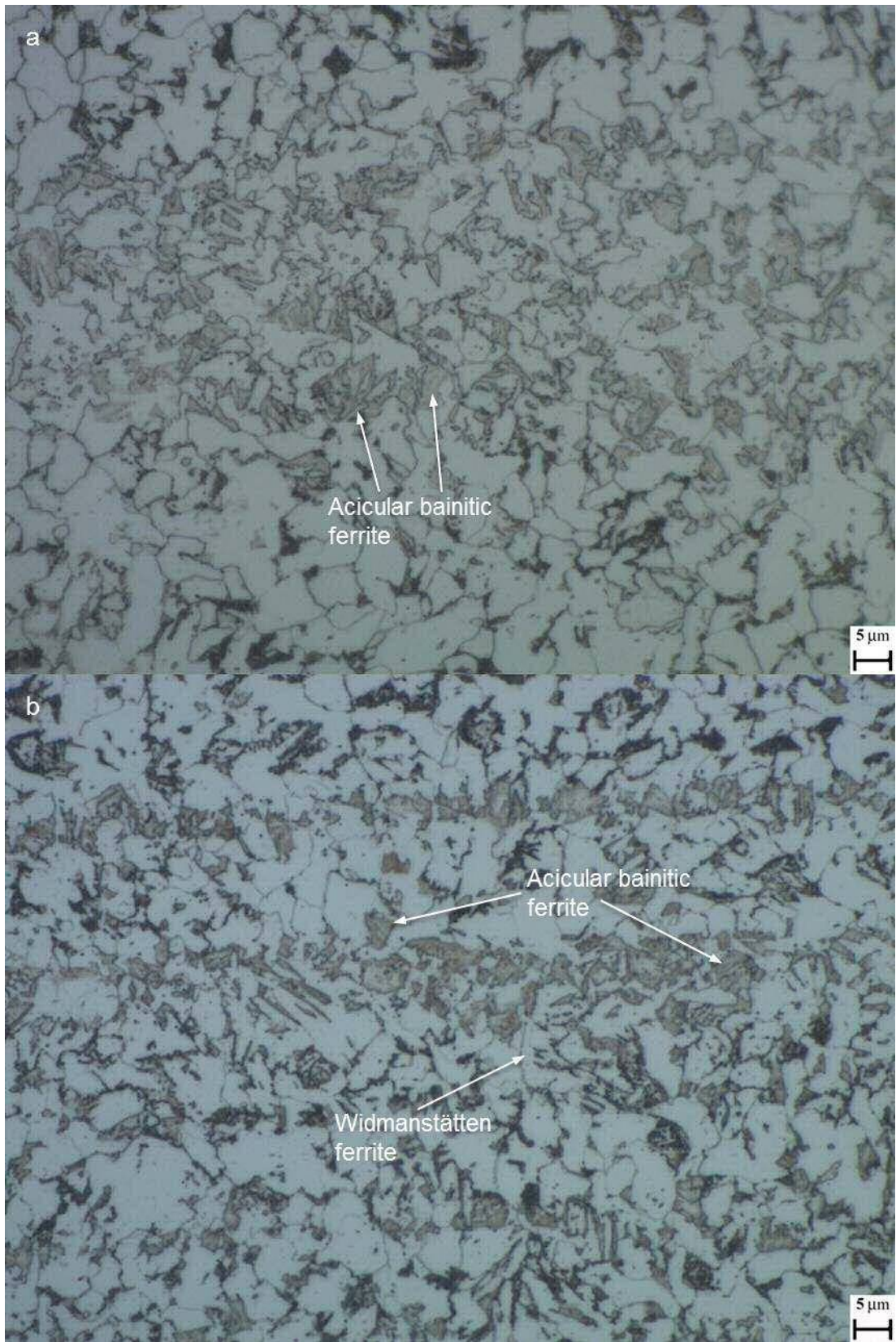
Figure 5.12. Microstructure [x1000, Etched] of (a) thermo-mechanically deformed at 50/s – 900°C; (b) thermally treated at 900°C
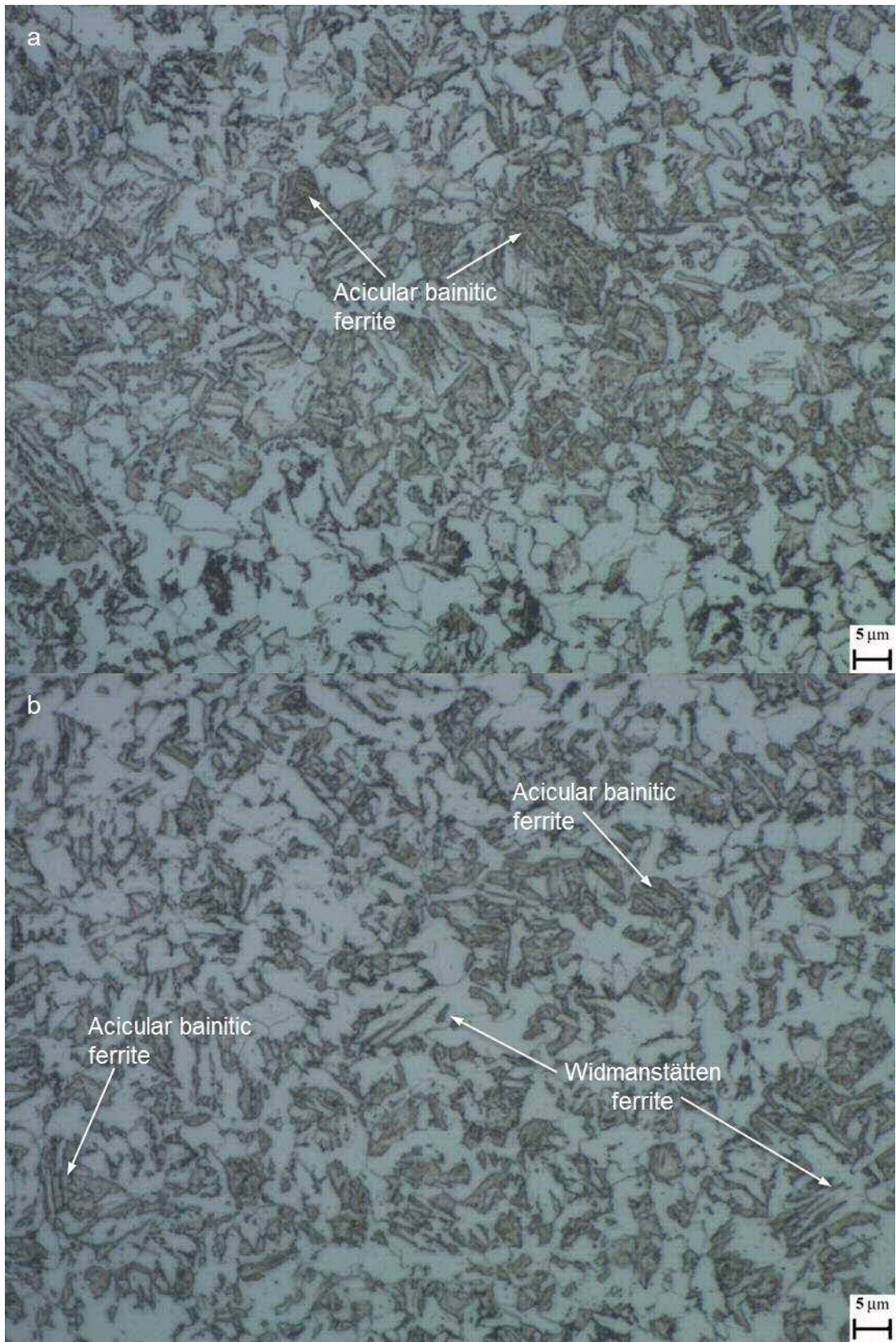
Figure 5.13. Microstructure [x1000, Etched] of (a) thermo-mechanically deformed at 10^2/s – 950°C; (b) thermally treated at 950°C

Comparable heterogeneous microstructures are observed in the samples tested at 1000°C; fine acicular bainitic ferrites are randomly dispersed within acicular and predominantly random geometry ferrite grains. As in the samples at 950°C, the applied deformation by hot compression has been unable to diversify the evolved microstructures. The central zone in both thermo-mechanically deformed and thermally treated samples at 950°C and 1000°C now resembles actual steel friction stir welds; an illustration is the TMAZ of the slow (Table 1.1) weld W04 (Figure 5.14) as it compares to Figure 5.13.

Figure 5.14. W04, microstructure of mid-TMAZ [x1000, Etched]

A further appreciable development is seen in the microstructure of all samples at 1100°C. Predominantly refined acicular bainitic ferrites are observed in the centre of the thermo-mechanically deformed sample at 50/s strain rate, with prior austenite grain boundaries visible (Figure 5.15a); acicular platelets are seen to nucleate from these boundaries (denoted in the same figure) as detailed in previous publications [5.41,5.42]. This is a heterogeneous microstructure because coarser acicular ferrite grains and blocky ferrite of random geometry are also present, along with suggestion of Widmanstätten ferrite (Figure 5.15a). Blocky ferrite (on the prior austenite grain boundary) outlining acicular ferrite is also observed in a separate

study on submerged arc welded (SAW) steel [5.43], whilst the concurrence of Widmanstätten and blocky ferrite is reported in earlier publications on SAW [5.39] and FSW [5.28,5.44] of steel. More importantly, the evolved microstructure is equivalent to a number of heterogeneous weld zone (TMAZ) microstructures presented in Chapter 2; for instance, it is closely matched to the intermediate weld W13 (Figure 5.15b).

Furthermore, the thermally treated sample at 1100^oC (its centre, Figure 5.16a, is seen as substantially modified from the corresponding sites in previous tests) is compared against the intermediate weld W12 (Figure 5.16b); the two predominantly acicular bainitic ferrite microstructures are almost identical, with regions of acicular ferrite and coarse grain boundary blocky ferrite also noticeable. Nucleation of acicular grains from prior austenite grain boundaries is well defined (marked in Figure 5.16a). This comparison offers further support to the argument that the thermal cycle simulates more than adequately the evolved microstructure of an actual DH36 steel friction stir weld, with no particular input by the compressive stress, especially when applying the very high temperatures and cooling rate recorded during steel FSW.

One more representative case of the thermo-mechanically deformed (10/s – 1100^oC) and thermally treated (1100^oC) samples equally displaying a microstructure comparable to a fast traverse speed weld zone is presented in Figure 5.17. This analogy confirms once again the importance of the thermal cycle in the developed microstructure and the negligible contribution by the compressive deformation that has been applied. Both thermo-mechanically deformed (Figure 5.17a) and thermally treated (Figure 5.17c) samples feature a heterogeneous but predominantly acicular bainitic ferrite microstructure with regions of acicular ferrite, exactly as in the TMAZ of fast weld W24 (Figure 5.17b) among other intermediate and fast welds (see relevant commentary in Chapter 2). As above, acicular platelets extend from clearly specified prior austenite grain boundaries (indicated on the figure). The presence of acicular bainitic ferrites (to such an extent) and prior austenite grain boundaries represents a considerable difference from all previous tests of lower peak temperature.

Figure 5.15. Microstructure [x1000, Etched] of (a) thermo-mechanically deformed at 50/s – 1100°C; (b) weld W13 (from Chapter 2)

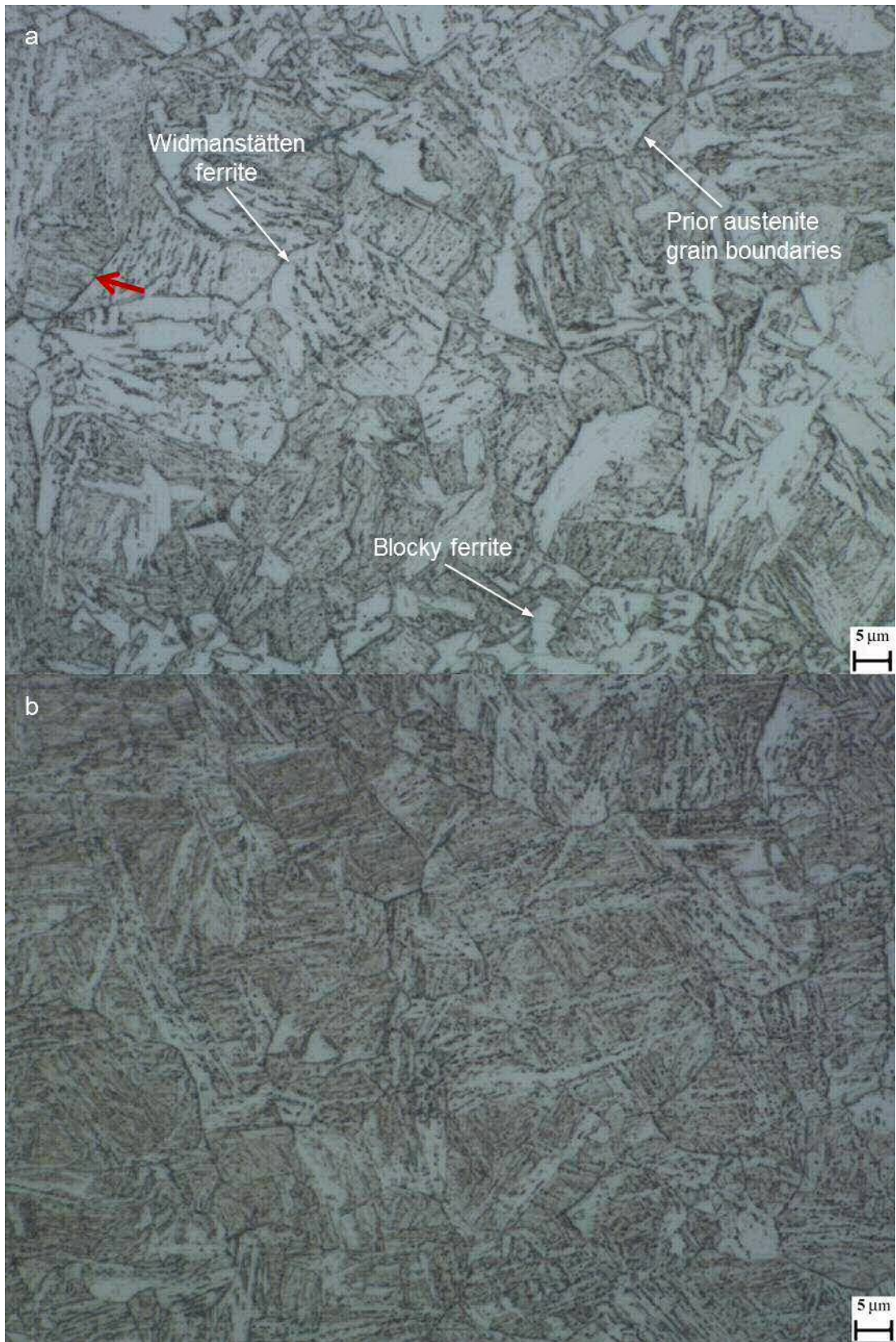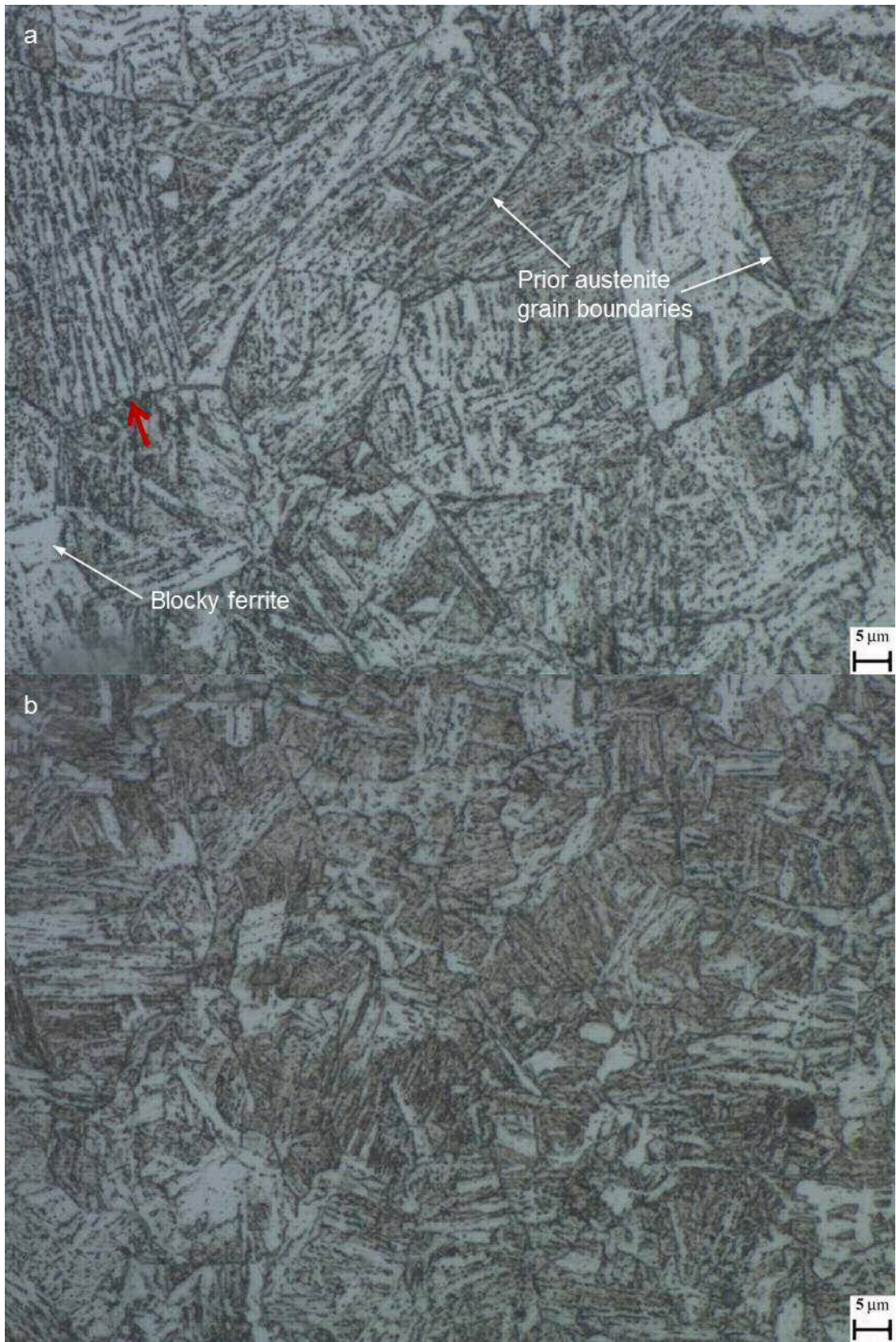**Figure 5.16. Microstructure [x1000, Etched] of (a) thermally treated at 1100°C; (b) weld W12 (refer to Chapter 2)**
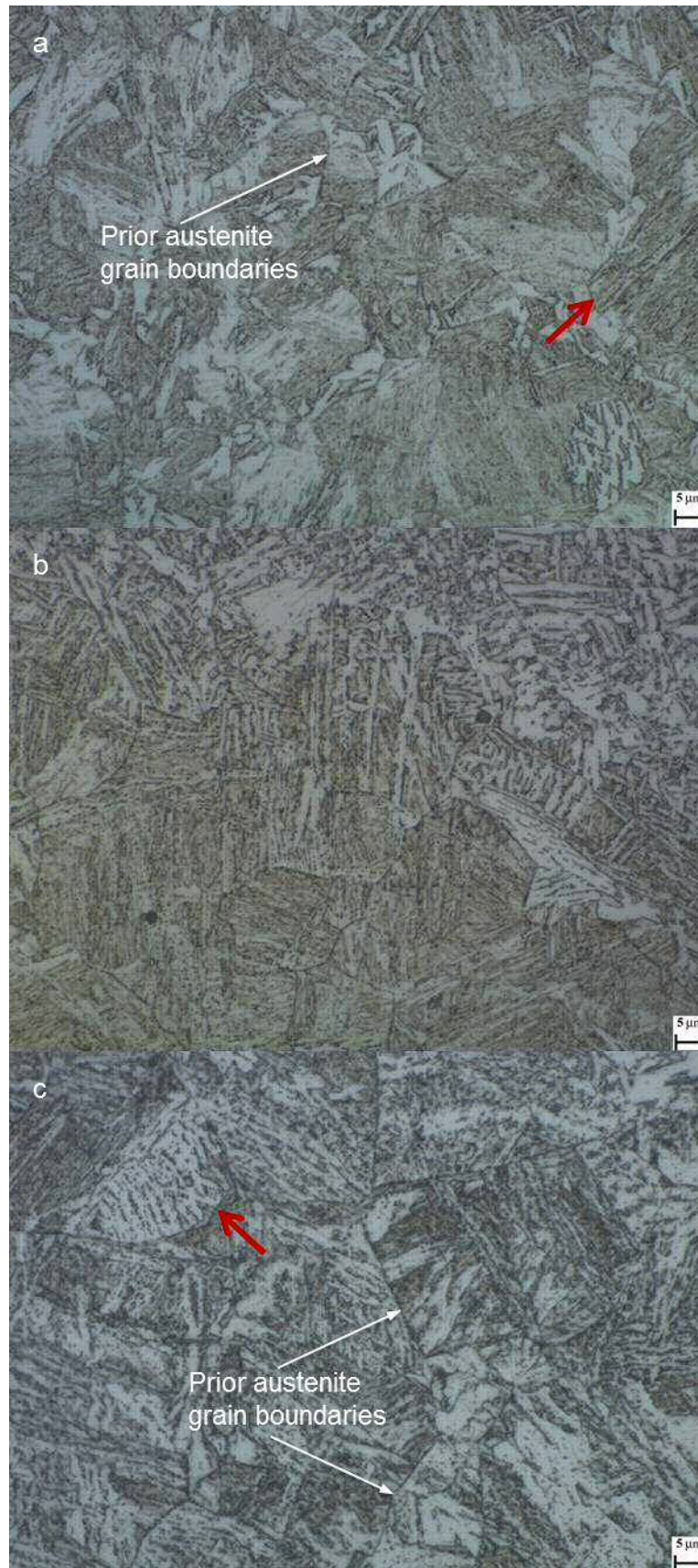
Figure 5.17. Microstructure [x1000, Etched] of (a) thermo-mechanically deformed at 10/s – 1100°C; (b) weld W24 (from Chapter 2); (c) thermally treated at 1100°C

As a general note, most of the examined microstructures are not in full agreement with regions within DH36 steel friction stir welds, as these are characterised in Chapter 2 and 4, but for specific features. These are limited to grain refinement by DRX and pearlite dissociation in the lower test temperatures (700°C–850°C), whereas the intermediate temperatures (900°C–1000°C) develop heterogeneous microstructures with fine acicular shaped bainitic ferrites and traces of Widmanstätten ferrite. The observed microstructures correspond to the TMAZ of actual intermediate and fast welds when high thermal energy is provided through the highest peak temperature of 1100°C. Comparable metallurgical features depending on the test temperature have been identified in the thermally treated samples. Therefore, the preceding examination reveals that the influence of the compressive deformation is decreasing with increasing test temperature, until it becomes insignificant in the tests at 1100°C; in contrast, the thermal cycle is seen to emerge as the dominant factor in the microstructural evolution.

As a physical simulation of FSW, the current testing programme appears to demonstrate that there is little contribution by the mechanical deformation during the actual welding process, especially for the high temperature weld regions such as below the tool shoulder and in the vicinity of the probe (Figure 5.1). This finding is in opposition to previous publications on FSW of steel in which the input by the severe plastic deformation is highlighted as significant [5.5,5.6]. Thus, hot axisymmetric compression testing has not produced the anticipated results in this study. This is attributed to the absence of mechanical stirring (in both series of tests); the latter is an essential part of the thermo-mechanical cycle during FSW [5.5]. The powerful effect of mass transportation in FSW has also been exhibited in Chapter 4, in which a material flow line with a microstructure contrasting from the adjacent phases within the top advancing side of the intermediate weld has been identified (see relevant commentary in section 4.3.1).

Although the prevalent testing method for simulation of common metalworking processes is hot compression (note the reviewed references in section 5.1), it is conceivable that the incorporation of shear stresses through hot torsion testing would be more suitable in simulating the FSW process. Cho *et al.* [5.41] argue that grain refinement in the TMAZ of API X100 grade steel is produced by DRX through shear stresses, the principal deformation mechanism in FSW [5.41]. Additionally, Thomas *et al.* [5.45] explain that adiabatic shearing forces also contribute to thermal energy generation as the material is deformed during welding. Accordingly, hot

torsion testing is potentially a method which can replicate the metallurgical system of steel FSW more closely. Torsion testing is routinely carried out for determination of a material's stress – strain curve at elevated temperatures [5.1,5.22]. For instance, researchers [5.46] assess the deformation parameters of an AISI 1045 medium carbon steel during high pressure torsion testing, which is implemented as a microstructural refinement process, in order to develop ultrafine grained microstructure through severe plastic deformation. Elsewhere [5.47], this method is used to simulate a heat treating process of pearlitic steels.

The shear compression specimen (SCS) represents one more option for flow stress analysis and physical simulation of FSW. The SCS is proposed by Rittel *et al.* [5.48] and evaluated in a thermo-mechanical deformation study of a Titanium alloy [5.49]. The SCS consists of a cylindrical sample with grooves machined on the longitudinal surface at a 45° angle (Figure 5.18). This method allows for hot deformation through the joint effect of shear and compressive forces which are applied on the material. The sample is deformed in axisymmetric compressive loading, therefore can be tested in conventional compression testing systems [5.49].
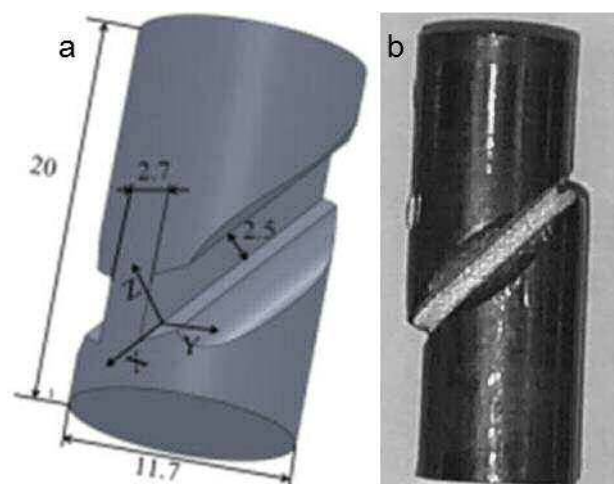
Figure 5.18. (a) Basic dimensions of a typical SCS [5.49]; (b) deformed SCS [5.48]

Finally, it is expected that the deformation conditions of a material are changing greatly as it flows from the advancing to the retreating side of a friction stir weld (e.g. temperature map of Figure 5.1). Thus, a more accurate replication of FSW with respect to the microstructural evolution in steel may require the assessment of changing strain rate during testing (at a fixed temperature) on top of any of the previously outlined options. The method of varying the strain rate has been researched by prior studies in the context of diverse processes. Indicatively, Abbod

et al. [5.50] conduct plane strain compression testing with changing strain rate during the deformation stage to analyse the flow stress of 316L stainless steel in conditions analogous to industrial rolling. Modifying the strain rate during hot compression is also used as a pre-straining method in a separate research work [5.26].

5.4. Conclusions

A detailed thermo-mechanical deformation study has been executed in testing conditions which simulate the FSW of steel in order to generate data not previously available for steel grade DH36 which are expected to improve the accuracy of any predictive modelling work on the subject and contribute towards the fundamental understanding of the process.

Analysis of the deformation behaviour of DH36 steel in hot axisymmetric compression tests on a Gleeble 3800 thermo-mechanical testing system has shown that the evolution of flow stress is significantly affected by the test temperature and rate of deformation; the alloy's flow stress is seen to increase with increasing strain rate and decreasing temperature. Thus, FSW parameters which create regions of high strain rate / low temperature conditions within the weld zone may develop embedded flaws due to reduced material flow. The flow stress in low strain rate / high temperature conditions demonstrates a typical softening phenomenon by DRX. However, the effect of DRX is clearly decreased in high strain rate conditions. The alloy's flow stress behaviour is only contradicted by the tests at 800°C in which the flow stress is seen to increase compared to that of a lower test temperature for a fixed strain rate. This atypical behaviour is attributed to the dual phase of ferrite and austenite which evolves at this intercritical temperature and the different flow stress of each phase. This represents an important observation on the optimum conditions for FSW of DH36 steel with regard to establishing process parameters and improving tooling and welding machine specifications.

To allow for an assessment of the influence of test temperature and strain rate on the evolved microstructure and enable an evaluation of the contribution of strain energy in a characteristic FSW microstructure, identical steel samples were subjected to the same thermal cycle but without deformation. Microstructural examination of the thermo-mechanically deformed and thermally treated samples

demonstrates that the strain rate has a moderate effect on microstructural evolution at lower temperatures, but this effect is seen to be much reduced up to negligible in higher peak temperatures. In summary, both series of tested samples exhibit only individual metallurgical features of actual steel friction stir welds in low (pearlite degeneration / dissociation, grain refinement by DRX as predicted by the present flow stress analysis, traces of acicular shaped grains) and intermediate (heterogeneous microstructure with small regions of acicular ferrite and fine acicular bainitic ferrite, evidence of Widmanstätten ferrite) test temperatures. The predominantly acicular bainitic ferrite microstructures developed in the highest test temperature of 1100°C, with features such as well-defined prior austenite grain boundaries, Widmanstätten and blocky ferrite are in excellent agreement with intermediate and fast speed DH36 friction stir welds.

The solid observation regarding the minimal contribution of deformation in the formed microstructures is in disagreement with the current understanding of the FSW process; this is ascribed to the lack of mechanical stirring of the material in hot compression testing. As a result, the application of shear forces in hot torsion testing and the method of varying strain rate are proposed as more fitting in the physical simulation of the metallurgical system generated by FSW.

5.5. References

[5.1]   Nowotnik A. Flow stress value and activation energy of hot deformed Inconel superalloys. Adv Manuf Sci Technol 2008;32:51–62.

[5.2]   Boisse P, Altan T, Luttervelt K van, editors. Friction and flow stress in forming and cutting. London: Kogan Page Science; 2003.

[5.3]   Dieter GE, Kuhn HA, Semiatin SL, editors. Handbook of Workability and Process Design. Materials Park, OH: ASM International; 2003.

[5.4]   Lin YC, Chen M-S, Zhong J. Effect of temperature and strain rate on the compressive deformation behavior of 42CrMo steel. J Mater Process Technol 2008;205:308–15.

[5.5]   Lienert T, Stellwag W, Grimmett B, Warke R. Friction stir welding studies on mild steel. Weld J Res Suppl 2003:1–9.

[5.6] Barnes SJ, Bhatti AR, Steuwer A, Johnson R, Altenkirch J, Withers PJ. Friction Stir Welding in HSLA-65 Steel: Part I. Influence of Weld Speed and Tool Material on Microstructural Development. Metall Mater Trans A 2012;43:2342–55.

[5.7] Rajput SK, Dikovits M, Chaudhari GP, Poletti C, Warchomicka F, Pancholi V, et al. Physical simulation of hot deformation and microstructural evolution of AISI 1016 steel using processing maps. Mater Sci Eng A 2013;587:291–300.

[5.8] Abbasi SM, Momeni A. Hot working behavior of Fe–29Ni–17Co analyzed by mechanical testing and processing map. Mater Sci Eng A 2012;552:330–5.

[5.9] Zhang J, Di H, Wang X, Cao Y, Zhang J, Ma T. Constitutive analysis of the hot deformation behavior of Fe–23Mn–2Al–0.2C twinning induced plasticity steel in consideration of strain. Mater Des 2013;44:354–64.

[5.10] Liu CY, Zhang RJ, Yan YN. Hot deformation behaviour and constitutive modelling of P92 heat resistant steel. Mater Sci Technol 2011;27:1281–6.

[5.11] Wei H, Liu G, Zhao H, Kang R. Hot deformation behavior of two C–Mn–Si based and C–Mn–Al based microalloyed high-strength steels: A comparative study. Mater Des 2013;50:484–90.

[5.12] Mirzadeh H, Cabrera JM, Prado JM, Najafizadeh A. Hot deformation behavior of a medium carbon microalloyed steel. Mater Sci Eng A 2011;528:3876–82.

[5.13] Kaibyshev R, Kazakulov I. Deformation behaviour of Fe-3Si steel. Mater Sci Technol 2004;20:221–8.

[5.14] Rao K, Prasad Y, Hawbolt E. Hot deformation studies on a low-carbon steel: Part 1-flow curves and the constitutive relationship. J Mater Process Technol 1996;56:897–907.

[5.15] Chai RX, Xu DH, Guo C. Prediction of constitutive behaviour of 20CrMnTiH steel under hot deformation conditions. Mater Sci Technol 2012;28:857–63.

[5.16] Zeng Z, Zhang Y, Jonsson S. Deformation behaviour of commercially pure titanium during simple hot compression. Mater Des 2009;30:3105–11.

[5.17] Gao L, Luo AA. Hot deformation behavior of as-cast Mg–Zn–Mn–Ce alloy in compression. Mater Sci Eng A 2013;560:492–9.

[5.18] Xu Y, Hu L, Sun Y. Deformation behaviour and dynamic recrystallization of AZ61 magnesium alloy. J Alloys Compd 2013;580:262–9.

[5.19] Zhang H, Jin N, Chen J. Hot deformation behavior of Al-Zn-Mg-Cu-Zr aluminum alloys during compression at elevated temperature. Trans Nonferrous Met Soc China 2011;21:437–42.

[5.20] McQueen HJ, Jonas JJ. Hot Workability Testing Techniques. In: Hoffmanner AL, editor. Met. Form. Interrelat. Between Theory Pract., New York: Springer; 1971, p. 393–428.

[5.21] Collaborative Research Project HILDA (High Integrity Low Distortion Assembly), E.U. Seventh Framework Programme (SCP2-GA-2012-314534-HILDA).

[5.22] Roebuck B, Lord JD, Brooks M, Loveday MS, Sellars CM, Evans RW. Measurement Good Practice Guide No 3. Measuring Flow Stress in Hot Axisymmetric Compression Tests. Teddington: 2002.

[5.23] Rasti J, Najafizadeh A, Meratian M. Correcting the stress-strain curve in hot compression test using finite element analysis and Taguchi method. Int J ISSI 2011;8:26–33.

[5.24] Cohen R. Metallurgical Study of the Hot Upsetting of 1035 Steel. In: Lenard J, editor. Model. Hot Deform. Steels, Berlin: Springer-Verlag; 1989, p. 39–69.

[5.25] Ozekcin A, Jin HW, Koo JY, Bangaru N V, Ayer R, Vaughn G, et al. A microstructural study of friction stir welded joints of carbon steels. Int J Offshore Polar Eng 2004;14:284–8.

[5.26] Essadiqi E, Jonas JJ. Effect of deformation on the austenite-to-ferrite transformation in a plain carbon and two microalloyed steels. Metall Trans A 1988;19:417–26.

[5.27] Wang M, Li Y, Wang W, Zhou J, Chiba A. Quantitative Analysis of Work Hardening and Dynamic Softening Behavior of low carbon alloy Steel Based on the Flow Stress. Mater Des 2013;45:384–92.

[5.28] Jafarzadegan M, Feng AH, Abdollah-zadeh A, Saeid T, Shen J, Assadi H. Microstructural characterization in dissimilar friction stir welding between 304 stainless steel and st37 steel. Mater Charact 2012;74:28–41.

[5.29]   McPherson N, Galloway A, Cater S, Hambling S. Friction stir welding of thin
         DH36 steel plate. Sci Technol Weld Join 2013;18:441–50.

[5.30]   Baillie P, Campbell SW, Galloway AM, Cater SR, McPherson NA. Friction
         stir welding of 6 mm thick carbon steel underwater and in air. Sci Technol
         Weld Join 2015;20:585–93.

[5.31]   McPherson N, Galloway A, Cater SR, Osman MM. A comparison between
         single sided and double sided friction stir welded 8mm thick DH36 steel
         plate. 9th Int. Conf. Trends Weld. Res., 2012.

[5.32]   Liscic B. Steel Heat Treatment. In: Totten GE, editor. Steel Heat Treat.
         Metall. Technol., Boca Raton, FL: CRC Press; 2007, p. 277–414.

[5.33]   Vander Voort G, editor. ASM Handbook Volume 9: Metallography and
         Microstructures. Materials Park, OH: ASM International; 2004.

[5.34]   Taguchi I, Hamada H. Development of new computer-aided microanalyzer
         and its application to iron and steel analysis. Anal Sci 1985;1:119–24.

[5.35]   Nayak SS, Misra RDK, Hartmann J, Siciliano F, Gray JM. Microstructure and
         properties of low manganese and niobium containing HIC pipeline steel.
         Mater Sci Eng A 2008;494:456–63.

[5.36]   Benedicks C, Löfquist H. Non-metallic Inclusions in Iron and Steel. London:
         Chapman & Hall; 1930.

[5.37]   Lloyd's Register. Rules for the Manufacture, Testing and Certification of
         Materials. London: 2014.

[5.38]   Bhadeshia HKDH. Diffusional formation of ferrite in iron and its alloys. Prog
         Mater Sci 1985;29:321–86.

[5.39]   Jang J, Indacochea JE. Inclusion effects on submerged-arc weld
         microstructure. J Mater Sci 1987;22:689–700.

[5.40]   Nandan R, DebRoy T, Bhadeshia HKDH. Recent advances in friction-stir
         welding - Process, weldment structure and properties. Prog Mater Sci
         2008;53:980–1023.

[5.41]   Cho H-H, Kang SH, Kim S-H, Oh KH, Kim HJ, Chang W-S, et al.
         Microstructural evolution in friction stir welding of high-strength linepipe steel.
         Mater Des 2012;34:258–67.

[5.42] Bhadeshia HKDH. Bainite in Steels. 2nd ed. London: IOM Communications; 2001.

[5.43] Wang SH, Luu WC, Ho KF, Wu JK. Hydrogen permeation in a submerged arc weldment of TMCP steel. Mater Chem Phys 2003;77:447–54.

[5.44] Konkol P, Mathers J, Johnson R, Pickens J. Friction stir welding of HSLA-65 steel for shipbuilding. J Sh Prod 2003;19:159–64.

[5.45] Thomas WM, Wiesner CS, Marks DJ, Staines DG. Conventional and bobbin friction stir welding of 12% chromium alloy steel using composite refractory tool materials. Sci Technol Weld Join 2009;14:247–53.

[5.46] Zrnik J, Pippan R, Scheriau S, Kraus L, Fujda M. Microstructure and mechanical properties of UFG medium carbon steel processed by HPT at increased temperature. J Mater Sci 2010;45:4822–6.

[5.47] Ferrer JP, Capdevila C, Caballero FG, García de Andrés C. Comparison of Globularisation Behaviour During Reheating Treatment of Different Pearlitic Microstructures. In: Chatterjee UK, Dhindaw BK, editors. Proc. Int. Conf. Adv. Mater. Mater. Process., Kharagpur, India: Indian Institute of Technology; 2006, p. 500–5.

[5.48] Rittel D, Ravichandran G, Lee S. Large strain constitutive behavior of OFHC copper over a wide range of strain rates using the shear compression specimen. Mech Mater 2002;34:627–42.

[5.49] Jing L, Fu RD, Li YJ, Shi Y, Wang J, Du DX. Physical simulation of microstructural evolution in linear friction welded joints of Ti–6Al–4V alloy. Sci Technol Weld Join 2015;20:286–90.

[5.50] Abbod MF, Sellars CM, Tanaka A, Linkens DA, Mahfouf M. Effect of changing strain rate on flow stress during hot deformation of Type 316L stainless steel. Mater Sci Eng A 2008;491:290–6.

6. Concluding remarks

This thesis has reported on a comprehensive investigation of steel FSW with a primary focus on marine and shipbuilding applications through a number of in-depth experimental testing programmes. The following commentary summarises the noteworthy findings of these testing programmes and traces the important research challenges which have emerged.

The process envelope development programme drawn up in Chapter 1 has produced 25 DH36 steel friction stir butt welds of 2000 x 400 x 6 mm by employing varying tool rotational and traverse speeds. The trialled welding traverse speeds commenced from the originally recommended by the FSW tool manufacturer (100 mm/min) and were gradually increased up to 500 mm/min. This work has determined that parameter selection is a complex process with many interdependent variables, the interrelation of which is still inadequately understood. By substantially increasing the range of attainable traverse speeds, this development programme has concluded that high speed FSW of steel is feasible and moreover, can deliver significant improvements in the techno-economic competitiveness of the process relative to fusion welding methods. As commented upon in the findings of the diverse testing programmes however, the identified high speed welding parameters require further refinement to enhance the welds' performance. In addition, expanding the process envelope even more should be made possible when various tooling issues (encountered during the present research) are addressed, as the FSW tool technology continues to improve.

High traverse speed FSW is expected to affect the weld quality. For this purpose, metallographic examination of all 25 welds was performed to characterise the evolved microstructure, thus offer an insight into the anticipated mechanical property behaviour of the weldments, and to identify possible flaws which may weaken this behaviour. This analysis has established that significant grain refinement of the original DH36 parent material microstructure is promoted during welding. Moreover, FSW of steel develops a complex metallurgical system which is highly dependent on the employed process parameters, chiefly tool traverse speed. The slow traverse speeds (100-200 mm/min) generate a microstructure of refined ferrite grains, the intermediate traverse speeds (250-400 mm/min) create an acicular bainitic ferrite-

rich microstructure and the fast traverse speeds (450-500 mm/min) give rise to heterogeneous microstructures of acicular ferrites and acicular bainitic ferrites. Although the assessed welding parameters have produced no defects in the main body of the weld zone hence increasing the confidence in the quality of high speed FSW, two types of process related flaws have been detected in most welds. Lack of penetration initiating a weld root flaw and the top surface breaking flaws require tackling through new developments in the processing conditions and the FSW tool for steel. A key research challenge remains the characterisation of the very fine precipitates that are likely to have evolved in the weld region and an assessment of their contribution to the strengthening mechanism of friction stir welds (as disclosed below) with the use of transmission electron microscopy.

Mechanical testing of the welds was conducted with the intention of assessing the evolution of mechanical properties with increasing tool rotational and traverse speeds and evaluating the impact of the previously established complex metallurgical system in steel FSW. Transverse tensile testing has consistently demonstrated that all slow and intermediate welds have higher yield and tensile strength compared to the parent material regardless of minor surface breaking flaws (as characterised above). Again, research on the role of the fine precipitates and grain refinement in the welds' increased strength will prove useful when fine-tuning process parameters. Nevertheless, most fast weld samples fractured in the weld zone or were classed as unstable, suggesting reduced tolerance to parameter variations; hence, better optimisation of the high speed welding parameters (450-500 mm/min) is required. The weld hardness is seen to increase with increasing traverse speed and this is attributed to the evolution of harder phases in the microstructure. Still, the majority of the examined welds show hardness distribution within classification society rules. Importantly, an improvement in impact toughness with increasing traverse speed has been recorded and this provides additional weight to the potential of high speed steel FSW. However, this particular subject requires further in-depth analysis of the reasons for increased impact toughness solely on the advancing side, its underlying mechanism and on routes to enhance it.

Since the fatigue performance of welded components is of paramount importance in marine applications, this has been thoroughly assessed by producing new welds which made use of the findings in the previously outlined testing programmes. Due to the lack of pertinent testing guidelines or specifications, an extensive standard operating procedure document, specific to FSW, was drafted and executed with the

objective of addressing the relevant knowledge gap for this process on low alloy steel and generating novel data for future assessment by classification societies. The weldments' yield strength, geometry, metallurgical features and hardness distribution were recorded in support of the fatigue testing. Furthermore, the effect of varying welding parameters was also established. Microstructural observations, hardness measurements and transverse tensile properties were in excellent agreement with the corresponding in the previous testing programmes. It has been demonstrated that all examined steel grade DH36 friction stir welds exhibit excellent fatigue performance; in fact, the recorded fatigue strength is better than relevant international recommendations for fusion welding and equal to high quality laser welding. Moreover, the relation between weld flaws and fatigue performance has been established through metallographic examination and exhaustive fracture surface analysis, and further supported by additional fatigue testing with the critical surface breaking defect removed. This has revealed that minor embedded flaws do not initiate cracks whilst surface breaking flaws, i.e. lack of penetration or the indentations on the weld top surface by the tool shoulder are recognised as the critical factor for crack propagation. The latter is an important challenge for future FSW process developments which, when addressed, is expected to upgrade the welds' fatigue life dramatically.

The above outlined examination has contributed towards the fundamental understanding of FSW, generating an extensive experimental dataset on DH36 steel which was not previously available, along with detailing the all-important link between evolved microstructures and resultant mechanical properties. Additionally, a number of parameter sets in the region of 500 mm/min (traverse speed) have been identified by microstructural examination and mechanical testing as generating an attractive combination of acceptable quality level and economically competitive processing conditions. Thus, there is significant merit in exploring any possible extension to the upper limits of the process envelope developed herein by producing and testing more high speed welds.

In parallel, knowledge of the thermo-mechanical response of the examined material is equally important with regard to further refinement of process parameters and future improvements in tooling and welding machine specifications. To this end, thermo-mechanical deformation studies were implemented by hot axisymmetric compression testing on a Gleeble thermo-mechanical simulator to generate original material property data at elevated temperatures for the validation of any predictive

modelling work on the subject and to develop a greater understanding of the steel's flow stress evolution in testing conditions, i.e. temperature and strain rate, which simulate the actual FSW process. This novel investigation has defined the deformation behaviour of DH36 steel in FSW conditions; the alloy's flow stress is appreciably affected by the test temperature and strain rate. It has been confirmed that the flow stress is increasing with decreasing temperature and increasing strain rate. This is an important finding concerning the FSW of steel since it suggests that process parameters which produce regions of low temperature and high strain rate in a friction stir weld may result in inadequate material flow thus promoting the formation of embedded flaws. In contrast, the same observation introduces an explanation for the typical absence of embedded flaws in slow friction stir welds, in which high temperature / low strain rate conditions are normally created. On this account, a detailed study of the material flow in extreme conditions, i.e. as a function of increasing traverse speed should inform any improvements in processing conditions.

The above described evolution of flow stress is only opposed by the tests at 800°C, in which increased flow stress is recorded as compared to a lower test temperature for constant strain rate. This irregular behaviour of DH36 steel is ascribed to the diverse flow stress of austenite and ferrite which have formed in this intercritical temperature and the varying ratio of these two phases. There is value in an in-depth consideration of this atypical flow stress behaviour as future work on steel metallurgy is concerned. With reference to FSW of DH36 steel, this observation provides an insight into future process parameter development efforts since it clearly specifies that welding in the vicinity of 800°C is better avoided to reduce the forces exerted on the FSW tool for steel.

Continuing this investigation, a second testing programme was performed by subjecting identical steel samples to the same thermal cycle in the absence of compressive deformation to evaluate individually the impact of peak temperature and strain energy on the evolved microstructure. Microstructural examination of the thermo-mechanically deformed and thermally treated samples has solely observed isolated metallurgical features of real friction stir welds. These are restricted to pearlite dissociation, grain refinement by DRX in agreement with the preceding flow stress analysis and minor traces of acicular shaped grains in low test temperatures, and heterogeneous microstructure with small regions of acicular ferrite and fine acicular bainitic ferrite and evidence of Widmanstätten ferrite in intermediate

temperatures. Nevertheless, both series of tests in the highest test temperature of 1100°C exhibit predominantly acicular bainitic ferrite microstructures with pronounced prior austenite grain boundaries, Widmanstätten and blocky ferrite; these are in excellent agreement with intermediate and fast speed DH36 friction stir welds. The corresponding analysis has demonstrated that the influence of the strain rate on the microstructural evolution is gradually reducing with increasing temperature, until this becomes negligible in the highest temperature. This behaviour of DH36 steel is contradicting the widely established thermo-mechanical deformation nature of FSW and this is attributed to the lack of mechanical stirring of the material through shear forces. This conclusion also serves as a reminder of the multi-physics, complex nature of FSW. Thus, deformation by hot compression testing in conditions that reproduce actual steel FSW has been partly unsuccessful in delivering the anticipated results. Consequently, diverse methods such as hot torsion testing and the application of varying strain rates during testing are proposed as more suitable in physically simulating the intricate metallurgical features of steel FSW.

6.1. Future research work

A significant conclusion from the experimental programmes reported above has been that microstructural examination, fatigue and tensile testing, and hardness and impact toughness measurements suggest acceptable (at a minimum) mechanical properties of the fast welds. Therefore, a step change improvement in the currently employed welding traverse speeds has been confirmed, but there is considerable scope for further examination of high speed welding. This would render more weight to the argument for introduction of steel FSW in industrial applications, verify the consistency of the welding process and more importantly, generate the required datasets which will promote the development of relevant classification society guidelines and specifications (in the context of the marine sector). Other evident research questions are the assessment of the effect of varying plate thickness on the weldments' mechanical properties and the evaluation of more grades of steel such as high strength and poor weldability (in fusion welding techniques), e.g. super bainitic steels.

Apart from the previously outlined research challenges that have come to light from

the fulfilled experimental testing programmes, an obvious requirement for wider introduction of steel FSW in large-scale manufacturing is the development of a cost-effective and durable tool which will consistently deliver high integrity welds; this is a matter broadly accepted as crucial in the uptake of the process. Such tools could be manufactured from exotic materials with remarkable properties as is the current research route. A different route however could well be the experimentation with low cost and chemically inert (to the welded steel) materials to produce a type of consumable tool. The use of consumables is standard practice in most sectors therefore it can be expected that such a tool would be commercially accepted more effortlessly than the currently available expensive options. While on the subject of tooling issues, it is worth exploring the pre-heat assisted (e.g. through induction heating) FSW which can be utilised to soften the steel ahead of the tool, hence exposing the latter to much reduced forces.

Moreover, the current tool technology for steel only allows for welding in two configurations; butt and lap. Critically, the future introduction of FSW in shipbuilding will not only dependent upon cost-related issues but also on the process's capability to weld more geometries and specifically, fillet welding. In view of the present tooling manufacturing methods and materials, this will require a step change advancement in tool technology.

Appendix A. Fatigue testing details

Table A.1. Summary of intermediate, slow and fast weld fatigue testing results

Stress range	Test	Cycles to fracture	Nominal Δσ (MPa)	Fracture region
Intermediate weld				
80% of YS	1	479,985	265.83	Weld, outer RT
	2	602,646	261.78	Weld, outer RT
	3	1,116,339	263.81	Weld, outer RT
	4	1,967,444	263.94	Weld, outer RT
	5	589,711	262.19	Weld, outer RT
	6	1,114,315	264.00	Weld, outer RT
	7	317,472	263.09	Weld, outer RT
	8	941,637	262.61	Weld, outer RT
	9	1,899,174	262.68	Weld, outer RT
	10	678,298	261.71	Weld, outer RT
90% of YS	1	310,992	296.96	Weld, outer RT
	2	335,264	298.81	Weld, outer RT
	3	254,089	296.83	Weld, outer RT
	4	359,445	296.29	Weld, outer RT
	5	337,432	295.01	Weld, outer RT
	6	312,883	296.96	Weld, outer RT
	7	350,413	295.41	Weld, outer RT
	8	629,054	296.29	Weld, outer RT
	9	664,426	296.42	Weld, outer RT
	10	492,379	295.48	Weld, outer RT

	1	1,489,360	230.67	Weld, outer RT
	2	2,600,000	228.72	Test terminated
70% of YS	3	2,020,530	229.51	Weld, outer RT
	4	1,384,622	227.93	Weld, outer RT
	5	2,210,534	229.32	Weld, outer RT

Slow weld

	1	422,074	266.00	Weld, AD side
	2	2,700,000	265.64	Test terminated
	3	2,500,000	265.21	Test terminated
	4	2,600,000	264.55	Test terminated
80% of YS	5	1,083,669	265.14	Weld, AD side
	6	2,500,000	266.06	Test terminated
	7	2,500,000	262.19	Test terminated
	8	2,600,000	265.81	Test terminated

Fast weld

	1	416,112	265.14	Weld root
	2	222,272	262.13	Weld, inner AD
	3	722,691	264.29	Weld root
	4	570,815	261.84	Weld root
80% of YS	5	129,490	263.39	Weld, inner AD
	6	731,208	261.59	Weld root
	7	136,844	264.36	Weld, inner AD
	8	516,949	261.36	Weld root

Appendix B. List of publications

B.1. Peer reviewed journal publications

1. Toumpis A, Galloway A, Cater S, McPherson N. Development of a process envelope for friction stir welding of DH36 steel – A step change. Mater Des 2014;62:64–75.

2. Toumpis AI, Galloway AM, Arbaoui L, Poletz N. Thermomechanical deformation behaviour of DH36 steel during friction stir welding by experimental validation and modelling. Sci Technol Weld Join 2014;19:653–63.

3. Maltin CA, Nolton LJ, Scott JL, Toumpis AI, Galloway AM. The potential adaptation of stationary shoulder friction stir welding technology to steel. Mater Des 2014;64:614-624.

4. Tingey C, Galloway A, Toumpis A, Cater S. Effect of tool centreline deviation on the mechanical properties of friction stir welded DH36 steel. Mater Des 2015;65:896-906.

5. Toumpis AI, Galloway AM, Molter L, Polezhayeva H. Systematic investigation of the fatigue performance of a friction stir welded low alloy steel. Mater Des 2015;80:116–28.

6. Micallef D, Camilleri D, Toumpis A, Galloway A, Arbaoui L. Local heat generation and material flow in friction stir welding of mild steel assemblies. Proc Inst Mech Eng Part L J Mater Des Appl 2015. DOI: 10.1177/1464420715583163.

7. Logan BP, Toumpis AI, Galloway AM, McPherson NA, Hambling SJ. Dissimilar friction stir welding of duplex stainless steel to low alloy structural steel. Sci Technol Weld Join 2015. DOI: 10.1179/1362171815Y.0000000063.

8. Polezhayeva H, Toumpis AI, Galloway AM, Molter L, Ahmad B, Fitzpatrick ME. Fatigue performance of friction stir welded marine grade steel. Int J Fatigue 2015;81:162–70.

9. Stevenson RJ, Toumpis AI, Galloway AM. Defect tolerance of friction stir welds in DH36 steel. Mater Des 2015;87:701–11.

10. Fowler S, Toumpis AI, Galloway AM. Fatigue and bending behaviour of friction stir welded DH36 steel. Int J Adv Manuf Technol 2015; Manuscript submitted for publication.

B.2. Article in an edited book:

Toumpis AI, Galloway AM, Polezhayeva H, Molter L. Fatigue assessment of friction stir welded DH 36 steel. Friction Stir Welding and Processing VIII, pp 11-20, Eds. RS Mishra, MW Mahoney, Y Sato, Y Hovanski, John Wiley & Sons Ltd. ISBN: 978-1-119-08249-1.

B.3. Papers in conference proceedings

1. Toumpis A, Galloway AM, Cater S, Micallef D, Camilleri D, Poletz N, Arbaoui L. Advances in Friction Stir Welding of Steel - Project HILDA. Transport Research Arena Conference, TRA2014, Paris, France, 14-17 April 2014.

2. Toumpis A, Galloway AM, Cater S, Molter L. A techno-economic evaluation of friction stir welding of DH36 steel. 10th International Friction Stir Welding Symposium, 10FSWS, Beijing, China, 20-22 May 2014.

3. Toumpis A, Galloway A, Cater SR, Burling P, Stanhope C. Friction stir welding of steel for marine applications. 33rd International Conference on Ocean, Offshore and Arctic Engineering, OMAE 2014, San Francisco, USA, 8-13 June 2014.

4. Toumpis AI, Galloway AM, Polezhayeva H, Molter L. Fatigue assessment of friction stir welded DH36 steel. TMS Annual Meeting and Exhibition, TMS2015, Orlando, USA, 15-19 March 2015.

5. Camilleri D, Micallef D, Arbaoui L, Toumpis A, Galloway A. Numerical modelling techniques applicable for the prediction of residual stresses and distortion due to mild steel DH36 friction stir welding. 4th International Conference on Friction Stir Welding and Processing, FSWP2015, Donostia-San Sebastian, Spain, 1-2 October 2015.

6. Toumpis AI, Galloway AM, Camilleri D, Arbaoui L. Recent developments in steel friction stir welding - project HILDA. ASME 2015 International Mechanical Engineering Congress & Exposition, IMECE2015, Houston, USA, 13-19 November 2015.